A R M S T R O N G   L A B O R A T O R Y

PRESSURE-CONTROLLED ATOMIZATION PROCESS (PCAP) FOR DIMENSIONAL RESTORATION OF AVIATION PARTS PART 1

John C. Tierney, Ronald J. Glovan, Ying-Ming Lee

MSE, Inc.
Post Box 4078
Butte MT 59702

ENVIRONICS DIRECTORATE
139 Barnes Drive, Suite 2
Tyndall AFB FL 32403-5323

July 1996

Final Technical Report for Period August 1990 - May 1995

19961108 018

AIR FORCE MATERIEL COMMAND
TYNDALL AIR FORCE BASE, FLORIDA 32403-5323
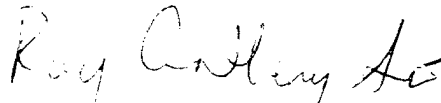
DTIC QUALITY INSPECTED 1

NOTICES

This report was prepared as an account of work sponsored by an agency of the United States Government. Neither the United States Government nor any agency thereof, nor any employees, nor any of their contractors, subcontractors, or their employees, make any warranty, expressed or implied, or assume any legal liability or responsibility for the accuracy, completeness, or usefulness of any privately owned rights. Reference herein to any specific commercial products, process, or service by trade name, trademark, manufacturer, or otherwise, does not necessarily constitute or imply its endorsement, recommendation, or favoring by the United States Government or any agency, contractor, or subcontractor thereof. The views and opinions of the authors expressed herein do not necessarily state or reflect those of the United States Government or any agency, contractor, or subcontractor thereof.

When Government drawings, specifications, or other data are used for any purpose other than in connection with a definitely Government-related procurement, the United States Government incurs no responsibility or any obligation whatsoever. The fact that the Government may have formulated or in any way supplied the said drawings, specifications, or other data, is not to be regarded by implication, or otherwise in any manner construed, as licensing the holder or any other person or corporation; or as conveying any rights or permission to manufacture, use, or sell any patented invention that may in any way be related thereto.

This technical report has been reviewed by the Public Affairs Office (PA) and is releasable to the National Technical Information Service, where it will be available to the general public, including foreign nationals.
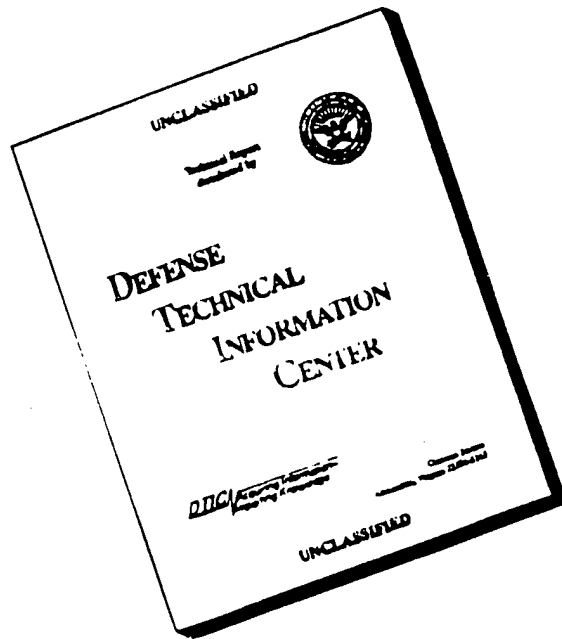
This report has been reviewed and is approved for publication.

FOR THE COMMANDER:

RAY A SMITH, 1Lt, USAF, BSC
Project Manager

ALLAN M. WEINER, Lt Col, USAF
Chief, Environmental Compliance Division

DISCLAIMER NOTICE

July 1996   Final Report   Aug 1990 to May 1995

Pressure-Controlled Atomization Process (PCAP) for
Dimensional Restoration of Aviation Parts: Part 1(pg 1-212)

John C. Tierney, Ronald J. Glovan, and Ying-Ming Lee

MSE, Inc.
P.O. Box 4078
Butte, MT 59702

APPROVED FOR PUBLIC RELEASE.   DISTRIBUTION UNLIMITED

The Pressure-Controlled Atomization Process (PCAP) is a new thermal spray process
in which a liquid metal is atomized in a supersonic nozzle, which also directs the
spray to a suitable substrate. The Spray Casting Project was jointly sponsored by
the United States Air Force, Armstrong Laboratory Environics Directorate at
Tyndall AFB, and the United States Department of Energy, Office of Technology
Development (DOE-OTD) under the U.S. Air Force-DOE Memorandum of Understanding
(MOU). The Air Force application uses the Pressure Controlled Atomization Process
(PCAP) to thermally spray metallic replacement coatings for electroplated hard
chromium.

The report presents a history of PCAP as it relates to the development of the
process, the development of the hardware to support the process development, and
the testing that was conducted to understand the process and generate engineering
data to support the replacement hard chromium electroplating with PCAP sprayed
coatings.

Thermal spraying of metals, hard chromium replacement.

UNCLASSIFIED   UNCLASSIFIED   UNCLASSIFIED   QUALITY INSPECTED 1

PREFACE

This final report describes the research and development work for developing a thermal spray process known as the Pressure-Controlled Atomization Process (PCAP) for the dimensional restoration of United States Air Force aviation parts. PCAP will replace electroplated hard chromium with a thermally sprayed coating of VERSAlloy 50, which is a nickel-based alloy.

EXECUTIVE SUMMARY

A. OBJECTIVE

The purpose of this document is to provide a final report for the research and development work conducted by MSE, Inc. (MSE), on Phase III of the Spray Casting Project for the United States Air Force (USAF). MSE is developing a thermal spray process known as the Pressure-Controlled Atomization Process (PCAP) for the dimensional restoration of USAF aviation parts. PCAP will replace electroplated hard chromium with a thermally sprayed coating of VERSAlloy 50, which is a nickel-based alloy.

B. BACKGROUND

The Spray Casting Project is jointly sponsored by the USAF, Environics Directorate of the Armstrong Laboratory at Tyndall Air Force Base, and the United States Department of Energy—Office of Technology Development (DOE-OTD). The project was conducted under a USAF-DOE Memorandum-of-Understanding (MOU), and its mission focused on waste minimization involving chromium electroplating of aviation components for the USAF and near-net shape fabrication of special nuclear material for DOE-OTD. The process under development, PCAP, is a new thermal spray process that atomizes liquid metals in the flow of inert gas passing through a supersonic nozzle.

The aspiration of liquid metals in supersonic nozzles was first studied in 1989 by EG&G, Idaho personnel at the Idaho National Engineering Laboratory (INEL); and a patent for the process (Patent No. 4,919,853) was issued in 1990. Phase I and Phase II of the Spray Casting Project were conducted at the INEL. Phase I demonstrated the feasibility of spraying high quality tin coatings on grit-blasted carbon steel coupons. Phase II goals were to build a spray coating system, spray coatings with high melting temperature materials suitable for replacing chromium, and evaluate the coatings. Phase III of the project started in 1990, and MSE became involved in developing the process and providing engineering design and fabrication capabilities for a production type system for installation in one of the USAF Air Logistics Service Centers (ALC). To facilitate testing, the laboratory equipment was moved to the Custom Spray Technologies facility in Rigby, Idaho, until modifications to the MSE Spray Casting Facility in Butte, Montana, were completed.

As MSE proceeded into Phase III of the Spray Casting Project, it became apparent that there were serious engineering shortcomings with the existing Phase II hardware. Specifically, the gas heater output temperature was insufficient to spray higher melting point alloys (>1000 °C), the supersonic nozzle was operating in a nonlinear region, and the spray nozzle eroded and reacted with the sprayed material. Additionally, MSE realized that a better understanding of the effects that nozzle geometry and system operating parameters had on the physical and mechanical properties of PCAP-produced deposits was necessary before a production unit could be designed and fabricated.

In 1991, at the request of the USAF, the direction of the USAF portion of the project changed from building prototype equipment to developing a test

program to qualify the PCAP-sprayed VERSAlloy 50 coatings to USAF standards. The test program involved an evaluation of the process by MSE, and an independent evaluation of the process by the Boeing Company and the USAF's Wright Laboratory. The test program also included continued development of process hardware for a first generation developmental pilot-scale unit to meet the needs of both the USAF and the DOE-OTD. After completing the MSE Test Series, the name of the process was changed from the Controlled Aspiration Process to the Pressure-Controlled Atomization Process (PCAP).

C. SCOPE

This document presents the research and development work that has been accomplished in replacing electroplated hard chromium with a PCAP thermally sprayed coating of VERSAlloy 50. Section I provides an overview of the project. Section II presents an overview of the qualification testing conducted by MSE for the MSE Test Series. The MSE Test Series consisted of two experimental designs, equipment upgrades, and computer modeling of the supersonic spray nozzles. Additionally, screening tests for nozzle candidate materials were investigated, and a comparison of PCAP-sprayed VERSAlloy 50 coatings to commercial electric twin-wire arc sprayed VERSAlloy 50 coatings was presented. A complete report of the MSE Test Series is in Appendix A. Section III is an overview of the qualification testing conducted by the Boeing Company for the Boeing Test Series. The Boeing Test Series consisted of tests for fatigue, abrasion, adhesion, internal stress, metallurgy, hardness, corrosion, materials compatibility and workability, and chemistry. In tests where it was practical, the sprayed VERSAlloy 50 coatings were compared directly to electroplated hard chromium. A complete report of the Boeing Test Series is in Appendix B. Section IV is an overview of the qualification testing conducted by the Wright Laboratory at Wright Patterson Air Force Base (WPAFB) for the Wright Laboratory Test Series. The Wright Laboratory Test Series consisted of tests for fatigue, hardness, and corrosion with a direct comparison to fatigue coupons coated with electroplated hard chromium. A complete report of the Wright Laboratory Test Series is in Appendix C. Section V presents an overview of parameter optimization testing conducted for the Wear- and Corrosion-Integrated Test (WIT) Series. The WIT Test Series consisted of a four-phase experimental design to determine system parameter settings for producing optimal characteristics for VERSAlloy 50 coatings. In addition to the experimental design, equipment modifications and computer modeling of a two-piece nozzle was conducted to support the design and fabrication of a developmental pilot-scale unit. A complete report of the WIT Test Series is in Appendix D. A summary and concluding remarks for work conducted on the Spray Casting Project are in Section VI. Recommendations for future work on the Project are in Section VII.

D. SYSTEM DEVELOPMENT, EXPERIMENTAL DESIGNS, AND TESTING

When the spray casting equipment was transferred from the Custom Spray Technologies facility in Rigby, Idaho, to the Spray Casting Facility in Butte, Montana, modifications were made to transform a piece of laboratory equipment into a reliable operating system with industrial controls. The fundamental operation of the process was also improved by incorporating a pressurized tundish system to inject liquid metal into the nozzle. These modifications were completed during the MSE Test Series.

The MSE Test Series was a group of tests and modeling work that was performed to gain an understanding of how the geometric and operating parameters of circular cross-section supersonic nozzles affected PCAP spray deposit characteristics. For the MSE Test Series, two experimental designs were used to evaluate the performance of PCAP while spraying tin. Results from the analysis provided the characterization data for nozzle geometry and operating control parameters that were used as the basis for process control parameter settings for spraying high temperature materials for the Boeing and Wright Laboratory Test Series.

During the MSE Test Series, a group of tests was also conducted to compare PCAP to a conventional thermal spray process, in this case, a Hobart/TAFA electric twin-wire arc system. Tests were conducted at varied process control settings to examine coating attributes of VERSAlloy 50 metal sprayed with the electric twin-wire arc system. Results of the tests were compared to PCAP sprayed VERSAlloy 50 coatings from the Boeing Test Series.

As part of the initial work performed for Phase III, it became apparent that erosion and/or corrosion was occurring in the spray nozzles fabricated from hexagonal boron nitride. Therefore, a series of tests was conducted to evaluate the compatibility of nozzle materials with selected spray materials such as VERSAlloy 50. The tests were static and consisted of placing a small metal coating sample on a sample of candidate nozzle material in a controlled atmosphere furnace. The candidate nozzle material samples were heated/cooled, then evaluated metallurgically for chemical attack.

The second series of testing conducted to qualify the process to USAF standards was designated as the Boeing Test Series. The Boeing Test Series used the experience of an aerospace company to evaluate PCAP-sprayed coatings produced by MSE. This test series was an intermediate set of engineering tests that evaluated VERSAlloy 50 coatings sprayed with the MSE-modified laboratory PCAP equipment. MSE sprayed 68 test samples that were evaluated by the Boeing Defense and Space Group in Kent, Washington.

The third series of testing conducted to qualify the process to Air Force standards was designated as the Wright Laboratory Test Series. As with the Boeing Test Series, coupons for the Wright Laboratory Test Series were sprayed with VERSAlloy 50 and were then sent for evaluation. MSE sprayed 75 test samples for the Wright Laboratory Test Series.

After completion of the Wright Laboratory Test Series, the spray casting system was modified to make the PCAP repeatable and the hardware controllable by a single operator. Modifications included installation of a vacuum/pressure spray chamber, design and installation of a new high temperature 1800 °C inert gas heating system, an automated tundish pressure control system, an electric metal feed system, a six-axis robotic arm, and a resistive heating element for the nozzle and tundish.

A final test series was conducted to investigate and characterize the VERSAlloy 50 coatings applied by the developmental pilot-scale hardware. Using a central composite experimental design with preliminary and validation testing, tradeoffs for optimizing coating parameters such as corrosion

resistance, wear resistance, porosity, and microhardness were quantified using statistical techniques. MSE sprayed 35 test samples and evaluated corrosion and wear characteristics. Microhardness, porosity, and grain size for the test specimens were evaluated by Tubal Cain Company.

E.   COMPUTER MODELING

During the MSE Test Series, INEL and MSE scientists modified and improved the quasi-one-dimensional computer code developed in Phase II and made simulation runs to support the pressurized nozzle design developed during the MSE Test Series.

After completing the Wright Laboratory Test Series, MSE scientists modelled a two-piece nozzle design using the quasi-one dimensional computer code.

F.   RESULTS

Results from the MSE Test Series show that the PCAP-sprayed VERSAlloy 50 coatings appear to have an advantage over the electric twin-wire arc sprayed VERSAlloy 50 because of the smaller grain size, lack of traverse cracking in the deposit, and lower porosity.

From the nozzle materials evaluation portion of the MSE test series, three candidate materials showed no visible signs of reaction from the 10-minute (screening) test, 10-hour test and 100-hour (duration) test. The candidate materials are: 1) alumina (98 percent dense); 2) silicon nitride; and 3) partially stabilized zirconia ($5.4Y_2O_3$).

Results from the Boeing Test Series show that the performance of PCAP-sprayed VERSAlloy 50 varied among the tests performed. Most notably, the PCAP coating enhanced the fatigue-resistance of AISI 4130 base steel coupon compared to reduced fatigue-resistance caused by electroplated hard chromium. The VERSAlloy 50 coating has a relatively high hardness but did not perform as well as electroplated chromium in Taber abrasion testing. The coating did not perform as well as the chromium plating in corrosion testing although the refinement of the spray process could reduce porosity in the coating and increase corrosion performance. The VERSAlloy 50 coating exhibited excellent adhesion to 15-5 PH stainless steel and 6A14V titanium, a material extremely difficult to electroplate.

Results from the Wright Laboratory Test Series also show that VERSAlloy 50 coating on the AISI 4130 steel fatigue coupons had significantly better fatigue resistance than the electroplated chrome AISI 4130 fatigue coupons. The VERSAlloy 50 coating performed poorly in the corrosion test. The period of time elapsed before the onset of corrosion is of concern for application where corrosion resistance is desirable.

Results from the WIT Test Series show that VERSAlloy 50 coatings applied with the developmental pilot-scale spray system are accurately predicted by the equations derived from the experimental design. As a result, the process can be tailored for optimizing different coating parameters.

G.   CONCLUSIONS

PCAP was tested and evaluated by MSE personnel and by two independent laboratories, the Boeing Company and the Wright Laboratory. The VERSAlloy 50 coatings applied with PCAP show promise for replacing hard electroplated chromium on external diameters of aviation flight hardware. As shown from the WIT experimental design, the coating characteristics can be improved substantially and can be optimized. Further investigation of adhesion strength of the coating needs to be conducted to better quantify this coating attribute.

The equipment development has evolved so that one trained operator controls the entire process. More development work is required on the metal feed system; on a spray nozzle fabricated from alumina, silicon nitride, or partially stabilized zirconia; and on an argon recirculation loop.

H.   RECOMMENDATIONS

Results from the Boeing and Wright Laboratory Test Series show that PCAP-applied VERSAlloy 50 coatings may be suitable for replacing hard electroplated chromium on USAF flight hardware. Further investigation into process operating control parameters and nozzle geometries to produce optimal coatings will be required before the process is ready for commercialization and/or installation at an USAF ALC. Using the two-phase flow computer model developed in Phase I and II and following an experimental design process, the investigation can be made with the existing spray casting system. Additional design work will also be required on the metal feed system to provide a means for supplying a continuous feed of material to the tundish.

To date, VERSAlloy 50, sprayed with the PCAP, has been identified as the candidate material to replace hard electroplated chromium; however, other wear-resistant coating alloys should be investigated and sprayed with the PCAP. As sprayed, coating characteristics for porosity, microhardness, adhesion strength, abrasion resistance, corrosion resistance, and fatigue resistance for each new alloy should be evaluated and compared to the VERSAlloy sprayed coatings.

PCAP should also be compared with other thermal spray processes that are commercially available. Specifically, vacuum plasma spraying, high velocity oxygen fuel spraying, and electric twin-wire arc spraying systems.

TABLE OF CONTENTS

LIST OF FIGURES

LIST OF FIGURES (CONT'D)

SECTION I
INTRODUCTION

With disposal costs and more stringent regulations for emission control of hexavalent chrome taking effect each year, an alternative method of applying wear-resistant materials on U.S. Air Force (USAF) components is becoming a necessity. The USAF has five Air Logistic Centers (ALC) that produce waste streams from hard chromium plating lines. The Pressure-Controlled Atomization Process (PCAP), a thermal spray process being developed at the Western Environmental Technology Office (WETO) by MSE, Inc. (MSE), is a possible technology alternative for the replacement of hard chrome plating. The PCAP atomizes molten materials and sprays finely atomized droplets onto aviation components as a means of dimensional restoration.

A. OBJECTIVE

The objective of the Spray Casting Project is to minimize the generation of hazardous waste from electroplated hard chromium by replacing the process with a thermally sprayed coating. Phase III goals were to qualify the process to USAF standards and to design and fabricate a developmental pilot-scale unit.

B. BACKGROUND

Phase I of the Spray Casting Project started in Fiscal Year 1989 and was conducted at the Idaho National Engineering Laboratory (INEL). The original title of the project was *Spray Coating of Metals*; however, the name of the project was changed in 1990 to reflect both the USAF mission as well as the United States Department of Energy–Office of Technology Development (DOE-OTD) mission. The objective for Phase I of the project was to demonstrate the feasibility of the process at low temperatures by spraying high-quality tin coatings on grit-blasted carbon steel coupons. Phase I involved building and testing an enclosed spray-coating system with controls and computerized equipment. Metallographic, bend, and adhesion tests were performed on sprayed samples. The results from Phase I testing showed that the process transferred a low amount of heat into the substrate and that low-temperature materials had good adhesion to the substrate.

Phase II of the Spray Casting Project was also conducted at the INEL. The objective for Phase II of the project involved upgrading the bench-scale apparatus developed in Phase I to spray high melting point metals and to investigate the replacement of hard chromium electroplating with sprayed chromium or chromium-bearing alloys. Additionally, the atomization and deposition mechanisms of the spray process were modeled. Nine successful coating experiments were performed with cobalt-chromium alloys, Stellite 6™, Coast 64™, and Haynes Ultimet™. One test to spray pure chromium was also attempted; however, the nozzle exit plugged before molten chromium was poured into the tundish, and no test specimens were produced.

Phase III of the Spray Casting Project was conducted at the WETO Spray Casting Facility in Butte, Montana. Phase II equipment was initially moved from the INEL on June 13, 1991, to the Custom Spray Technologies facility in

1

Rigby, Idaho. Eight spray experiments were conducted at Custom Spray Technologies to provide operator training, component fabrication, and testing of circular cross-sectional spray nozzles. The Phase II equipment was moved from the Custom Spray Technologies facility to the MSE Spray Casting Facility on October 23, 1991.

C.   SCOPE

The original objective for Phase III of the project was to design, fabricate, and test pilot-scale spray casting equipment to be used at an USAF repair facility. However, at the direction of the USAF, the objective of Phase III was changed to first qualify the spray casting process to meet USAF standards and then to build a developmental pilot-scale system. The qualification process was divided into three separate test series: the MSE Test Series, the Boeing Test Series, and the Wright Laboratory Test Series. In addition to qualification testing, new process hardware equipment was continually designed, fabricated, and installed to meet the USAF requirements of building a developmental pilot-scale system. A final test series was also conducted to characterize and improve the coatings applied by the Pressure-Controlled Atomization Process (PCAP). The final test series, designated the Wear- and Corrosion-Integrated Test (WIT) Series, utilized experimental design techniques to provide optimal coating characteristics for wear resistance, corrosion resistance, microhardness, and porosity.

Based on the recommendations from Phase II testing at the INEL, other metal alloys were investigated for coating USAF parts. MSE identified a family of nickel-based alloys produced by Protective Metal Alloys that have relatively low temperature melting ranges that are ideal for PCAP spraying for wear resistant applications. To date, pure tin and VERSAlloys 25 and 50 have been sprayed by MSE. The VERSAlloy series are a family of nickel-based alloys that contain relatively high amounts of carbon, boron, and silicon. The chemical composition of VERSAlloy 25 and 50 are shown in Table 1.

Table 1.   NOMINAL CHEMICAL COMPOSITIONS, WEIGHT PERCENT.

Alloy	Melt Temp (°F)	C	Cr	Si	B	Fe	Ni
VERSAlloy 50	1950	0.60	11.0	4.0	3.0	4.0	Bal
VERSAlloy 25	1975	0.10	----	3.2	1.6	1.0	Bal

All of the Phase III high-temperature qualification testing was conducted with VERSAlloy 50. The total number of spray tests conducted for the MSE, Boeing, Wright Laboratory Test Series, WIT Series, and for the DOE-OTD work are shown in Table 2.

2

TABLE 2. NUMBER OF SPRAY TESTS.

Test Series	Number of Tests
MSE Test Series	78
Boeing Test Series	68
Wright Laboratory Test Series	75
Wear- and Corrosion-Integrated Test (WIT) Series	35
DOE-OTD	127

Phase III work included developing a reliable high-temperature inert gas heating system and an electric metal feed system; installing a six-axis robotic arm; replacing an induction coil nozzle/tundish heating system with a graphite resistant heating element; designing, fabricating, and installing a vacuum/pressure chamber to control atmosphere and contain particle overspray; and installing a 0.02 micron filter to control particle emissions from the process. Work for qualification testing consisted of coating specimens with tin or VERSAlloy 50 and then evaluating and quantifying the coating properties by using standardized test methods. A list of standardized tests used in the evaluation of VERSAlloy 50 coated specimens are given in Table 3.

TABLE 3. STANDARDIZED TESTS.

Test Method Number	Description
ASTM B117	Neutral Salt Fog Spray Test
ASTM G85	Acetic Acid Salt Fog Spray Test
Federal Test Method 141C, Method 6192.1	Taber Abrasion Wear Resistance
ASTM C633-79	Adhesion Testing of Thermally Sprayed Coatings

D.   OVERVIEW-HARDWARE DEVELOPMENT

Phase II equipment was delivered to the Spray Casting Facility on October 23, 1991, and the first spray test at the Spray Casting Facility was conducted December 31, 1991. Prior to commencing the MSE Test Series, two major modifications were made to the system. First, the fundamental process of injecting the liquid feedstock material into the nozzle was changed from operating in an aspirating mode to operating in a pressurized mode. Second, a computer controlled X-Y translation device was installed to manipulate

3

substrate material into the spray plume. The system operated during the MSE Test Series is shown in Figures 1 and 2.

During the MSE Test Series, a resistive graphite heating element, power supply, and process controller system, was designed, fabricated, and installed to replace the induction power supply, coil, and susceptor system used to heat the nozzle and tundish. Additionally, a gas heating system developed by American Furnace Company was fabricated and installed into the process hardware. The gas heating system was installed to achieve the gas temperatures required to spray high-temperature materials (>1000 °C) for the Boeing Test Series. Prior to starting the Boeing and Wright Laboratory Test Series, an oxygen analyzer, pressure control valve, and PID controller to regulate tundish pressure were also installed in the system. The system operated during the Boeing and Wright Laboratory Test Series is shown in Figures 3 and 4.

After completing the Wright Laboratory Test Series, a metal feed system, a two-piece nozzle, and a new inert gas heater were designed, fabricated, and installed into the process hardware. Additionally, a six-axis robotic arm, manufactured by Staubli Unimation, was installed to manipulate parts in the spray plume. A new vacuum/pressure spray chamber, manufactured by Advanced Vacuum Systems, was also installed and integrated in the process. The developmental pilot-scale system was designed to be a reliable system that can be operated by one skilled technician. Figures 5, 6, and 7 show features of the spray system during the WIT Series.

E.   OVERVIEW OF PRESSURE-CONTROLLED ATOMIZATION PROCESS (PCAP)

The basic components of the developmental pilot-scale PCAP unit are a gas delivery system, a converging/diverging supersonic nozzle, a pressurized tundish control system, a nozzle/tundish resistance graphite heating system, an inert gas resistant graphite heating system, a metal feed system, a six-axis robotic arm, and an integrated control system. A schematic drawing of the PCAP developmental pilot-scale system is shown in Figure 8. The process flows inert gas, typically argon (99.997 percent pure), through the gas heating system into the heated nozzle. The heated gas is accelerated to a supersonic velocity and exits the spray nozzle. As the gas accelerates through the nozzle throat, liquid metal is pressurized in the tundish and injected into the nozzle throat through an orifice where atomization takes place. The atomized metal droplets are then deposited onto a moving substrate or part. Figure 9 represents the relationship between gas velocity, gas temperature, particle velocity, and particle temperature versus the spray distance from the nozzle throat when the nozzle operates in the pressurized mode. Figure 10 represents the relationship between gas velocity, gas temperature, particle velocity, and particle temperature versus the spray distance from the nozzle throat when the nozzle operates in the aspiration mode. The data in both illustrations was generated with the quasi-one dimensional computer code developed during Phase II of the project. In both graphs, the particle temperature and velocity are based on a 10 micron particle of VERSAlloy 50. Through experimental testing and analysis, it was determined that the desired mode of operation for the spray casting system is the pressurization mode.

4

The most important component in the PCAP is the supersonic nozzle that has a circular cross section and is nominally 2.33 inches long. The converging section is approximately 1.62 inches long and has a 6-degree angle of convergence. The throat is 0.080 inch in diameter and is 0.10 inch long. The diverging section is approximately 0.660 inch long and has a 2-degree angle of divergence. The liquid orifice is 0.011 inch in diameter. An engineering drawing of the MSE two-piece nozzle is shown in Figure 11.
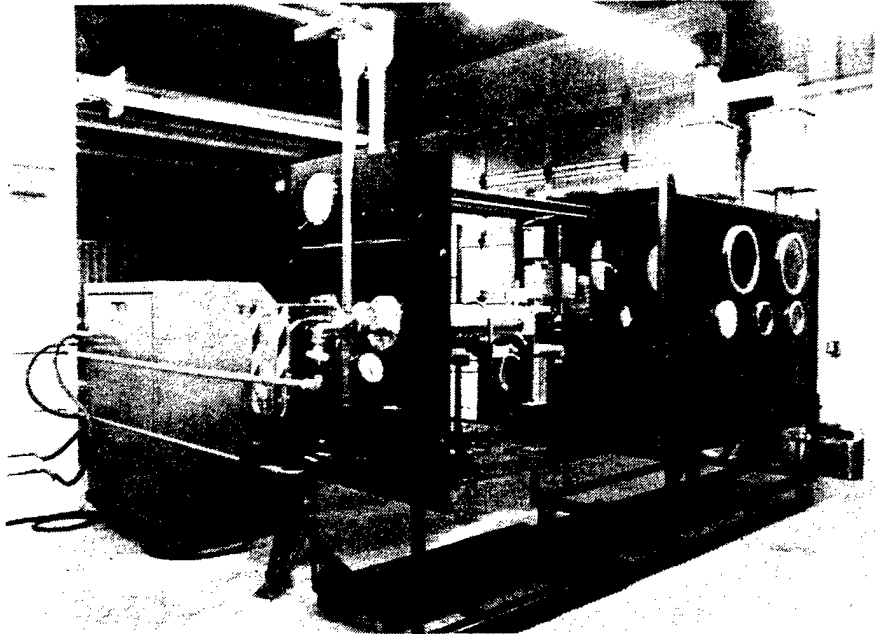
Figure 1. Overall View of Spray Casting Equipment During MSE Test Series.
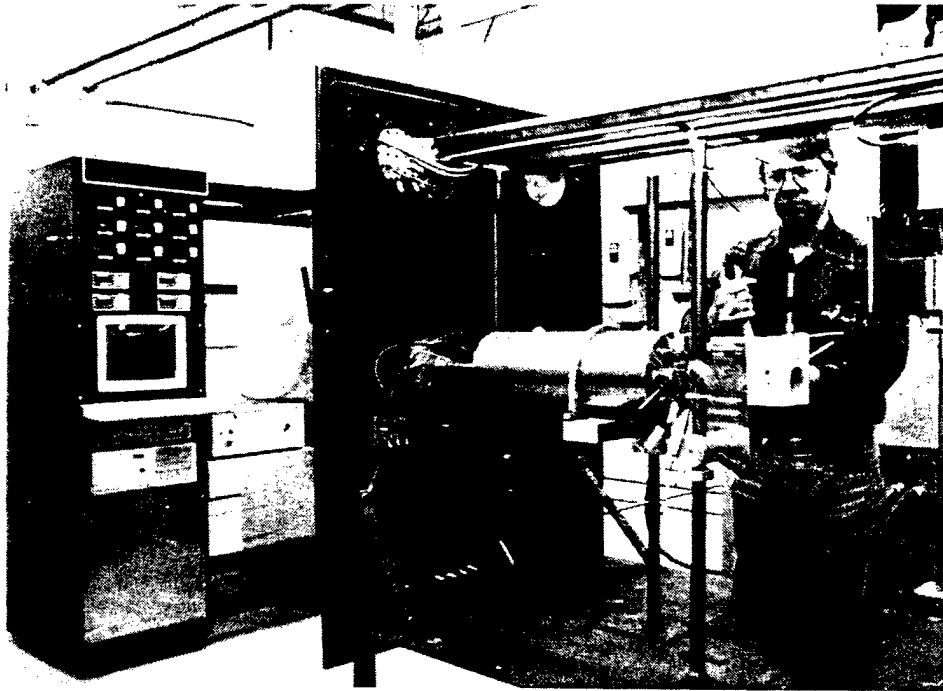
Figure 2.   View of Gas Heater During MSE Test Series.
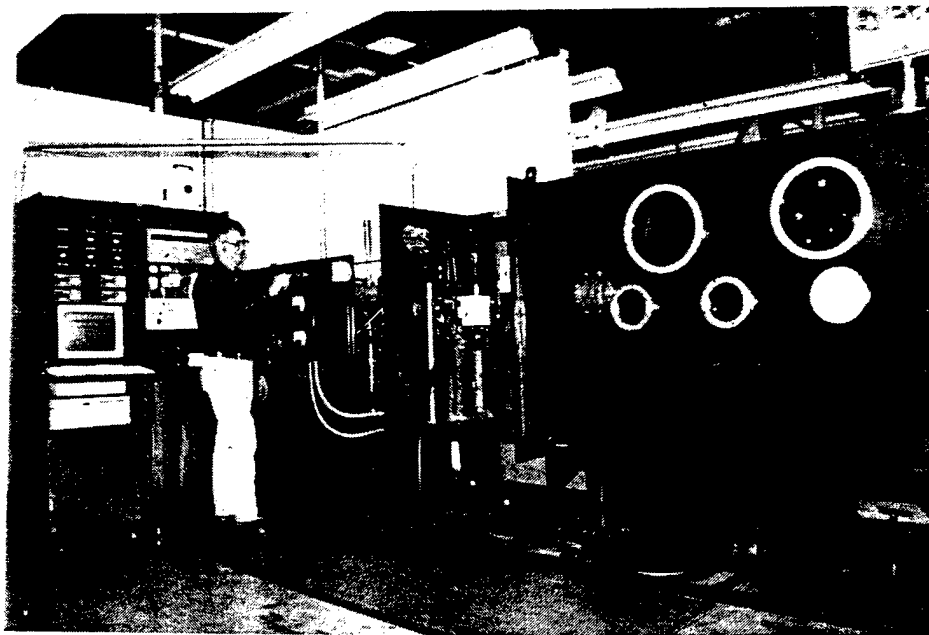
Figure 3.   Overall View of Spray Casting Equipment During
Boeing and Wright Laboratory Test Series.
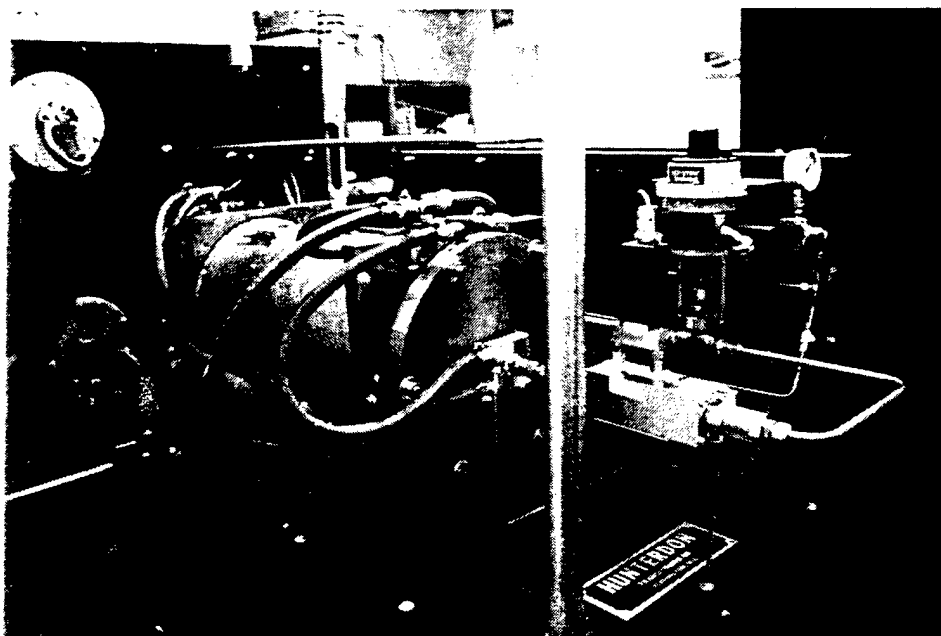
Figure 4.   Gas Heating System During Boeing and Wright
            Laboratory Test Series.
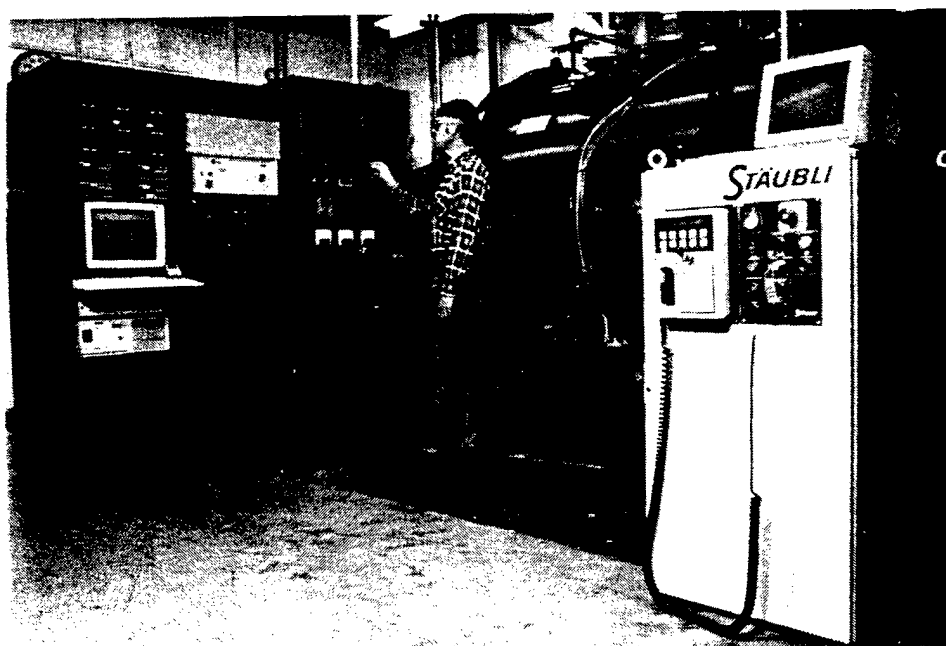
Figure 5.   Overall View of Spray Casting Equipment During
            Wear- and Corrosion-Integrated Test Series.
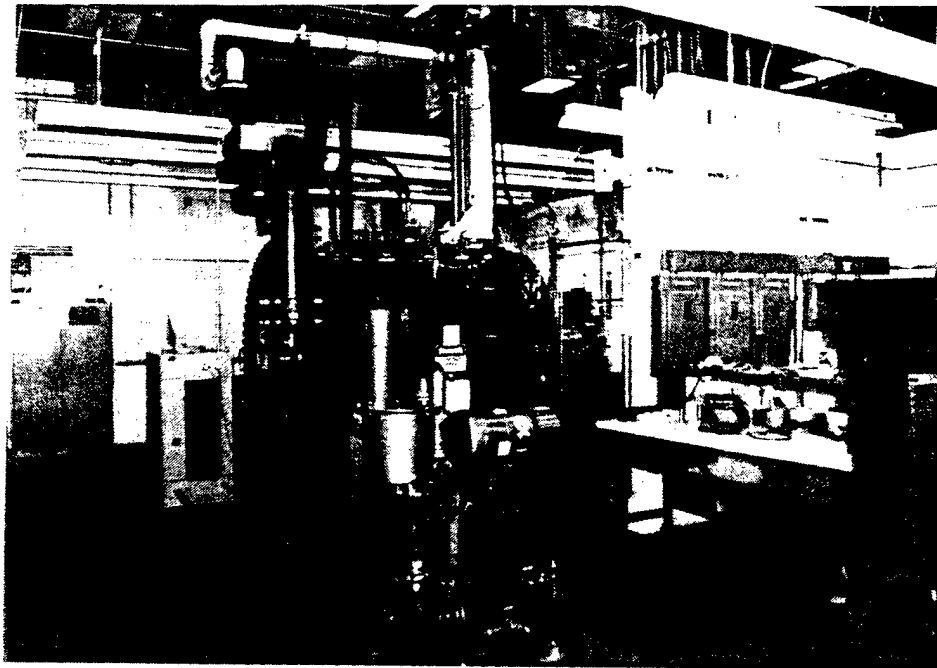
Figure 6.   Opposite Side View of Spray Casting Equipment
During Wear- and Corrosion-Integrated Test
Series.
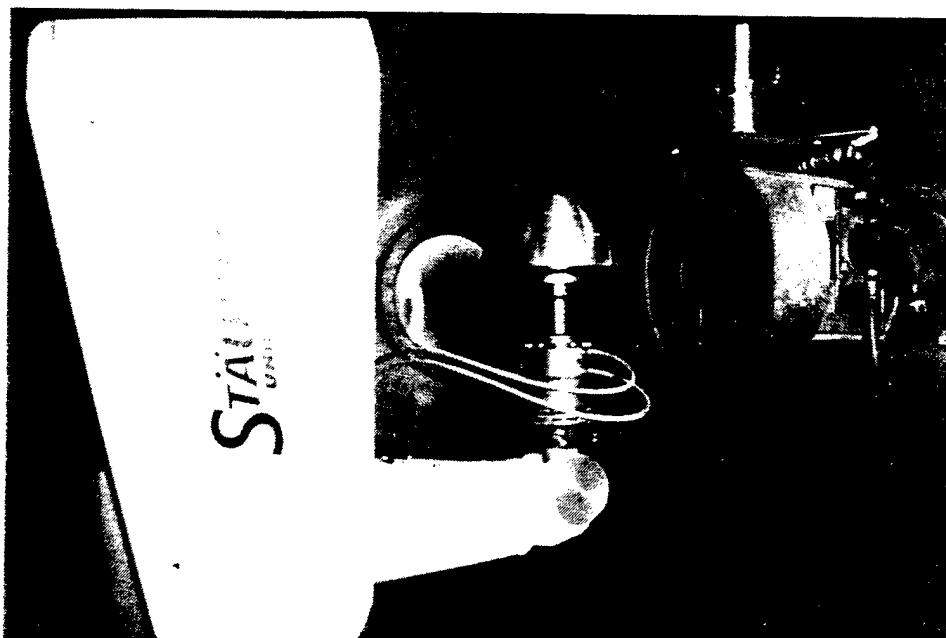
Figure 7.   Robotic Arm and Nozzle/Tundish Housing During
Wear- and Corrosion-Integrated Test Series.
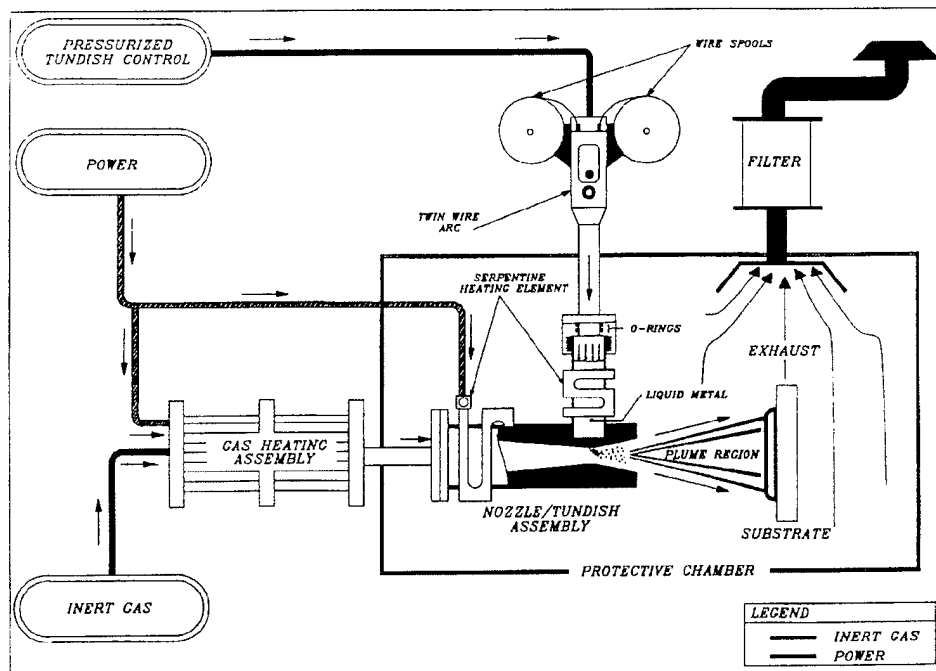
Figure 8. Schematic of Pressure-Controlled Atomization Process (PCAP).
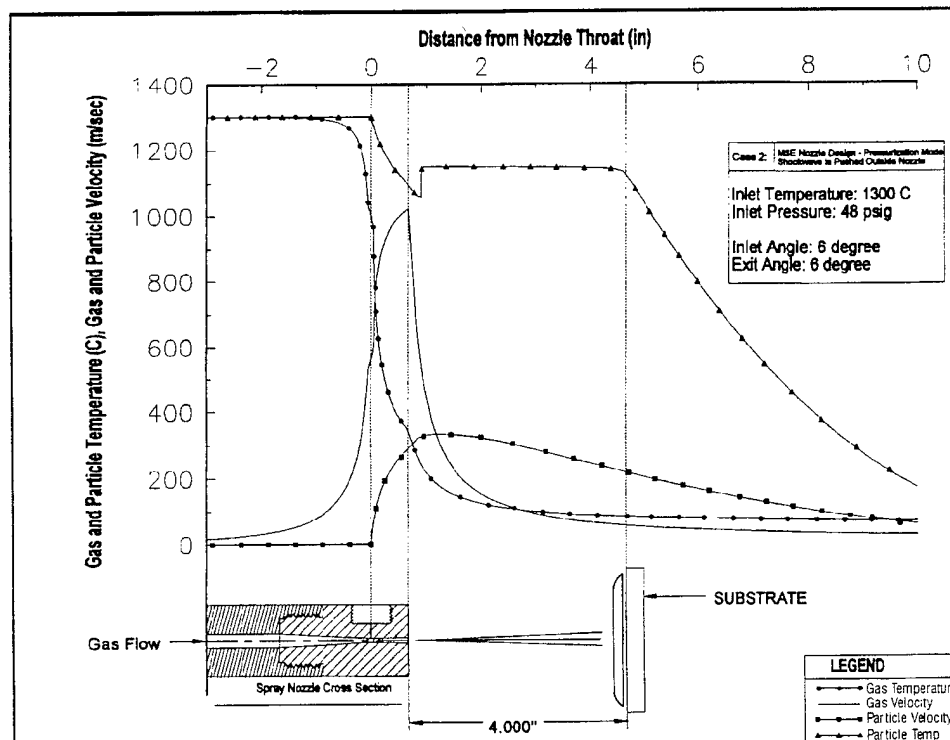
Figure 9. Nozzle Characteristics Operating in Pressurized Mode.
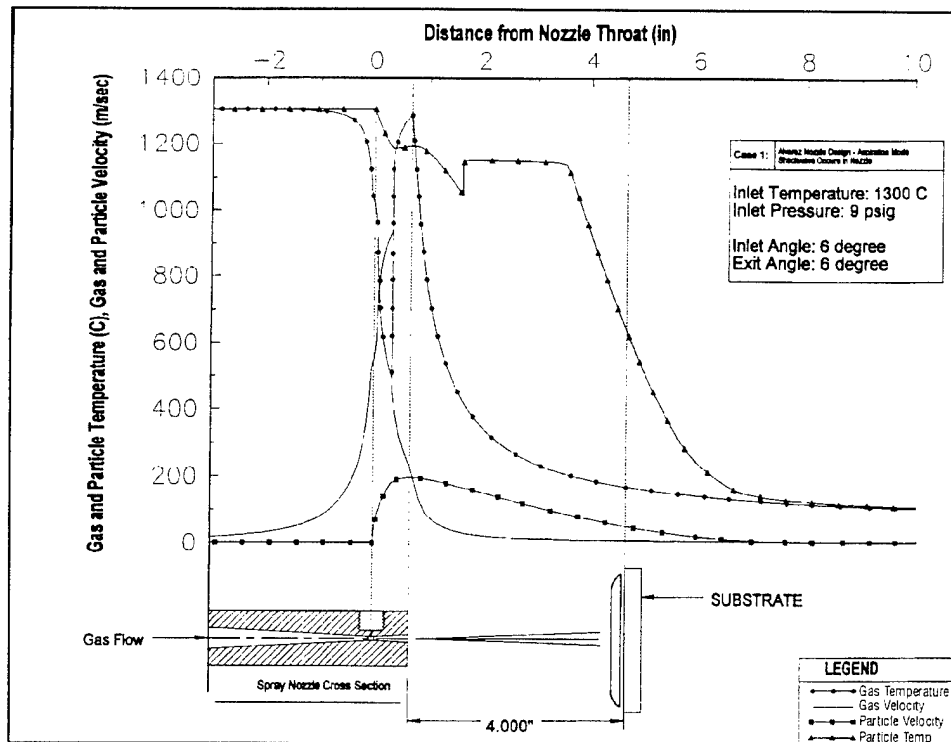
Figure 10. Nozzle Characteristics Operating in Aspiration Mode.
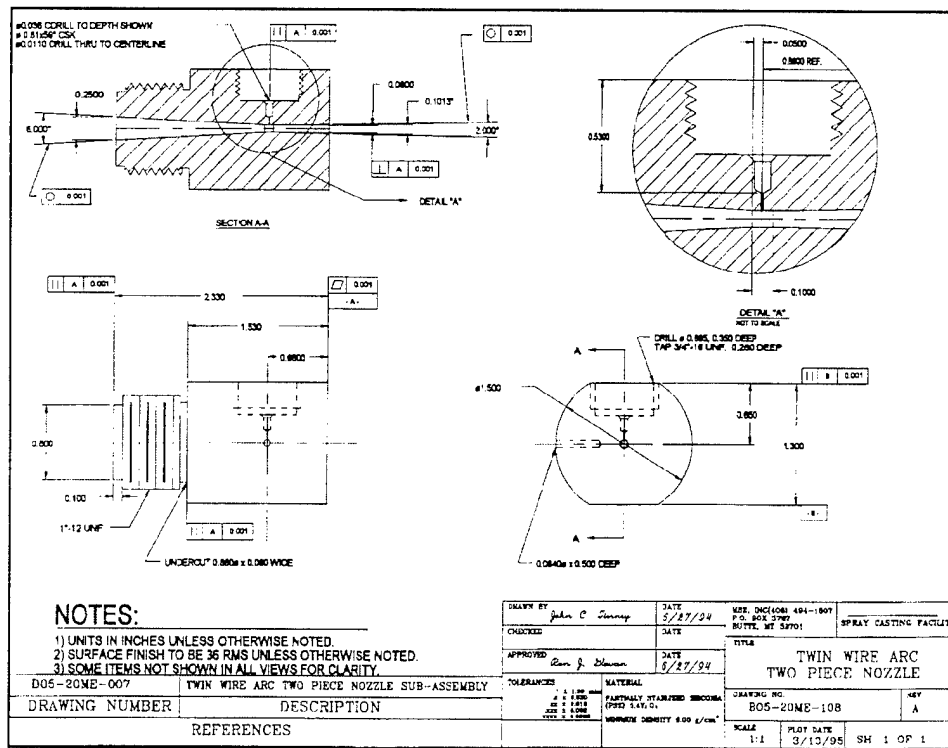
Figure 11. Drawing of 2-Degree Nozzle.

10

SECTION II
QUALIFICATION TESTING: MSE TEST SERIES

The MSE Test Series report is divided into the following sections:

1) Spray Tests
   -Equipment Modifications/Development
   -Experimental Design
   -Comparison to Commercial Spray Tests;

2) Nozzle Materials Evaluation Tests; and

3) Numerical Simulation and Modeling.

Prior to conducting spray tests for the MSE Test Series, a substantial effort was undertaken to modify the Phase II spray system from laboratory equipment into a reliable operating system with industrial controls. Additionally, the fundamental operation of the process was improved by incorporating a means of pressurizing the tundish to inject liquid metal into the nozzle.

Two experimental designs were used to evaluate the performance of the PCAP for spraying tin during the MSE Test Series. The first test group, designated 92-EXD, investigated nozzle geometry effects on coating attributes, and the second test group, designated 92-CPC, investigated process control parameter effects on coating attributes. For each test in the experimental designs, tin was sprayed onto low carbon sheet steel plates and six adhesion specimens. Typical process operating parameters for the MSE Test Series are given in Figures 12 and 13.

For the 92-EXD test group, a statistically pure eight-run, full-factorial experimental design was selected to study nozzle geometry effects on adhesion strength, microhardness, and mean grain size. Nozzle geometry variations included different orifice locations, different orifice diameters, and different nozzle throat diameters.

For the 92-CPC test group, a 16-run fractional-factorial experimental design was selected to study process control parameters including inlet pressure, gas temperature, substrate translation speed, spray distance, melt temperature, and differential spray pressure. Response parameters were adhesion strength, microhardness, and mean grain size.

A group of tests were also conducted to compare the PCAP to a conventional thermal spray process. Eight tests using a Hobart/TAFA electric wire arc system at different operating parameters were conducted spraying VERSAlloy 50. Coating attributes analyzed in these tests included, adhesion strength, microhardness, and porosity. The results of the tests provided data necessary to compare the PCAP to an industrial process. PCAP sprayed VERSAlloy 50 coatings from the Boeing Test Series were used to compare the VERSAlloy 50 coatings sprayed with the electric wire arc system.

Current spray nozzles are fabricated from hexagonal boron nitride, a relatively soft, machinable ceramic material that is resistant to attack by

various liquid metals. However, the material erodes and corrodes during spraying so other candidate nozzle materials needed to be identified for developing a developmental pilot-scale system. An initial group of static tests were performed in a controlled atmosphere furnace by placing a small metal sample onto a coupon of the candidate nozzle material. The furnace was heated to a predetermined temperature and maintained at the predetermined temperature for 10 minutes. For materials showing no reaction during the 10-minute tests, another sample of metal and candidate nozzle material were tested at the same predetermined temperature for 1 hour. The process was repeated for 10-hour and 100-hour duration tests.

The quasi-one-dimensional nozzle and plume computer codes were modified by MSE and INEL personnel during the MSE Test Series. Improvements to the code included: the addition of volume fraction effects for thicker sprays; the addition of the gas dynamic pressure gradient force in the throat region; modification to correctly model supersonic exit conditions of the nozzle; modifications to handle subsonic flow in the nozzle; a new equation to calculate friction factor in the nozzle; and a new equation to calculate the viscosity of dilute gas in the nozzle. A pressurized nozzle was modelled and characterization studies were performed to validate results of the computer code.

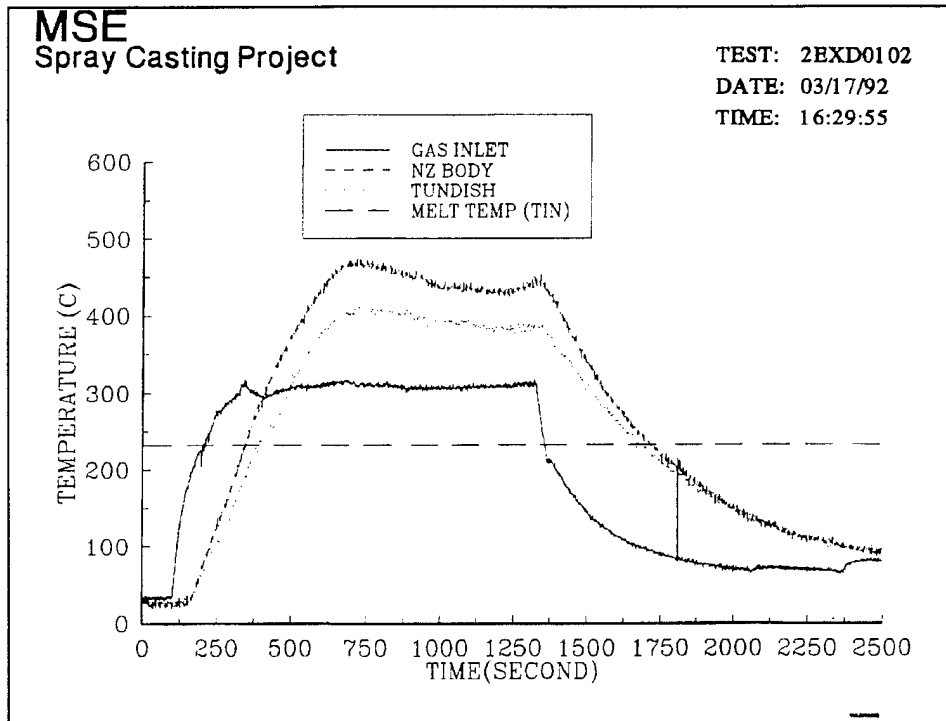A complete report of the MSE Test Series is in Appendix A.

Figure 12.   Typical Operating Parameters During MSE Test
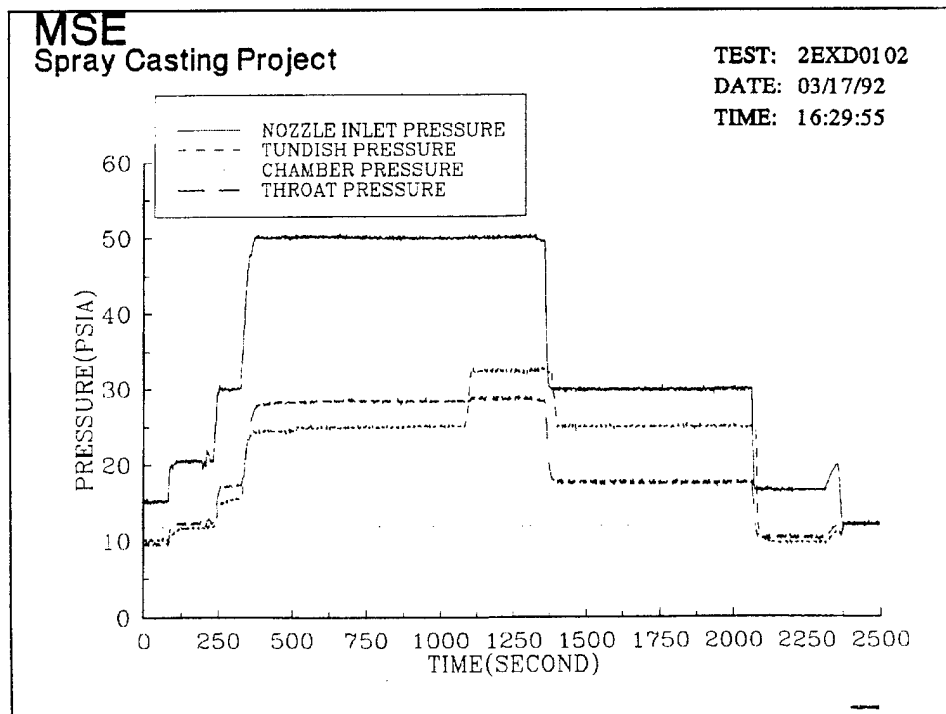Series.

Figure 13.   Typical Operating Parameters During MSE Test
Series.

13
(The reverse of this page is blank)

SECTION III
QUALIFICATION TESTING: BOEING TEST SERIES

The Boeing Test Series report is divided into the following two sections:

1) Additional MSE Testing; and

2) Boeing Report: Spray Casting - Chromium Substitutes.

In addition to the testing conducted by the Boeing Company, the report also contains the results of a short group of tests conducted by MSE to evaluate the effects of specimen preheat and specimen configuration on adhesion strength. Adhesion testing was conducted per ASTM C633-79, Standard Test Method for Adhesion of Cohesive Strength of Flame Sprayed Coatings.

The Boeing report contains the results of tests performed on coupons spray coated with VERSAlloy 50. Testing was performed by the Materials, Processes and Physics, Chemical and Environmental Technology organization within the Boeing Defense and Space Group. The group of tests performed included fatigue, abrasion, adhesion, corrosion, hardness, internal stress, metallurgical, chemistry, and material compatibility/workability. In tests where it was practical, the VERSAlloy 50-coated specimens were compared directly to specimens electroplated with engineering chromium. Specimen configuration, test conduct, photographs of tested specimens, and photo micrographs of the coatings are presented. Typical process operating parameters for the Boeing Test Series are in Figures 14 and 15.

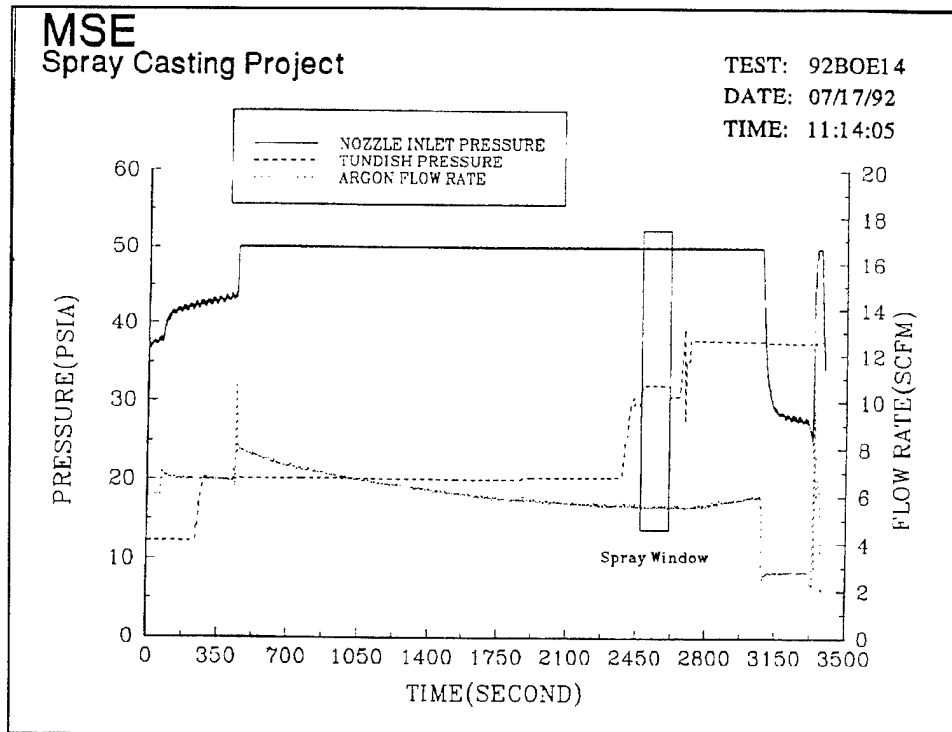A complete report of the Boeing Test Series is in Appendix B.

15

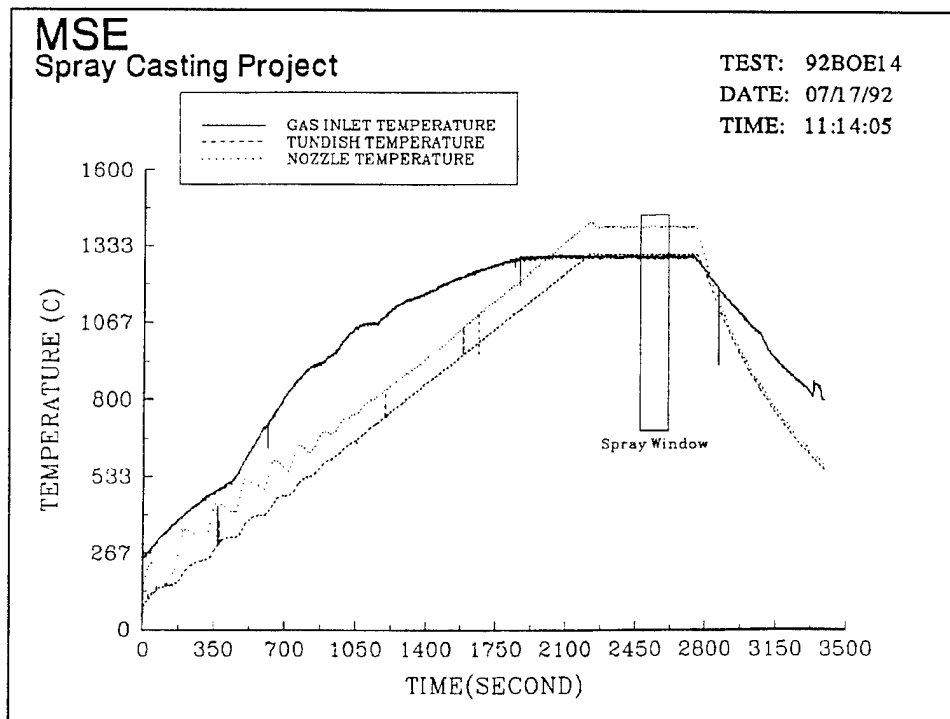Figure 14. Typical Operating Parameters During Boeing Test Series.

Figure 15. Typical Operating Parameters During Boeing Test Series.

SECTION IV
QUALIFICATION TESTING: WRIGHT LABORATORY TEST SERIES

The Wright Laboratory Test Series report is divided into the following sections:

1) Evaluation Report--Evaluation of Spray-Casted Materials; and

2) Evaluation Report--Spray Casting Evaluation.

The Wright Laboratory report contains the results of tests performed on coupons spray coated with VERSAlloy 50. Testing of the coupons was performed by the Materials Directorate Systems Support Division, WL/MLS at Wright Patterson Air Force Base. Coupons sprayed for the Wright Laboratory Test Series were identical in configuration to the coupons for the Boeing Test Series. The group of tests performed included: fatigue, corrosion, and hardness. PCAP sprayed VERSAlloy 50 was applied to eight 4130 steel fatigue coupons, eight 3- by 5- by 0.062-inch AISI 4130 steel corrosion coupons, and eight 1- by 5- by 0.125-inch AISI 4130 steel metallurgical coupons. Corrosion testing was performed per ASTM B-117, Method of Salt Spray (Fog) Testing. Fatigue coupons coated with VERSAlloy 50 were compared directly to fatigue coupons with hard chromium plating. Test conduct, equipment setups, coupon photographs before and after testing, and photo micrographs of the coatings are presented. Typical process operating parameters for the Wright Laboratory Test Series are in Figures 16 and 17.

In addition to spraying the Boeing designed AISI 4130 steel fatigue coupons, Wright Laboratory requested that 15 coupons be fabricated from 304 stainless steel and that 15 coupons be fabricated from Ti6Al4V. The additional coupons were also coated with VERSAlloy 50. A drawing of the Boeing designed fatigue coupons is in Figure 18.

After testing the Boeing-designed fatigue coupons, Wright Laboratory requested that an additional 12 fatigue coupons be fabricated to ASTM E-466. A drawing of the ASTM E-466 fatigue specimen is in Figure 19. The ASTM E-466 coupons were fabricated from AISI 4130 steel and were coated with VERSAlloy 50 and were sent to the Wright Laboratory for evaluation. Results of fatigue testing for the ASTM E-466 coupons were not reported by Wright Laboratory.

A complete report of the Wright Laboratory Test Series is in Appendix C.
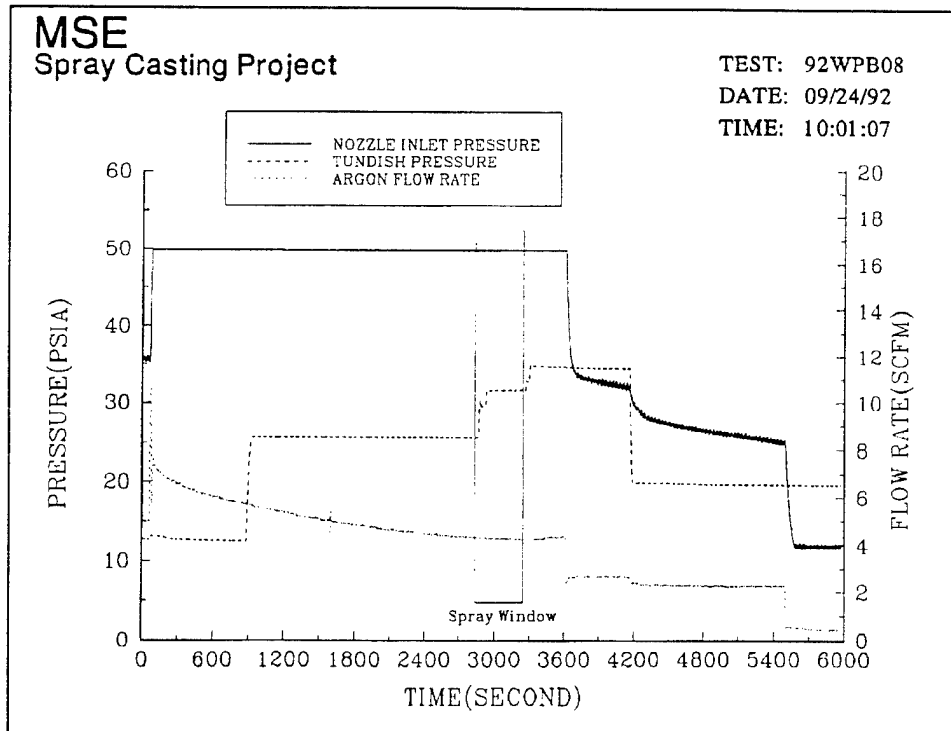
17

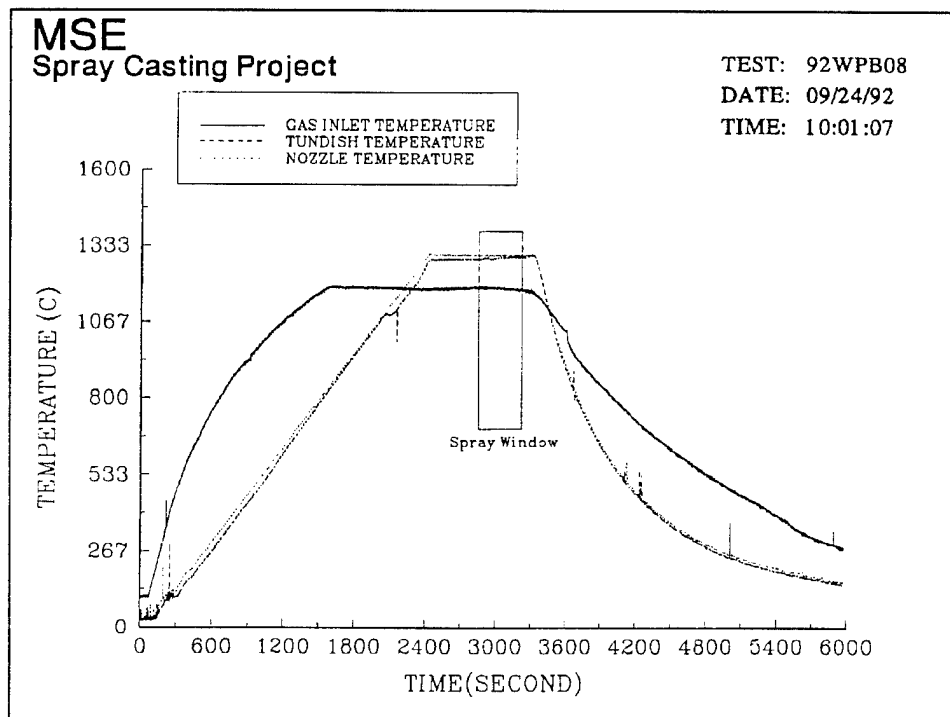Figure 16. Typical Operating Parameters During Wright
Laboratory Test Series.

Figure 17. Typical Operating Parameters During Wright
Laboratory Test Series.

Figure 18. Boeing-Designed Fatigue Specimen.

Figure 19. Wright Laboratory-Designed Fatigue Specimen.

SECTION V
WEAR- AND CORROSION-INTEGRATED TEST SERIES

The final Test Series performed for Phase III of the Spray Casting Project were known as the Wear- and Corrosion-Integrated Tests (WIT). The WIT Test Series report is divided into the following sections:

1. Hardware Development
   - Gas Heating System
   - Metal Feed System
   - Spray Chamber and Filter System
   - Nozzle/Tundish Heating System
   - Two-Piece Nozzle;

2. Computer Modeling
   - Two-Piece Nozzle; and

3. Experimental Design Spray Tests
   - Phase I
   - Phase II
   - Phase III
   - Phase IV.

Prior to conducting spray tests for the WIT Test Series, industrial equipment was designed, fabricated, and integrated so that one skilled operator could control the process. The system was designated as the developmental pilot-scale hardware. In addition to hardware modifications, a two-piece nozzle design was modelled with the quasi-one-dimensional nozzle computer code developed during Phase II of the project. A two-piece nozzle was then fabricated from hexagonal boron nitride and installed, tested, and characterized during the WIT Test Series.

An experimental design was performed to determine process repeatability and process optimization characteristics with the developmental pilot-scale hardware. Improvements in corrosion resistance, wear resistance, microhardness, and porosity for VERSAlloy 50 coatings applied with the PCAP were sought. The experimental design was comprised of four phases and required a total of 35 runs. The design consisted of one spray test for Phase I, eight spray tests for Phase II, 22 spray tests for Phase III, and four spray tests for Phase IV. For Phase I testing, a single plate of sheet steel was sprayed at five different spray distances with VERSAlloy 50. For the remaining 34 spray tests, VERSAlloy 50 was applied to coupons fabricated from AISI 4130 steel. One fatigue coupon, one corrosion coupon, and one metallurgical coupon were sprayed for each spray test. The spray fixture used during the tests is shown in Figure 20. Typical process operating parameters for the WIT Test Series are in Figures 21 and 22.

The purpose of Phase I testing was to calculate the standard deviation for the cross-sectional height of a single spray pass at five different spray distances. The standard deviations were used to determine the overlap between consecutive spray passes for Phase II, III, and IV testing. A photograph of the sprayed plate is in Figure 23.

21

Phase II testing consisted of a completely random eight-run experimental design to determine the effects of four different spray patterns. The patterns used the same basic motion but differed in the amount of overlap between consecutive passes. The patterns were based on the standard deviation (σ) for a 6-inch spray distance. The four patterns used spray track gaps (center to center distance between consecutive passes) of .5σ, σ, 2σ, and 3σ. Response variables for Phase II testing included corrosion, wear, microhardness, and porosity. The wear and corrosion tests were performed at the Spray Casting Facility, and the coating microstructure characteristics for microhardness and porosity were performed by Tubal Cain, Inc.

Phase III testing consisted of a 22-run central composite design to investigate the effects of varying spray distance, operating pressure, and pressure differential. The PCAP was operated at five different levels for each parameter investigated during the experimental design. A statistical analysis of each coating was then performed to determine which parameter settings produced the optimal coating for corrosion resistance, wear resistance, microhardness, and porosity characteristics. Response variables for Phase III testing included corrosion, wear, microhardness, and porosity. The wear and corrosion tests were performed at the Spray Casting Facility and the coating microstructure characteristics for microhardness, and porosity were performed by Tubal Cain, Inc.

Phase IV testing consisted of four runs to verify that the operating parameters predicted in Phase III testing and analysis produced the optimal coating characteristics. This phase of testing was to determine the credibility of the Phase I, II, and III testing. Response variables for Phase IV testing included corrosion, wear, microhardness, and porosity. The wear and corrosion tests were performed at the Spray Casting Facility, and the coating microstructure characteristics for microhardness, and porosity were performed by Tubal Cain, Inc.

A complete report of the Wear- and Corrosion-Integrated Test Series is in Appendix D.
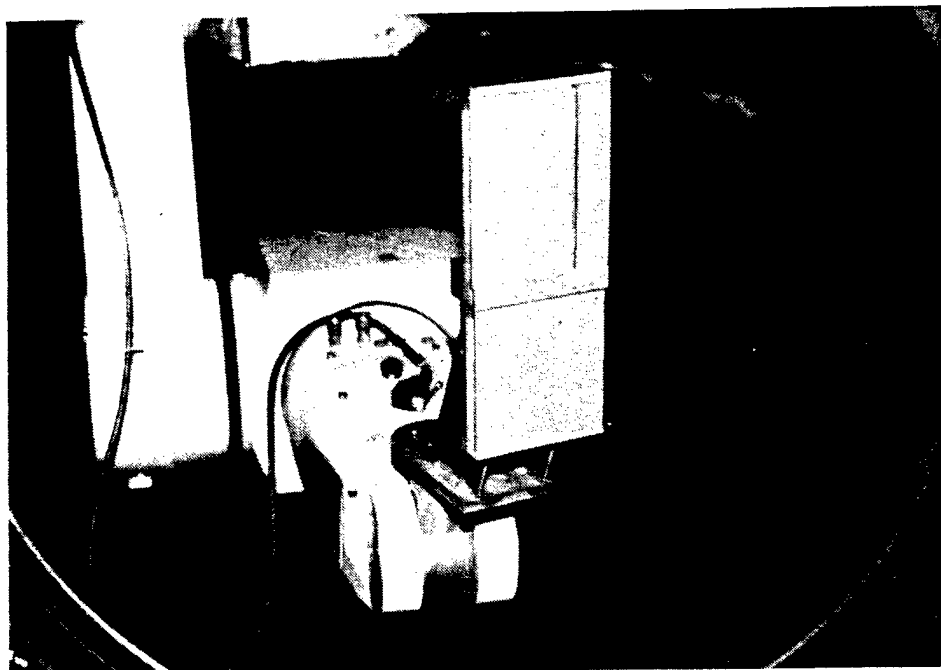
Figure 20. Wear and Corrosion Spray Fixture Mounted on Robotic Arm.
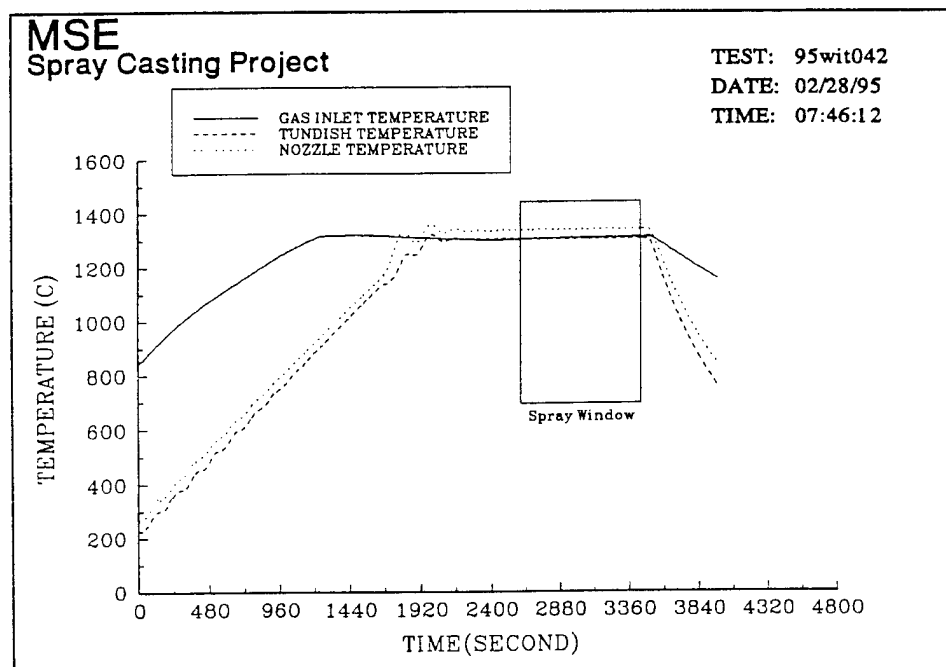

Figure 21. Typical Operating Parameters During Wear- and Corrosion-Integrated Test Series.
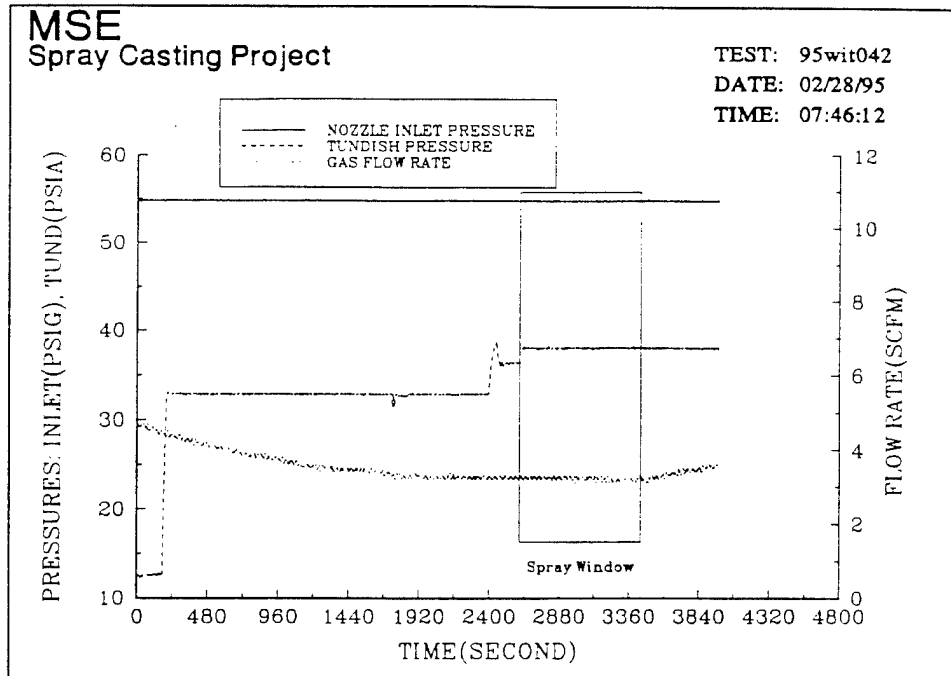
23

Figure 22. Typical Operating Parameters During Wear- and Corrosion-Integrated Test Series.
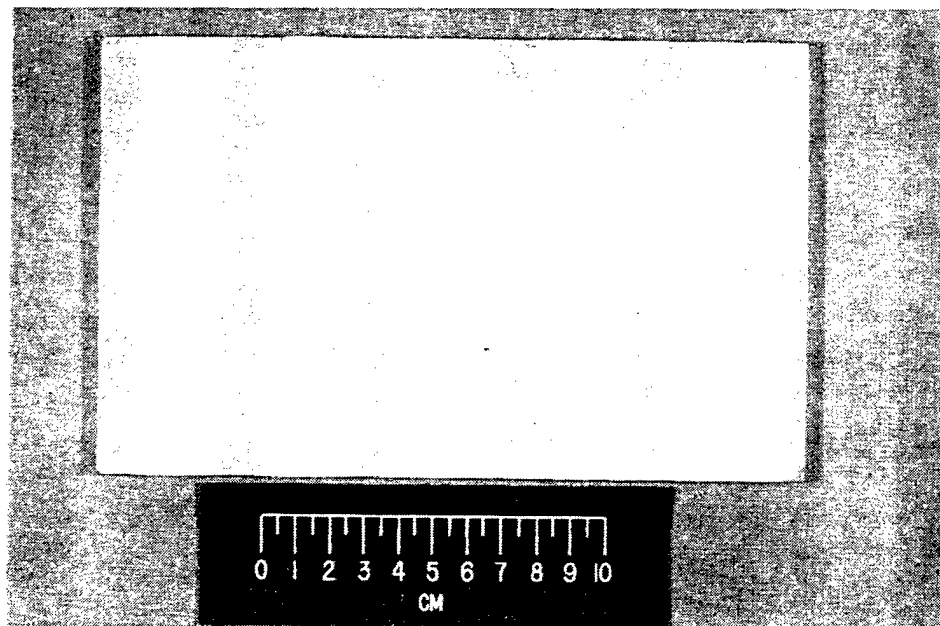

Figure 23. Flat Plate from Phase I of Wear- and Corrosion-Integrated Test Series (at Five Spray Distances).

SECTION VI
SUMMARY AND CONCLUSIONS FOR PHASE III

A developmental pilot-scale system was designed and characterized for spraying VERSAlloy 50. Graphite resistant heating systems were designed and installed for heating the nozzle/tundish assembly and for providing heated inert gas to the nozzle. Output temperature of the MSE gas heating system was tested to 1800 °C. The graphite heating element in the gas heater proved to be reliable and has been used for 144 spray tests (288 hours). The nozzle/tundish heating system was tested to 1750 °C; however, the nozzle/tundish resistive element was replaced after 40 spray tests when the power lead connection cracked. Combined together the graphite heating elements in the nozzle/tundish system has been used for 130 tests (260 hours).

Oxygen concentrations in the vacuum/pressure chamber were measured between 0.01 and 0.2 percent. When operating below these oxygen levels, the resistive heating elements showed no signs of oxidation. Additionally, no oxide particles have been found in the coating microstructure. This would indicate that a vacuum level from 0.001 to 0.050 Torr and then backfilling with commercial grade argon (99.997 pure) produces an acceptable oxygen concentration in the spray chamber. Chamber pump down and an argon backfill takes 30 minutes.

Static tests for candidate nozzle materials indicate that aluminum oxide (99.7 percent dense), silicon nitride, and partially stabilized zirconia (5.4Y_2O_3) have the best resistance to chemical attack by the VERSAlloy 50.

Particulate overspray accumulated on the spray chamber floor with only a fraction of the particulate making it to the 0.02 micrometer filter. As a result, further consideration is required in the design of the chamber for particle collection. Another consideration would be to add an argon recirculation loop through the filter and chamber to carry particulate into the filter.

An independent evaluation of the PCAP was conducted by the Boeing Company and Air Force's Wright Laboratory. Results from the two independent laboratories indicate enhanced fatigue resistance from PCAP applied VERSAlloy 50. An adhesion strength of the nickel-based alloy, VERSAlloy 50, was measured at 8068 psi with a standard deviation (σ) of 682 psi. This data was obtained by MSE as an additional test during the Boeing Test Series. No adhesion strength comparisons between VERSAlloy 50 and chrome-plated coupons were conducted using the ASTM C633-79 Standard.

A Taber Wear Index of 13.9 was achieved when applying VERSAlloy 50 with optimized process parameters from the WIT Test Series. This Taber wear index is well within the range of hard chromium indexes published by ASM International.

Corrosion of VERSAlloy 50 sprayed coatings (0.006 to 0.008 inch thick) have been tested for 48 hours in a neutral salt f/og spray and show no corrosion when the coating is sprayed with optimized process parameters from the WIT Test Series.

25

Porosity varie depending upon which coating property was being optimized, but averaged less than 1 percent and was never measured to be higher than 4.5 percent.

Microhardness measurements of VERSAlloy 50 coatings also varied depending upon which coating property was being optimized, but averaged 650 Vickers for the WIT Test Series.

Lastly, the one-dimensional computer code provided information that reduced the trial and error process in designing nozzles. By predicting nozzle response for gas temperature, gas velocity, and gas pressure, the correct process operating ranges can be selected for alternate nozzle geometries.

SECTION VII
RECOMMENDATIONS

Results of Phase III testing during the Boeing and Wright Laboratory Tests Series show that PCAP applied VERSAlloy 50 coatings may be suitable for replacing hard electroplated chromium on USAF flight hardware. Further investigation into operating control parameters and nozzle geometries to produce optimal coatings will be required before the process is ready for commercialization. Control parameters to be considered include:

- nozzle inlet pressure;
- nozzle/tundish differential pressure;
- inlet gas temperature;
- liquid metal superheat temperature; and
- substrate translation speed.

Optimized coating characteristics to be considered include:

- adhesion strength;
- surface finish (by grinding); and
- coating thickness.

Investigations into surface preparation should also be conducted for grit size and grit material. The effect of grit size on adhesion strength and on fatigue resistance of the substrate will be required before a PCAP system is demonstrated in an ALC.

In addition to investigating process and nozzle parameters, more design work and testing will be required for the process hardware, i.e., a metal feed system to supply a continuous feed of material to the tundish, reliable level detection of liquid material in the tundish, a wear and chemical resistant two-piece nozzle fabricated from one of candidate nozzle materials, and an argon recirculation loop.

Other wear-resistant coating alloys should be investigated and sprayed with the PCAP. For Phase III, VERSAlloy 50, has been identified as the candidate material to replace electroplated hard chromium. Sprayed coatings for each new alloy should be evaluated for porosity, microhardness, adhesion strength, abrasion resistance, corrosion resistance, and fatigue resistance and then be evaluated and compared to results of VERSAlloy 50 sprayed coatings.

Since there are existing thermal spray processes commercially available, PCAP-sprayed VERSAlloy 50 coatings should be compared to VERSAlloy 50 coatings applied by other thermal spray processes, i.e., vacuum plasma, high velocity oxygen fuel, and electric twin-wire arc systems. Coating characteristics evaluated from each process would include, corrosion resistance, fatigue resistance, wear resistance, microhardness, and porosity measurements.

APPENDIX A

SPRAY CASTING PROJECT
MSE TEST SERIES REPORT

(The reverse of this page is blank)

SPRAY CASTING PROJECT
MSE TEST SERIES REPORT

J. Tierney
R. Glovan
Y. M. Lee
W. Daniel
S. Witt

Prepared by

MSE, Inc.
P.O. Box 3767
Butte, Montana 59702

Prepared for

November 1992

REVIEWS AND APPROVALS:

Reviewed and approved by: _Ronald J. Gloria_____
                                                        Project Manager

32

CONTENTS

FIGURES

FIGURES (Cont'd)

FIGURES (Cont'd)

TABLES

1. INTRODUCTION

Phase III of the Spray Casting Project is being conducted by MSE, Inc., at its facilities in Butte, Montana. The primary purpose of the Phase III work is to qualify the spray casting process to meet Air Force standards and then to design, fabricate, and test the pilot-scale spray casting equipment to be used at an Air Force repair facility. The qualification process has been broken down into three separate test series: the MSE Test Series, the Boeing Test Series, and the Wright Laboratories Test Series. A separate report will be prepared for each of these test series.

The MSE Test Series was a group of tests and modeling work that was primarily performed immediately after the Air Force spray casting equipment was moved from the Custom Spray Technologies (CST) facility in Rigby, Idaho, to the MSE Spray Casting facility (SCF) in Butte, Montana. The purpose of the testing and modeling was to gain an understanding of how the geometric and operating parameters of circular cross section supersonic nozzles affect spray deposit charcteristics; this work was complimented by a substantial equipment upgrade effort. In addition to these endeavors, it was recognized early in the project that erosion/corrosion of nozzles had the potential to be a major problem in developing the total process for production coating in an Air Force facility. Therefore, a test series was conducted to screen potential candidate nozzle materials.

2. SPRAY TESTS

To demonstrate the controlled aspiration process (CAP) as a sound technological process, a series of qualification tests must be completed to develop an engineering database. The database will allow the Air Force to determine if the process is qualified to be used in refurbishment/repair facilities. Qualification testing is broken down into three test series: 1) MSE Testing, 2) Boeing Testing, and 3) Wright Laboratory Testing. The following sections detail the results of the MSE Test Series for equipment modifications development, operating parameter tests, nozzle geometry tests, and comparison to commercial spray tests.

2.1 EQUIPMENT MODIFICATIONS/DEVELOPMENTS

When the spray casting equipment was moved from the CST facility in Rigby, Idaho, to the SCF in Butte, Montana, modifications were made to transform a piece of laboratory equipment into a reliable operating system with industrial controls. Specifically, a computer controlled X-Y translation device, an oxygen sensor, a mass flow sensor, a pressure control valve and PID controller, and a new gas heating system were installed. Additionally, the fundamental operation of the process was improved by incorporating a pressurized tundish system to inject liquid metal into the nozzle. These modifications were made during the MSE Test Series.

2.1.1 Gas Heating System

To spray high temperature melting point materials, e.g., VERSAlloy-50, an argon gas temperature equivalent to the melting point is required to avoid cooling the nozzle. MSE personnel recognized this requirement and found a vendor to design and build a gas heating system that was capable of heating to 1,700 °C. This vendor was American Furnace Company of Knoxville, Tennessee.

1

The gas heating system is a water-cooled, cold wall, American Society of Mechanical Engineers (ASME) stamped and registered pressure vessel that uses a tubular graphite resistance heating element to provide source heat to a low thermal mass, high surface area, rigid carbon heat exchanger core. The system is designed to control exit gas temperatures over a range of 20-1,700 °C and outlet pressures over a range of 0-50 pounds per square inch gage (psig). The system is fully instrumented with Powers 512, 535, and 320 process controllers for pressure, temperature, and overtemperature protection, respectively. The pressure measurement feedback signal to the Powers 512 process controller is provided by a Model 5525G Computer Instruments Corporation pressure transmitter; the exit gas temperature measurement feedback signal to the Powers 535 temperature controller is provided by a type "S" open-tipped thermocouple; and overtemperature measurement of the heating element is provided by a Mikron-77 two-color optical pyrometer.

The vessel is horizontally mounted on the power supply, and all system controls are housed in a National Electrical Manufacturer's Association (NEMA) 12-control enclosure. Power to the furnace is provided by a current-limiting silicon/controlled rectifier (SCR)/stepdown transformer system. A 4-20 milliamp signal from the temperature controller regulates the SCR output to the primary feed of the 480-volt, 60-Hz, 55-kW transformer. Electrical connections from the transformer to the furnace electrodes are through 350 MCM, copper-braided, water-cooled flex cables. The new gas heating system and the gas heating vessel are shown in Figures 1 and 2.

Safety systems for the furnace include flow and thermal switches that interrupt power to the furnace. If coolant water flow is lost or if the cooling water overheats, an audible alarm sounds, and the system will not resume power until the alarm condition has been acknowledged and manually reset. The entire gas heating system was designed so a single operator can monitor and control the process.

2.1.2 Computer Controlled X-Y Translation Device

The translation manipulator is an off-the-shelf system capable of linear traverse rates of up to 30 inches per second and consists of a lead screw drive table, a linear slide, and a MAC 100 motion logic controller built by the Techno/isel Company. The system was installed to increase reliability and repeatability of translating the substrates to be sprayed. Figure 3 shows the computer controlled x-y translation device.

The system uses MAC software on a Dell 325 IBM compatible computer to program motion commands that are compiled and stored to a computer file. Precise speed and position information in the compiled file is downloaded from the Dell 325 to the MAC 100 controller via a standard RS232 cable. Selecting and downloading a file with the desired motion pattern allows substrate movement to be duplicated test after test.

2.1.3   Mass Flow Measurement

Argon mass flow is measured with a Sierra Side-Trak 830 series flow transducer that has been integrated into the gas heating system. The mass flow measurement is currently used for diagnostic purposes and for the computer modeling effort; however, future work may involve using the mass flow measurement as a feedback signal to the process controller, which will allow the control valve to control argon gas flow rate instead of system pressure.
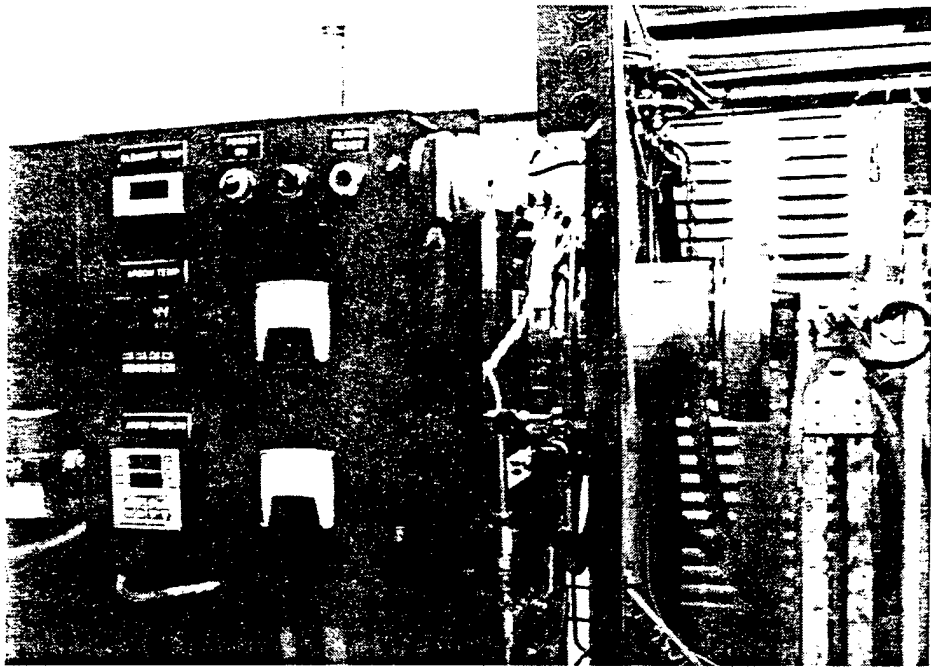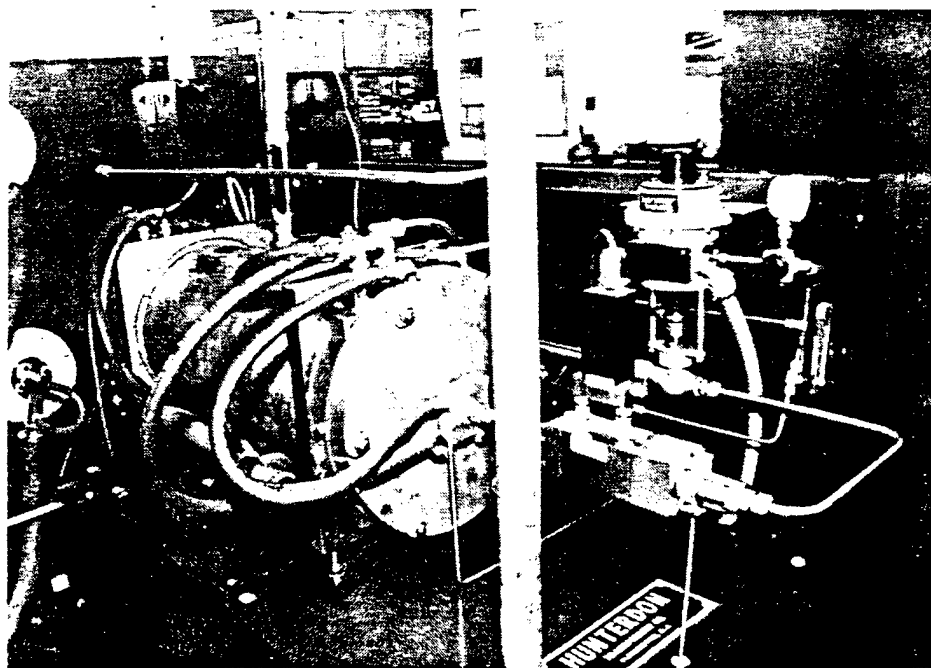
2

Figure 1. New gas heating system.
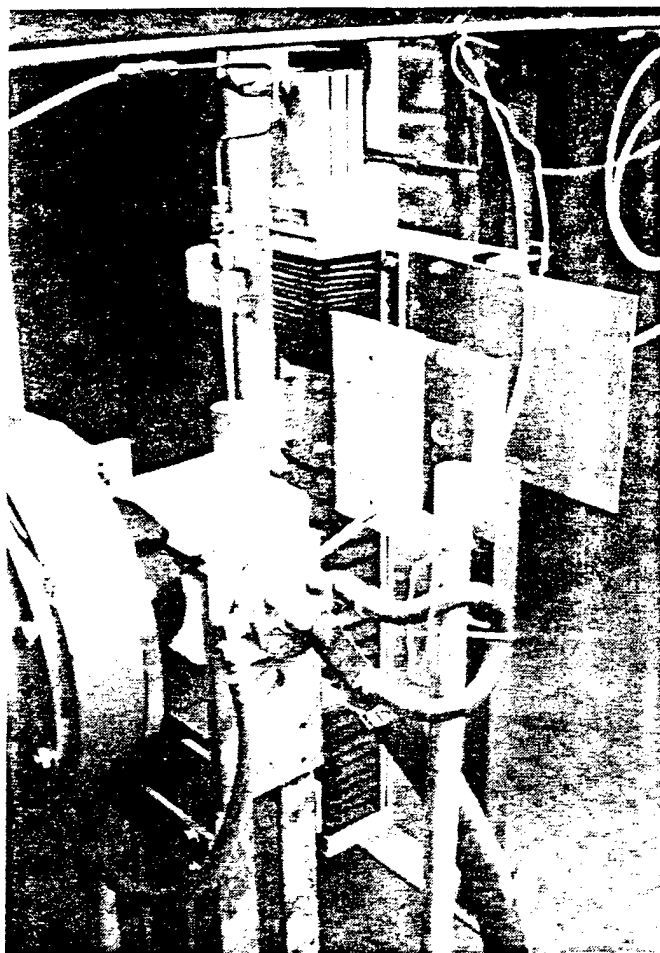

Figure 2. Gas heating vessel.

3

Figure 3. Computer-controlled x-y translation device.

2.1.4 Oxygen Sensor

Oxygen content in the spray chamber is measured with a Rosemount Model 755R oxygen analyzer. This analyzer provides a direct readout of 0 to 100 percent oxygen concentration and was installed to determine the time required to purge the chamber to less than 1 percent oxygen. The analyzer also monitors the leakup rate of the chamber so that a minimum argon purge can be adjusted to maintain the oxygen content at less than 1 percent.

2.1.5 Pressurized Tundish System

A pressurized tundish system was incorporated into the controlled aspiration process to achieve higher particle velocities and to control the mass flow rate of the liquid metal (see Figure 4). The concept eliminated operating in the narrow inlet gas pressure range of conventional atmospheric nozzles and essentially allowed for unlimited inlet gas pressures. Figure 5 illustrates the difference in particle velocities of an atmospheric nozzle and a pressurized tundish nozzle.
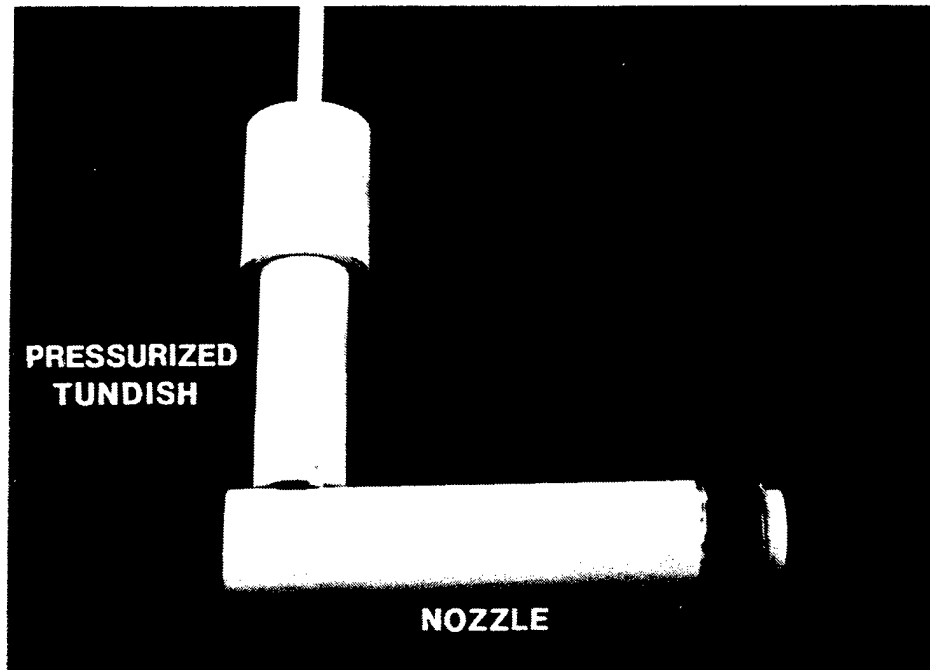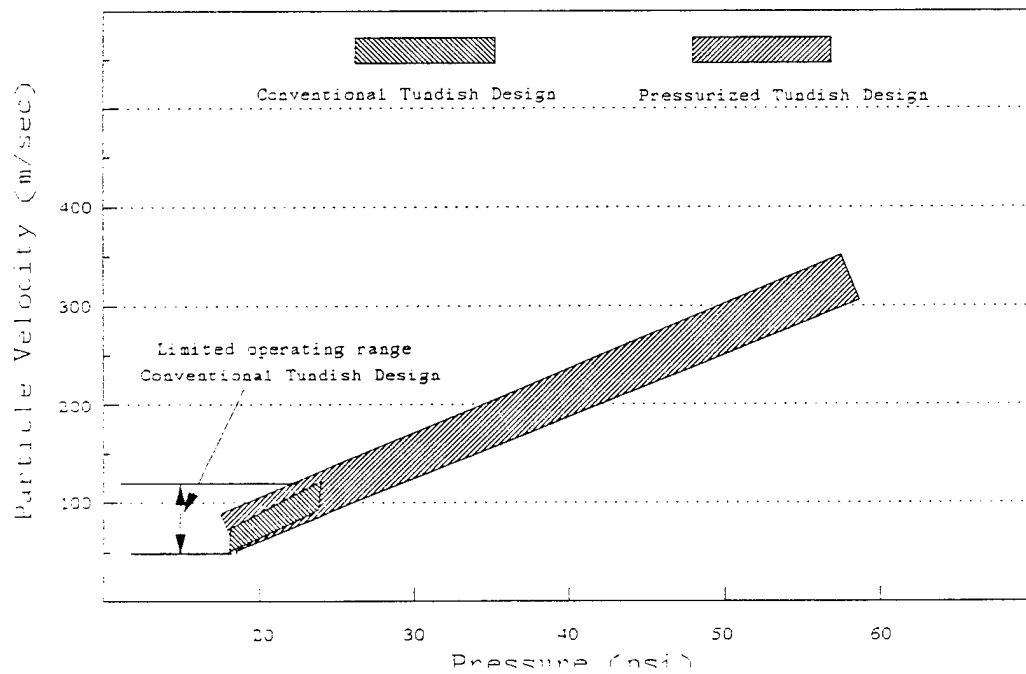
Figure 4. Pressurized tundish and spray nozzle.

Figure 5. Particle velocity comparison.

The pressurized tundish system will also allow a twin-wire arc system to be incorporated as a continuous metal feed system. (The current system is a batch process and is limited to spraying approximately 30 grams of feedstock material). Because the twin-wire arc system normally uses pressurized gas to carry molten metal away from the spray gun, the system will readily adapt into the pressurized tundish system of the CAP.

2.2 EXPERIMENTAL DESCRIPTION

An experimental study of the CAP for tin coatings was performed at the MSE SCF. The coatings were studied using design of experiment methods of Box and Hunter (Ref. 1) and identified the effects of nozzle geometry and control parameters on coating attributes. Two experimental designs were conducted using full factorial and fractional-factorial techniques. Estimates of the effects of each parameter in the experimental design were calculated from the data, and normal probability plots were generated to determine the significance of the effects. Results of the analysis provide characterization data for nozzle geometry and operating control parameters that will be used as the basis for process control parameter settings for high temperature spraying.

2.2.1 Experimental Setup

The system used for this project uses a protective enclosure, a gas heating assembly, a molten metal assembly, and a converging/diverging supersonic nozzle to spray molten metal droplets onto base metals to form thin, dense, adherent coatings or thicker near-net shape parts. A schematic drawing of the process is shown in Figure 6. The process flows inert gas, in this case argon, through the gas heating assembly into the heated nozzle. Simultaneously, liquid metal is pressurized and injected into the nozzle throat where small metal droplets are formed and deposited onto a moving substrate.

2.2.2 Experimental Procedure

For the MSE Test Series, two experimental designs were used to evaluate the performance of the CAP. The first test series, designated 92-EXD, investigated nozzle geometry effects on coating attributes, and the second test series, designated 92-CPC, investigated process control parameter effects on coating attributes; both of these experiments deposited thin coatings onto a substrate. These statistical investigations provide information on operating parameters and equipment sensitivity for the CAP. Process parameters examined for the CAP were inlet gas pressure, tundish pressure, gas temperature, and metal melt temperature, whereas deposition process variables were spray distance and substrate traverse rate.

For each test in the experimental designs, tin (99.8 percent pure) was sprayed onto low carbon sheet steel plates (12"L x 6"W x 1/8"D) and six adhesion specimens (AISI 4340 heat treated to 40 HRC). Figure 7 represents a typical spray configuration. As mentioned in Section 2.1.5, a pressurized tundish system was also incorporated into the system for control of the liquid metal injection flow rate.
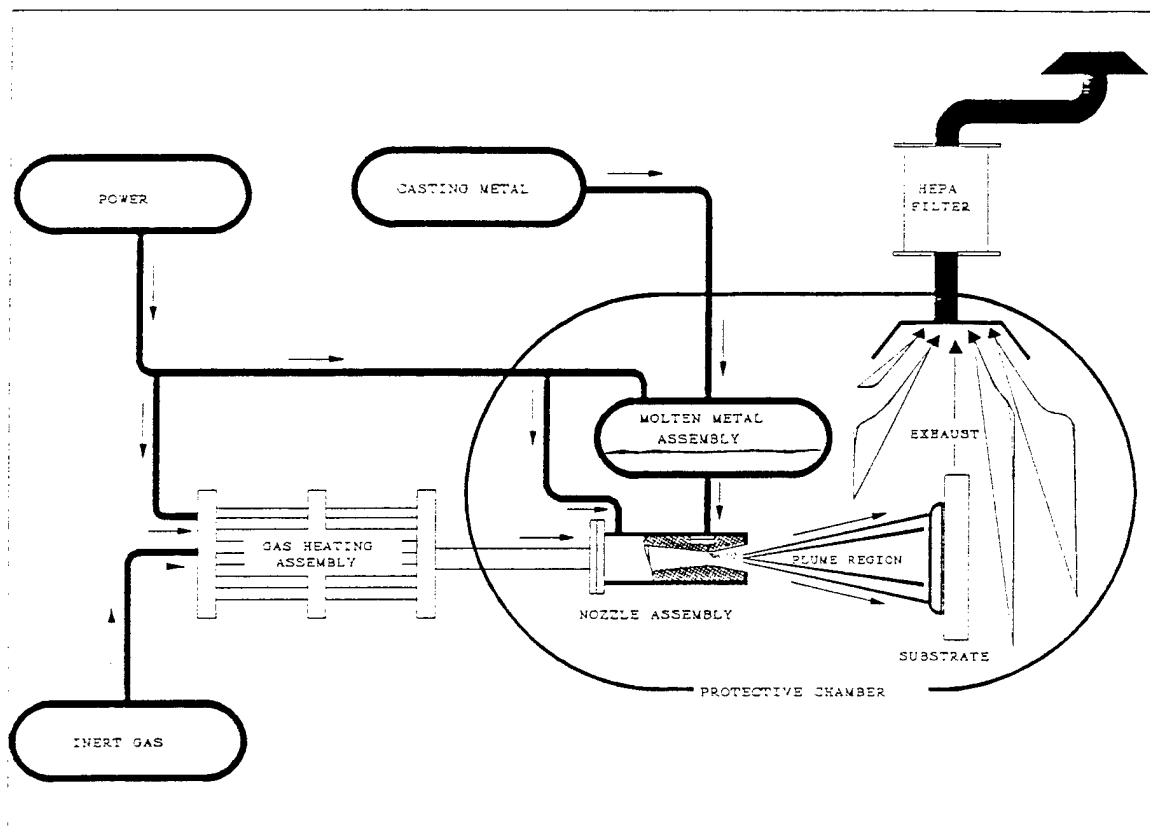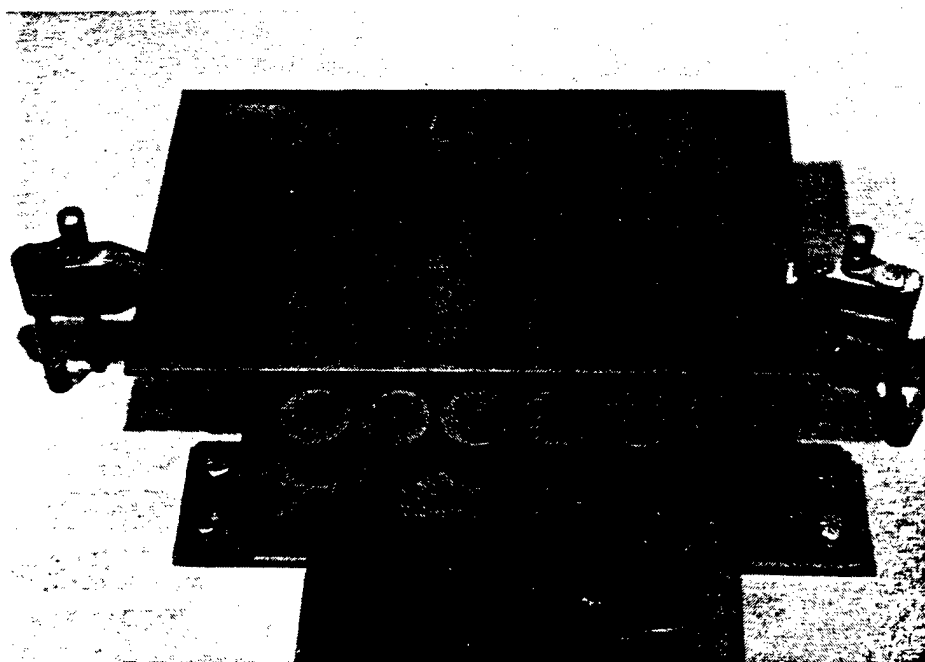
6

Figure 6. Controlled aspiration process.

Figure 7. Typical spray configuration.

7

2.2.3 Design of Experiment

Design of experiment methods of Box and Hunter were used for the MSE test series (Ref. 1), and recommendations from these authors include performing up-front investigations to properly target experimental design parameters. Therefore, a number of experimental tests, designated as the 92-TRAIN tests, were performed before developing the 92-EXD test series. In all, 10 92-TRAIN tests were performed, and the results of these initial investigations led to the development of the 92-EXD experimental design. Results from the 92-EXD test series were then analyzed and were used to "freeze" the nozzle geometry for the subsequent 92-CPC test series. Before developing the 92-CPC experimental design, four more experimental investigation tests were conducted. These tests, designated 92-ADH, investigated the effect of control parameters on adhesion strength.

2.2.3.1 Nozzle Configuration Tests (92-EXD)

For the 92-EXD test series, a statistically pure 2^3, eight-run, full-factorial experimental design studying three parameters at two levels each was selected to study nozzle geometry effects on coating attributes, in particular, adhesion strength, microhardness, and mean grain size. Table 1 shows the full factorial matrix, variables to be studied, and the high and low levels chosen for each parameter. Control parameters held constant for the test series are given in Table 2.

Table 1.   92-EXD experimental design parameters.

TEST SEQUENCE	STANDARD ORDER	ORIFICE LOCATION	ORIFICE DIAMETER	THROAT DIAMETER	NOZZLE IDENTIFICATION
2	1	0.050	0.009	0.080	92-3B
6	2	0.100	0.009	0.080	92-3E
4	3	0.050	0.011	0.080	92-3B$_1$
5	4	0.100	0.011	0.080	92-3D
1	5	0.050	0.009	0.100	92-3A
8	6	0.100	0.009	0.100	92-3E$_1$
7	7	0.050	0.011	0.100	92-3A$_1$
3	8	0.100	0.011	0.100	92-3C

Table 2.   92-EXD constant operating parameters.

NOZZLE TEMPERATURE (°C)	ARGON GAS TEMPERATURE (°C)	INLET PRESSURE (PSIA)	PRESSURE DIFFERENTIAL (PSIA)	SPRAY DISTANCE (INCHES)	TRAVERSE RATE (IPS)	SURFACE PREPARATION (AL$_2$O$_3$)
372	300	50	2	4	5	36 Mesh at 80 psi

An appropriate statistical model for this design is

$$y = \beta_0 + \frac{1}{2}(\beta_1 x_1 + \beta_2 x_2 + \cdots + \beta_7 x_7) + \epsilon$$ (1)

where:

y = response variable;
x_1 = orifice location;
x_2 = orifice diameter;
x_3 = throat diameter;
x_4 = $x_1 x_2$;
x_5 = $x_2 x_3$;
x_6 = $x_3 x_1$;
x_7 = $x_1 x_2 x_3$; and
ϵ = experimental error.

Each control variable is coded so that -1 represents the low level and +1 represents the high level. The last four variables are the two-way and three-way interactions of the main factors x_1, x_2, and x_3. Coefficients β_1, β_2,...,β_7 in equation 1 are the factor effects—the change in response y from the low level to the high level, respectively, for each factor. Each effect may be estimated from the data by subtracting the average response at the low level from the average response at the high level of the corresponding factor.

2.2.3.2 Process Variable Tests (92-CPC)

For the 92-CPC test series, a 2^{6-2}, 16-run, fractional-factorial design studying 6 parameters at 2 levels was selected. Additionally, two center point replicates were included to complete the design. Table 3 shows the fractional-factorial matrix, variables, and levels chosen for each parameter. Parameters held constant for the test series are given in Table 4. Response variables are adhesion strength, mean grain size, and porosity.

The experimental design is a resolution IV design; consequently, main effects are confounded with three-way and higher interactions, and two-way interactions are confounded with each other.

An appropriate statistical model for this design is:

$$y = \beta_0 + \beta_c x_c + \frac{1}{2}(\beta_1 x_1 + \beta_2 x_2 + \cdots + \beta_{15} x_{15}) + \epsilon$$ (2)

where:

y = response variable;
x_1 = inlet pressure = $x_2 x_3 x_5$ = $x_4 x_5 x_6$;
x_2 = argon temperature = $x_1 x_3 x_5$ = $x_3 x_4 x_6$;
x_3 = traverse rate = $x_1 x_2 x_5$ = $x_2 x_4 x_6$;
x_4 = spray distance = $x_2 x_3 x_6$ = $x_1 x_5 x_6$;

Table 3. 92-CPC experimental design parameters.

TEST SEQUENCE	STANDARD ORDER	INLET PRESSURE (psia)	ARGON GAS TEMP. (°C)	RATE (ips)	SPRAY DISTANCE (inches)	MELT TEMP. (°C)	DIFF. PRESSURE (psia)
17	1	30	300	2	2	382	1
4	2	60	300	2	2	582	1
9	3	30	600	2	2	582	2
5	4	60	600	2	2	382	2
18	5	30	300	10	2	582	2
8	6	60	300	10	2	382	2
14	7	30	600	10	2	382	1
3	8	60	600	10	2	582	1
10	9	30	300	2	4	382	2
2	10	60	300	2	4	582	2
15	11	30	600	2	4	582	1
11	12	60	600	2	4	382	1
7	13	30	300	10	4	582	1
12	14	60	300	10	4	382	1
1	15	30	600	10	4	382	2
13	16	60	600	10	4	582	2
16	17*	45	450	6	3	482	1.5
6	18*	45	450	6	3	482	1.5

Table 4. 92-CPC constant operating parameters.

NOZZLE IDENTIFICATION	ORIFICE LOCATION	ORIFICE DIAMETER	THROAT DIAMETER	SURFACE PREPARATION
92-3B;	0.050	0.011	0.080	36 Mesh at 60 psi

x_5 = melt temperature = $x_1x_2x_3$ = $x_1x_4x_6$;

x_6 = pressure differential = $x_2x_3x_4$ = $x_1x_4x_5$;

$x_7 = x_1x_2 = x_3x_5$;

$x_8 = x_1x_3 = x_2x_5$;

$x_9 = x_1x_4 = x_5x_6$;

$x_{10} = x_1x_5 = x_2x_3$;

$x_{11} = x_1x_6 = x_4x_5$;

$x_{12} = x_2x_4 = x_3x_6$;

$x_{13} = x_2x_6 = x_3x_4$;

$x_{14} = x_1x_2x_4 = x_3x_4x_5 = x_1x_3x_6 = x_2x_5x_6$;

$x_{15} = x_1x_3x_4 = x_2x_4x_5 = x_1x_2x_6 = x_3x_5x_6$; abd

ϵ = experimental error.

Factor x_c is the indicator variable for the corner points in the design ($x_c = 1$ at the corner points, and $x_c = 0$ at the center points). The extra factor x_c is needed to separate the average contribution of the corner points from the average contribution of the center points to response y. Coefficient β_c measures the overall curvature of the response surface in this experimental region.

The six control variables x_1 through x_6 are assumed coded to -1 at the low value, 0 at the center value, and +1 at the high value. Due to the fractional nature of the 2^{6-2} design, there is considerable confounding of effects in this design. The above definitions include all confounded interactions of order three or less. All confounding relations for this design can be easily found from the defining relation:

$$I = x_1x_2x_3x_5 = x_2x_3x_4x_6 = x_1x_4x_5x_6 \tag{3}$$

where I denotes the multiplicative identity (+1). For example, to find the effects (aliases) confounded with main effect x_1, multiply both sides of equation 3 by x_1 to obtain:

$$x_1 = x_2x_3x_5 = x_1x_2x_3x_4x_6 = x_4x_5x_6 \tag{4}$$

where $x_1^2 = +1$ at the corner points and can be omitted as a factor in any product. Note that the three-way interactions in equation 4 are the same aliases previously listed in the definition of x_1. It is customary in screening tests to ignore higher order interactions; therefore, in this analysis, it is assumed that four-way and higher interactions are negligible.

2.2.4 RESULTS

This section presents the results of two experimental designs performed on the CAP.

Results from the 92-EXD nozzle geometry tests are shown in Table 5, and results from the 92-CPC control parameter tests are shown in Table 6. Response variables for mean grain size and porosity were determined through computer-assisted image analysis, and microhardness was determined using a Vickers indentor with a 50-gram load. For a complete report on the material analysis of the tin coatings for 92-EXD and 92-CPC, see Appendix A.

Table 5. Response variables for the DOE 92-EXD test series.

TEST SEQUENCE	STANDARD ORDER	ADHESION STRENGTH (PSI)	MICROHARDNESS HV50 AVERAGE	MEAN GRAIN SIZE (MICRONS)
2	1	1251	15.8	3.0
6	2	1281	16.3	1.0
4	3	1389	12.2	2.0
5	4	1202	18.9	0.5
1	5	1364	16	2.0
8	6	1254	17.9	1.5
7	7	1320	16.2	1.5
3	8	1338	16.5	2.5

Typical microstructures from the 92-EXD nozzle geometry tests and the 92-CPC control parameter tests are given in Figures 8 and 9, respectfully. Adhesion strength was measured and determined according to ASTM C 633-79. Figure 10 is the adhesion testing fixture, and Figure 11 is a typical result of an adhesion specimen failure. Adhesion strength response was determined by averaging the six individual specimen strengths.

For the 92-EXD tests, the factor effects were computed by fitting the statistical model given by equation 1 directly to the experimental data using the Statistical Analysis System (SAS) software package. These effects are plotted in Figures 12 through 14 for each response variable (the intercept is not included in these plots) and are an average response at the low and high levels for each parameter. For example, the average response effect for orifice location on adhesion strength is calculated by averaging the responses at the low and the high levels and then subtracting the average low from the average high. Mathematically this is:

Low Level: $(1,251+1,389+1,364+1,320)/4 = 1,331$

High Level: $(1,281+1,202+1,254+1,338)/4 = 1,269$

Difference: $1,269 - 1,331 = - 62$

Note that the difference is negative, which indicates that as orifice location increases or moves forward in the nozzle throat, the adhesion strength decreases.

Since there were no replications in this design, there can be no estimate of the experimental error independent of the model. However, normal probability plots of the factor effects can be used to determine if any effects appear significant in relation to the other effects. These plots appear in Figures 15 through 17. If no effects are significant, the probability plots will appear to be nearly straight lines, provided the unknown experimental errors are normally distributed as $NID(0,\sigma^2)$.

12

Table 6. Response variables for the DOE 92-CPC test series.

TEST SEQUENCE	STANDARD ORDER	ADHESION STRENGTH (PSI)	MEAN GRAIN SIZE (MICRONS)	MAXIMUM POROSITY (MICRONS)
17	1	1588	3.5	0
4	2	904	3.0	0
9	3	1977	2.0	0
5	4	1210	0.5	0
18	5	1481	1.0	34
8	6	1383	0.5	0
14	7	1500	0.5	0
3	8	1459	0.5	0
10	9	5220	3.0	0
2	10	1182	0.5	0
15	11	1439	1.0	0
11	12	1171	0.5	0
7	13	1810	3.0	22
12	14	1996	0.5	6
1	15	1070	2.0	0
13	16	1375	1.0	0
16	17	1308	1.0	0
6	18	1302	1.0	0

From Figures 12 through 17, it appears that at least some of the main effects and interactions are significant for each response variable; these are the effects that deviate most from the overall straight line pattern in the normal probability plots and are typically the largest effects in magnitude. From Figure 15, it appears that the orifice location x_1 and the $x_1x_2x_3$ interaction are the most significant factors affecting adhesion strength; from Figure 16, it appears that the orifice location x_1 and the x_1x_3 interaction are the most significant effects affecting mean grain size; and from Figure 17, it appears that the orifice location x_1 and the $x_1x_2x_3$ interaction are the most significant factors affecting microhardness. The existence of relatively large interactions for each response variable implies that the three response variables are fairly complicated functions of the three control variables over the experimental region investigated. All three control variables appear to have a significant affect on nozzle performance in the experimental region explored by the EXD test.

For the 92-CPC tests, the factor effects (the βs) are estimated from least squares fits of equation 2 to the experimental data for each response variable investigated. As before, the SAS statistical package
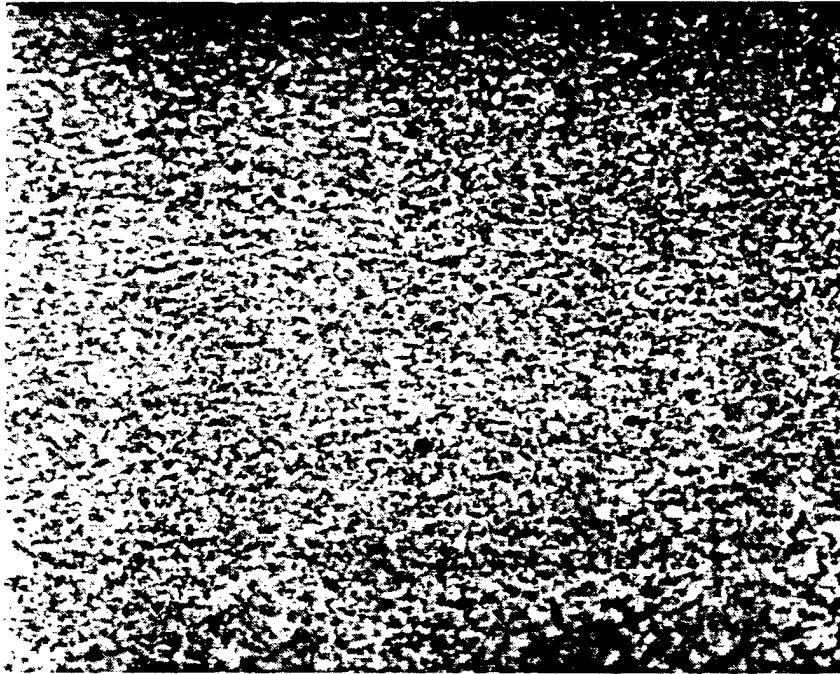
Figure 8. A typical microstructure for a 92-EXD test. (Mag = 500X)
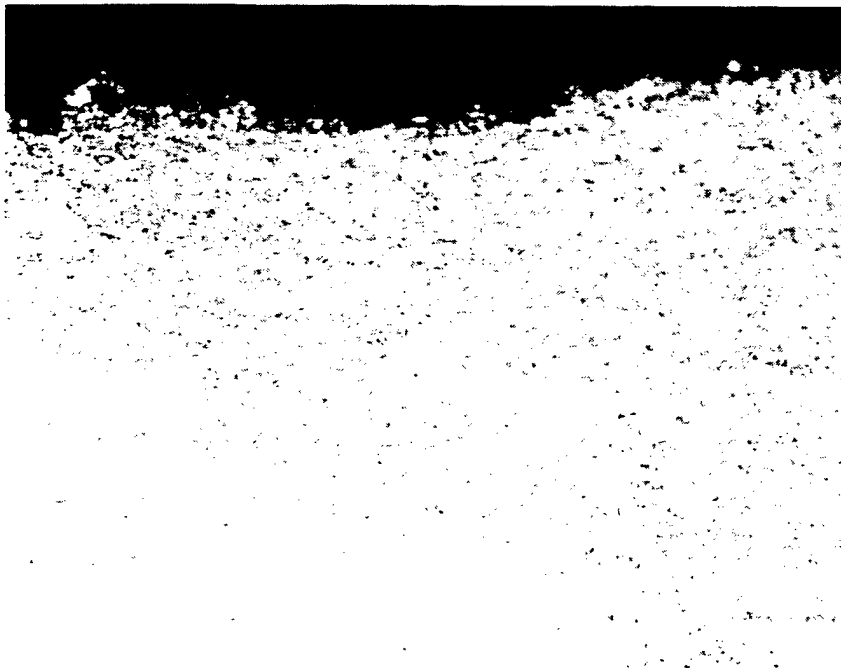
Figure 9. A typical microstructure for a 92-CPC test. (Mag = 500X)

14
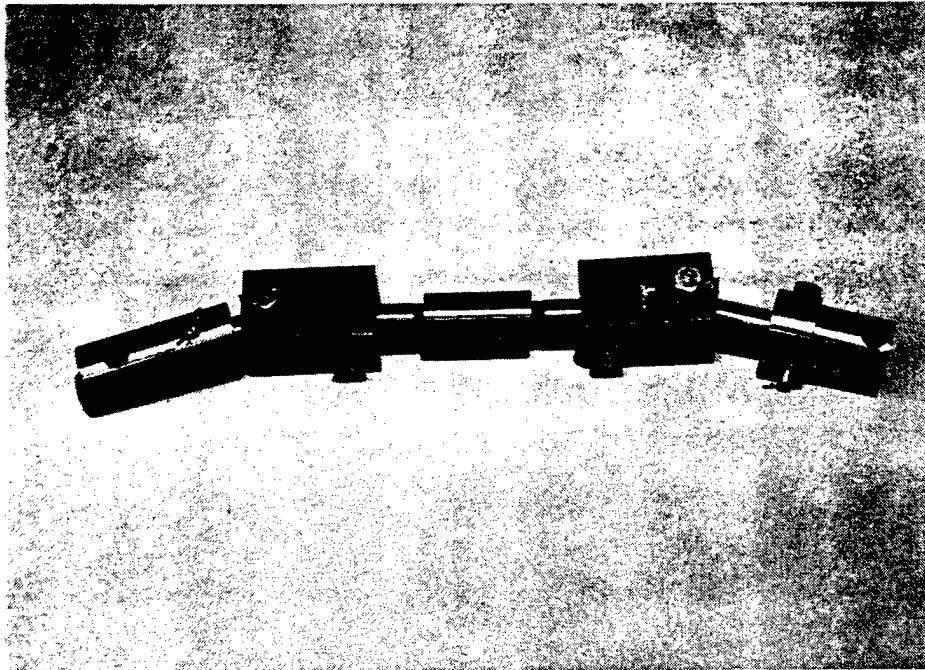
Figure 10. Testing fixture per ASTM C633-79.
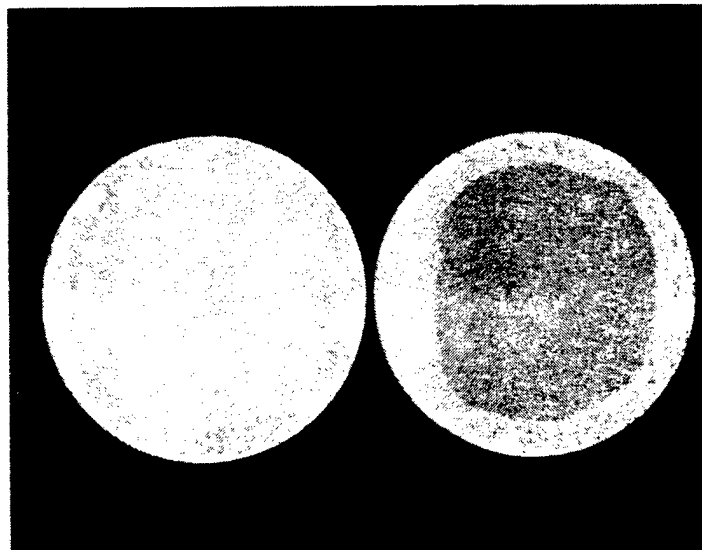
Figure 11. Fracture surface halves of test 92ADH0402.
(Mag = 1.7X)

NOTE: The fracture was a combination of adhesion (dark surface on right half) and cohesion (light surface on right half).
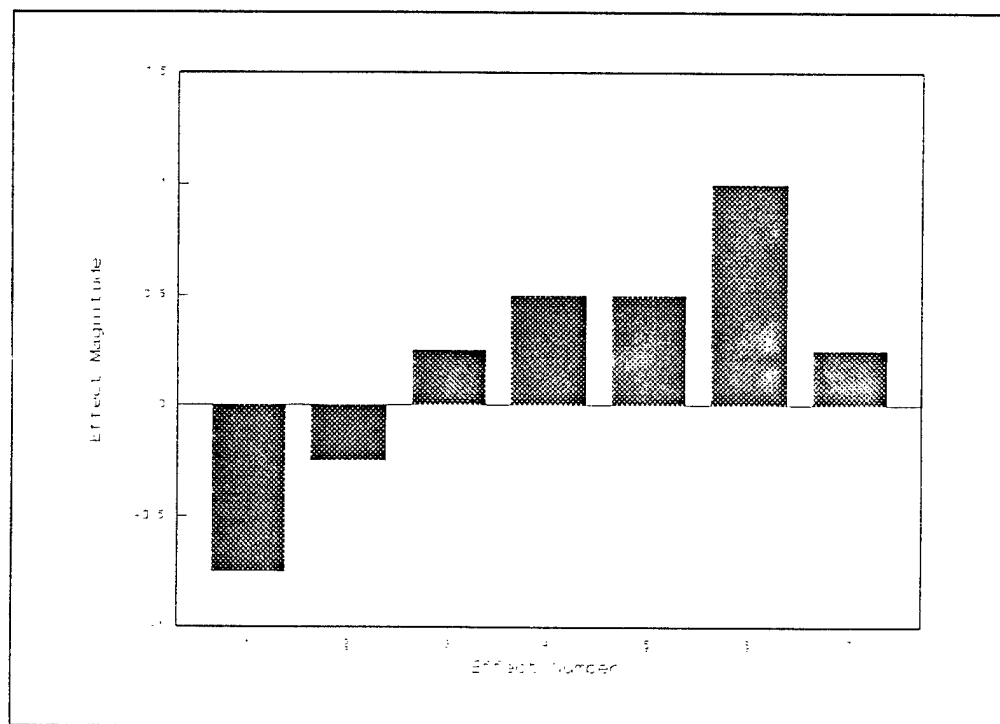
53
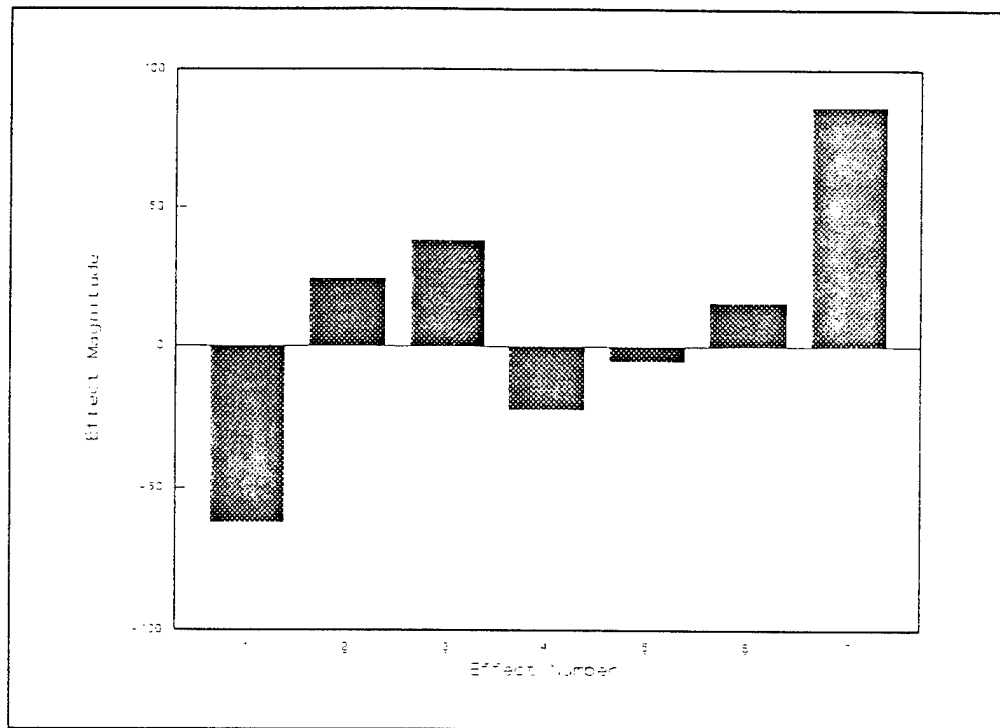
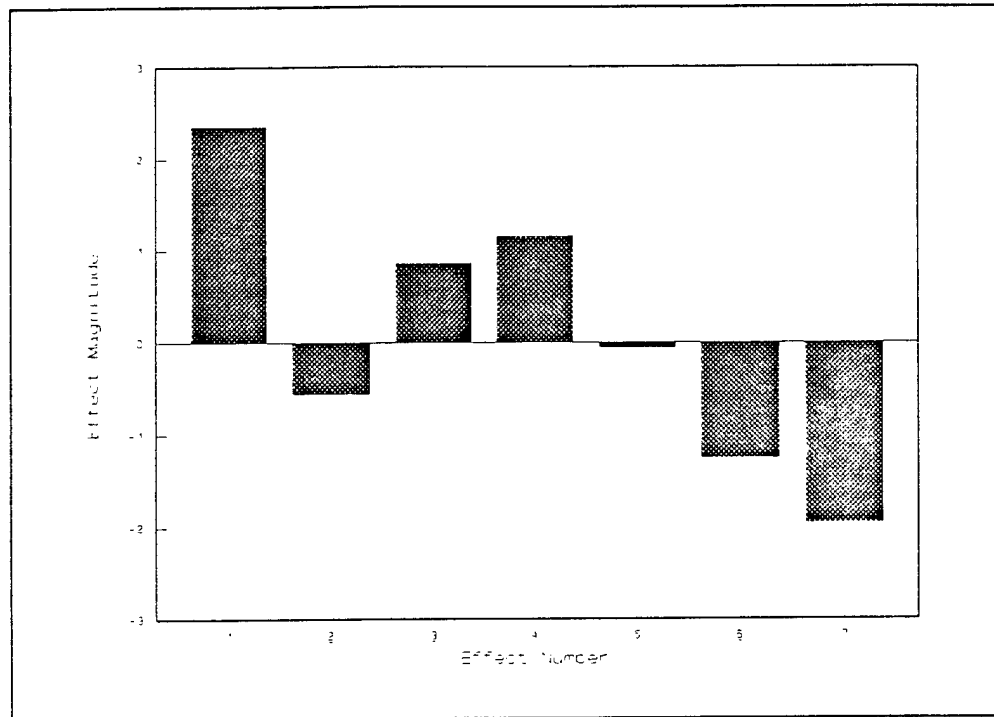*Figure 12. Adhesion effects.*

Figure 13. Mean grain size effects.

Figure 14. Microhardness effects.
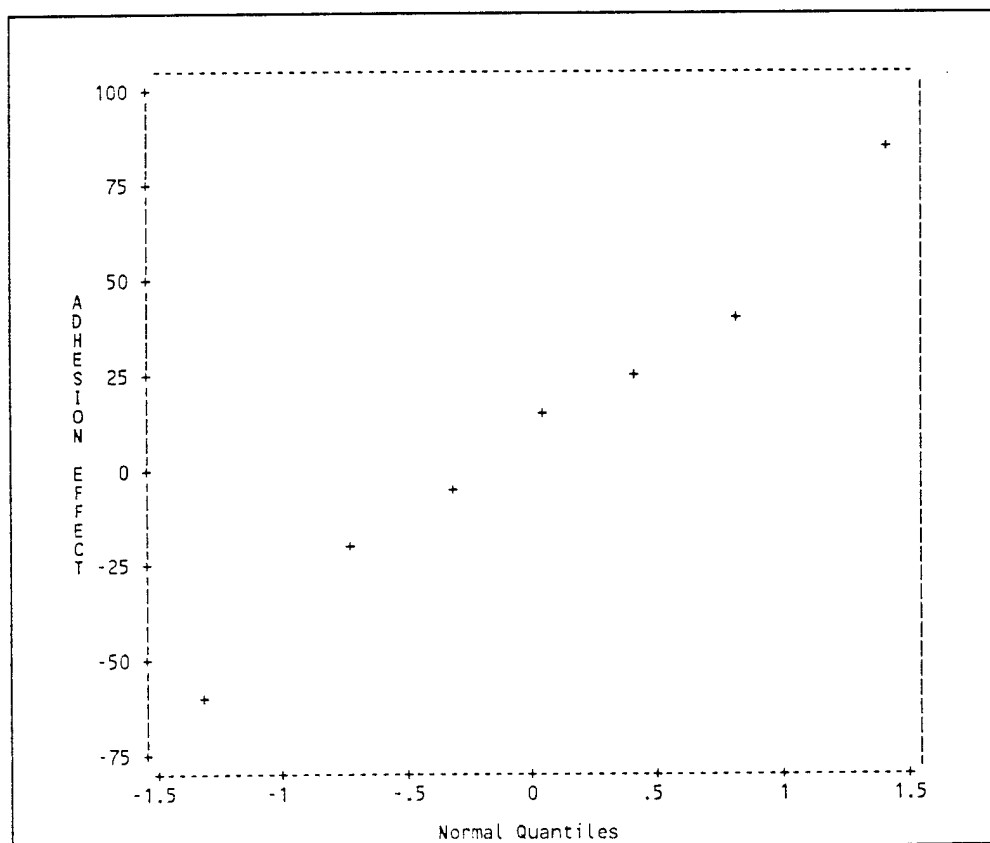
Figure 15. Normal probability plot—adhesion effects.

17
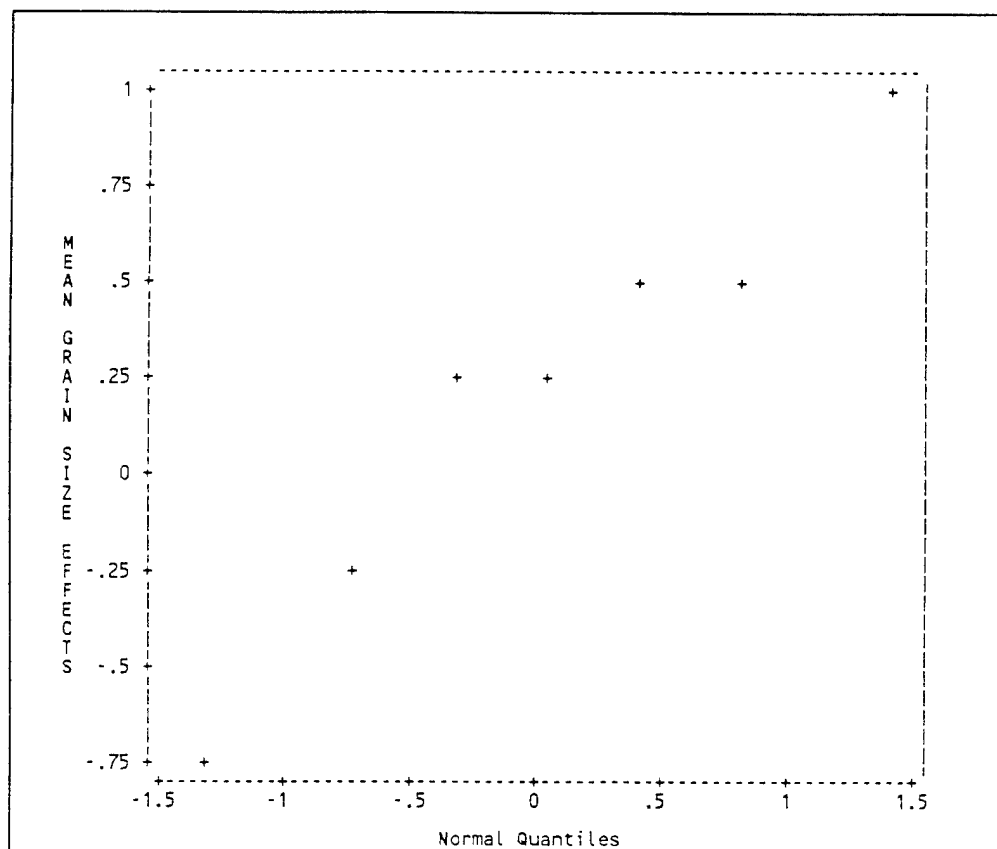
Figure 16. Normal probability plot—mean grain size effects.

is used to perform this task, although the estimates also could be found by hand calculations using Yates' algorithm (an error-prone method for a model this complicated).

The factor effects are plotted in Figures 18 through 20, and the corresponding normal probability plots are shown in Figures 21 through 23 (the intercept and corner effect are not included in these plots).

Based on the error estimate (with 1 degree of freedom) obtained from the two center point replicates, all effects appear highly significant (with t test probabilities below 0.01). However, the error estimate may not be completely reliable since it is based on only two replicates at the center of the design. Alternately, the normal probability plots may be used to determine which effects appear significant in relation to the other effects, provided the experimental errors are normally distributed as $NID(0, \sigma^2)$. From Figure 21, it appears that all factors significantly influence adhesion strength. In Figure 22, no effect stands out as significant in relation to the others; however, all are likely to affect mean grain size based on the t tests results. From Figure 23, it appears the argon temperature x_2, the traverse rate x_3, and their interaction have the most influence on porosity. Although not shown in the figures, the overall curvature effect appears to be significant for each response variable based on the tests. Consequently, the three response variables appear to be fairly complicated functions of the six control variables over the experimental region investigated. All six control variables appear to have a significant effect on spray performance in the experimental region explored by the CPC test.
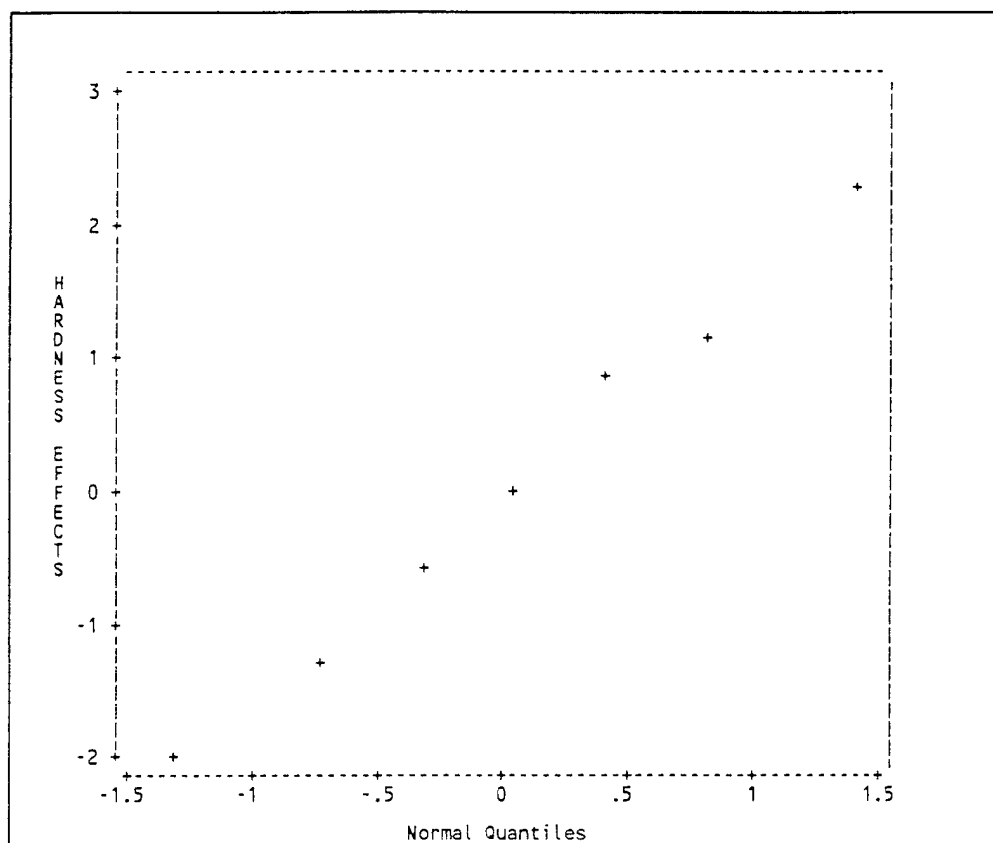
Figure 17. Normal probability plot—microhardness effects.
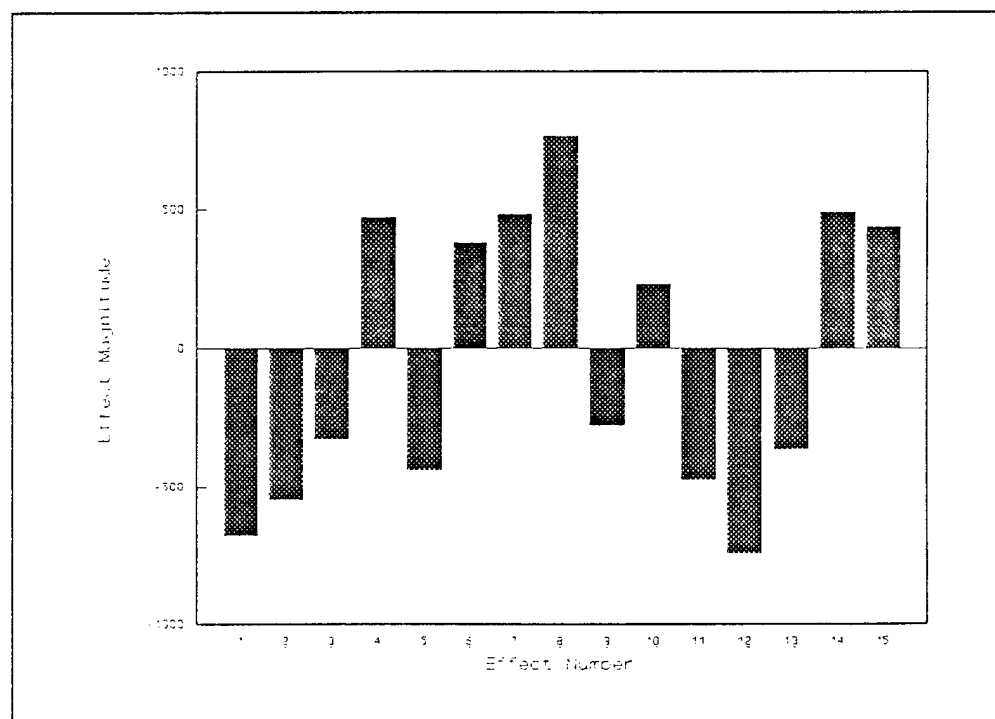
Figure 18. Adhesion effects.

19
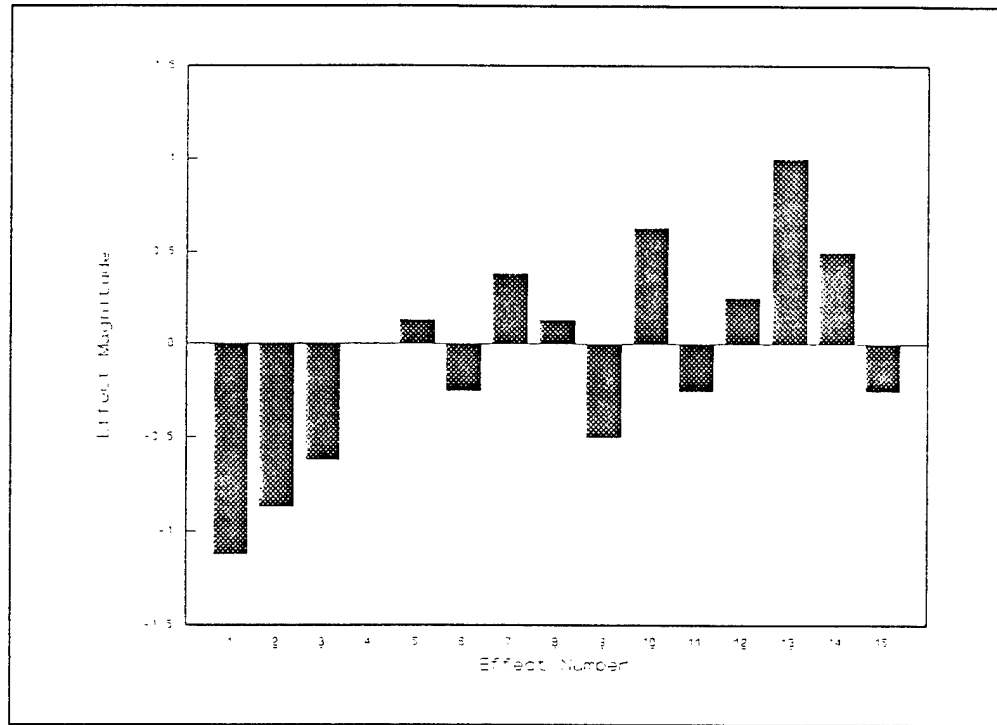
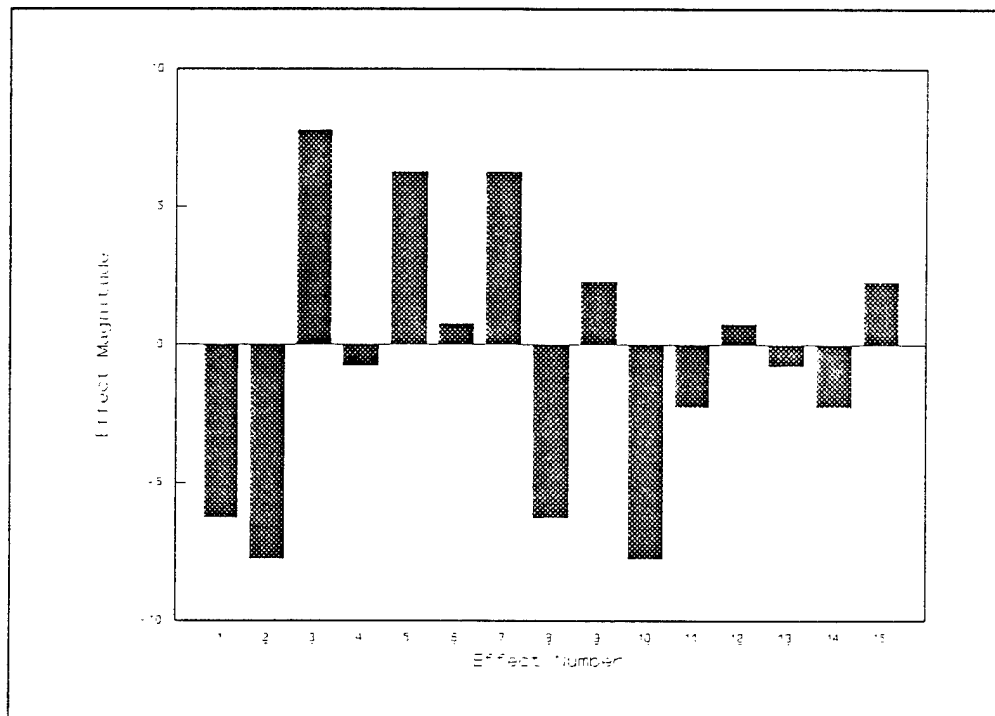*Figure 19.   Mean grain size effects.*
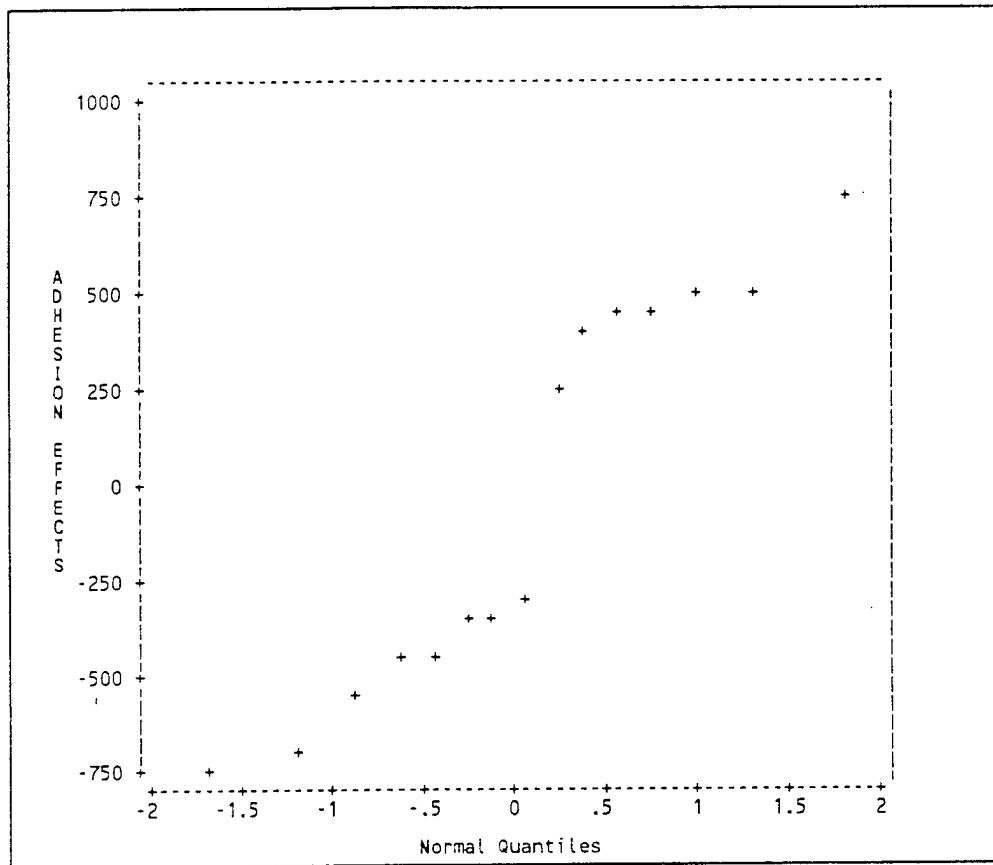

Figure 20.   Porosity effects.

20

Figure 21. Normal probability plot—adhesion effects.

2.2.5 SUMMARY AND CONCLUSIONS

Experimental studies of the CAP were performed for nozzle geometry and process control parameters. The experiments used a fractional-factorial approach and were characterized by evaluating coating qualities. Coating quality response was determined from adhesion strength, mean grain size, microhardness, and porosity.

2.2.5.1 92-EXD Tests

For the 92-EXD tests, adhesion strength ranged from 1,202-1,389 pounds per square inch (psi). Microhardness ranged from 12.2-18.9 HV50, and mean grain size ranged from less than 1-8 microns. Orifice location and the three-way interaction between orifice location, orifice diameter, and throat diameter most significantly affected adhesion strength. Mean grain size was most influenced by orifice location and the two-way interaction of orifice location and orifice diameter. Microhardness was most influenced by orifice location and the three-way interaction between orifice location, orifice diameter, and throat diameter.
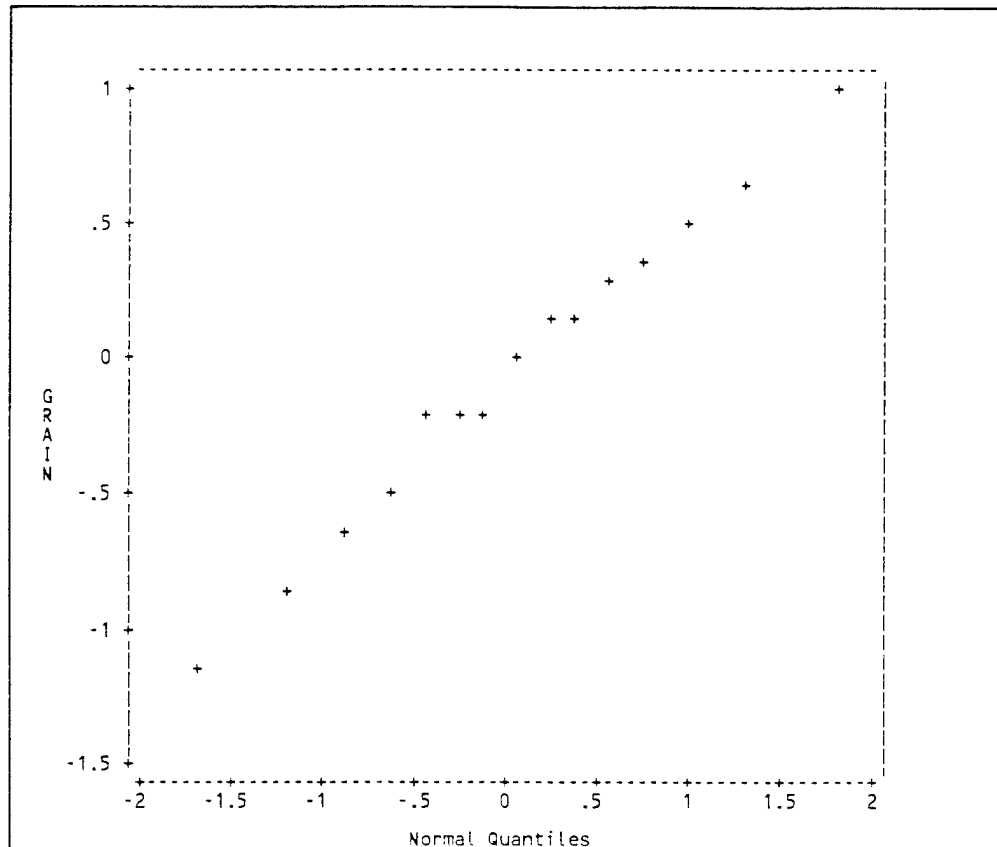
Figure 22. Normal probability plot—mean grain effects.

The complex interactions of the variables indicate that all three variables significantly effect the nozzle performance. Therefore, because no one geometry aspect dominated the others, the optimum nozzle geometry was based on the test with the largest microhardness and the smallest mean grain size.

2.2.5.2 92-CPC Tests

For the 92-CPC tests, adhesion strength ranged from 904-5,220 psi, porosity from 0 to 34 microns, and mean grain size from less than 1 to 40 microns. All factors influence adhesion strength and mean grain size—no effect significantly stands out from the others. Porosity was most influenced by argon temperature and traverse rate.

This screening test indicates that all six control variables have significant effect on the spray performance of tin. The experimental region explored will become the basis for the equipment settings for higher melting temperature materials.

2.3 COMPARISON TO COMMERCIAL SPRAY TESTS

This test series was conducted in order to compare the CAP to a conventional thermal spray process, in this case, a Hobart/TAFA electric twin-wire arc system. Eight tests at varied process control

60
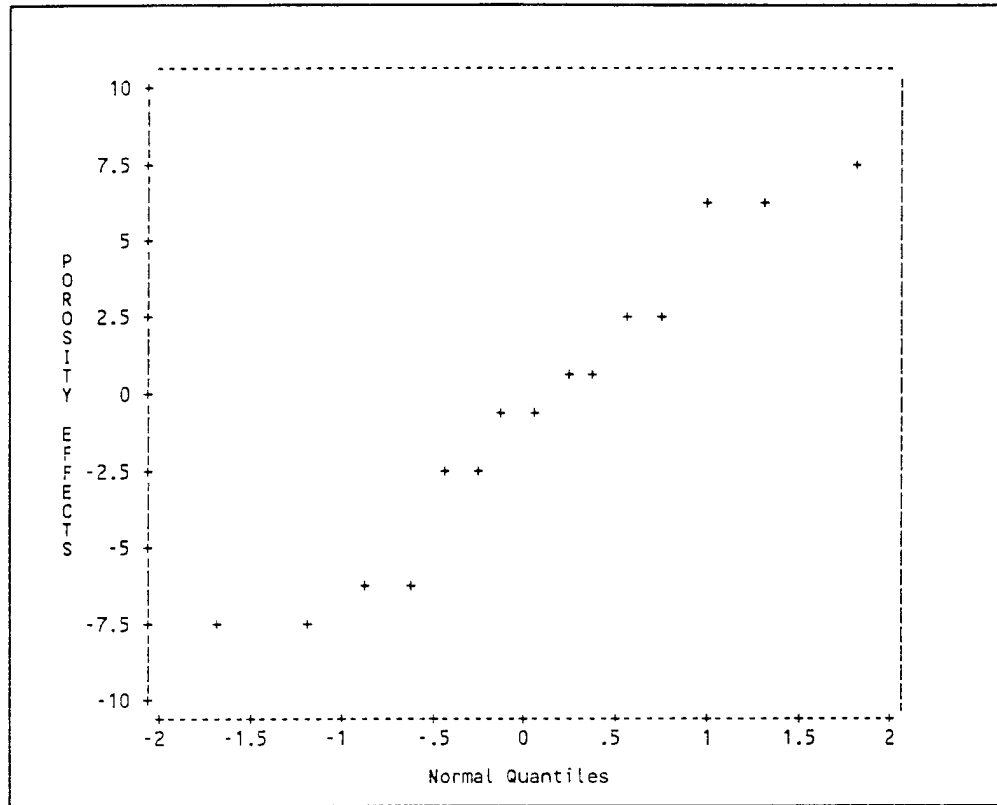
Figure 23. Normal probability plot—porosity effects.

parameter settings were conducted to examine coating attributes of VERSAlloy-50 metal alloy sprayed with the electric drive system. Coating attributes analyzed in these tests were identical to the MSE work with tin and include adhesion strength, microhardness, and porosity. Results of the tests are to provide Air Force personnel the data necessary to compare the CAP to an industrial process.

2.3.1 Experimental Setup

The electric arc spray system applies coatings of selected wire-form metals. The system uses push/pull motors to feed two electrically charged wires through an arc gun. The wires contact at the gun tip and create an arc, which melts the wire at temperatures higher than 7,200 °F. Compressed air then atomizes the molten metal and projects it onto the substrate. The process schematic is shown in Figure 24.

2.3.2 Experimental Procedure

For this test series, eight tests were conducted to evaluate the performance of the Hobart/TAFA electric drive system. Of the eight tests, four were conducted at varied operating conditions to spray VERSAlloy-50 onto sheet steel plates (12"L x 6"W x 1/8"D). The remaining tests were duplicates of the first four tests except VERSAlloy-50 was sprayed on six adhesion specimens (AISI 4340 heat treated to 40 HRC). Control process parameters selected for the study are given in Table 7.

23

Table 7. Control process parameters.

TEST SEQUENCE NUMBER	GAS PRESSURE (PSIG)	WIRE CURRENT (AMPS)	SURFACE PREPARATION (Al$_2$O$_3$)	SPRAY DISTANCE (INCHES)
1	50	150	30 Mesh	4
2	50	150	30 Mesh	6
3	50	100	30 Mesh	6
4	50	200	30 Mesh	6
5	50	150	30 Mesh	4
6	50	150	30 Mesh	6
7	50	100	30 Mesh	6
8	50	200	30 Mesh	6
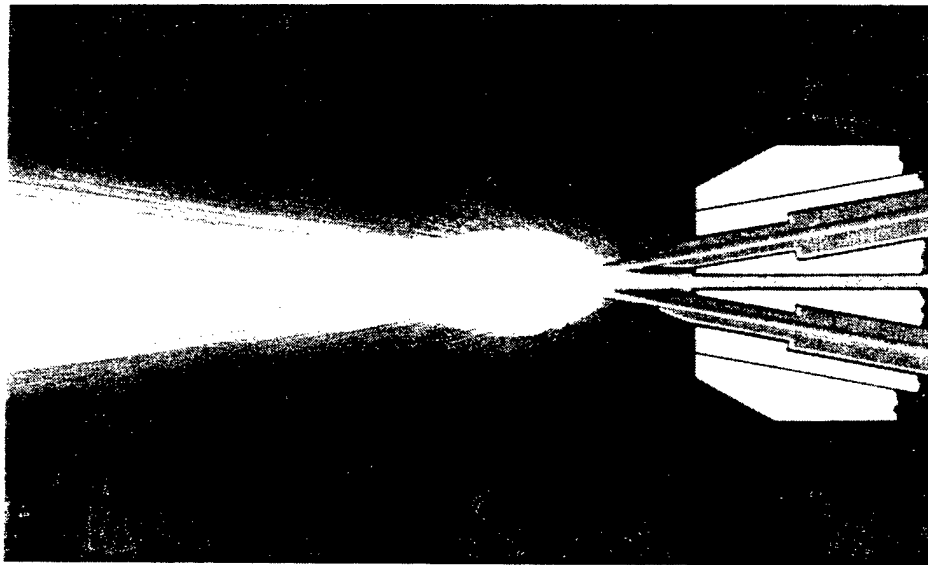
Figure 24. Twin-wire arc process.

2.3.3 Results

Results of the electric twin-wire arc tests are shown in Table 8. As in the MSE Test Series, coating attributes for mean grain size and porosity were determined through computer-assisted image analysis, and microhardness was determined using a Vickers indentor with a 50-gram load. Adhesion strength was determined according to ASTM C 633-79 and is an average of six individual specimen strengths. A typical microstructure for the twin-wire arc process is given in Figure 25.

Table 8. Coating results—twin-wire arc system.

TEST NUMBER	ADHESION STRENGTH (PSI)	MICROHARDNESS HV50 AVERAGE	MAX POROSITY (MICRONS)
1	-	645.5	2.044
2	-	594.5	2.725
3	-	660.5	2.064
4	-	538.9	3.038
5	7071	-	-
6	7077	-	-
7	6587	-	-
8	6717	-	-

Figure 25. Typical microstructure of twin-wire arc sprayed deposit. (Mag = 500X)

25

Results of the CAP sprayed tests are shown in Table 9. The same test standards and techniques were used to collect this data as were used for the twin-wire arc tests. However, a specific test series was not conducted to generate this data; it was collected from spray tests that were part of the Boeing Test Series. A typical microstructure for these tests is shown in Figure 26.

Table 9. Coating results—CAP system.

Test Number	Adhesion Strength (psi)
92-BOE-02	3062
92-BOE-04	6736
92-BOE-20	3440
92-BOE-37	4288

Figure 26. Typical microstructure of CAP sprayed deposit. (Mag = 500X)

26

2.3.4 Summary and Conclusions

A comparision of the twin-wire arc spray system and the CAP spray system processes is summarized in Table 10.

Table 10. Comparison of twin-wire arc and CAP test results.

Process	Average Adhesion Strength (PSI)	Average Microhardness Range - HV	Mean Grain Size (Microns)	Porosity % (Microns)
Twin-Wire Arc	6863	540-670	---	2.35
CAP	4394	490 - 505*	4	1.00*
* The average of seven tests.				

It should be noted that the data generated from the CAP sprayed samples was not part of a designed experiment to generate such data; the samples were part of the Boeing Test Series.

Based on the analysis of the data generated, it appears the CAP has the advantage over the twin-wire arc process because of the much smaller grain size, lack of transverse cracks in the deposit, and lower porosity. Although the adhesion strength and the hardness were somewhat higher for the twin-wire arc process, it is believed these properties can be signifigantly improved for the CAP through the use of designed experiments. It is also believed that the porosity and grain size numbers can be further improved.

3. NOZZLE MATERIALS EVALUATION TESTS

During the initial work that was performed for Phase III of the Spray Casting Project, it became apparent that a more erosion/corrosion-resistant nozzle material would be necessary to perform the process qualification testing required by the Air Force. The currently used nozzle material is hexagonal boron nitride, which is soft, easy to machine, and resistant to attack by liquid metals at relatively low temperatures. However, at the temperatures necessary to melt the cobalt- and nickel-base alloys that might be examined in Phase III (approximately 1,700 °C), the boron nitride material experienced excessive erosion/corrosion and excessive nozzle wear. This situation would have made it difficult if not impossible to duplicate test results that would be required for successful process qualification testing. For this reason, a series of tests that would evaluate the compatability of candidate nozzle materials with selected coating materials was designed. These tests are described below.

3.1 SCREENING TESTS AND RESULTS

In order to examine a relatively large number of nozzle material/coating combinations, a screening test was developed. The test was static in nature and consisted of placing a small metal coating sample on a sample of candidate nozzle material in a controlled atmosphere furnace. An example of this test setup is shown in Figure 27, and the furnace used for the testing is shown in Figure 28. The temperature of the furnace was then raised to a predetermined temperature and maintained at that

Figure 27. Test setup.
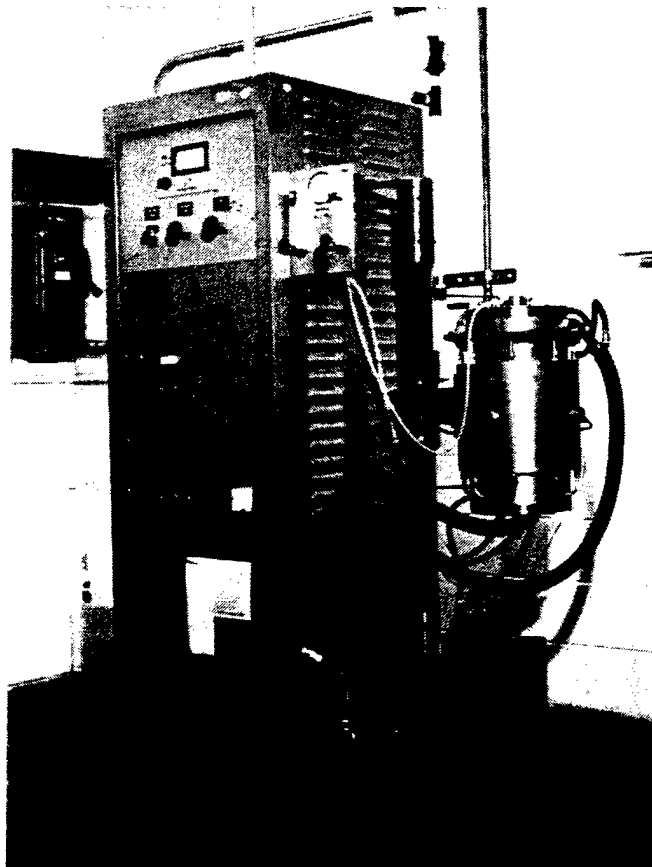
Figure 28. Test furnace.

66

temperature for 10 minutes; the furnace was then cooled to room temperature. A typical furnace cycle is shown in Figure 29.

The predetermined temperature for the samples that were reacted with Stellite 6, Inconel 92, and carbon steel was 1,700 ± 25 °C; the predetermined temperature for VERSAlloy-50 was 1,150 ± 25 °C and for VERSAlloy-25 was 1,300 ± 25 °C. The variations in test temperatures are a result of initailly looking at the higher temperature materials first and then finding the lower melting range of VERSAlloy materials, which will be the materials used for the Process Qualification Test Series. If a candidate nozzle material did not display an easily detected reaction with the sample metal, another sample was heated to the same temperature and held for 1 hour at that temperature.

The candidate nozzle materials that were investigated included the following:

- alumina;
- silicon carbide;
- aluminum nitride;
- silicon nitride;
- boron carbide;
- silicon carbide/boron carbide composite;
- hexagonal boron nitride/mullite composite; and
- hexagonal boron nitride/aluminum nitride composite.

Hexagonal boron nitride was also run through this screening test as a control material because it was the material from which all previous nozzles were fabricated. It should also be noted that two different densities of alumina were also screened.

The coating materials that were tested included the following alloys, which were intended to represent a particular class of alloy:

- Stellite 6 (cobalt-base alloys);
- Incoloy filler metal 92 (nickel-base alloys);
- plain carbon steel (iron-base alloys);
- VERSAlloy-50 (nickel/boron/silicon alloy); and
- VERSAlloy-25 (nickel/boron/silicon alloy).

The chemical content of each of the above alloys is shown in Table 11.

Table 11. Nominal composition of base metals - weight %.

Base Metal	C	Fe	Cr	Co	Ni	W	B	Si
Stellite 6	1.0	---	26.0	Bal	---	5.0	---	---
Inconel 92	.03	6.6	16.4	---	71.0	---	---	0.2
Carbon Steel	.10	Bal	---	---	---	---	---	---
VERSAlloy-25	.10	1.0	---	---	Bal	---	1.6	3.2
VERSAlloy-50	.60	4.0	11.0	---	Bal	---	3.0	4.0

Typical Astro Furnace Thermal Cycle
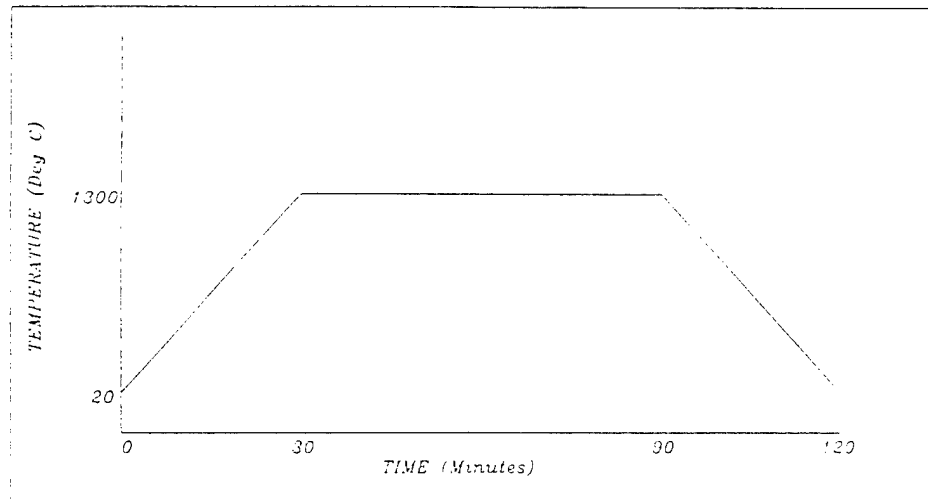
Figure 29. Typical furnace cycle.

After the samples were removed from the furnace, they were mounted and/or polished for examination with a metallurgical microscope, stereo microscope, or scanning electron microscope (SEM). The samples were sectioned so that a cross sectional view through the reaction zone was shown in the mounted specimen. A plan view photograph of the unsectioned sample was also taken for the test record.

Evaluation of the screening tests was conducted by examining the cross sections with a suitable microscope, and in some cases, with a SEM equipped with an energy dispersive x-ray (EDX) analysis system. The microscopic examination quickly revealed whether or not the coating alloy and the candidate nozzle material had reacted with each other. In the cases where there appeared to be little or no reaction between the alloy and the ceramic nozzle material, the SEM was used to determine the level of reaction.

3.1.1 Ten-Minute Tests

The candidate nozzle materials that did not pass the 10-minute exposure tests were hexagonal boron nitride, silicon carbide, silicon nitride, boron carbide, and the silicon carbide/boron carbide composite. Examples of these 10-minute tests are shown in Figures 30 through 33. As can be seen from an examination of the photographs, the reaction of the nozzle materials and the metals was quite evident and pronounced.

30

Figure 30. Cross sectional view of the 10-minute screening test between silicon carbide and Stellite 6. (Mag = 3X)

NOTE: The sample cross section was mounted and polished in a standard phenolic mounting material. The sample is in the center of the photograph, with the Stellite 6 being indicated by the arrow. The silicon carbide is the black rectangular material directly below the Stellite 6. The white rectangular pieces surrounding the sample are alumina that was placed in the mount to ensure the sample was ground and polished to a flat surface. These alumina pieces appear in all mounted cross sections. An analysis of the photograph revealed the Stellite 6 had undergone a substantial reaction with the silicon carbide, as indicated by the reaction zone that has penetrated the silicon carbide. This condition renders the silicon carbide unfit for service as a nozzle material.

3.1.2 One-Hour Tests

The candidate nozzle materials that passed the 10-minute tests were then exposed for 1 hour at temperature. The candidate nozzle materials that passed this test were alumina, silicon nitride, hexagonal boron nitride/mullite composite, and the hexagonal boron nitride/aluminum nitride composite. The only material to fail this test was the aluminum nitride. A photograph of aluminum nitride and stellite is shown in Figure 34.

3.2 DURATION TESTS

After the screening tests were run, duration tests of 10 hours were conducted using the same test format of spray metal sample on a candidate ceramic nozzle material. The particular metal/ceramic combinations tested are shown below:

31
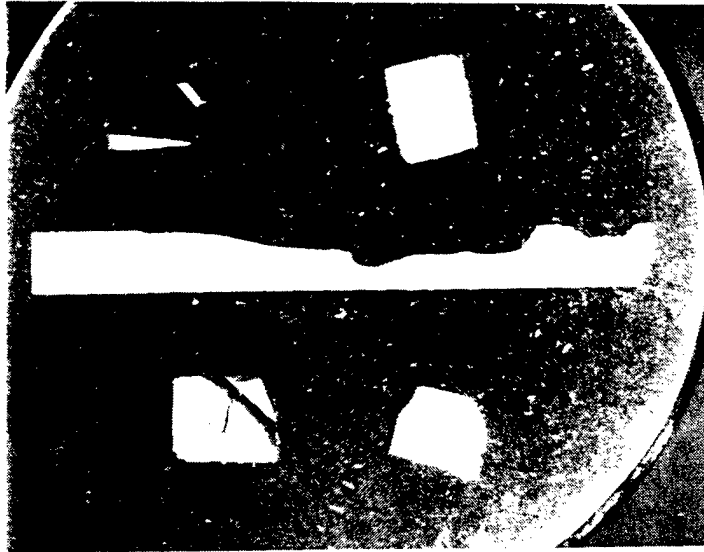
Figure 31. Cross sectional view of the 10-minute screening test between hexagonal boron nitride and carbon steel (iron). (Mag = 3X)

NOTE: This photograph shows a substantial reaction has taken place between the boron nitride and the Inconel. The arrow in the photograph shows the location of the reaction zone and the subsequent loss of cross section.
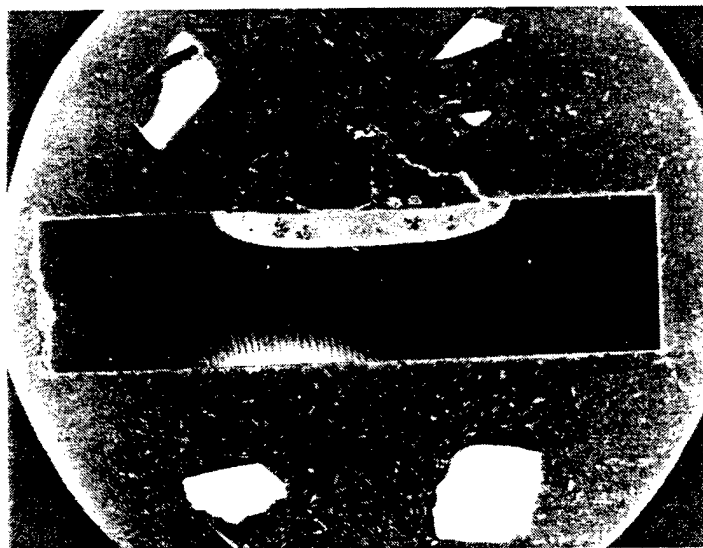
Figure 32. Cross sectional view of the 10-minute screening test between a silicon carbide/titanium diboride composite and Inconel alloy 92. (Mag = 3X)

NOTE: Examination of the above photograph revealed that a considerable reaction had taken place between the composite and the Inconel. The reaction zone is the light area indicated by the arrow.
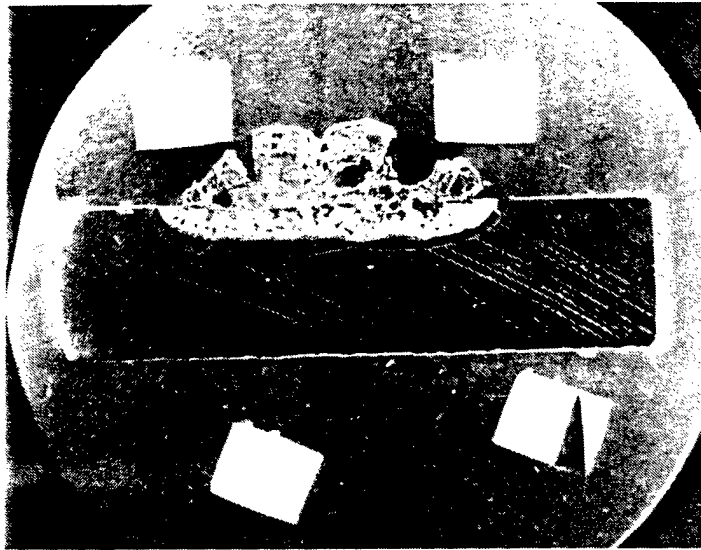
Figure 33. Cross sectional view of the 10-minute screening test between boron carbide and Inconel alloy 92. (Mag = 3X)

NOTE: Notice the considerable reaction that has taken place between the test materials.
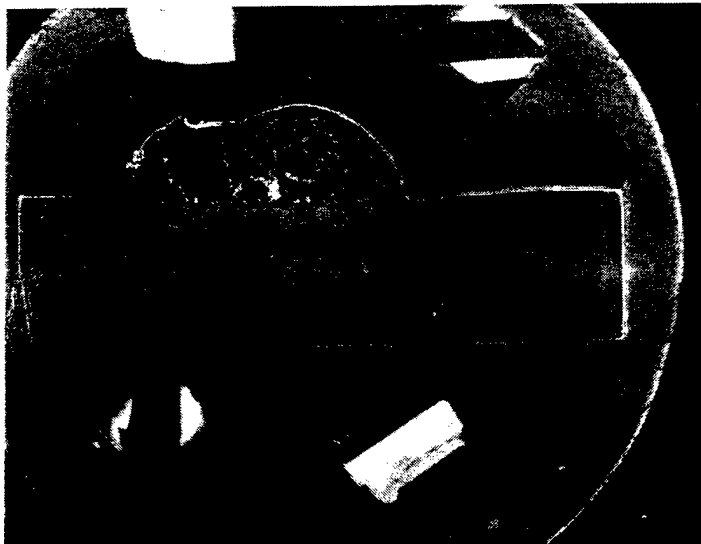
Figure 34. Cross sectional view of the 1-hour screening test between aluminum nitride and Stellite 6. (Mag = 3X)

NOTE: Examination of the photograph above shows the Stellite has wet the aluminum nitride surface, and a reaction has taken place, as evidenced by the recession of the ceramic surface.

33

- mullite/boron nitride composite and VERSAlloy-25*;
- aluminum nitride/boron nitride composite and VERSAlloy-25*;
- alumina and VERSAlloy-50**; and
- silicon nitride and VERSAlloy-25*.

* tested at 1,300 ± 25 °C
** tested at 1,150 ± 25 °C

The ceramic coupons were cross sectioned through the reaction zone and were given microscopic examinations. Photographs of the cross sections are shown in Figures 35 through 38.

The final test of the duration series was a 100-hour test between alumina and VERSAlloy-50, which was conducted at 1,150 ± 25 °C. A cross sectional view of the alumina in this test is shown in Figure 39.
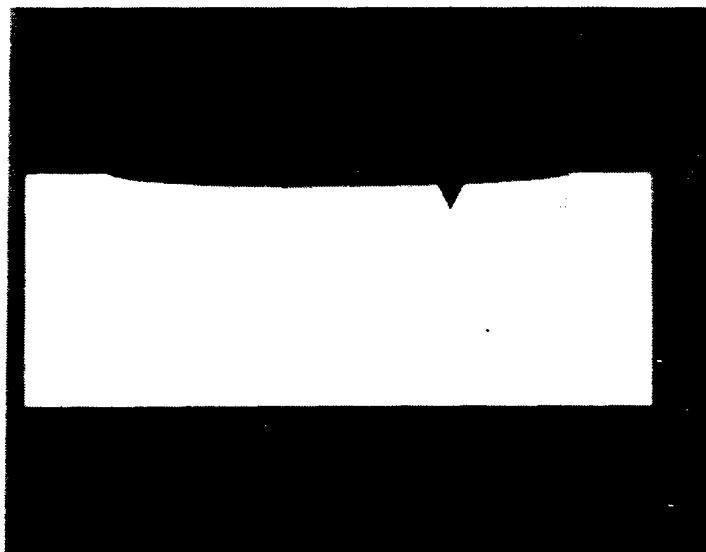
Figure 35. Cross sectional view of the 10-hour duration test between the mullite/hexagonal boron nitride composite and VERSAlloy-25. (Mag = 3X)

NOTE: The photograph shows that no visible reaction has taken place on the composite material. The arrow in the photograph shows where the VERSAlloy-25 was sitting on the composite during the test.

34
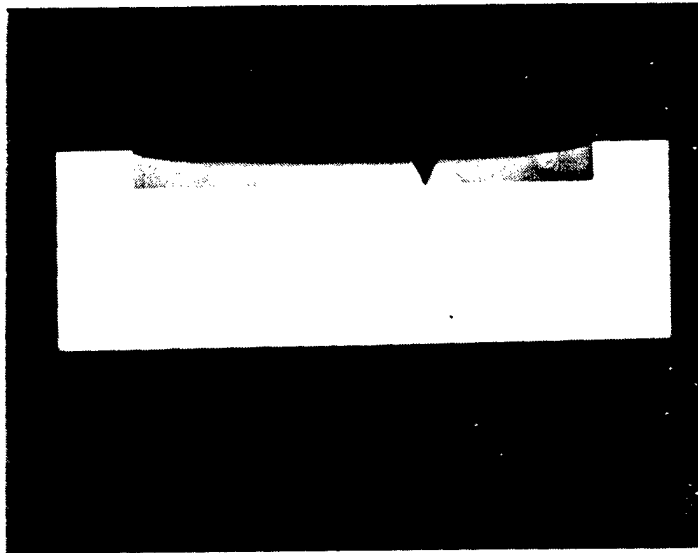
Figure 36. Cross sectional view of the 10-hour duration test between the aluminum nitride/hexagonal boron nitride composite and VERSAlloy-25. (Mag = 3X)

NOTE: The photograph shows the composite material has discolored at some surfaces; a severe chemical reaction was not observed. The arrow shows where the VERSAlloy-25 was sitting on the composite during testing.
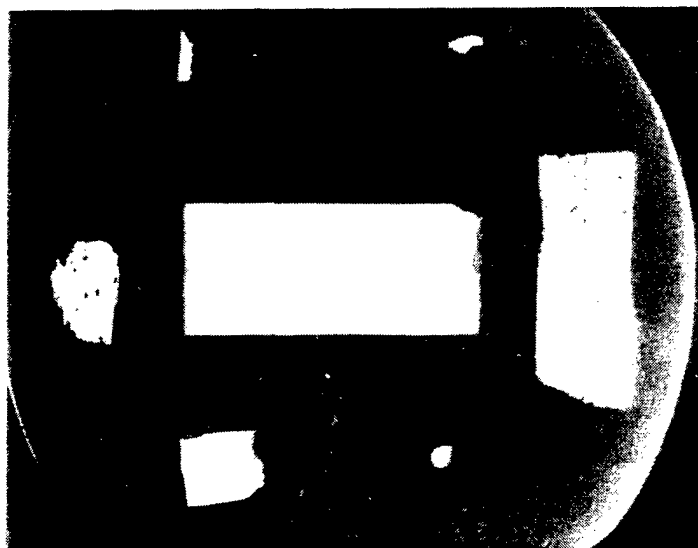
Figure 37. Cross sectional view of the 10-hour duration test between alumina and VERSAlloy-50. (Mag = 3X)

NOTE: The photograph shows that no visible reaction has taken place on the alumina.

35
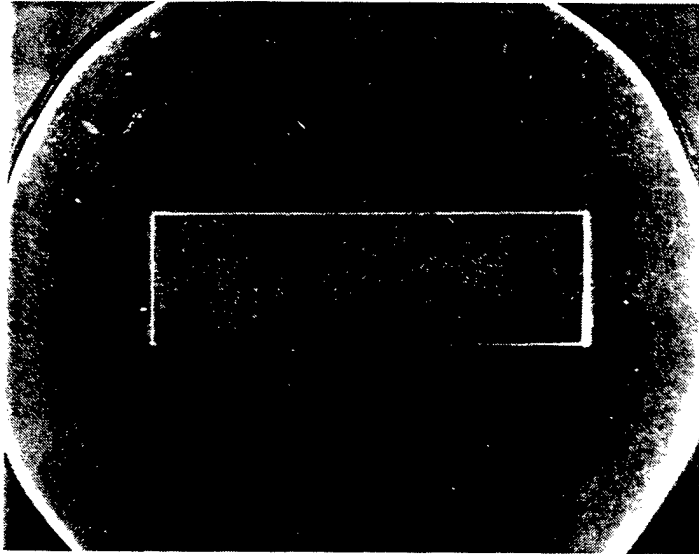
Figure 38. Cross sectional view of the 10-hour duration test between silicon nitride and VERSAlloy-25. (Mag = 3X)

NOTE: The photograph shows that no visible reaction has taken place on the silicon nitride. The arrow shows the location of the VERSAlloy-25 during the test.
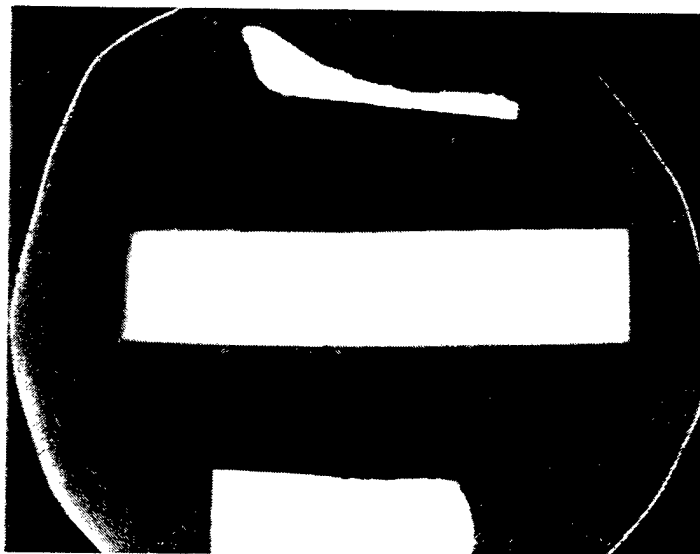
Figure 39. Cross sectional view of the 100-hour duration test between alumina and VERSAlloy-25. (Mag = 3X)

NOTE: The photograph shows that no visible reaction has taken place on the alumina.

3.3 CONCLUSIONS

Based on the results of the screening and duration tests, the four candidate nozzle materials that appear to be suitable for nozzle use are:

- alumina (98 percent dense);
- silicon nitride;
- mullite/hexagonal boron nitride composite; and
- aluminum nitride/hexagonal boron nitride composite.

Each of these materials have positive and negative charcteristics. The alumina and silicon nitride, because of their relative high hardness, will probably have superior resistance to erosion; however, this hardness also makes them difficult to machine into a nozzle configuration. These materials are also prone to cracking because of thermal stresses during startup and shutdown; published data indicates silicon nitride will outperform alumina in this regard (Ref. 2). Because of their fabrication difficulties, these materials will only be considered for nozzles during the pilot-scale development portion of the project.

The composite materials are relatively easy to machine and will be the choice for nozzles that are fabricated during the MSE and Boeing testing phases of the project. The erosion resistance of these materials will also be evaluated during these test series.

4. NUMERICAL SIMULATION AND MODELING

4.1 Quasi-One-Dimensional Nozzle and Plume Modeling

The Idaho National Engineering Laboratory (INEL) quasi-one-dimensional nozzle and plume computer codes were used to examine the experimental data and nozzle configurations. The code was put together for MSE by INEL scientists for use with the Air Force Spray Casting Program. During the MSE test series period, INEL and MSE scientists modified and improved the computer code and made various simulation runs to support the new pressurized nozzle design and data analyses. This section describes the modification and improvement work performed by INEL and MSE personnel, simulation work performed at MSE, and other supporting modeling and analysis work for the project.

4.1.1 New Modifications and Improvements

During the MSE test series period, INEL and MSE personnel made modifications to the quasi-one-dimensional computer code for better simulation. Following are some of the improvements done to the code.

- Volume fraction effects: For thicker sprays where the spray is more concentrated, the displacement of droplets/particles of the carrier gas can not be neglected as it is for dilute sprays. Because the local volume fraction of gas is reduced, the net effect for the gas is similar to a net reduction of the flow cross-sectional area. In the computation algorithm, this change was implemented through modification of the mass flux variable $x = \rho uA$, which becomes in the new version $x = \alpha \rho uA$ where α is the local volume fraction of gas.

37

- Gas dynamic pressure gradient forces (buoyancy force): The pressure gradient force term may only be significant in regions of large gas accelerations such as in the throat region of the nozzle or through the shock wave. This force is due to the pressure gradient in the gas phase in the same manner as the buoyancy force in a quiescent fluid is due to the gravity force.

- Supersonic exit conditions: Modifications were made so that if the shock wave is pushed to the exit plane of the nozzle in the course of the code trying to match the exit plane pressure, the shock wave was dispensed with, and the exit pressure condition was not matched.

- Subsonic throughout the nozzle: If a spray nozzle is driven in a manner so the flow is not choked, the original code would not correctly simulate the nozzle/spray dynamics. A new version of the code was constructed to handle subsonic throughout case with full coupling to the injection system dynamics and with inflight droplet/particle undercooling, recalescence, and solidification possible.

- Plume Program: The Plume Program was rewritten based on empirical input for the entrainment rate as opposed to the expansion angle.

- New friction factor equation: A new equation by Chen was used to calculate the friction factor in a closed conduit (Ref. 3). The equation can be expressed as:

$$\frac{1}{\sqrt{f}} = -2.0 \log[\frac{\epsilon}{3.7065D} - \frac{5.0452}{Re} \times \log(\frac{1}{2.8257}(\frac{\epsilon}{D})^{1.1098} + \frac{5.8506}{Re^{0.8981}})] \tag{5}$$

- New viscosity equation: A widely used Sutherland formula was adopted to calculate the viscosity of dilute gases. The final formula is:

$$\frac{\mu}{\mu_0} \approx (\frac{T}{T_0})^{1.5} \frac{T_0 + S}{T + S} \tag{6}$$

where S is an effective temperature, called the Sutherland constant, which is characteristic of the gas.

4.1.2 Nozzle Design and Simulation Task

Parametric studies were performed with the quasi-one-dimensional model to estimate the importance of various parameters in the liquid metal spray casting process. Since the idea of pressurized tundish was discussed, a series of simulation was performed to verify MSE personnel's assumption. The simulation result shows characteristics of the nozzle can be adjusted through the changes of the nozzle geometry. Much higher particle velocity also can be obtained by using pressurized tundish, which is now standard equipment.

- The nozzle design for tin series: This design series was an attempt to improve the flow properties through the changes of the nozzle geometry. The new design is a modified and improved version of a CST round nozzle design. By eliminating some questionable design features, improvements were made to the old CST design. The basic philosophy of this design is to reduce any strong discontinuities (shock waves) and increase the particle spray velocity. A series of computer modeling runs were done to CST- and MSE-designed nozzles to see the differences in these areas (no pressurized tundish). The values of parameters used are as follows:

  - argon inlet pressure: 19.06 psi;
  - argon inlet temperature: 100 °C;
  - nozzle wall temperature: 272 °C;
  - liquid tin temperature: 272 °C; and
  - assumed particle size: 100 μm.

  NOTE: These values are suggested for future baseline testing.

Figures 40 to 43 show the result from computer modeling efforts. Figure 40 is the gas velocity distributions between MSE and CST nozzles; the MSE nozzle displays weaker shock wave strength and smoother velocity transition. Figure 41 displays the particle velocity distributions between MSE and CST nozzles; the MSE nozzle produces 40 percent higher particle velocity when particles leave the nozzle. Figure 42 shows the MSE nozzle produces smoother gas temperature variation in the nozzle. Figure 43 shows the MSE- and CST-designed nozzles deliver similar particle temperature history; the particles start to solidify at a location less than 4 inches from the nozzle exit with either nozzle design. In conclusion, the result from the computer modeling shows the MSE-designed nozzle produces higher particle spray velocity and smoother flow characteristics than a CST-designed nozzle.

- Pressurized tundish design: Conventional nozzle design depends on the negative pressure differential at the throat region to pull the liquid metal into the spray nozzle, which restricts the gas (argon) inlet pressure ranges it can be operated on. The pressurized tundish idea provides the freedom of almost unlimited gas (argon) inlet pressure ranges, which allows for tailoring of the nozzle design for different applications. Figure 44 displays the particle velocity distributions for different argon inlet pressures. Higher particle velocities are achieved through higher argon inlet pressures, which should give MSE personnel total control of the process.

- Characterization study: Nozzle design 92-3B1, which was used during the second experimental design testing of the MSE Spray Casting Project, was examined for the characterization comparison. The test data from the characterization testings on April 24, 1992 (no name for this test), and 3B1-CHAR-3 (April 24, 1992) have been compared against the results from the one-dimensional nozzle and plume code; the relationship between the nozzle inlet and throat pressures were used for the study. For this study, 17 computer runs were executed.

Assumptions:

nozzle inlet temperature (argon): 300 °C; and
nozzle wall temperature: 382 °C.
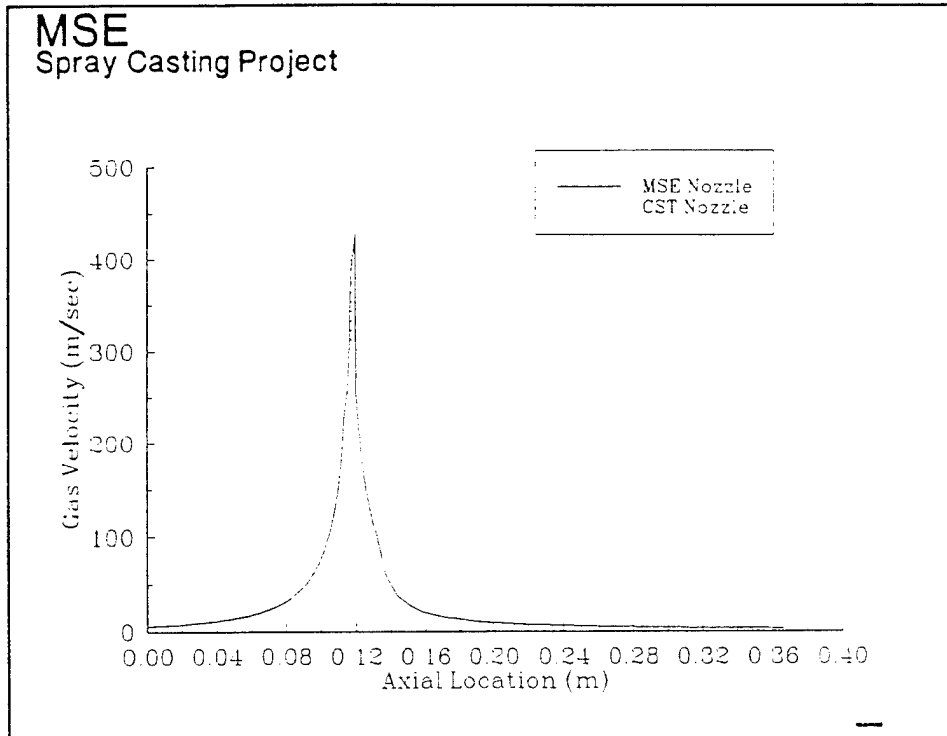
Figure 40. Gas velocity distribution.
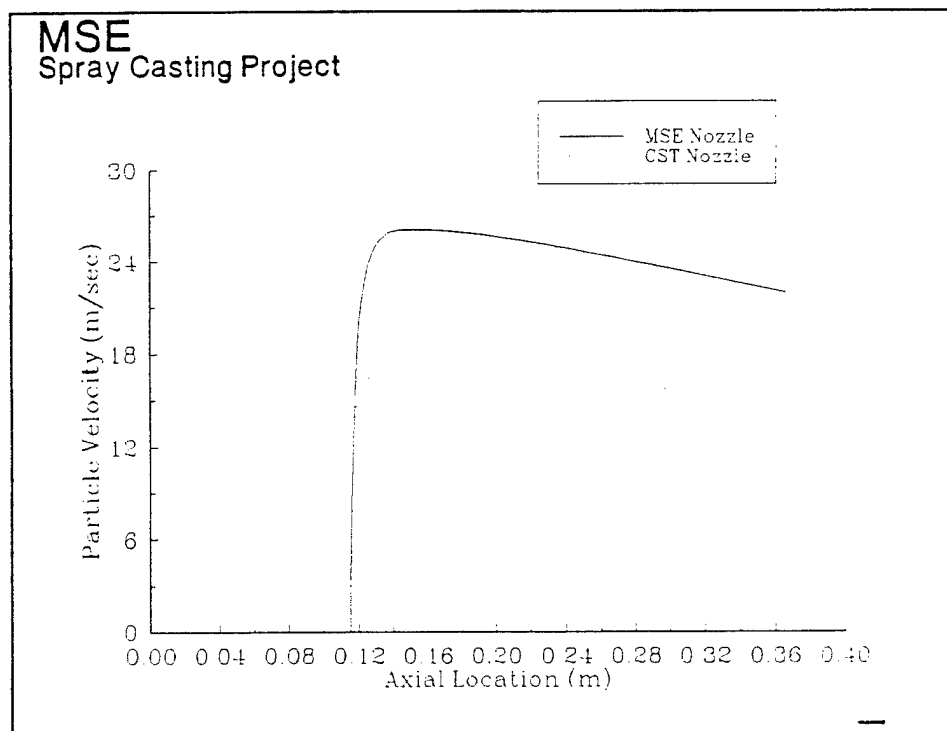
Figure 41. Particle velocity distribution.

40
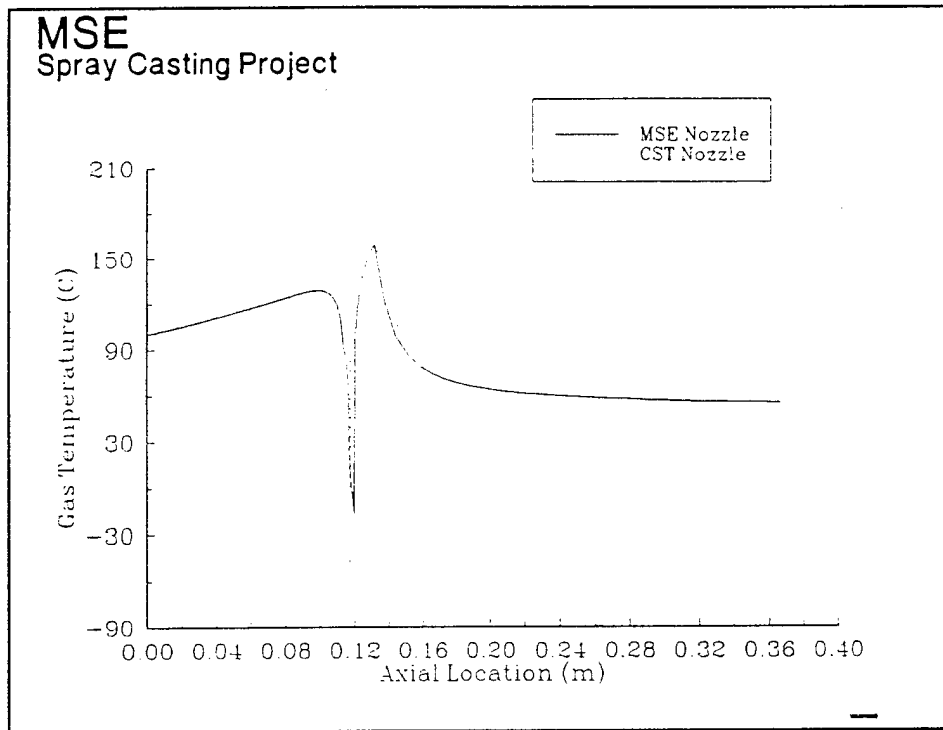
Figure 42. Gas temperature distribution.
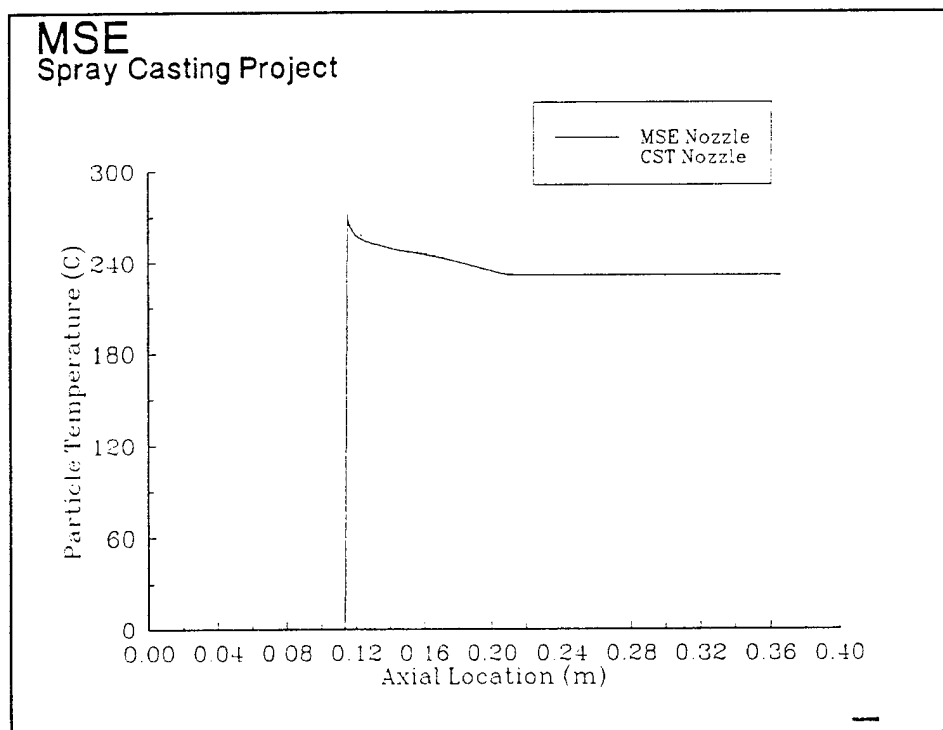
Figure 43. Particle temperature distribution.

41
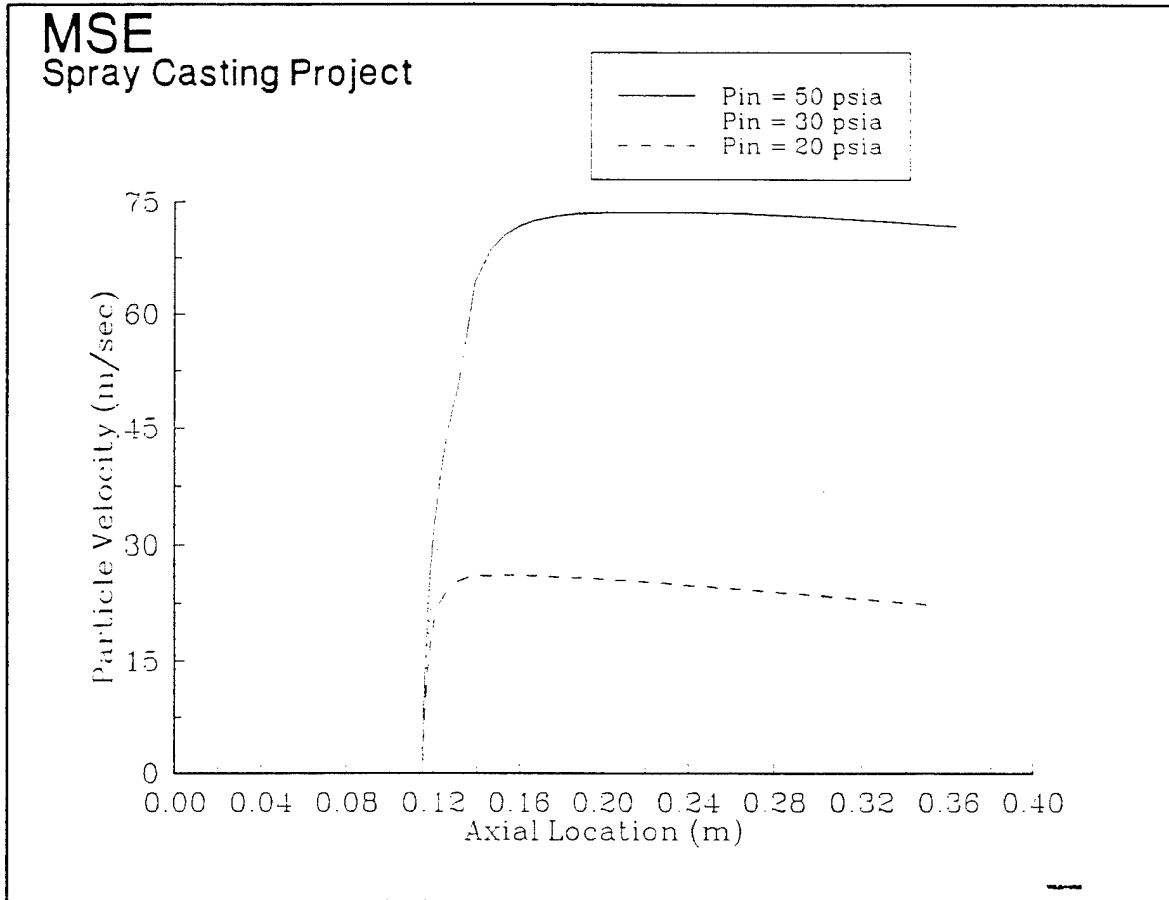
Figure 44. Particle velocity distribution.

Figure 45 shows the comparison between the computer modeling result and the data from the characterization testing on April 24, 1992. Figures 46 to 48 show the throat pressure against the inlet pressure under different temperature settings from the test data of test 3B1-CHAR-3. Figure 49 shows the modeling result against the test data of testing 3B1-CHAR-3.

The modeling results show agreement with the test data, especially at the low nozzle inlet pressure range. It seems the one-dimensional code hits its limit when the 3D effects in the nozzle flow become important at the higher nozzle inlet pressures.

The throat pressure does not respond fast enough with the inlet pressure changes. It is clear from the figures, that the throat-to-inlet pressure ratio does not maintain at constant value during sudden inlet pressure changes, but the ratio goes back to the steady-state value after staying at the same new inlet pressure value for a period of time. The throat pressure-to-inlet pressure ratio changes with the tundish/gas temperatures, but only by a small amount.

- One-Dimensional Spray Nozzle and Plume Examples: Figures 50 and 51 are used to illustrate the typical result of the data analysis. Figure 50 shows typical particle velocities for the different sizes of particles, and Figure 51 shows typical particle temperatures for the different sizes of particles.
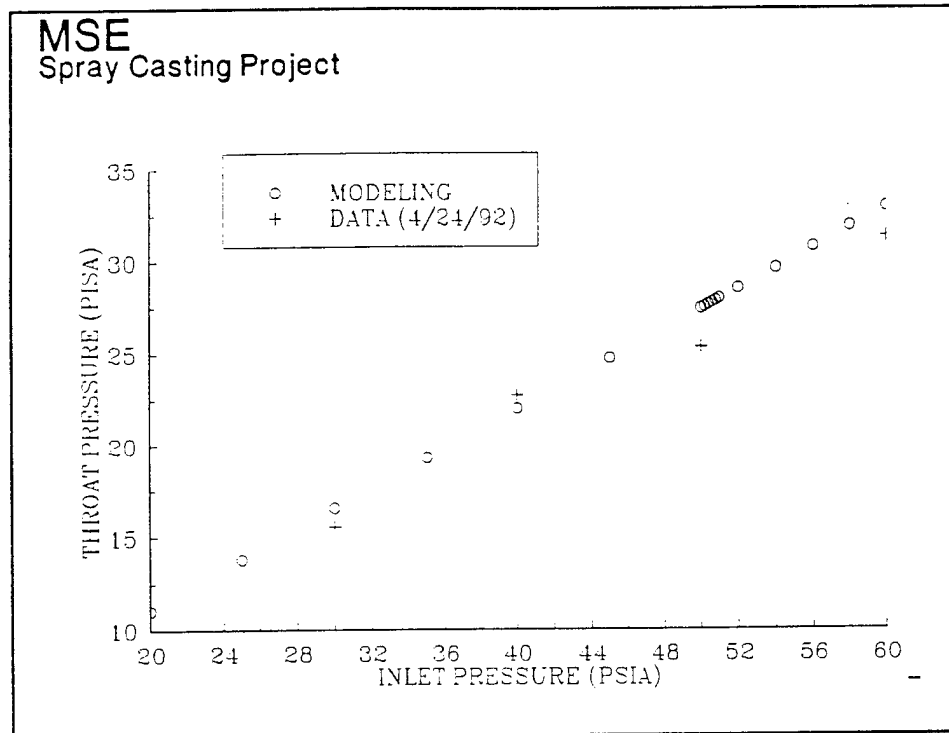
Figure 45. Inlet and throat pressure distribution.
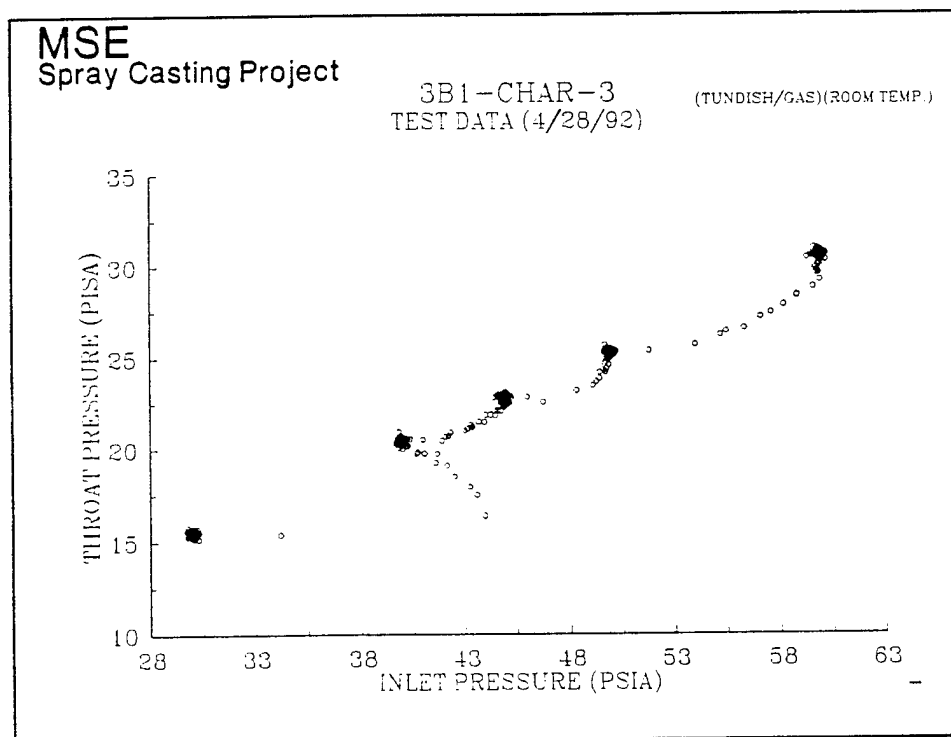
Figure 46. Inlet pressure vs. throat pressure (room temperature).

43
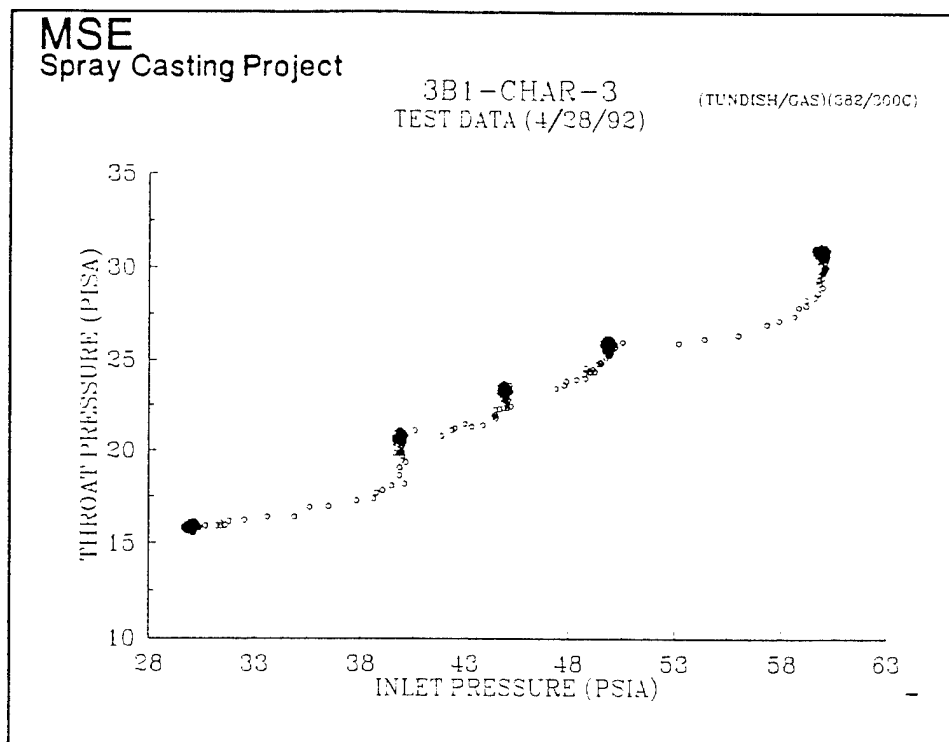
Figure 47. Inlet pressure vs. throat pressure (382/300C).
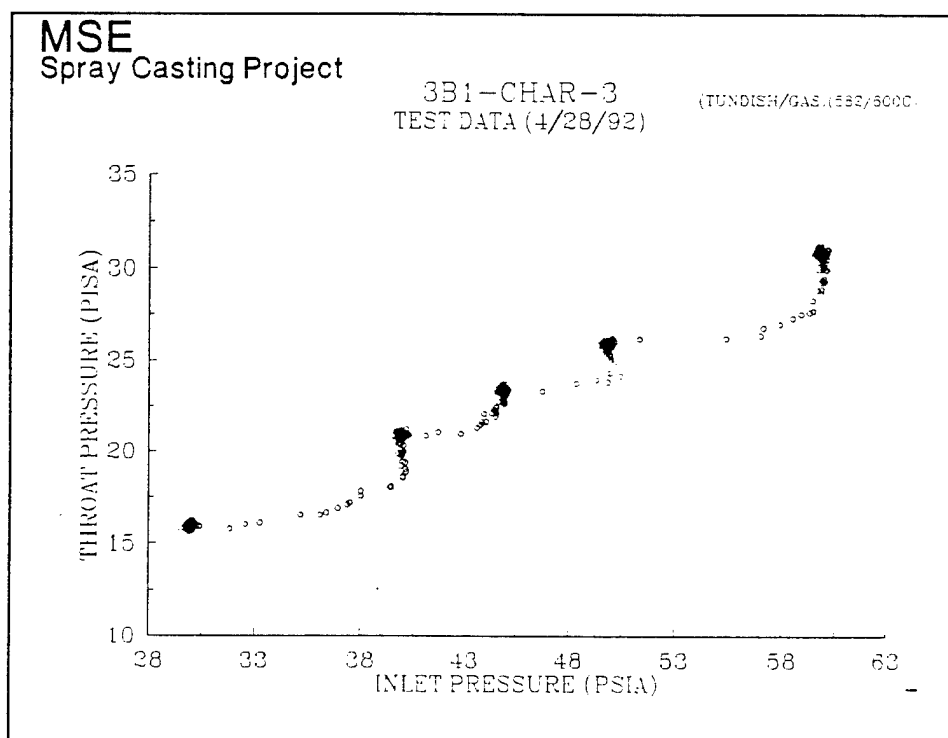
Figure 48. Inlet pressure vs. throat pressure (582/600C).

44
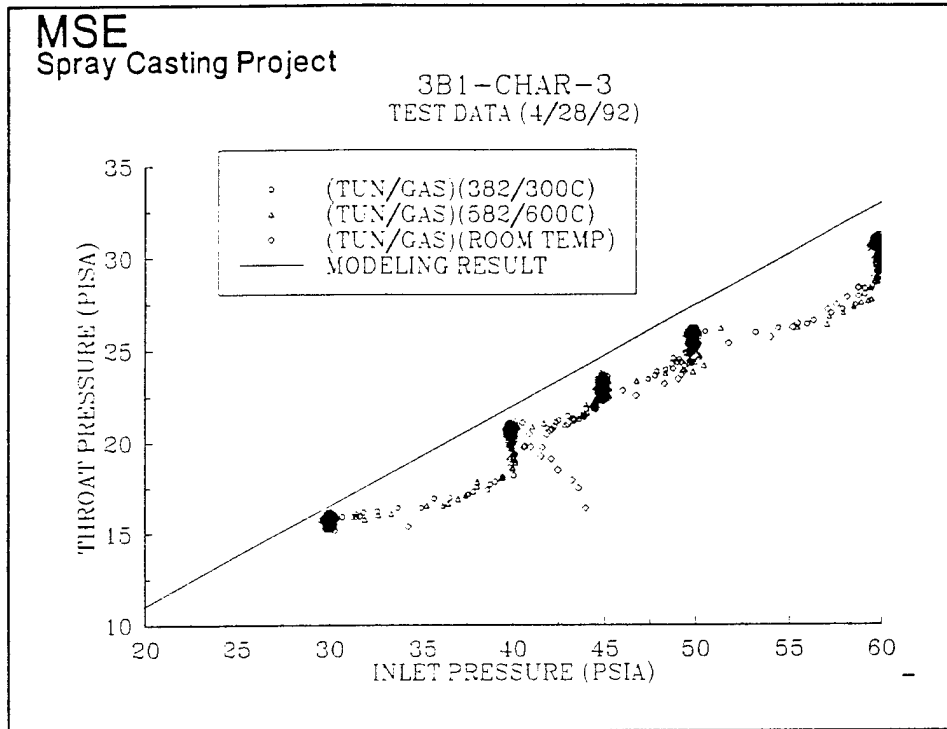
Figure 49. Inlet pressure vs. throat pressure.
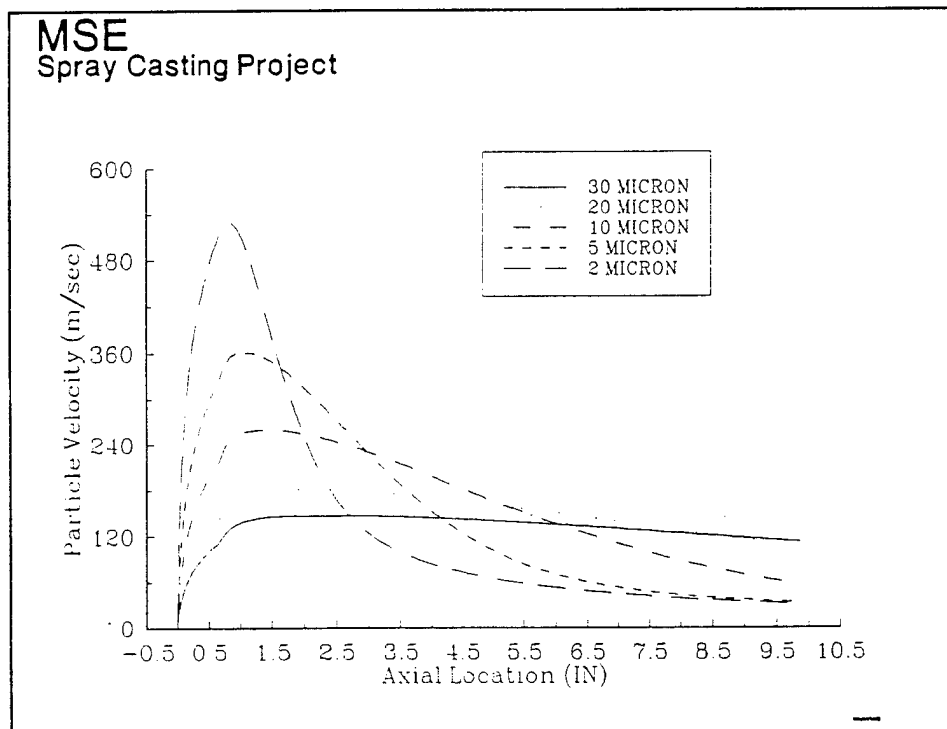
Figure 50. Particle velocities for different sizes of particles.

45
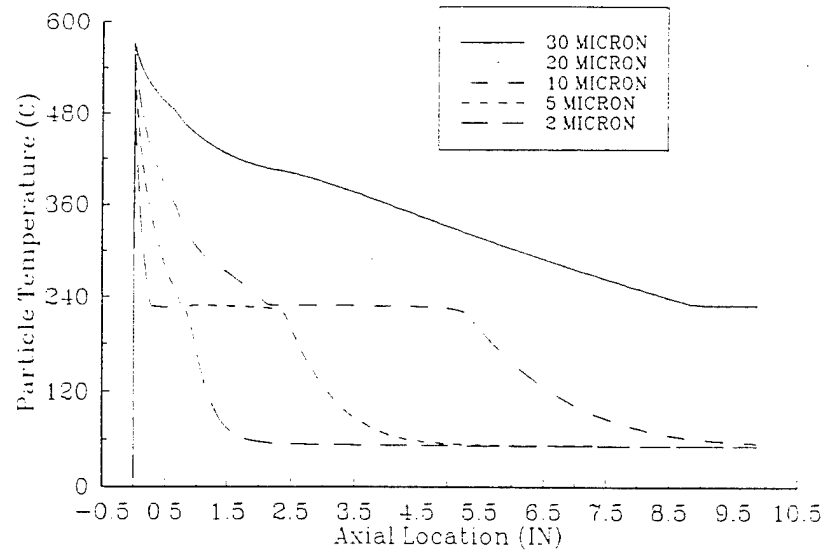
Figure 51. Particle temperature for different sizes of particles.

46

REFERENCES

1. Box, G. E. P.; Hunter, W. G.; and Hunter, J. S., *Statistics for Experimenter's*, Wiley Publishing, New York, NY, 1978.

2. American Ceramic Society, *Ceramic Source*, Vol. 7, p. 313, 1991.

3. Janna, William S., *Engineering Heat Transfer*, PWS Publishers, Boston, MA, 1986.

APPENDIX A

TubalCain Company
Report on Material Analysis: Tin Coatings

MSE Tin Data

	A	B	C	D	E	F	G	H
1	Sample	92-EXD-1	92-Train-10	92-3B-CR	92EXD-1-2	92EXD0201	92EXD0301	92EXD0401
2								
3	Base Metal Thk	3.325	3.315	3.278	3.347	3.317	3.294	3.289
4	B.M. + Coating	3.503	3.499	3.739	3.96	3.66	3.573/3.752	3.465/3.559
5	Coating Thk.	0.178	0.184	0.461	0.613	0.343	.277 - .456	.176 - .270
6	Mount Thickness	0.175	0.183	0.43	0.479	0.343	0.353	0.149
7								
8								
9	Max Grain Size	33μ	10μ	8μ	5μ	4μ	5μ	4μ
10	Mean Grain Size	3-5μ	2-3μ	2μ	3μ	3μ	2-3μ	2μ
11								
12	HV50 #1	15.4	16	14.6	13.8	14.7	15.1	11.6
13	HV50 #2	14.6	16.4	16.2	15.5	16.2	14.9	11.9
14	HV50 #3	14.4	16.3	15.6	16.2	16.5	16.2	12.3
15	HV50 #4	14.1	13.6	16.6	16.2	17	17.3	12.5
16	HV50 #5	14.7	13.8	13.8	16.7	16.1	17	12.7
17	HV50 #6	14.4	13.2	13.8	16.3	16.1	17	
18	HV50 #7	14.5	15.2	14.3	16.2	15.7	16.8	
19	HV50 #8	14.6	15	14.3	16.5	15.7	16.7	
20	HV50 #9	15.2	13.9	15.5	16.9	15.1	17.3	
21	HV50 #10	14.4	15.3	17	15.7	14.9	17.3	
22								
23	HV50 Average	14.6	14.9	15.1	16	15.8	16.5	12.2*
24								
25	Surf Prof/Base Metal	4.92	6.08	3.84	6.95	5.23	6.69	5.86
26								
27								
28	Maximum Porosity Size	None	None	None	None	None	None	None

A-1

MSE Tin Data

	I	J	K	L	M	N	O	P
1	92EXD0501	92EXD0601	92EXD0602	92EXD0701	92EXD0801	92ADH0101	92ADH0201	92ADH0301
2								
3	3.297	3.289	3.365	3.363	3.338	3.411	3.363	3.383
4	3.488/3.505	3.59	3.565	3.464	3.572	3.793	3.375	3.375
5	.191 - .208	0.301	0.2	0.101	0.234	0.382	0.012	0.012
6	0.226	0.264	0.172	0.117	0.2	0.4	0.0025	0.126
7								
8								
9	<1μ	7μ	3μ	8μ	3μ	<1μ	1μ	44μ
10	<1μ	2μ	1μ	1-2μ	1-2μ	<1μ	1μ	1μ
11								
12	16.5	18	14.9	16	16.9	18.4		15.5
13	20	17.6	16.2	16.6	18.2	18.1		16.4
14	19.3	18.6	16.9	16.4	17.6	18		15.4
15	18.9	18	16	15.4	17.1	17.6		14.6
16	19.2	16.8	16.8	16.4	19.5	17.5		16.7
17	19.7	18	16.8		19	18.1		17.3
18	19.1	18.1	16.2		18	19.8		16.7
19	19.3	16.4	16.4		18.9	17.5		18.1
20	18.5	15.1	16.2		18.1	17.6		16.7
21	18.9	17.3	16.2		16.1	17.4		16.7
22								
23	18.9	17.4	16.3	16.2	17.9	18		16.4
24								
25	4.63	6.23	5.86	4.63	6.96	6.9	5.92	4.39
26								
27								
28	None	None	None	None	None	None	None	None

A-2

90

MSE Tin Data

	Q	R	S	T	U	V	W	X
1	92ADH0401	92CPC0101	92CPC0201	92CPC0202	92CPC0301	92CPC0401	92CPC0402	92CPC0501
2								
3	3.382	3.427	3.415	3.449	3.462	3.506	3.452	3.5
4	3.485	3.537	3.616	3.649	3.534		3.703	3.873
5	0.103	0.11	0.201	0.2	0.062		0.251	0.373
6	0.125	0.108	0.199	0.182	0.074	0.025		0.383
7								
8								
9	60μ	2μ	6μ	<1μ	<1μ	1μ	25μ	<1μ
10	1μ	2μ	<1μ	<1μ	<1μ	1μ	3μ	<1μ
11								
12	16.4	12.4	19	15	*	*	14.4	16.1
13	17.5	13.7	19.5	15.6			13.9	16.6
14	17.9	13.2	15.9	16			14.1	16.1
15	15.7	13.4	18.3	18.2			14.2	17
16	17	14.5	17.8	18.3			15.5	16.7
17	16.4	12.6	18.5	18.7			15.2	16.4
18	18.2	13.4	19.5	18.1			14.9	15.1
19	17.4	12.3	19.5	17.6			14	15.5
20	18.5	10.8	20.1	17.1			13.1	15.7
21	17.7	12.4	19.6	16.8			13	16.1
22								
23	17.3	12.9	18.8	17.1	*	*	14.2	16.1
24								
25	6.19	4.65	4.92	5.88	3.62	3.77	5.26	5.4
26								
27								
28	None	None	None	None	None	10μ	None	None

A-3

MSE Tin Data

	Y	Z	AA	AB	AC	AD	AE	AF
1	92CPC0601	92CPC0702	92CPC0801	92CPC0901	92CPC1001	92CPC1101	92CPC1201	92CPC1301
2								
3		3.514		3.504	3.464			
4	3.573	3.639	3.63	3.693	3.582	3.528	2.964	2.935
5		0.125		0.189	0.118			
6	0.194	0.146	0.194	0.206	0.098	0.117	0.081	0.033
7								
8								
9	1μ	38μ	<1μ	20μ	43μ	6μ	2μ	1μ
10	1μ	3μ	<1μ	2μ	3μ	<1μ	<1μ	1μ
11								
12	13.3	16	15.6	15.4	*	*	*	*
13	12.9	17	16.7	14.5				
14	12.1	15.9	16.9	15.7				
15	13.2	16.5	16.4	13.6				
16	14.4	13.2	17.2	14.4				
17	13.8	15.8	17.7	14.9				
18	12.6	15.5	18.5	14.4				
19	13.5	15.8	17.5	14.5				
20	12.2	16.1	17.6	13.4				
21	14.2	14.7	15.9	13.8				
22								
23	13.2	14.1	17	13	*	*	*	*
24								
25	5.56	4.32	4.98	6.2	5.58	5.31	4.33	3.46
26								
27								
28	None	22μ	None	None	None	None	6μ	None

A-4

MSE Tin Data

	AG	AH	AI	AJ	AK
1	92CPC1401	92CPC1501	92CPC1601	92CPC1701	92CPC1801
2					
3			2.88	2.97	2.897
4	2.933	2.919	3.057	3.192	3.088
5			0.177	0.218	0.091
6	0.051	0.026	0.189	0.288	0.06
7					
8					
9	8μ	1μ	2μ	40μ	2μ
10	<1μ	1μ	1μ	3-4μ	1μ
11					
12	*	*	11.9	10.8	*
13			12.1	10.4	
14			12.3	10.6	
15			12.2	10.8	
16			12	10.9	
17			12.5	10.9	
18			12.3	10.9	
19			12.3	10.9	
20			12.2	10.5	
21			11.7	10.7	
22					
23	*	*	12.2	10.7	*
24					
25	4.19	3.49	4.64	4.18	5.36
26					
27					
28	None	None	None	None	34μ
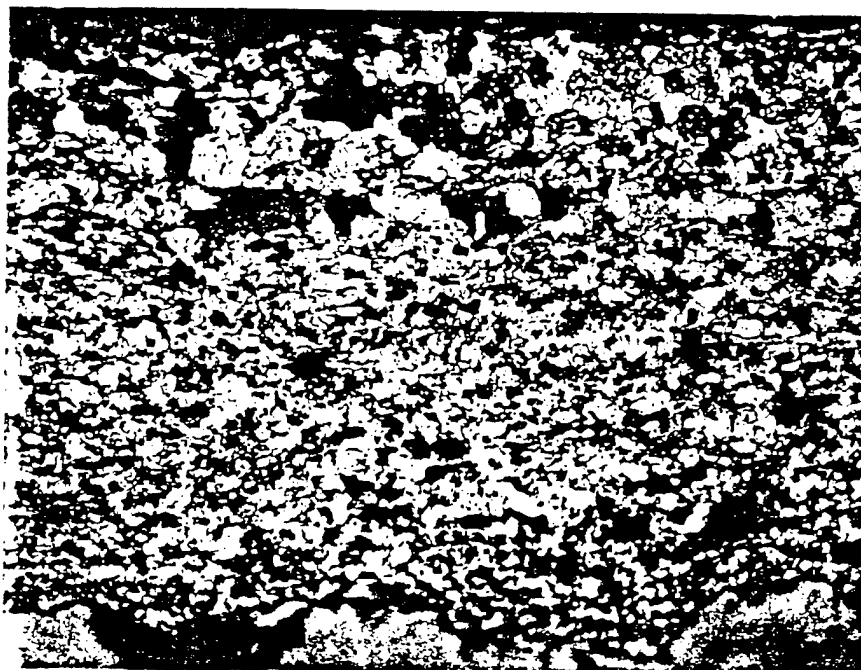
Figure 20. 92-EXP-1, Procedure #4. Etched with Keller's Reagent, 15 seconds. 500X
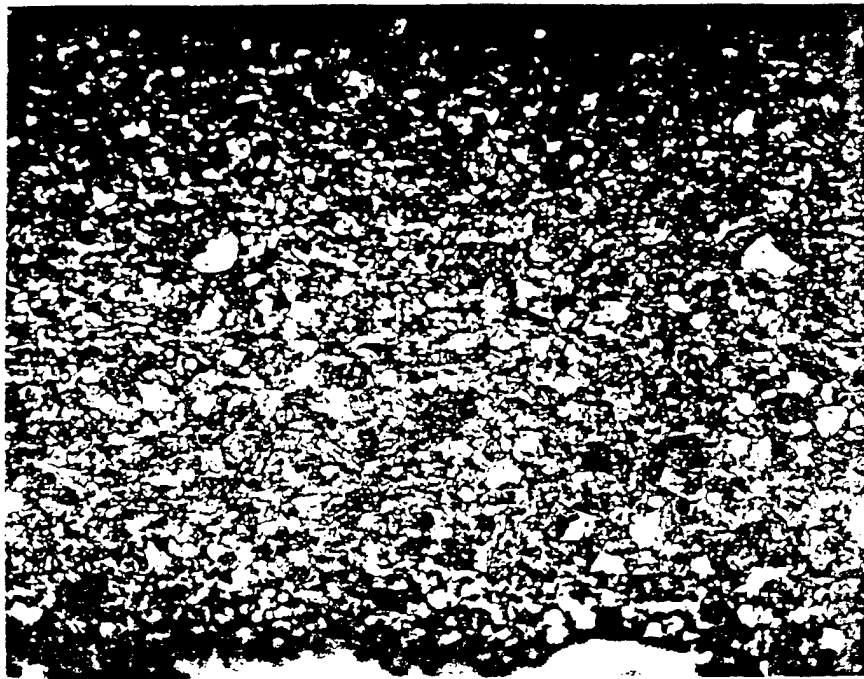
Figure 21. 92-Train-10, Procedure #4. Etched with Keller's Reagent, 15 Seconds. 500X.
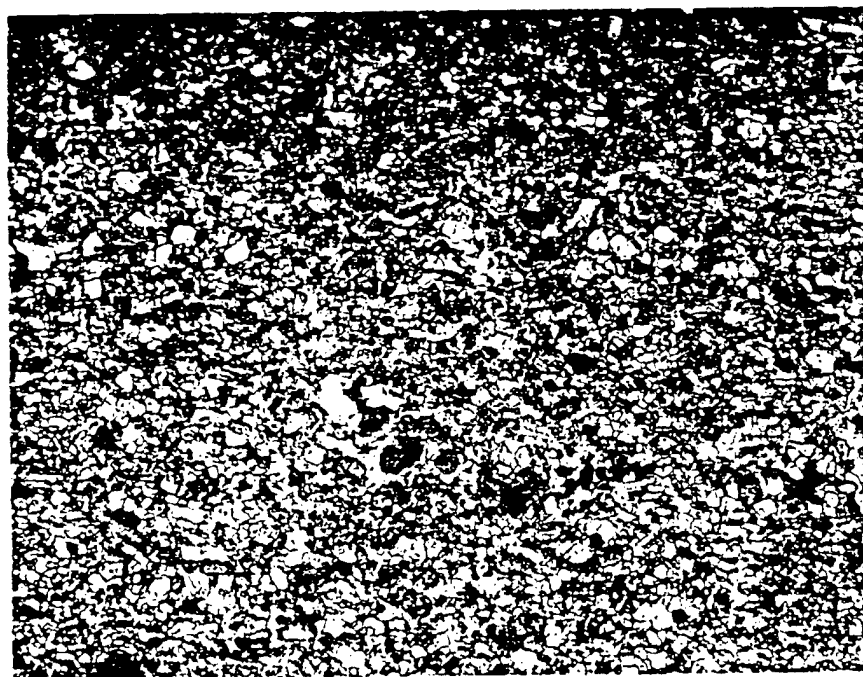
Figure 22. 92-3B-CR, Procedure #4. Etched with Keller's Reagent, 15 Seconds. 500X.

A-7
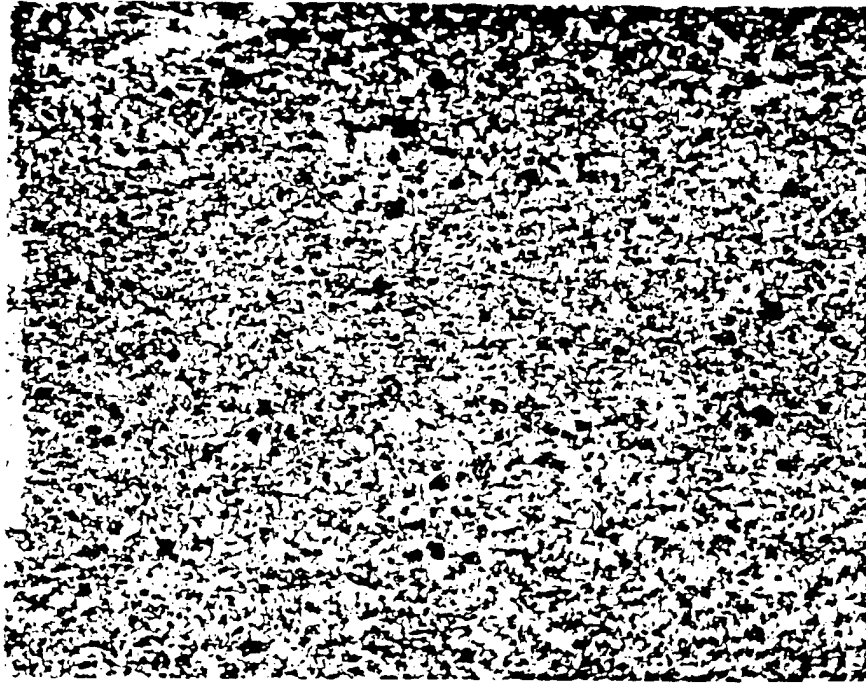
Figure 23. 92-EXD-1-2, Procedure #4. Etched with Keller's Reagent, 15 Seconds. 500X.
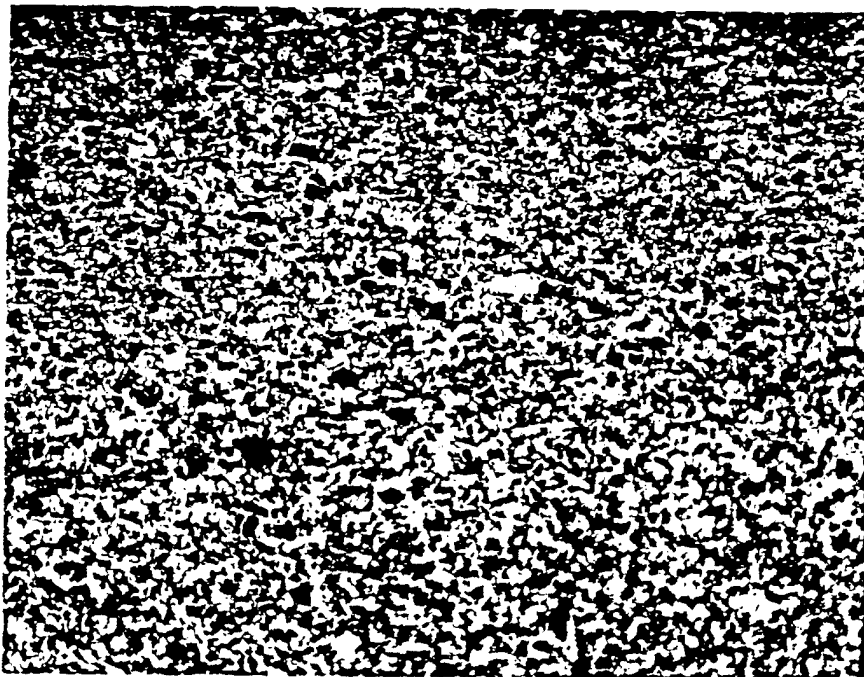
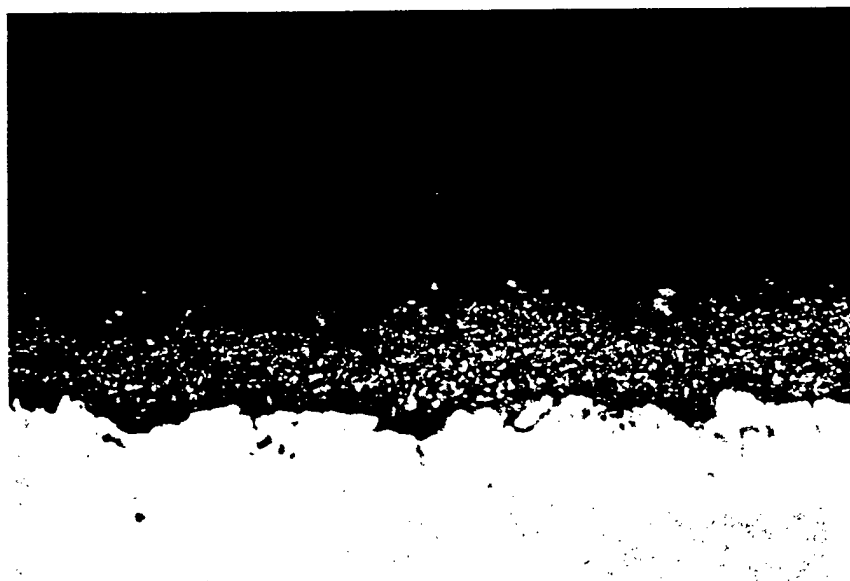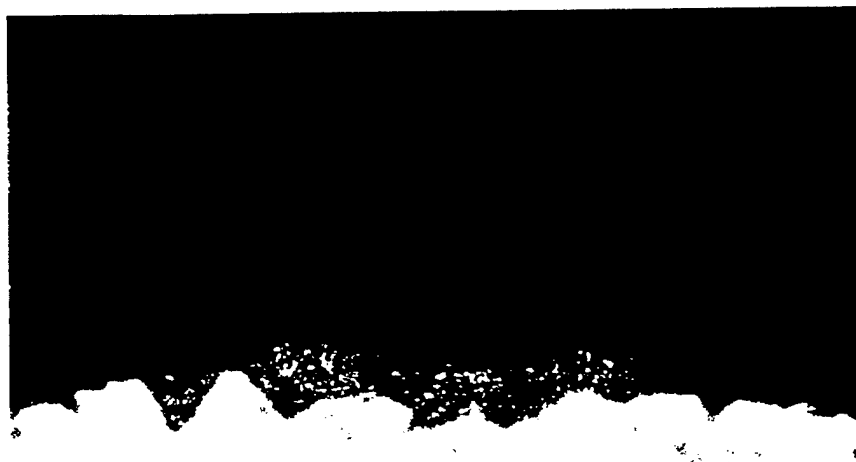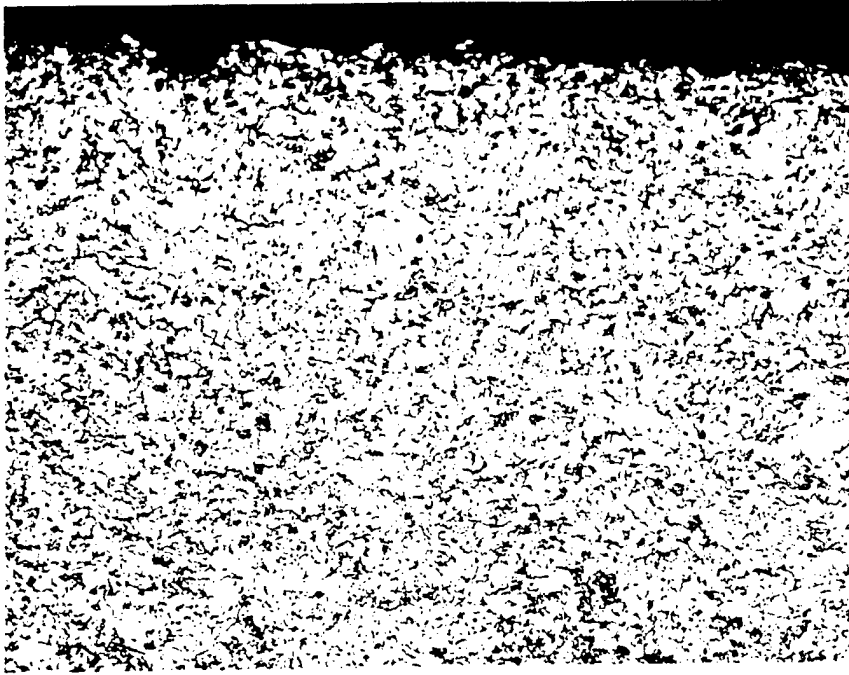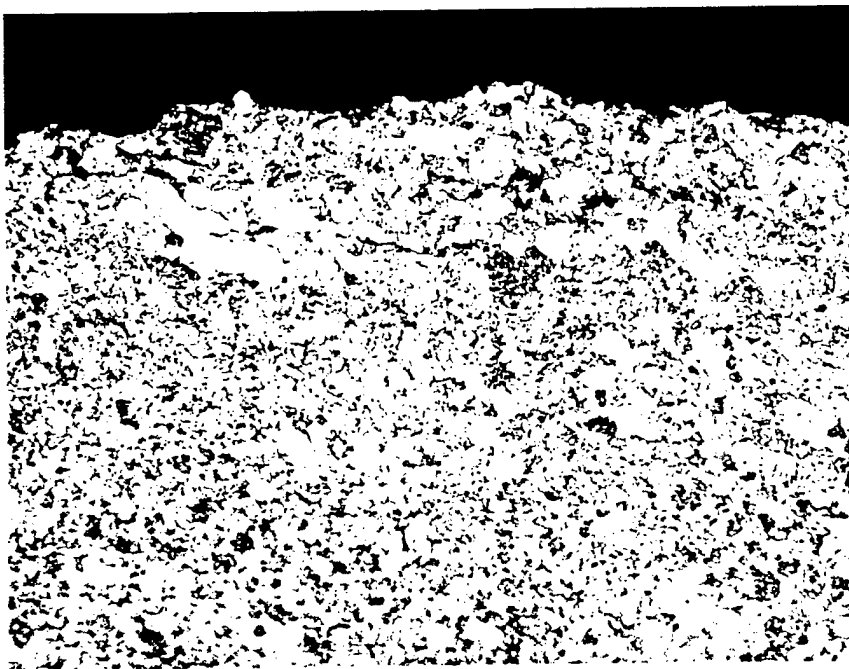Figure 24. 92EXD0201, Procedure #4. Etched with Keller's Reagent, 15 Seconds. 500X.

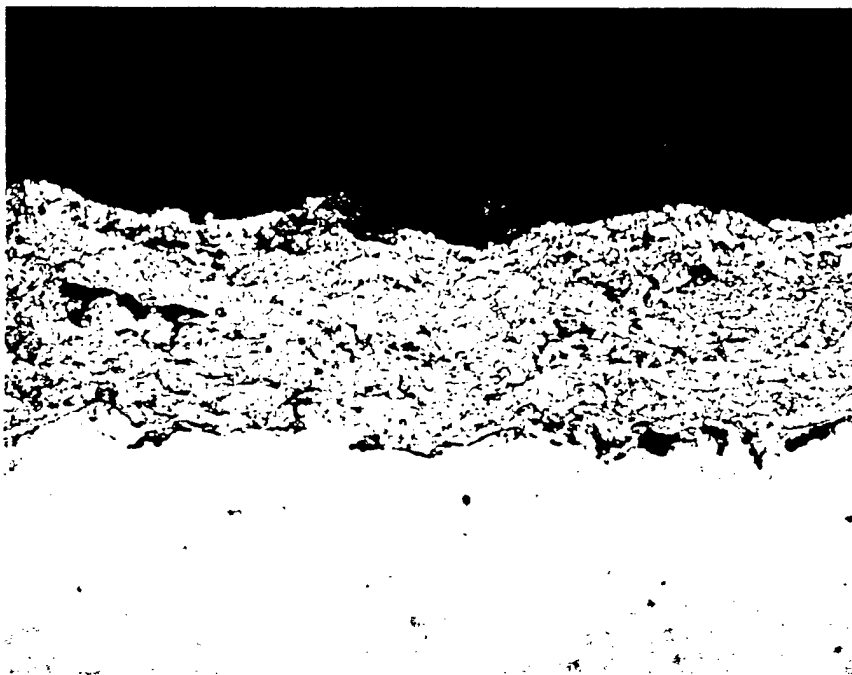Figure 25. 92-EXD0301, Procedure #4. Etched with Keller's Reagent, 15 Seconds. 500X.
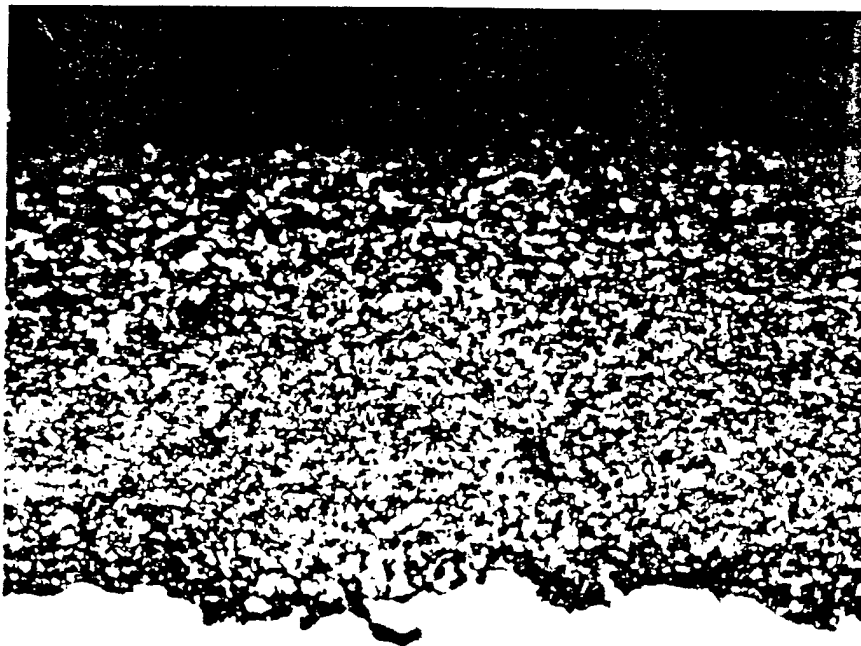
Figure 26. 92EXD0401, Procedure #4. Etched with Keller's Reagent, 15 Seconds. 500X.

A-9
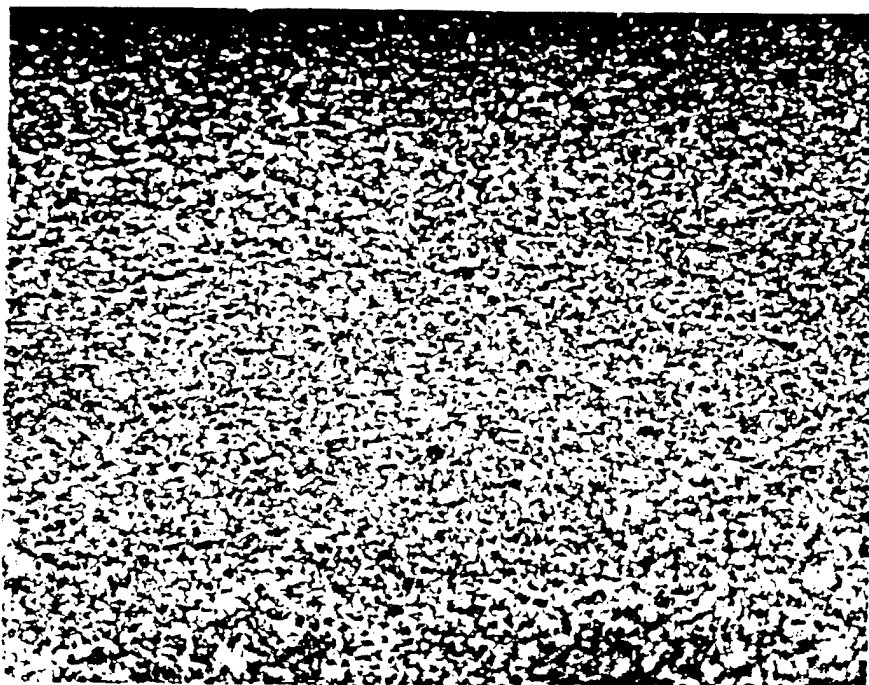
Figure 27. 92-EXD0501, Procedure #4. Etched with Keller's Reagent, 15 Seconds. 500X.
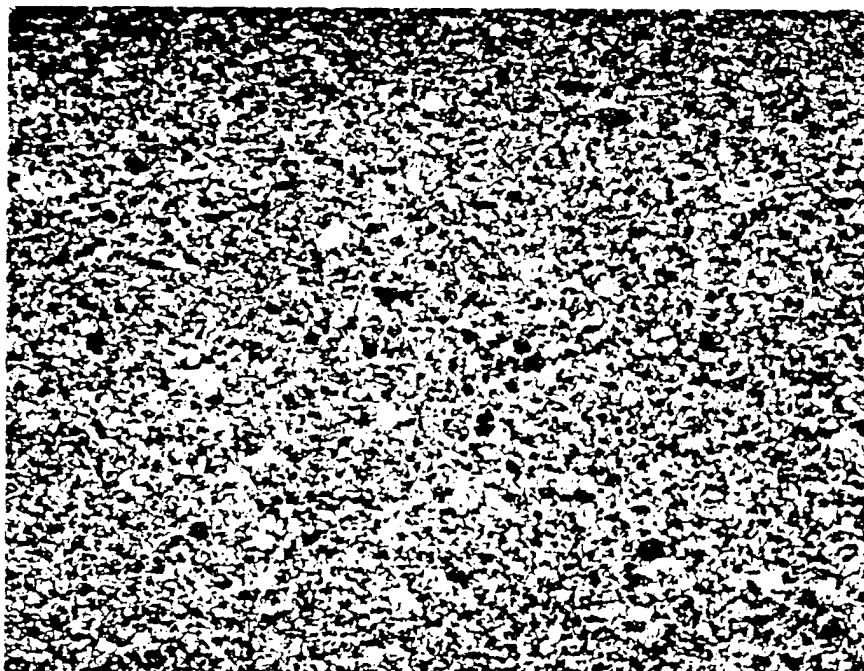
Figure 28. 92EXD0601, Procedure #4. Etched with Keller's Reagent, 15 Seconds. 500X.
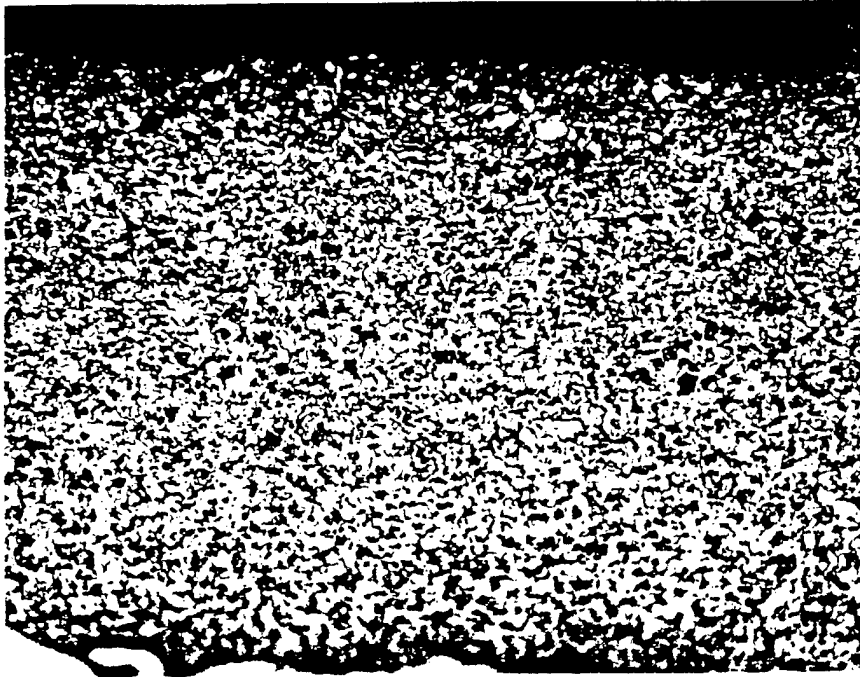
Figure 29. 92-EXD0602, Procedure #4. Etched with Keller's Reagent, 15 Seconds. 500X.
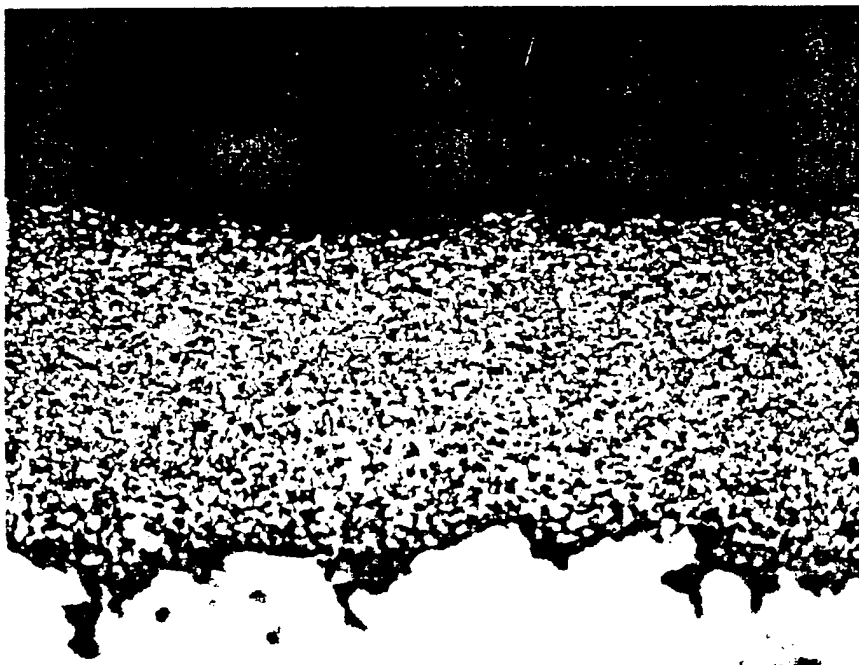
Figure 30. 92EXD0701, Procedure #4. Etched with Keller's Reagent, 15 Seconds. 500X.
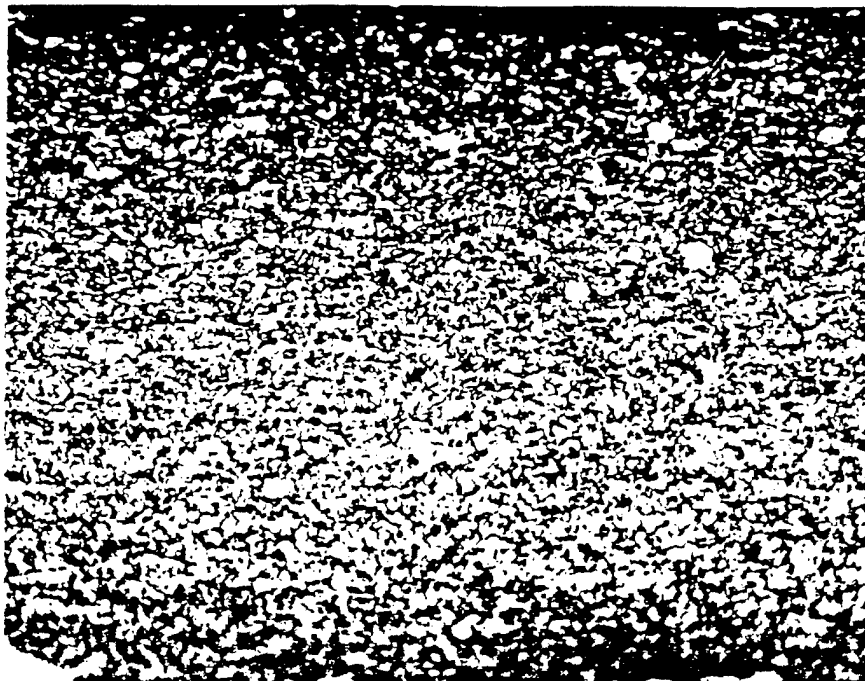
Figure 31. 92-EXD0801, Procedure #4. Etched with Keller's Reagent, 15 Seconds. 500X.
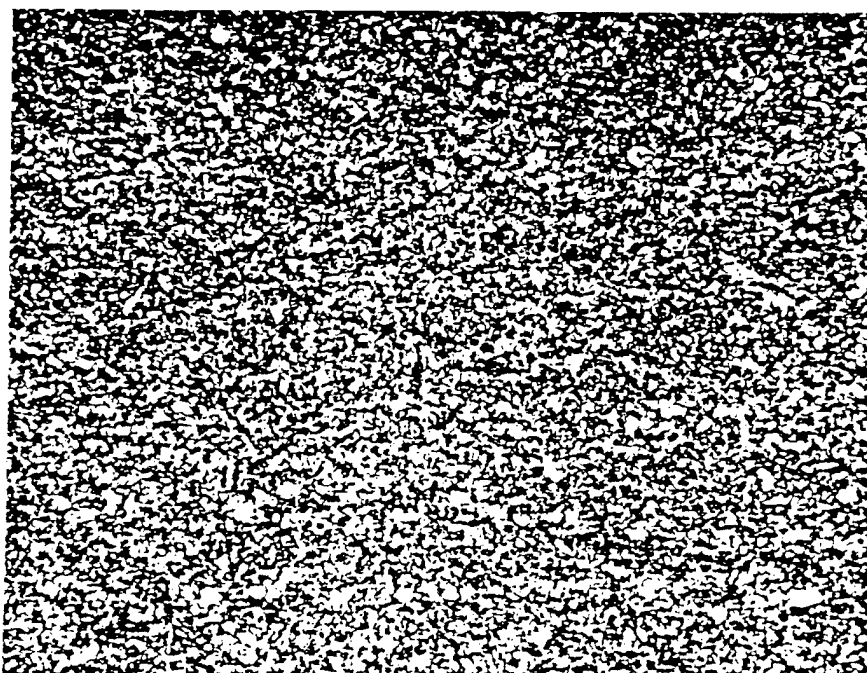
Figure 32. 92ADH0101, Procedure #4. Etched with Keller's Reagent, 15 Seconds. 500X.

A-12

Figure 33. 92ADH0201, Procedure #4. Etched with Keller's Reagent, 15 Seconds. 500X.

Figure 34. 92ADH0301, Procedure #4. Etched with Keller's Reagent, 15 Seconds. 500X.

A-13

Figure 35. 92ADH0401, Procedure #4. Etched with Keller's Reagent, 15 Seconds. 500X.

Figure 34. 92ADH0402, Procedure #4. Etched with Keller's Reagent, 15 Seconds. 500X.
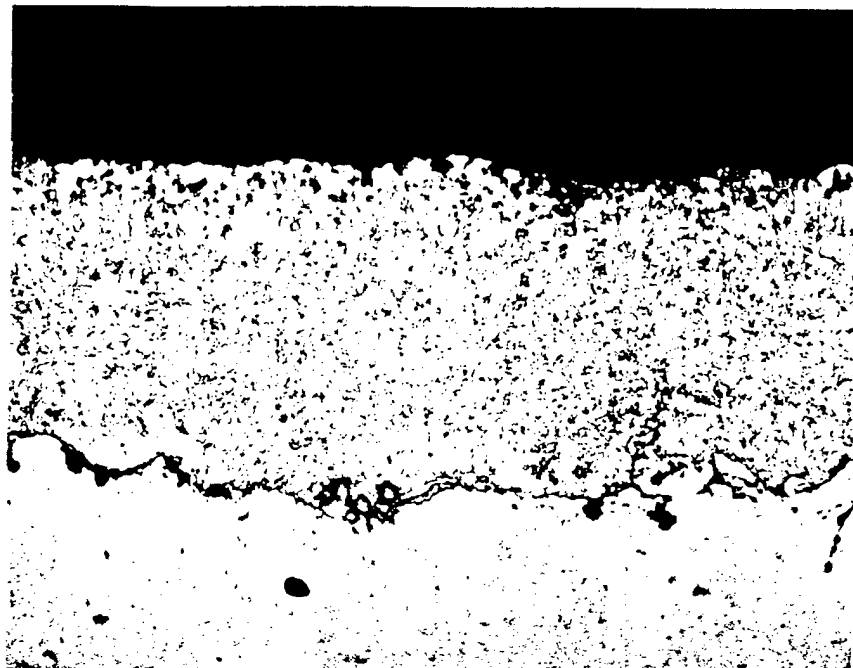
Figure 37. 92CPC0101, Procedure #4. Etched with Keller's Reagent, 15 Seconds. 500X.
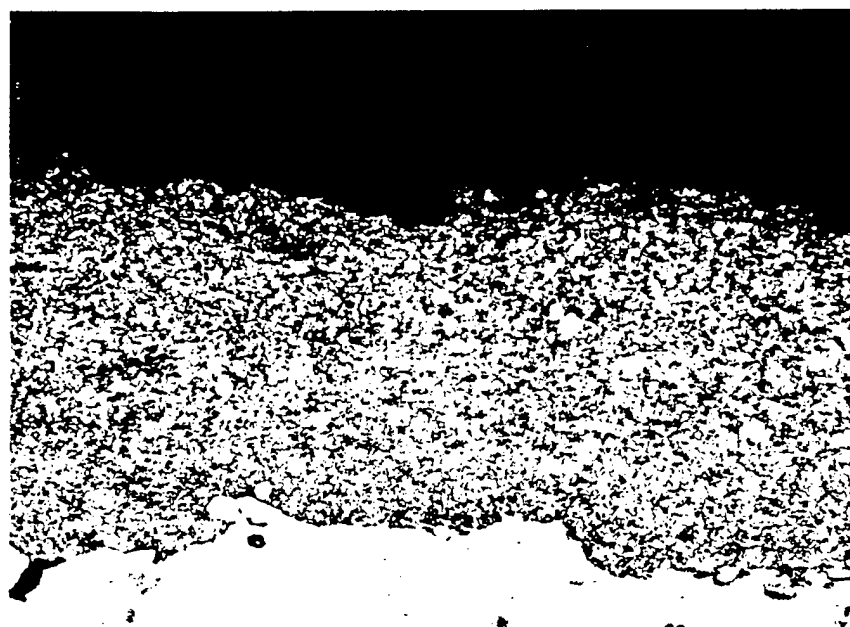
Figure 38. 92CPC0201, Procedure #4. Etched with Keller's Reagent, 15 Seconds. 500X.
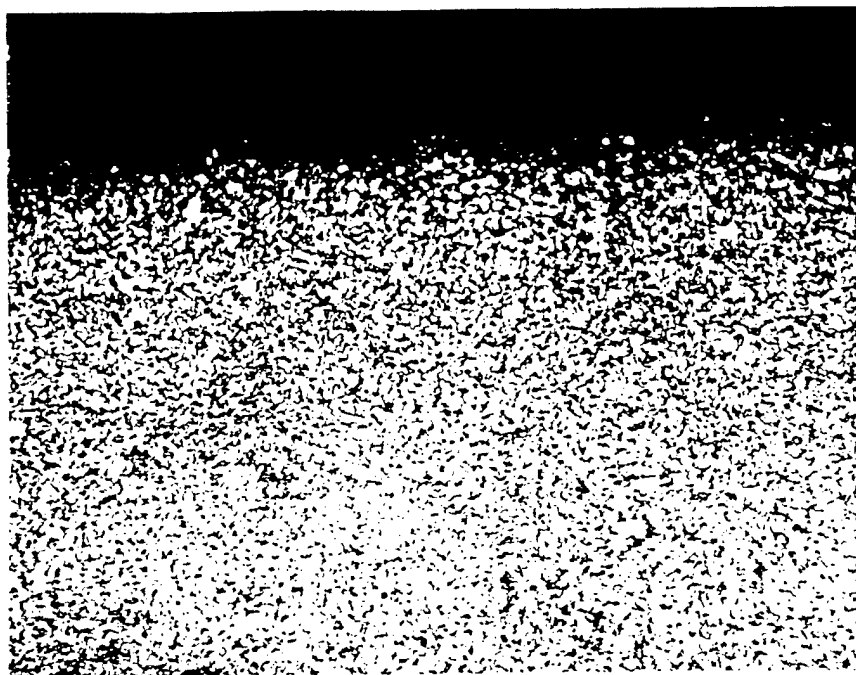
Figure 39. 92CPC0202, Procedure #4. Etched with Keller's Reagent, 15 Seconds. 500X.
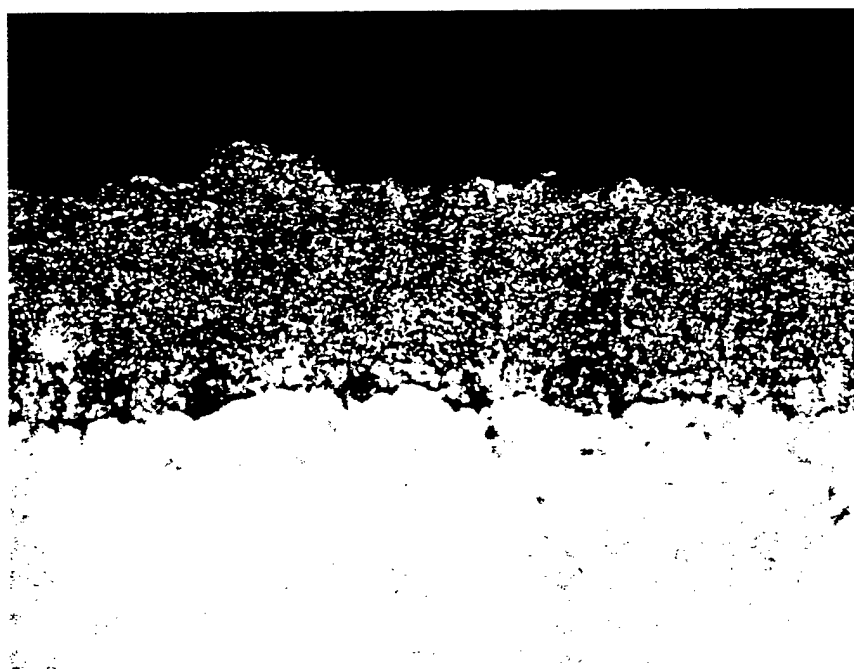
Figure 40. 92CPC0301, Procedure #4. Etched with Keller's Reagent, 15 Seconds. 500X.

A-16
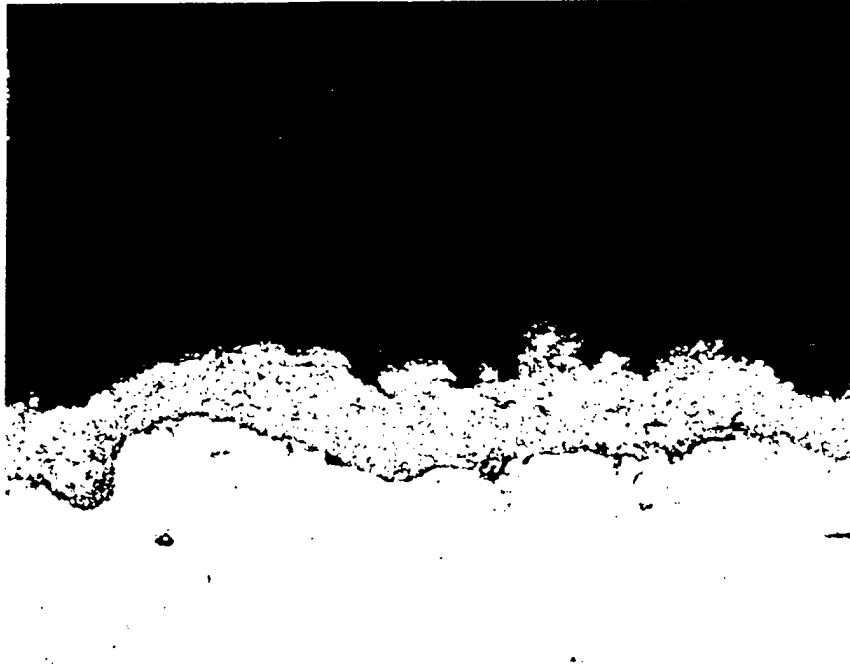
Figure 41. 92CPC0401, Procedure #4. Etched with Keller's Reagent, 15 Seconds. 500X.
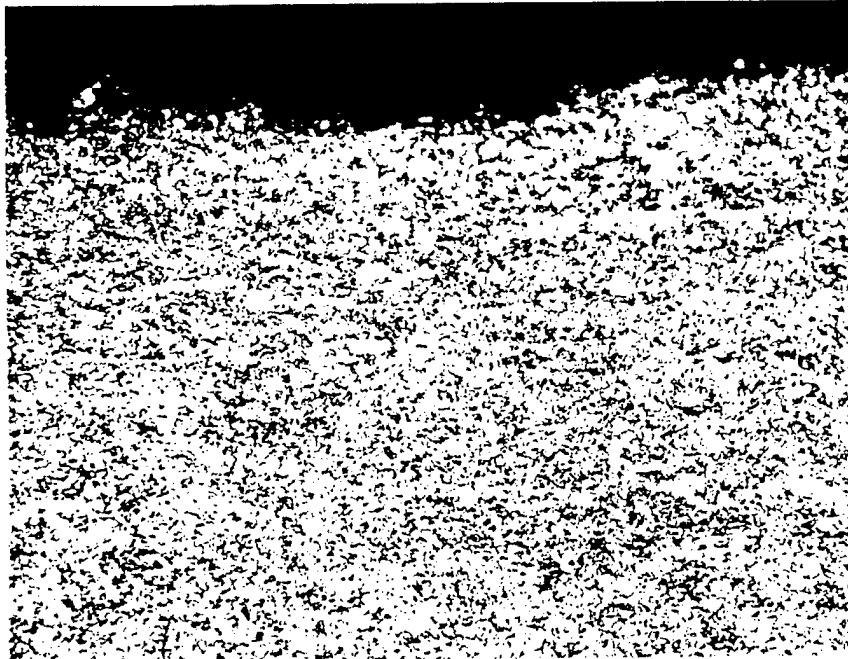
Figure 42. 92CPC0501, Procedure #4. Etched with Keller's Reagent, 15 Seconds. 500X.
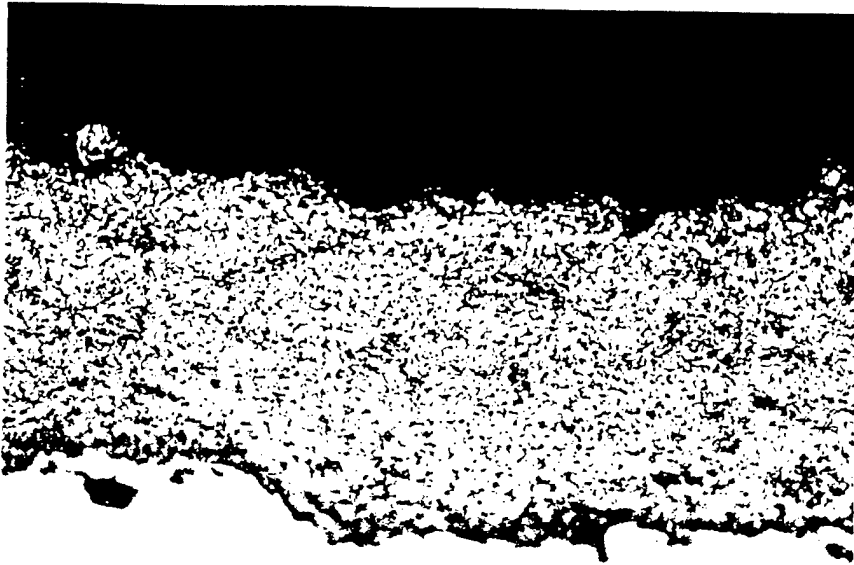
Figure 43. 92CPC0601, Procedure #4. Etched with Keller's Reagent, 15 Seconds. 500X.
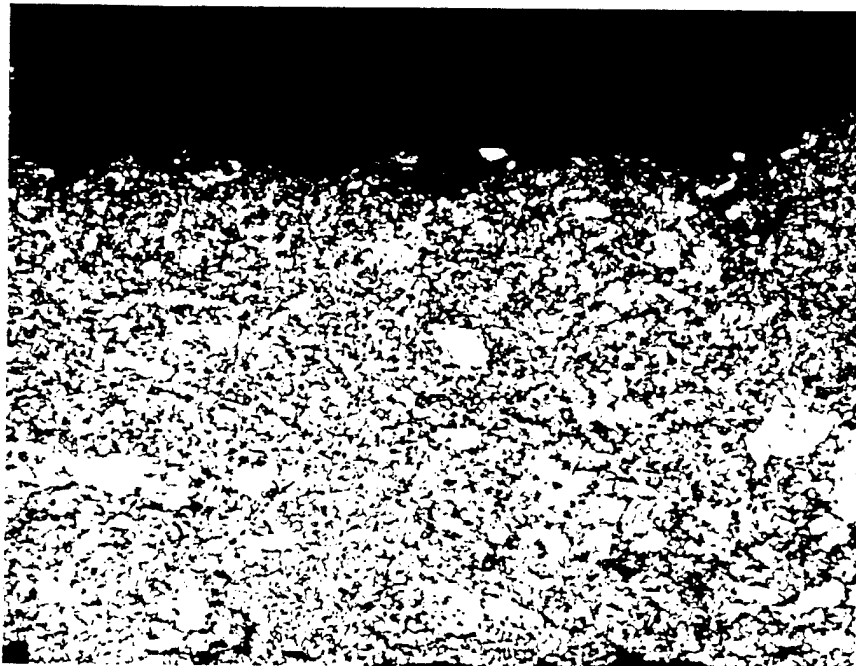
Figure 44. 92CPC0702, Procedure #4. Etched with Keller's Reagent, 15 Seconds. 500X.

Figure 45. 92CPC0801, Procedure #4. Etched with Keller's Reagent, 15 Seconds. 500X.
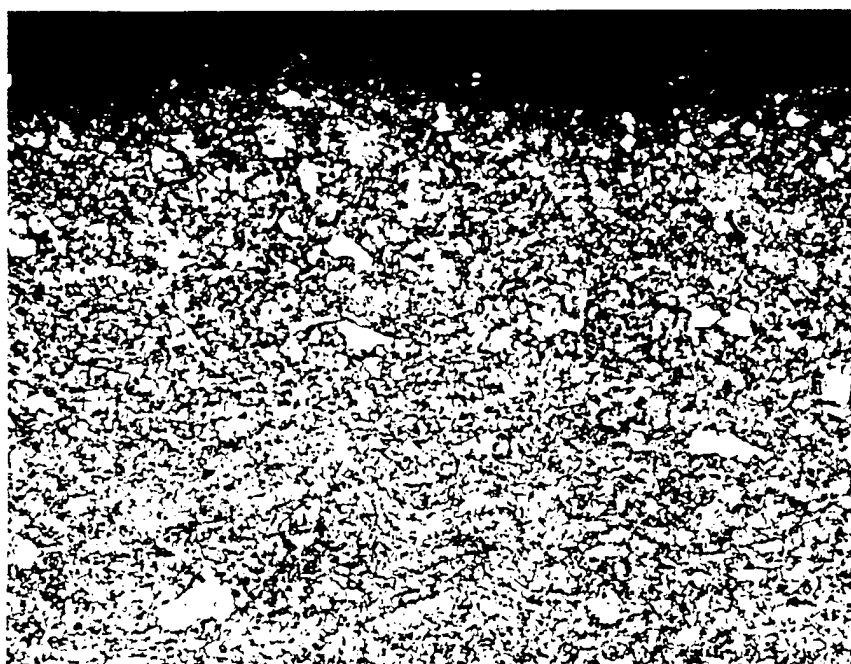
Figure 46. 92CPC0901, Procedure #4. Etched with Keller's Reagent, 15 Seconds. 500X.
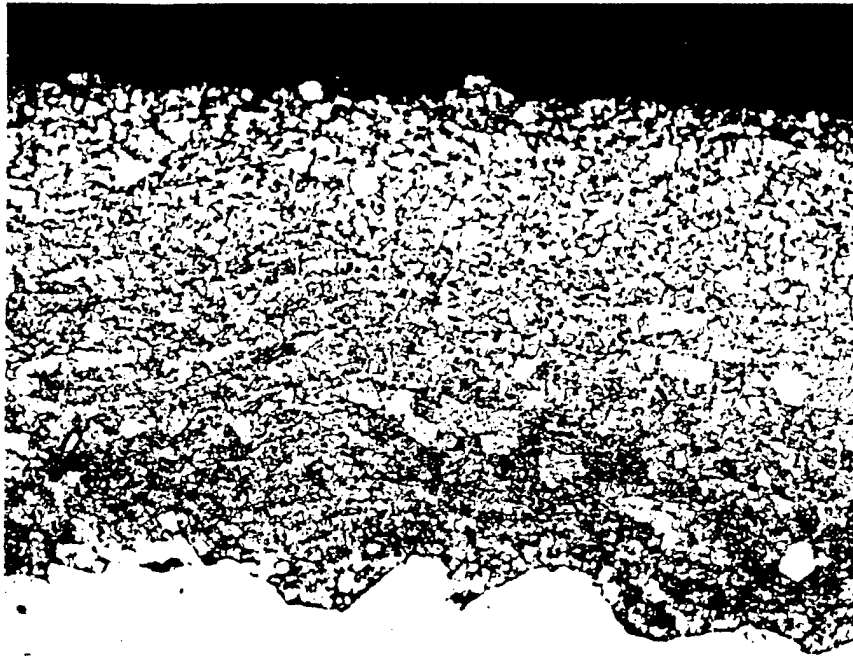
Figure 47. 92CPC1001, Procedure #4. Etched with Keller's Reagent, 15 Seconds. 500X.
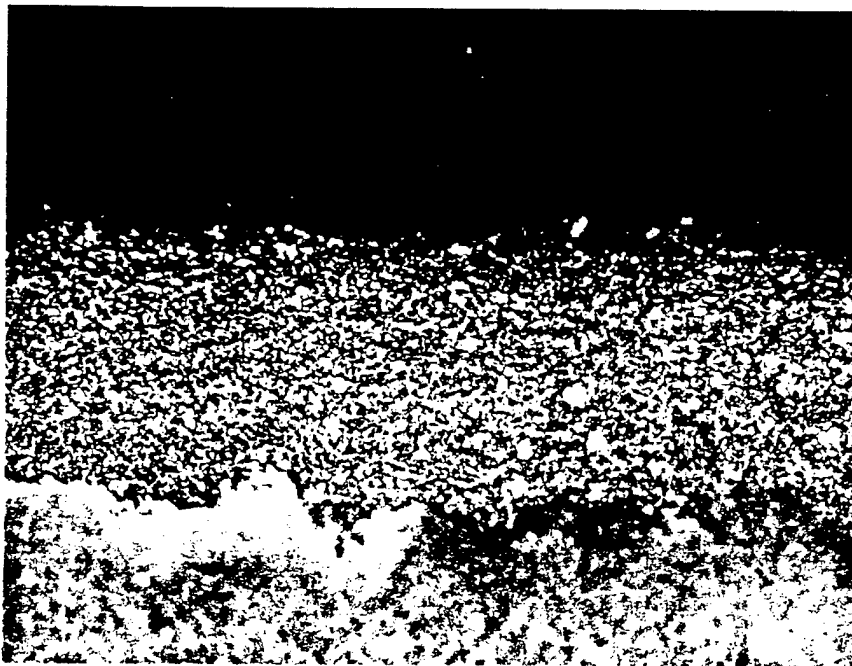
Figure 48. 92CPC1101, Procedure #4. Etched with Keller's Reagent, 15 Seconds. 500X.
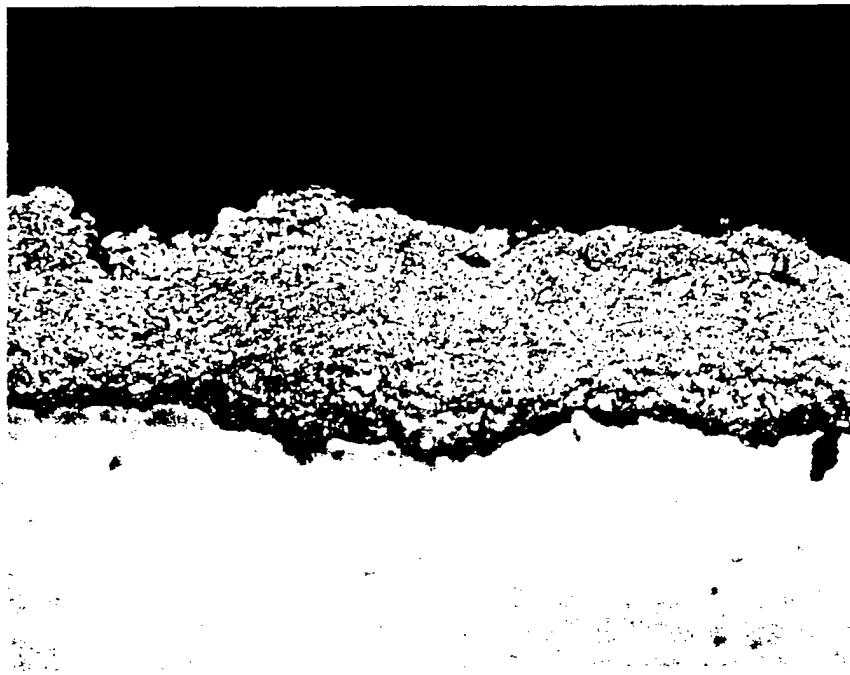
Figure 49. 92CPC1201, Procedure #4. Etched with Keller's Reagent, 15 Seconds. 500X.

Figure 50. 92CPC1301, Procedure #4. Etched with Keller's Reagent, 15 Seconds. 500X.

A-21

Figure 51. 92CPC1401, Procedure #4. Etched with Keller's Reagent, 15 Seconds. 500X.

Figure 52. 92CPC1501, Procedure #4. Etched with Keller's Reagent, 15 Seconds. 500X.

Figure 53. 92CPC1601, Procedure #4. Etched with Keller's Reagent, 15 Seconds. 500X.

Figure 54. 92CPC1701, Procedure #4. Etched with Keller's Reagent, 15 Seconds. 500X.

Figure 55. 92CPC1801, Procedure #4. Etched with Keller's Reagent, 15 Seconds. 500X.

APPENDIX B

SPRAY CASTING PROJECT
BOEING TEST SERIES REPORT

SPRAY CASTING PROJECT
BOEING TEST SERIES REPORT

Prepared by

MSE Inc.
P.O.Box 3767
Butte, Montana 59702

Prepared for

U.S. Department of Energy
Under Contract DE-AC22-88ID12735

April 1993

REVIEWS AND APPROVALS:

Prepared by: _John C. Tierney_ _____
Project Engineer

Reviewed by: _Ronald J. Gloran_ _____
Project Manager

Approved by: _M. H. Lewis for. N. EGAN_ _____
Program Manager

CONTENTS

1. INTRODUCTION

Phase III of the Spray Casting Project is being conducted by MSE Inc., at its Spray Casting Facility in Butte, Montana. The primary purpose of Phase III work is qualifying the spray casting process to meet Air Force standards and then designing, fabricating, and testing of pilot spray casting equipment that will be used at an Air Force Logistics and Service Center. The qualification process has been broken down into three separate test series: the MSE Test Series, the Boeing Test Series, and the Wright Laboratories Test Series; a separate report will be prepared for each of these series.

The Boeing Test Series used the experience of an aerospace company to evaluate sprayed coatings that were produced by MSE. This test series was an intermediate set of engineering tests that evaluated spray cast coatings before a final analysis and determination is made by the Air Force using the Wright Laboratory Test Series. The group of tests performed included fatigue, abrasion, adhesion, corrosion, hardness, internal stress, metallurgical, chemistry, and materials compatibility/workability. MSE sprayed 68 test samples that were then evaluated by the Boeing Defense and Space Group in Kent, Washington. In some of the tests, the sprayed coatings were compared directly to electroplated engineering chromium.

In addition to the tests evaluated at the Boeing Company, MSE conducted a short series of tests that evaluated the effects of specimen preheat and specimen configuration on adhesion strength.

The complete text of the Boeing report, *Spray Casting - Chromium Substitutes*, is included as Appendix A.

The data reports for the individual spray tests are available as a separate document.

2. ADDITIONAL MSE TESTING

In addition to the bend-type adhesion test specimens sprayed for Boeing, MSE also sprayed several series of coupons fabricated and tested per ASTM C 633-79, *Standard Test Method for Adhesion or Cohesive Strength of Flame Sprayed Coatings*. This type of adhesion/cohesion testing is quantitative, whereas the bend adhesion tests are qualitative. A numerical value was necessary because an evaluation of substrate preheating was also examined: a numerical value of adhesion strength is also useful for purposes of comparison to other thermal spray processes.

Substrate preheating was evaluated by spraying coupons without preheat and at two different preheat temperatures (140 and 220 °C). The test data is shown in Table 1 and is the average of six tests.

Table 1. Effect of preheat on adhesion/cohesion strength.

Test No.	Coating Thickness (in)	Preheat (°C)	Adhesion/Cohesion Strength (psi)	Standard Deviation (psi)
93WPB44	0.008	None	4,786	420
93WPB45	0.007	140	4,018	252
93WPB46	0.012	140	3,958	634
93WPB47	0.011	220	3,467	579

During the MSE Test Series, adhesion/cohesion bond strength data generated per ASTM C 633-79 was used extensively. However, a paper given by Han et al., during the 1992 International Thermal Spray Conference and Exposition reported that standard sample cylinders could have a 25 to 30 percent higher-than-average stress than what is assumed by ASTM C633-79 (Ref. 1); consequently, bond strengths would be underreported by a significant amount. With this condition in mind, MSE developed its own design of a sample cylinder; Figure 1 is a photograph of the before and after sample cylinders. The new configuration maintains an even stress distribution across the diameter of the sample cylinder.

A set of six of these new sample cylinders were sprayed under conditions identical to the samples sprayed in test 93WPB44; the data for this test is shown in Table 2. As can be seen from an analysis of the data, the new configuration had a substantially higher adhesion/cohesion strength.

Table 2. Adhesion/cohesion strength data for improved coupons.

Test No.	Coating thickness (in)	Adhesion/Cohesion Strength (psi)	Standard Deviation (psi)
93WPB53	0.009	8,068	682

From this data, it can be concluded that the adhesion/cohesion bond strength of Versalloy 50 sprayed onto an AISI 4340 substrate is comparable to other thermal spray processes.

121

2
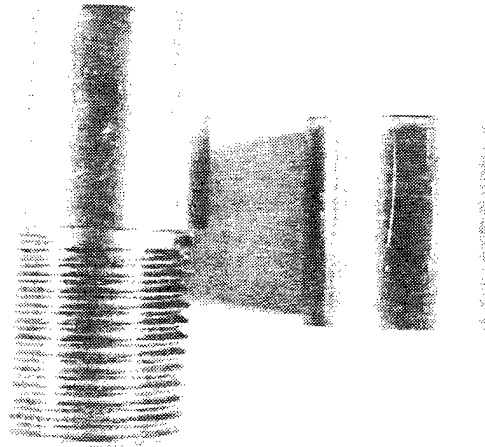
Figure 1. View of adhesion test coupons.

(The MSE-developed coupon is on the left, and the ASTM C633-79 coupon is on the right.)

The Boeing report also indicated that the abrasion resistance of the Versalloy 50 coatings was less than that of engineering chromium—that was certainly true for the chromium plating produced by Boeing. However, not all engineering chromium has abrasion resistance at that level. Volume 18 of the AMS Handbook, *Friction, Lubrication, and Wear Technology*, shows Taber abrasion results that are comparable to those achieved with Versalloy 50 (Taber Index ≈ 15) (Ref. 2). A copy of this reference is included as Appendix B.

3. REFERENCES

1. Han, Rybicki, and Shadely, *Bond Strength Testing of Thermal Spray Coatings Using ASTM C633-79: Effect of Specimen Size on Test Results*, Proceedings of the International Thermal Spray Conference & Exposition, Orlando, Florida, May-June 1992.

2. ASM Handbook, *Volume 18: Friction, Lubrication, and Wear Technology*, ASM International, October 1992, pp. 835-836.

APPENDIX A

Boeing Company Report

Boeing Defense & Space Group

P.O. Box 3999

Seattle, WA   98124-2499

Title: Spray Casting - Chromium Substitutes

Contract: 2-C138-C

Release Date: 3/15/93

Prepared by: S. M. Aasness   *J. M. Aasness* 3/15/93

Approved by: E. C. Groshart   3/16/93

Approved by: T. H. Luhman   *Thomas L. Luhman* 3/16/93

ABSTRACT

This report contains the results of tests performed on a coating of Versalloy 50 applied by MSE, Inc using the spray casting process developed by the Idaho National Engineering Laboratory (INEL) and the U.S. Air Force. These tests were performed by the Materials, Processes and Physics, Chemical and Environmental Technology organization within Boeing Defense & Space Group and included evaluation of chemical composition, microstructure, internal stress, hardness, corrosion resistance, abrasive wear resistance, adhesion, galvanic compatibility, and fatigue.

KEY WORDS

TABLE OF CONTENTS

LIST OF TABLES

LIST OF FIGURES

132

6

133

1.0 INTRODUCTION

This report contains the results of evaluation tests performed on a spray casted coating of Versalloy 50, applied by MSE, Inc with the objective of providing the engineering data which will allow the spray casting process to be used on flight hardware.

The spray casting process is unique in that the material to be applied is melted and, while in the molten condition, sprayed much like a paint to form a coating. Each droplet is kept molten through the spray system with hot gas and becomes solid only after entering the coating, where it cools very rapidly. Because of this uniqueness, the objective of the test program was to completely characterize the coating.

2.0   EXECUTIVE SUMMARY

Nine categories of tests were performed to characterize the coating including determination of coating composition and structure and evaluation of engineering properties.

2.1   Chemistry

The objective of this test was to compare the composition of the coating against the chemistry of the alloy from which it was derived to determine whether or not chemical reactions had taken place during the spraying process. The elemental composition of the coating was found to be essentially the same as that of the unsprayed alloy. It was not possible to determine the molecular composition of either the coating or the unsprayed alloy due to equipment limitations.

2.2   Metallurgical Tests

The objectives of this test were to: (a) determine the microstructure of the coating and compare it to the unsprayed alloy; (b) examine the surface of the coating for cracks; and (c) determine the effect of thermal cycles on (a) and (b).

The coating was determined to have an amorphous structure with a low level of porosity, in the range of 5 to 10%, and the unsprayed alloy was determined to have a crystalline structure. Surface cracks varying in length from 0.003" to 0.010" were detected in the three specimens examined. Thermal cycles of 375°F, 650°F and 900°F for 6 hours did not produce a detectable change in microstructure or appear to propagate or initiate cracks in the coating.

2.3   Internal Stress

The objective of this test was to determine the internal stress of the coating by measuring the bend induced in coated almen shot peen test strips. It was found that the grit blast operation, used as a substrate surface preparation, induced significant compressive stress in the test strips. Subsequent application of the coating partially relieved this stress. This may be attributed to tensile stress in the coating or thermal or mechanical impact effects of the spraying process. The net result was a slight residual compressive stress at the specimen surface.

137

2.4 Hardness Tests

Microhardness measurements were made on the coating in the as sprayed condition and following 6 hour bakes at 375°F, 650°F and 900°F. These measurements were compared to the unsprayed alloy and chrome plate. The microhardness of the as sprayed coating was significantly higher than the unsprayed alloy. There was no significant effect on microhardness following the 375°F bake, but the 650°F and 900°F bakes increased coating microhardness. The microhardness of chrome was slightly higher than the as sprayed alloy, but comparable the microhardness of the coating following a 650°F bake.

2.5 Corrosion Tests

The objective of this test was to compare the corrosion protection of the coating against chrome plate. Initial testing was performed in acetic acid salt spray, however, this test was found to be too aggressive. Testing was then performed in neutral salt spray using the worn taber abrasion panels. Red corrosion products were evident on both the spray coated and chrome plated panels after 24 hours and the test was discontinued after 48 hours. Corrosion was found to be more severe on the spray coated panels than the chrome plated panels. These results however, may have been influenced by the high surface roughness of the as sprayed coating. Additional testing was performed with the sprayed coating ground to a surface roughness comparable to chrome plate. Red corrosion products were again evident on both coatings after 24 hours in neutral salt spray and testing was discontinued after 48 hours. Corrosion was again found to be more severe on the spray coated than the chrome plated panels.

2.6 Abrasion Test

The objective of this test was to compare the abrasive wear resistance of the coating against chrome plate. The Taber wear index was found to be significantly higher for the sprayed coating, both lubricated and unlubricated, than for chrome plate, indicating that the coating is not as resistant to abrasive wear.

2.7 Adhesion Tests

The objective of this test was to qualitatively evaluate the adhesion of the coating to various substrates. The sprayed coating was found to have excellent adhesion to 15-5 PH stainless steel and 6Al4V titanium. Some loss of adhesion occurred with AISI 4130 and AISI 1018 steel substrates.

2.8 Materials Compatibility and Workability Tests

The objective of this test was to evaluate the condition and adhesion of the coating following shot peen, and to determine the galvanic compatibility of the coating with various substrates.

Following shot peen, coating condition and adhesion to 15-5 PH stainless steel was comparable for the sprayed coating and chrome plate, with no loss of adhesion evident. Adhesion of the sprayed coating to 6Al4V titanium was superior than chrome plate, with only slight loss appearing on two of the three specimens tested. Adhesion of the sprayed coating to heat treated 4340M was not as high, with some degree of adhesion loss noted on all three specimens compared to no adhesion loss for chrome plate.

The coating was found to be galvanically compatible with 15-5 PH stainless steel, with neither the coating nor the substrate preferentially corroded. The coating was found to be galvanically incompatible with 4340M steel, with the substrate preferentially corroded indicating that the coating is more galvanically noble. The coating was found to be galvanically incompatible with 6Al4V titanium, with the coating preferentially corroded indicating that the coating is more galvanically active.

2.9 Fatigue Test

The objective of this test was to compare the effect of the coating on the fatigue strength of high strength steel and against chrome plate. Chrome plate was found to significantly reduce the fatigue strength of heat treated AISI 4130 steel by as much as an order of magnitude. The coating however, was found to enhance the fatigue strength, possibly due to residual compressive stresses.

3.0 APPROACH

The sprayed (coating) material was to be completely characterized. This approach was taken because of the nature of the coating process. The material to be sprayed is melted and, while in the molten condition, sprayed much like a paint to form a coating. Each droplet is kept molten through the spray system with hot gas and becomes solid only after entering the coating, where it cools at a very fast rate. The fast cooling rate leaves the metal in what is believed to be an amorphous state, which is not the normal physical state of the metal alloy before spraying.

The following tests were conducted to characterize the sprayed coating.

3.1 Chemistry

The sprayed coating's composition was checked against the chemistry of the alloy from which it was derived. This analysis was to confirm whether or not chemical reactions had taken place during the melt phase. Three tests were made using the metallurgical tests specimens referenced in section 3.2.2 (a).

3.2 Metallurgical Tests

The objectives of this test were to: (a) determine the microstructure of the coating and compare it to the unsprayed alloy; (b) examine the surface of the coating for cracks; and (c) determine the effect of thermal cycles on (a) and (b).

3.2.1 Specimen

Serial No.	Description
A1 - A4, A6 and A7	1" x 5" x .095" (AISI 1018 steel) sprayed to a thickness of 0.003 inch, minimum

3.2.2   Tests

(a) Specimens A1, A2 and A3 were cross sectioned, polished, etched and microscopically analyzed within an inch of one end using 500X magnification to show any grain structure or porosity. A sample of the unsprayed alloy was used as a standard.

(b) Specimens A4, A6 and A7 were examined for surface cracks and photographed using 200X magnification.

(c) The specimens examined in (b) were placed in an air oven, one at each of the following conditions:

Specimen	Thermal Cycle
A4	375±25° F for 6 hours
A7	650±25° F for 6 hours
A6	900±25° F for 6 hours.

(d) The surface of each baked specimen was re-examined for cracks and photographed using 200X magnification.

(e) The baked specimens were cross sectioned, polished, etched and microscopically analyzed using 500X magnification and compared with (a) and the alloy standard.

3.3   Internal Stress

The objective of this test was to determine the internal stress of the coating by measuring the bend induced in coated almen shot peen test strips.

3.3.1   Specimen

Serial No.	Description
1-12	Almen shot peening test strips per MIL-S-13165, Type A. Coating thickness 0.003 inch minimum.

Test strip specifications:

Analysis of stock - SAE 1070
Cold rolled spring steel
Square edge number one (on 3" edge)
Finish - blue temper (or bright)
Uniformly hardened and tempered to 44-5- HR_C
Flatness - ± .0015" arc height as measured on gauge shown in MIL-S-13165

3.3.2 Test

Twelve specimens were spray coated as near as possible to the same conditions. Internal stress in the coating will cause the strips to bend. The bend on each sprayed specimen was measured and recorded as well as two specimens which were grit blasted only. The specimens were placed in an air oven at the following conditions:

Specimen	Thermal Cycle
1,2,3	375±25 °F for 3 hours
4,5,6	650±25 °F for 3 hours
7,8,9	Confirmation set
10,11,12	None

After cooling, the extent of bending was remeasured. If the stresses were thermally relieved, the specimen would have relaxed and the bend reduced. Thermal cycling of these sets was repeated until maximum relaxation was achieved. Specimens 7, 8 and 9 were exposed to the total time/temperature cycle affecting the maximum relaxation to confirm results.

3.4 Hardness Tests

The objective of this test was to compare the microhardness of the coating to the unsprayed alloy and chrome plate.

3.4.1 Specimen

Serial No.	Description
B1, B2	1" x 5" x 0.095" (AISI 1018 steel) sprayed to a thickness of 0.010 inch minimum.

143

3.4.2 Test

Each specimen was cut in half and the four resulting samples were placed in an air oven at:

Specimen	Thermal Cycle	
B2-1	375±25° F	for 6 hours
B2-2	650±25° F	for 6 hours
B1-1	900±25° F	for 6 hours
B1-2	One control specimen.	

Following cooling, a minimum of three microhardness measurements were made on each of the four specimens and compared to the unsprayed alloy standard and to chrome.

3.5 Corrosion Tests

The objective of this test was to compare the corrosion protection of the coating against chrome plate.

3.5.1 Specimen

Serial No.	Description
1-8, 10	3" x 5" x 0.047" (AISI 1018 steel) coated to 0.004" to 0.0075".

3.5.2 Test

The specimens were baked as follows:

Specimen	Thermal Cycle
1,2,3	(3) at 375±25° F for 3 hours
4,5,6	(3) at 650±25° F for 3 hours
7,8,10	(3) unbaked.

Specimens 3, 6 and 10 were subsequently bent along the center line to take a 30° set. The nine specimens were placed in an acetic acid salt spry maintained and operated according to ASTM G85. The planned test time was 21 days (500 hours), checked daily for the first three days, then checked periodically. The first sign of rust was noted and the test discontinued when severe corrosion had occurred.

3.6 Abrasion Test

The objective of this test was to compare the abrasive wear resistance of the coating, unlubricated and with dry film lubricant applied, against chrome plate.

3.6.1 Specimen

Serial No.	Description
1-6	4" x 4" x 0.040 (AISI 4130 steel) coated to 0.003 inch minimum.
C1-C3	4" x 4" x 0.040 (AISI 4130 steel) chrome plated to 0.003 inch minimum.

3.6.2 Test

The sprayed specimens were thermally conditioned at 375±25° F for 3 hours. Three of the sprayed alloy specimens, serial numbers 1, 2 and 3 and the three chrome plated specimens were tested according to Fed. Test Method Standard 141C, Method 6192.1 using a 1000 gram load with a CS17 wheel.

The remaining three sprayed specimens were coated with dry film lubricant MIL-L-46101 to a thickness of 0.0005±0.00002 inch, then tested using the same load and wheel as above.

3.7 Adhesion Tests

The objective of this test was to qualitatively evaluate the adhesion of the coating to various substrates.

3.7.1 Specimen

AISI 1018 steel:	3" x 5" x 0.047 panel
AISI 4130 steel:	Fatigue specimen per drawing 23-1803
17-4PH stainless, hardened to 200 ksi:	1/2" x 6" round rod
4340M steel, heat treated to 280-300 ksi:	1/2" x 6" round rod
6Al4V titanium, annealed:	3/4" x 6" round rod

3.7.2   Test

AISI 1018 steel   The specimen was bent on a one inch diameter and examined for peeling or flaking of the coating from the substrate

AISI 4130 steel   A saw was used to cut through the coating
17-4PH cres bar   to the substrate. The edges of the cut
4340M steel bar   were then probed with a sharp instrument
6Al4V titanium bar   and the coating examined for loss of adhesion.

3.8   Materials Compatibility and Workability Tests

The objective of this test was to evaluate the condition and adhesion of the coating following shot peen, and determine the galvanic compatibility of the coating with various substrates.

3.8.1   Specimen

1/2" round rod 6 inches in length, coated to a thickness of 0.006 to 0.010 inch. Six specimens of each of the following materials required:

Serial No.	Description
S1-S6	17-4 PH stainless steel, hardened to 200 ksi
1-6	4340M steel, heat treated to 280-300 ksi
T1-T6	6Al4V titanium, annealed.

3.8.2   Test

The sprayed specimens were thermally conditioned at 375±25° F for 3 hours.

(a) Three sprayed specimens of each base material (serial numbers S1-S3, 1-3 and T1-T3) were shot peened according to MIL-S-13165 using hardened steel shot to the intensity of 0.010A. The specimens were then examined for adhesion loss and condition of the coating.

(b) The remaining specimens were ground according to the following sketch and evaluated for the ability to grind:

63 √

0.003 to 0.005

▨ Removed Metal
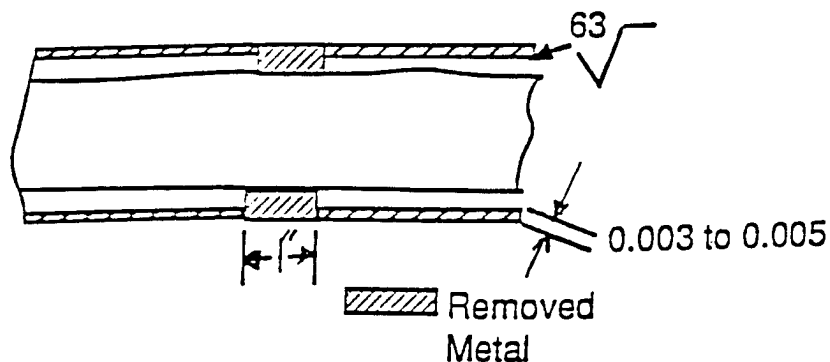
(c) The machined specimens in (b) were placed in a neutral salt spray cabinet maintained and operated according to ASTM B117 for 21 days (500 hours). Following salt spray, the specimens were evaluated for pitting and undercutting at the dissimilar metal junction.

3.9 Fatigue Test

The objective of this test was to evaluate the effect of the coating on the fatigue strength of high strength steel and compare to chrome plate.
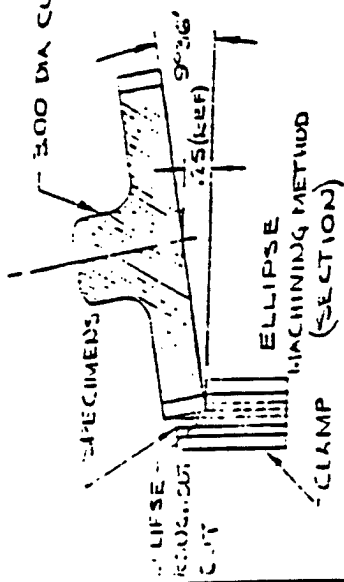
3.9.1 Specimen

Specimens were fabricated per drawing 23-1803 (Figure 3.9-1) using 1/8" sheet AISI 4130 steel, heat treated to 180-200 ksi.

Serial No.	Description
1-15	Specimens sprayed to a thickness of 0.0045±0.001" on the flat sides only; edges left bare.

Serial No.	Description
C1-C15	Specimens chrome plated all around to a thickness of 0.0062±0.0005 mils.
31-42	Specimens left bare.

Figure 3.9-1. Drawing of fatigue specimen.

3.9.2   Test

S/N curves (maximum stress vs. fatigue life cycles) were generated for bare, metal sprayed and chrome plated specimens. Testing was performed under the following conditions:

    Loading - Axial
    Stress ratio: 0.10
    Temperature - Room Temp
    Environment - Air
    Specimen Surface Condition: As sprayed/ plated
    Shot peen prior to coat / plate: None.

4.0 RESULTS

4.1 Chemistry

The composition of the coating and of the unsprayed alloy was evaluated using an electron microprobe and was determined to be as shown in Table 4.1-1 and in Figures 4.1-1 through 4.1-4. Images of the surface topography taken during composition analysis appear in Figures 4.1-5 through 4.1-7.

Table 4.1-1. Composition of Sprayed and Unsprayed Versalloy 50 Alloy

Element	Weight Percent					
	Sample A1	Sample A2	Sample A3	Average	Unsprayed	Unsprayed Literature Values
Nickel	76.96	72.58	77.61	75.72	71.04	Balance (74.08)
Chromium	14.62	13.87	14.24	14.24	21.43	13.5
Silicon	3.63	3.34	3.76	3.58	3.35	4.25
Iron	4.79	10.21	4.39	6.46	3.97	4.25
Carbon	-	-	-	-	-	0.67
Boron	-	-	-	-	-	3.25

The composition of the coating compared closely with the literature values of the unsprayed alloy. The analysis of the unsprayed alloy sample, however, showed a higher chrome content than the literature values. The cause of this discrepancy is not obvious and additional samples should be analyzed to confirm this result.

4.2 Metallurgical Tests

(a)   Cross sections of the as sprayed coating appear in Figures 4.2-1 through 4.2-6. As expected, the coating was found to be essentially amorphous in the as sprayed condition. Spherical particles are present in the coating which appear to be metal particles that solidified prior to surface impact. There is a low level of porosity in the coating, in the range of 5 to 10%, which in some cases is associated with the spherical particles. There are a few dark vertical

PRZ Correction 20.00 KV 40.00 deg
).of Iterations = 3

Element   K-ratio   Z   A   F   ZAF   Atom%   Wt%
  Ni-K   0.752   1.003   1.020   1.000   1.023   73.54   76.96
  Cr-K   0.155   1.016   1.020   0.909   0.943   15.56   14.62
  Si-K   0.017   0.890   2.349   0.999   2.090   7.15   3.63
  Fe-K   0.054   1.017   1.029   0.850   0.891   4.75   4.79
                                                     Total= 100.00%

BCRG Microprobe Lab.   R.G.Racus   TUE 22-SEP-92 05:47
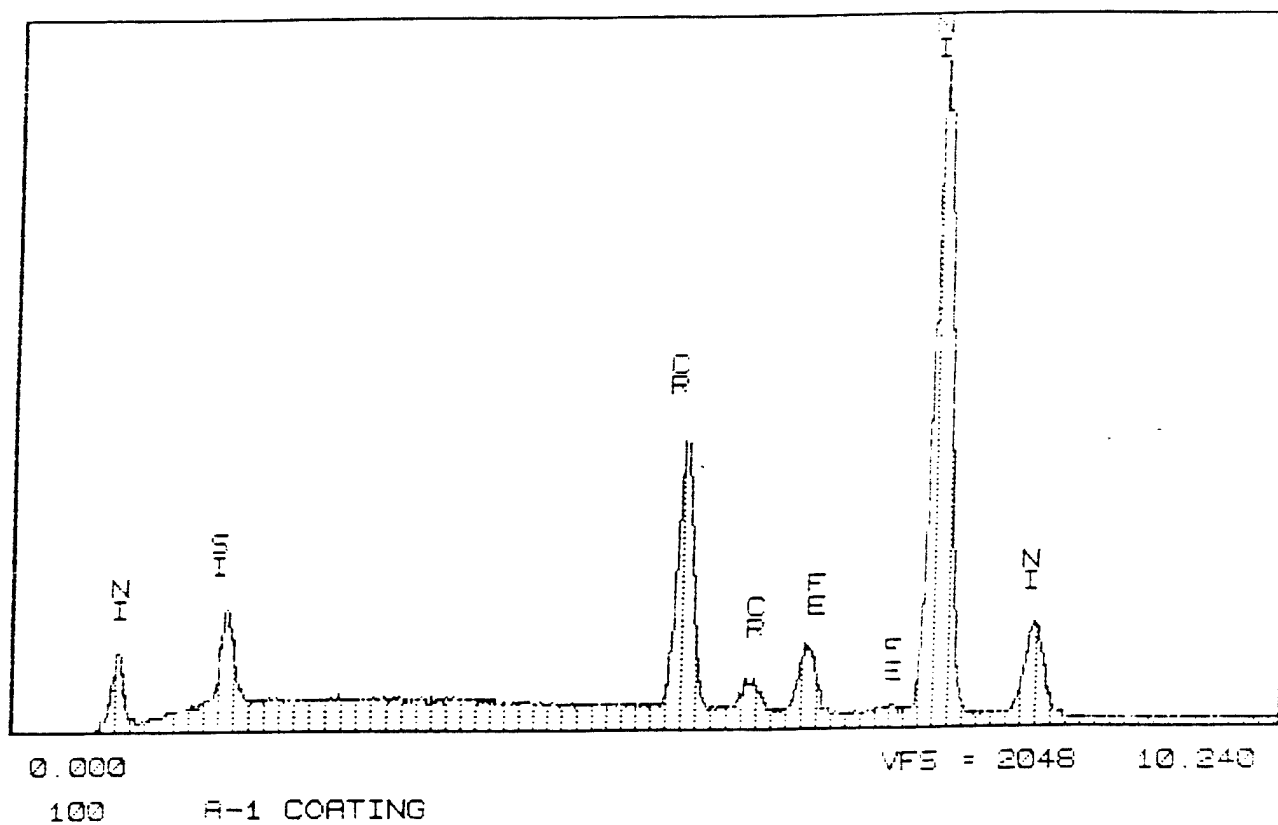Cursor: 0 000KeV = 0

Figure 4.1-1. Electron microprobe composition analysis of coating for specimen A1.

PRZ Correction 20.00 kV 40.00 deg
No.of Iterations = 2

Element	K-ratio	Z	A	F	ZAF	Atom%	Wt%
Ni-K	0.706	1.002	1.026	1.000	1.027	68.50	72.58
Cr-K	0.147	1.015	1.020	0.909	0.941	14.78	13.87
Si-K	0.016	0.889	2.339	0.999	2.078	6.59	3.34
Fe-K	0.113	1.016	1.028	0.865	0.904	10.13	10.21
						Total=	100.00%

ECRG Microprobe Lab.   R.G.Racus   TUE 22-SEP-92 06:51
Cursor: 0.000keV = 0

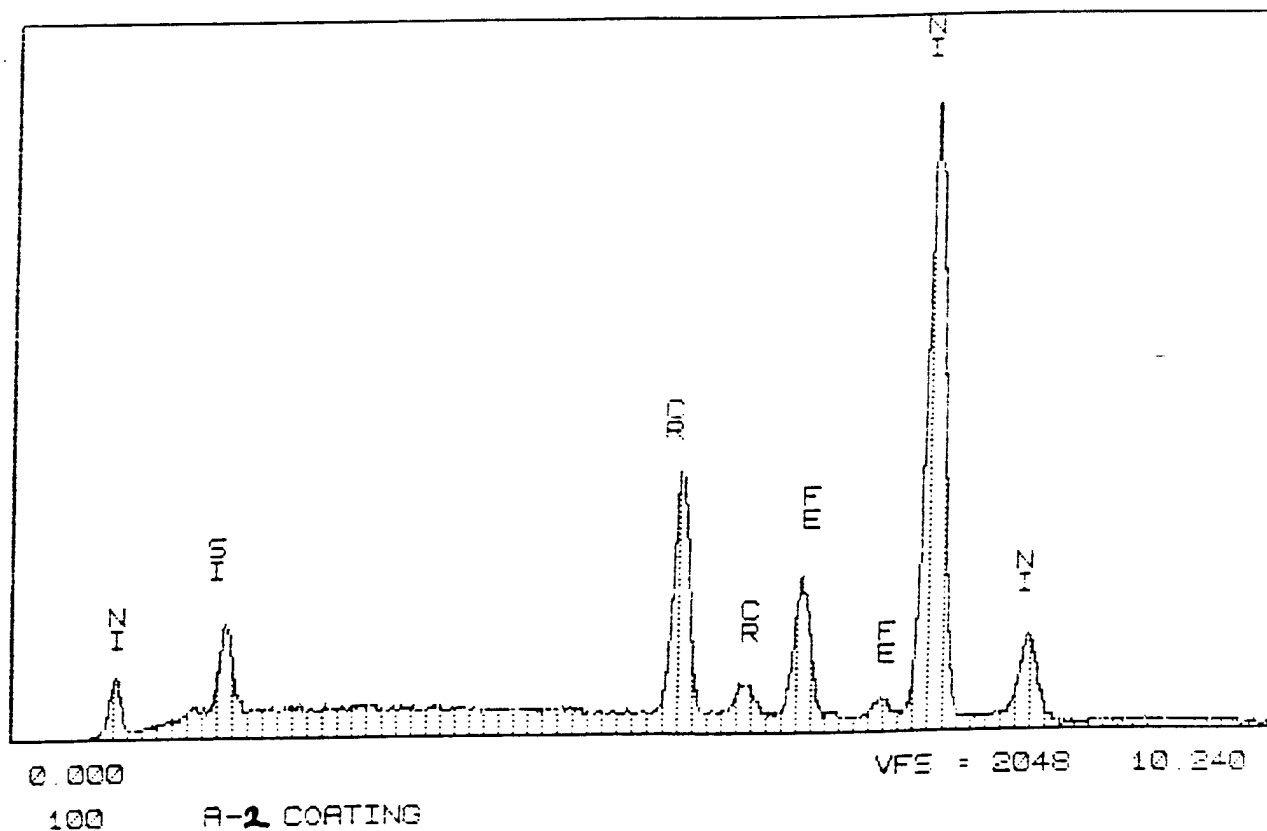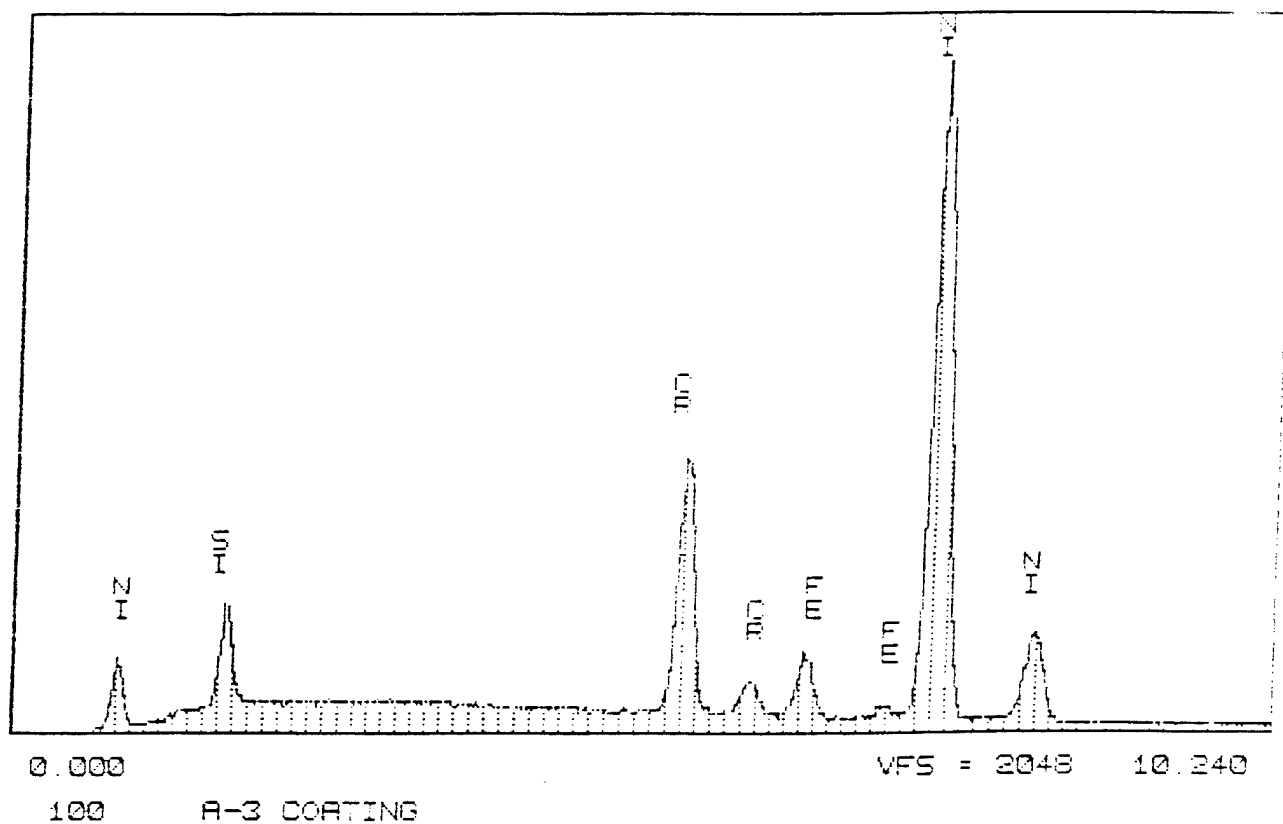0.000
100   A-2 COATING

VFS = 2048   10.240

Figure 4.1-2. Electron microprobe composition analysis of coating for specimen A2.

153

24

RZ Correction 20.00 kV 40.00 deg
No.of Iterations = 2

Element	K-ratio	Z	A	F	ZAF	Atom%	Wt%
Ni-K	0.759	1.003	1.019	1.000	1.022	73.10	77.61
Cr-K	0.151	1.017	1.020	0.908	0.942	15.15	14.24
Si-K	0.018	0.890	2.352	0.999	2.093	7.41	3.76
Fe-K	0.049	1.018	1.029	0.847	0.887	4.34	4.39
						Total=	100.00%

ECRG Microprobe Lab   R.G.Racus   TUE 22-SEP-92 07:05

Cursor: 0 000keV = 0

0.000   VFS = 2048   10.240

100   A-3 COATING

Figure 4.1-3.   Electron microprobe composition analysis of coating for specimen A3.

154

25

PRZ Correction 20.00 kV 40.00 deg
No.of Iterations = 3

ement	K-ratio	Z	A	F	ZAF	Atom%	Wt%
Fe-K	0.043	1.016	1.040	0.874	0.923	3.92	3.97
Cr-K	0.225	1.015	1.019	0.921	0.952	22.69	21.43
Ni-K	0.691	1.002	1.025	1.000	1.027	66.62	71.04
Mn-K	0.002	1.032	1.010	0.896	0.934	0.22	0.22
Si-K	0.016	0.889	2.311	0.999	2.052	6.56	3.35
Mo-L	0.000	1.129	1.303	0.997	1.466	0.00	0.00
Ti-K	0.000	1.008	1.046	0.927	0.977	0.00	0.00
Nb-L	0.000	1.117	1.386	0.998	1.545	0.00	0.00
Al-K	0.000	0.909	3.171	0.999	2.880	0.00	0.00
Cu-K	0.000	1.050	1.020	1.000	1.071	0.00	0.00

Total= 100.00%

BCAG Microprobe Lab.   R.G.Racus   THU 22-OCT-92 09:26
Cursor: 0.000KeV = 0

0.000   VFS = 4096   10.240

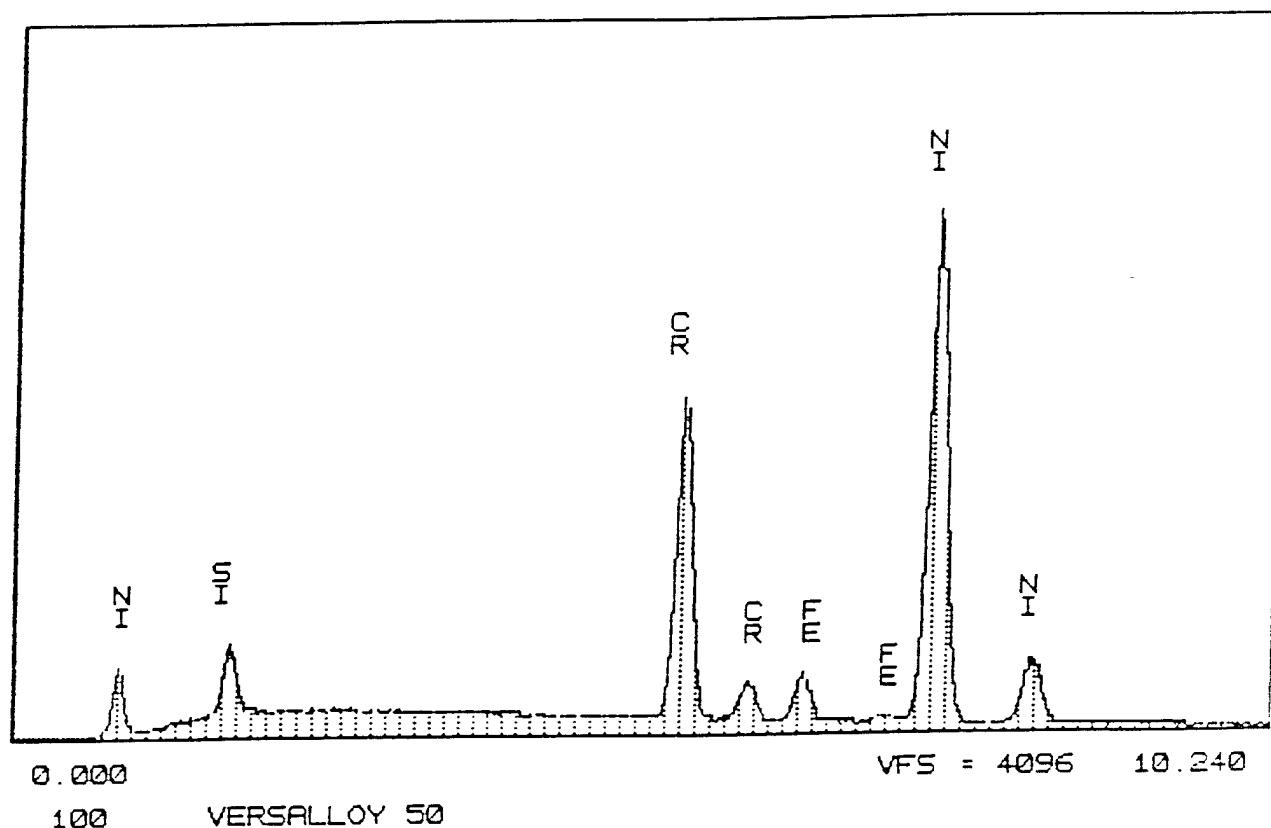100   VERSALLOY 50

Figure 4.1-4.   Electron microprobe composition analysis of
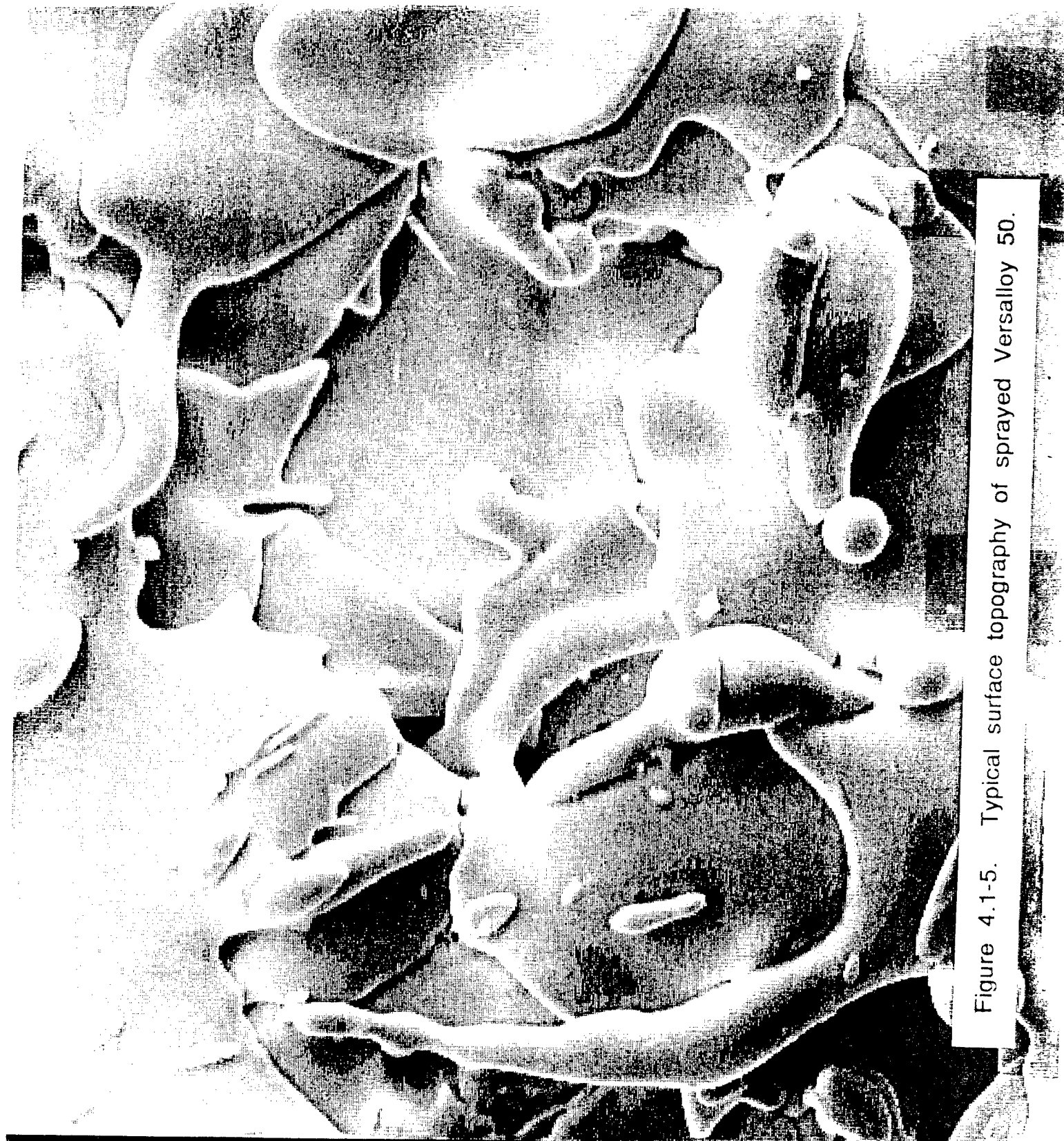   Versalloy 50 alloy, unsprayed.

155

26

Figure 4.1-5.   Typical surface topography of sprayed Versalloy 50.

156

Figure 4.1-6. Typical surface topography of sprayed Versalloy 50.

Figure 4.1-7. Typical surface topography of sprayed Versalloy 50.

Figure 4.2-1.   (Specimen A1, 500X) Cross section of Versalloy 50
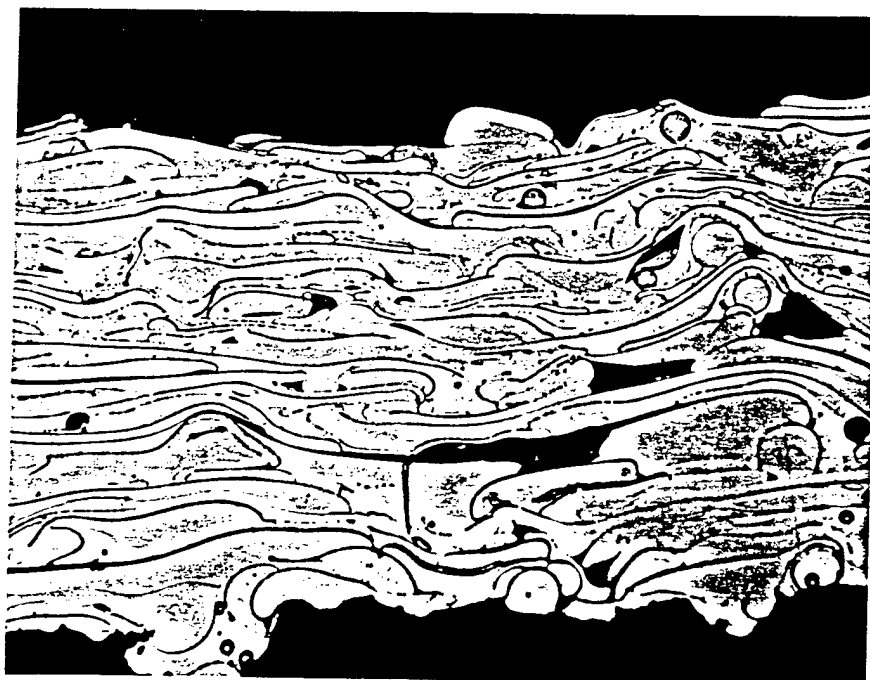coating in as sprayed condition.

Figure 4.2-2.   (Specimen A1, 500X) Cross section of Versalloy 50
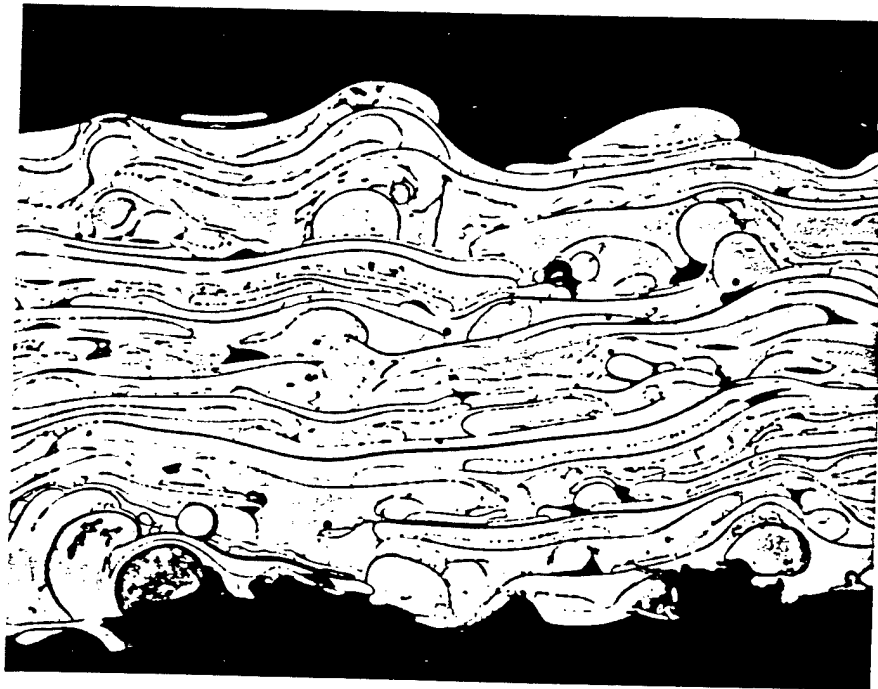coating in as sprayed condition.

Figure 4.2-3.   (Specimen A2, 500X) Cross section of Versalloy 50
coating in as sprayed condition.

Figure 4.2-4.   (Specimen A2, 500X) Cross section of Versalloy 50
coating in as sprayed condition.

Figure 4.2-5.   (Specimen A3, 500X)   Cross section of Versalloy 50 coating in as sprayed condition.

Figure 4.2-6.   (Specimen A3, 500X)   Cross section of Versalloy 50 coating in as sprayed condition.
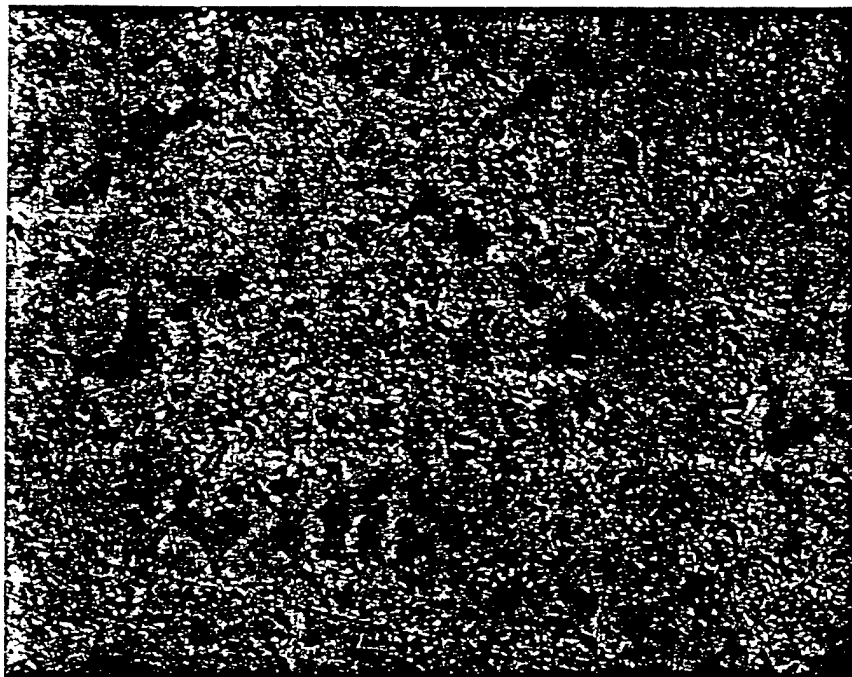
Figure 4.2-7.   Cross section of Versalloy 50 alloy, polished.
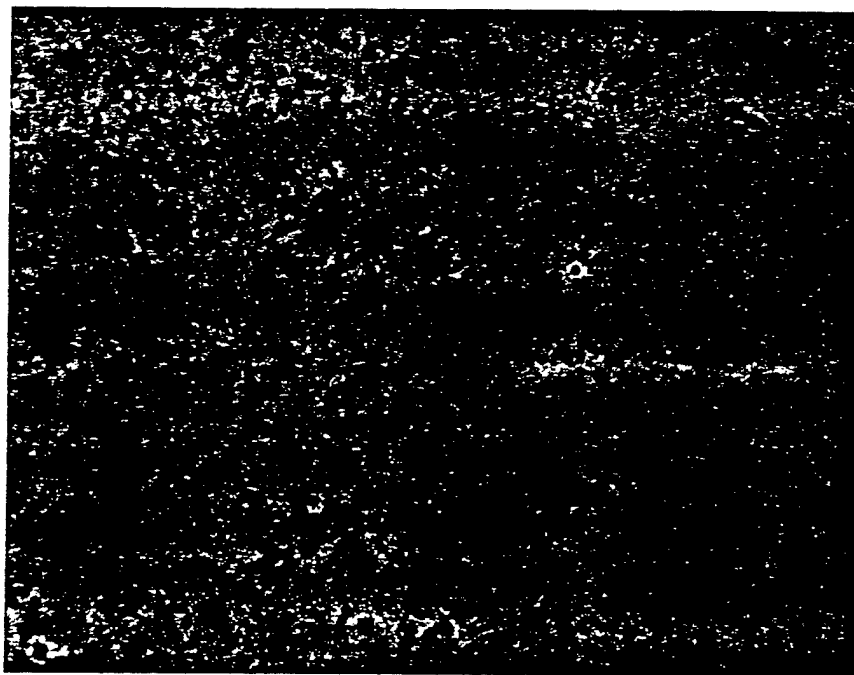

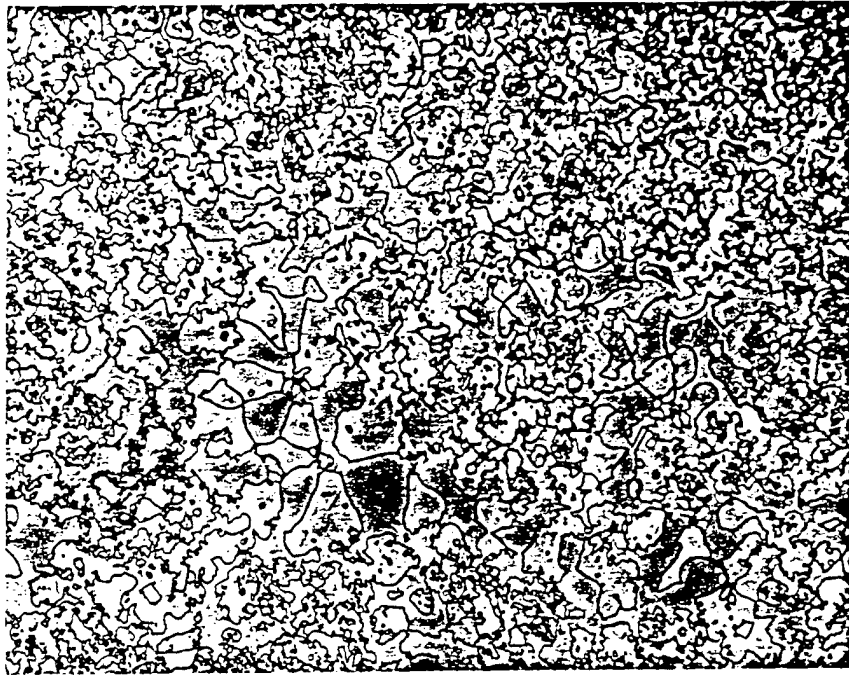Figure 4.2-8.   Cross section of Versalloy 50 alloy, polished.

Figure 4.2-9.   Cross section of Versalloy 50 alloy, polished and etched.
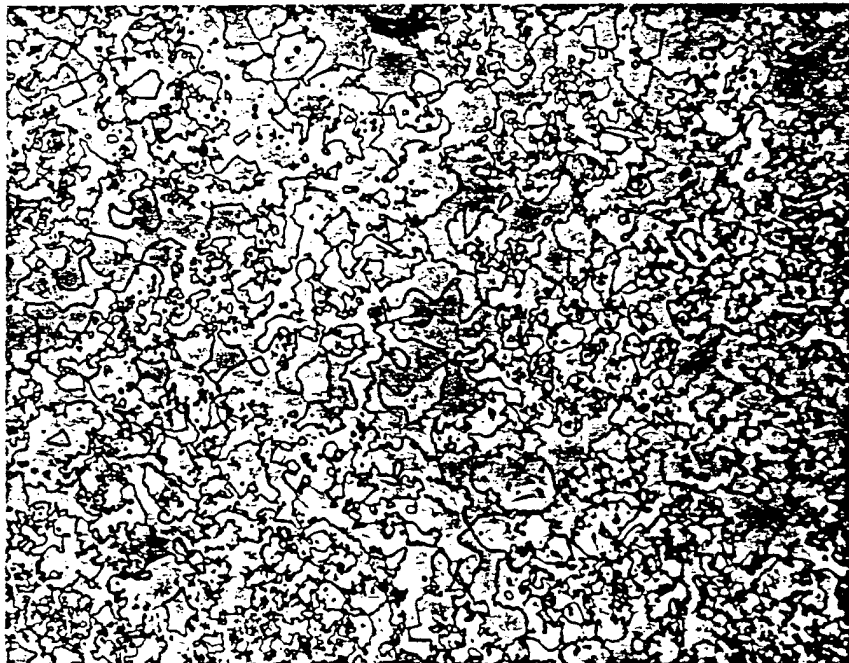

Figure 4.2-10.   Cross section of Versalloy 50 alloy, polished and etched.

lines within the coating which may be cracks. These are most apparent in Figures 4.2-1 and 4.2-2. The structure of the unsprayed alloy was found to be crystalline, photographs of which appear in Figures 4.2-7 through 4.2-10.

(b) The surface of three sprayed specimens were examined for cracks at 200X magnification. Photographs appear in Figures 4.2-11 through 4.2-16. Two of the specimens, A6 and A7, were found to have surface cracks ranging from 0.005" to 0.010" in length. The third specimen, A4, was found to have fewer cracks with a maximum crack length of approximately 0.003". These cracks may be related to residual internal stresses in the coating.

(c,d) The specimens in (b) were re-examined after baking in accordance with section 3.2.2 (c). Photographs of the specimen surfaces appear in Figures 4.2-17 through 4.2-22. The bake cycles did not appear to propagate existing cracks or initiate new ones.

(e) Cross sections of the sprayed coating after baking appear in Figures 4.2-23 through 4.2-28. The structure appears essentially the same as in part (a) with no observable structural change occurring in the coating as a result of baking.

4.3   Internal Stress

The results of the internal stress evaluation are shown in Figures 4.3-1 through 4.3-3. The vertical axis is the degree of bend measured in the specimen. Negative values indicate compressive stress in the coating and positive values indicate tensile stress. The values shown for grit blast are representative values for the effect of grit blasting the almen test strips. As shown in the figures, grit blasting induces compressive stresses in the part which is partially relieved upon application of the coating. As shown in Figure 4.3-1, thermal cycling at 375° F has no effect on the internal stress of the part. Figure 4.3-2 shows that thermal cycling at 650° F has a slight effect during the first two cycles, but virtually no effect during the third. Figure 4.3-3 shows the effect of one extended bake at 650° F for 6 hours. It was expected that there would be a slight relaxation of compressive stress as was seen following the two shorter cycles at 650°F. However, as seen in the figure, there was no real effect.

Figure 4.2-11.   (Specimen A4, 200X)   Magnified view of surface
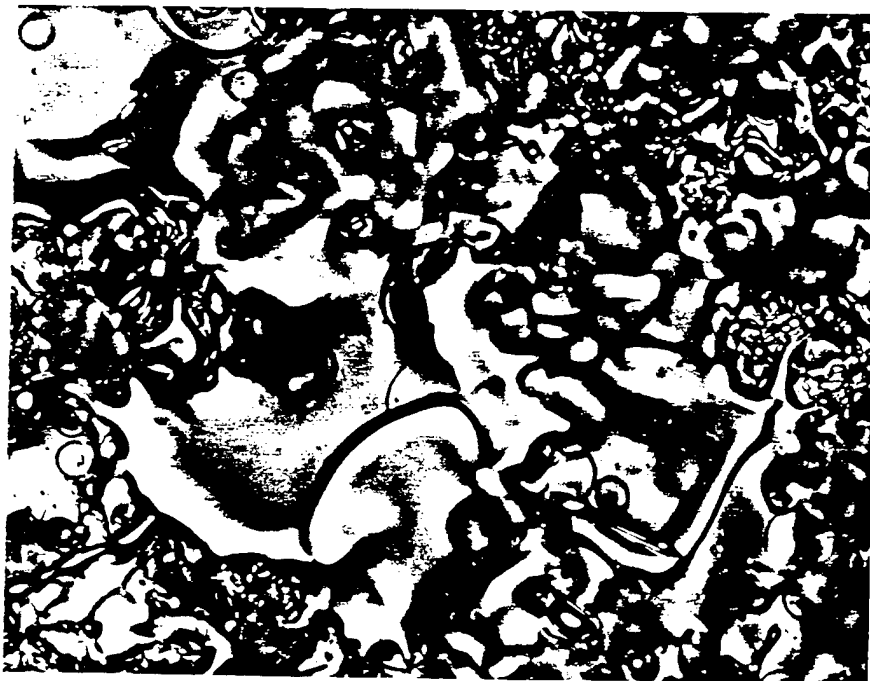cracks in as sprayed coating.

Figure 4.2-12.   (Specimen A4, 200X)   Magnified view of surface
cracks in as sprayed coating.

Figure 4.2-13.   (Specimen A7, 200X)   Magnified view of surface cracks in as sprayed coating.
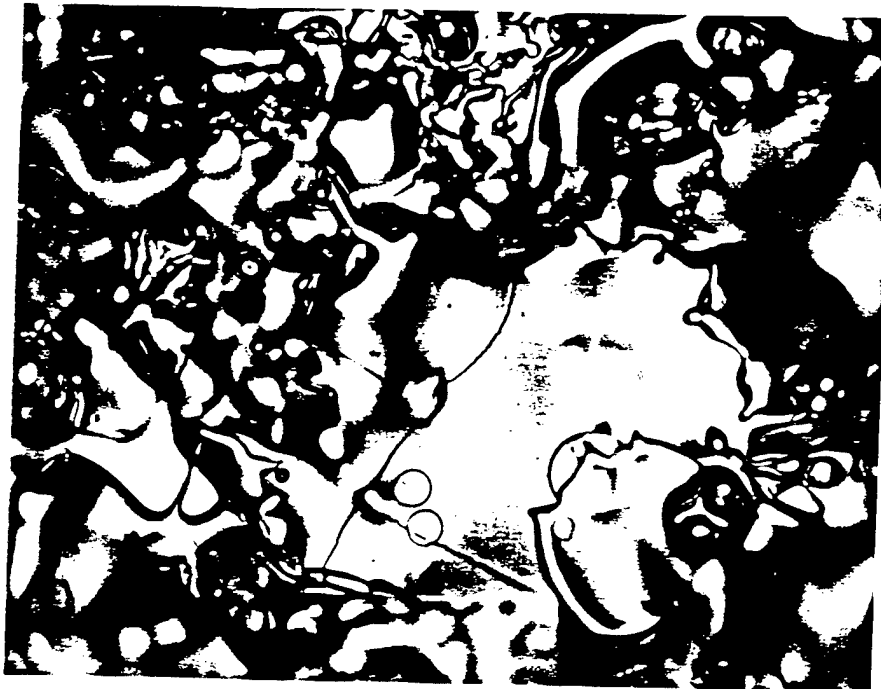

Figure 4.2-14.   (Specimen A7, 200X)   Magnified view of surface cracks in as sprayed coating.

Figure 4.2-15.   (Specimen A6, 200X)   Magnified view of surface
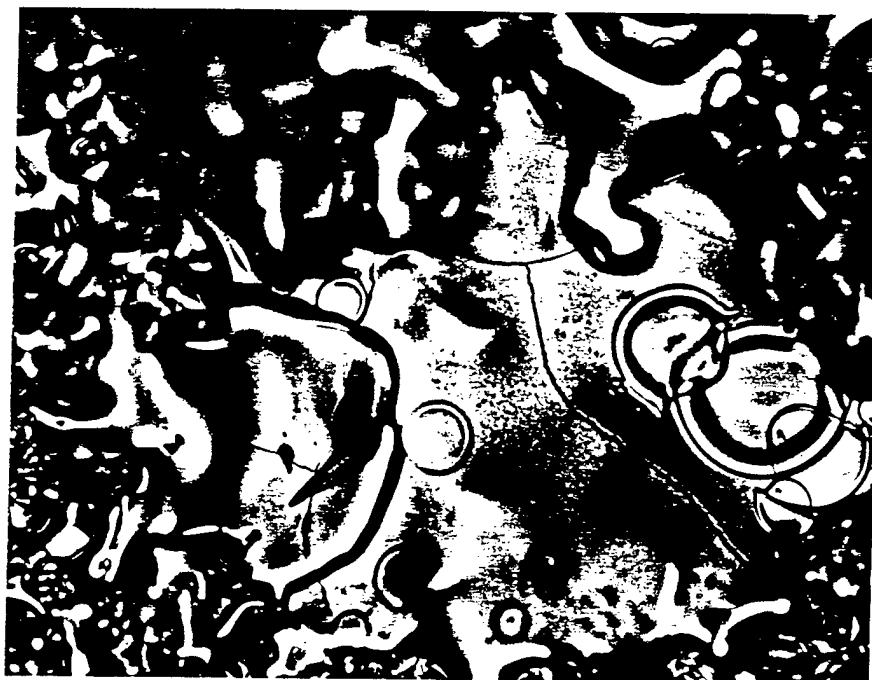cracks in as sprayed coating.

Figure 4.2-16.   (Specimen A6, 200X)   Magnified view of surface
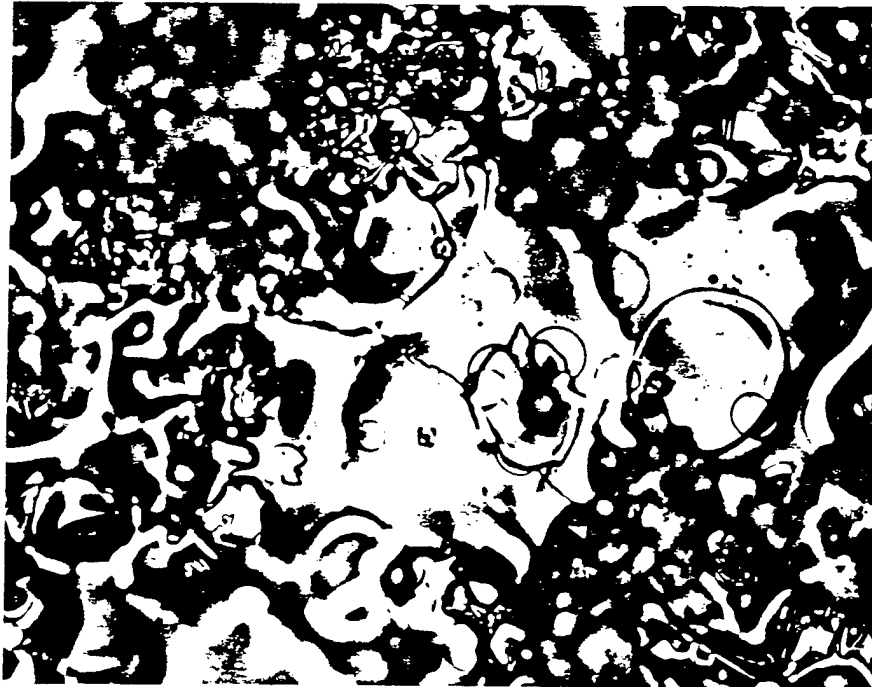cracks in as sprayed coating.

Figure 4.2-17.   (Specimen A4, 200X)   Magnified view of surface cracks in coating after 375°F, 6 hour bake.
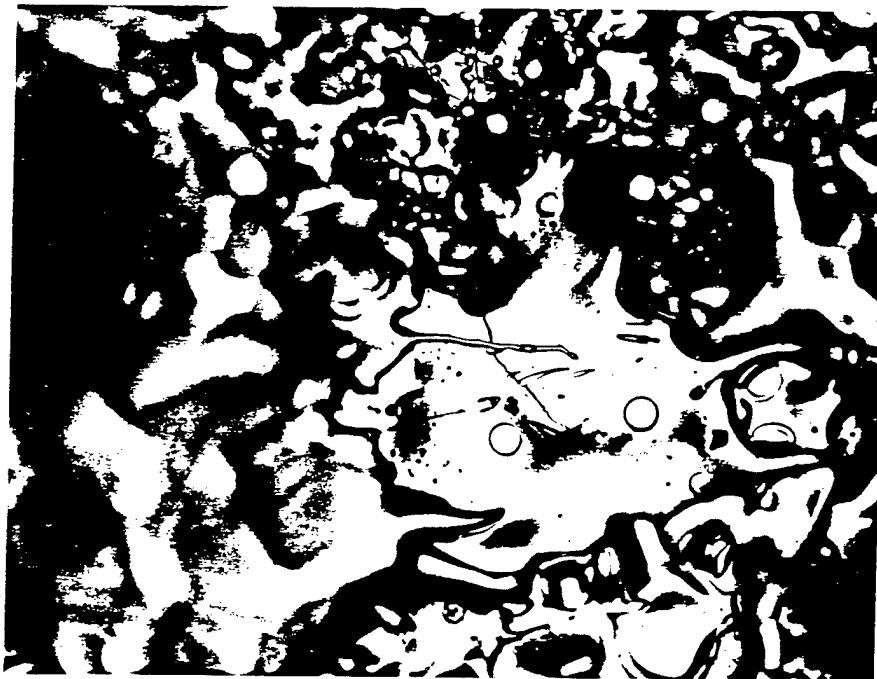

Figure 4.2-18.   (Specimen A4, 200X)   Magnified view of surface cracks in coating after 375°F, 6 hour bake.

Figure 4.2-19.   (Specimen A7, 200X)   Magnified view of surface
                  cracks in coating after 650°F, 6 hour bake.

Figure 4.2-20.   (Specimen A7, 200X)   Magnified view of surface
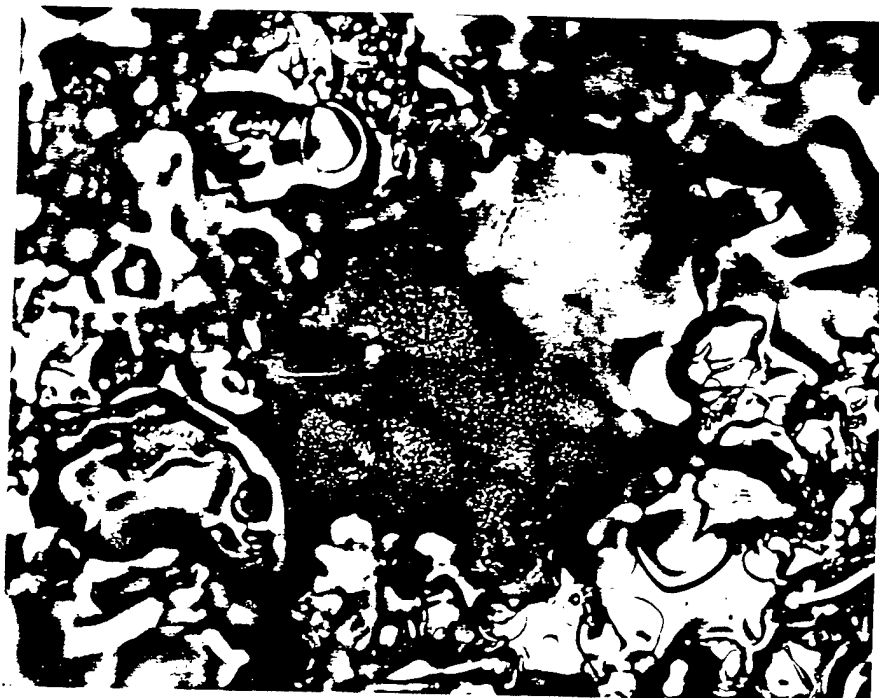   cracks in coating after 650°F, 6 hour bake.

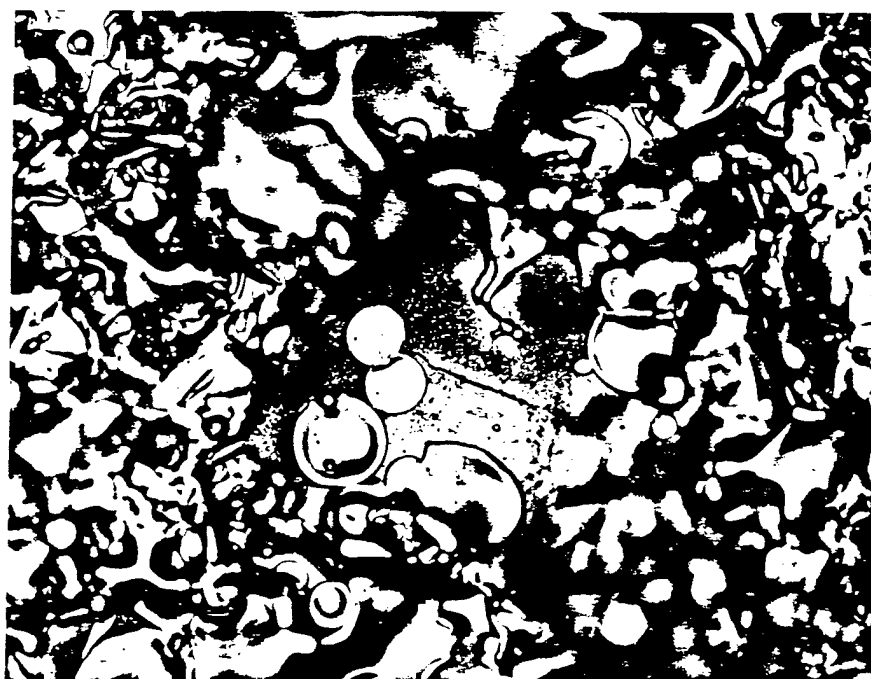Figure 4.2-21. (Specimen A6, 200X) Magnified view of surface cracks in coating after 900°F, 6 hour bake.

Figure 4.2-22. (Specimen A6, 200) Magnified view of surface cracks in coating ai 900°F, 6 hour bake.

Figure 4.2-23. (Specimen A4, 500X) Cross section of Versalloy 50 coating after 375°F, 6 hour bake.
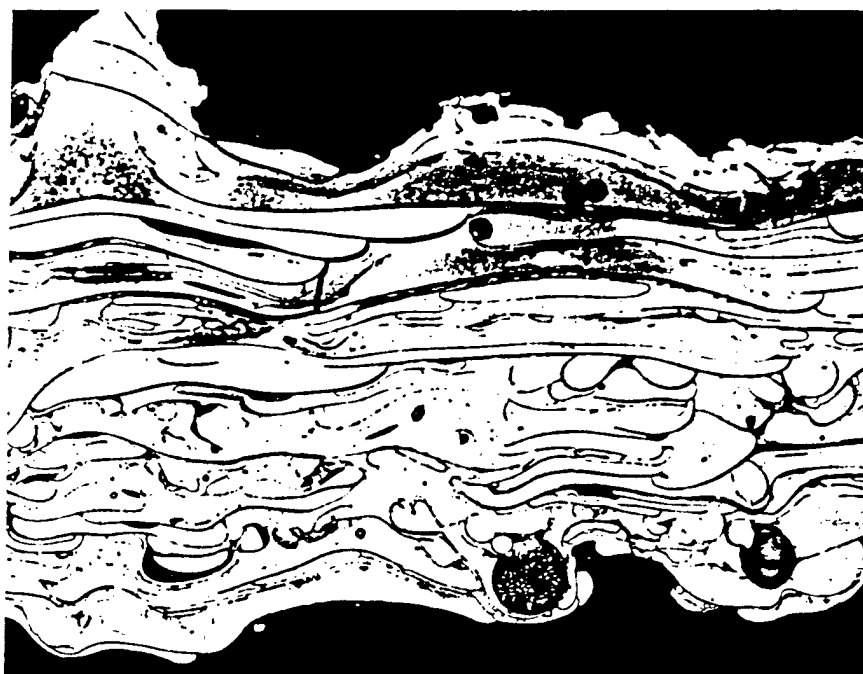

Figure 4.2-24. (Specimen A4, 500X) Cross section of Versalloy 50 coating after 375°F, 6 hour bake.

Figure 4.2-25.   (Specimen A7, 200X)   Cross section of Versalloy 50
coating after 650°F, 6 hour bake.

Figure 4.2-26.   (Specimen A7, 200X)   Cross section of Versalloy 50
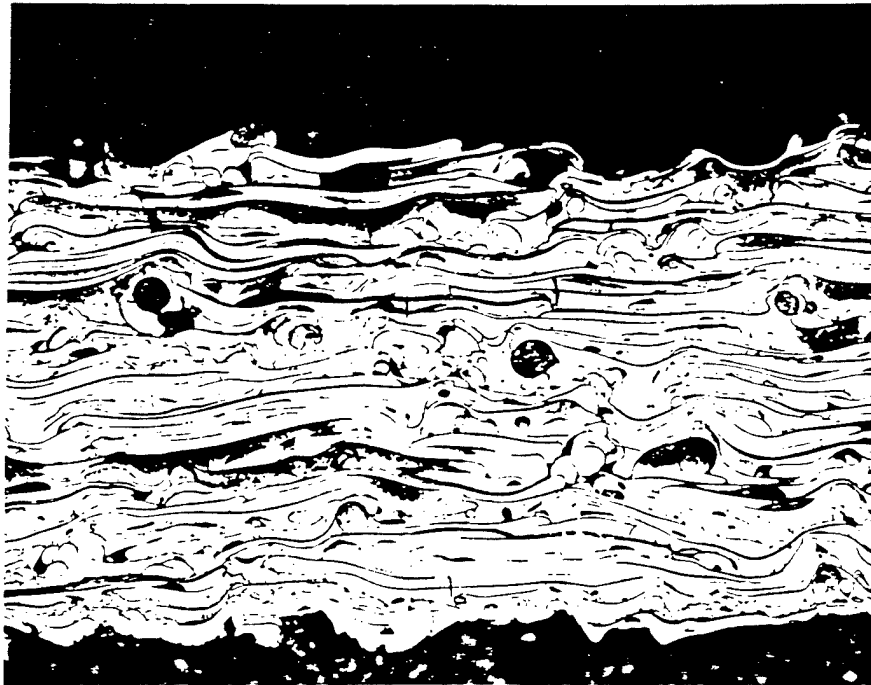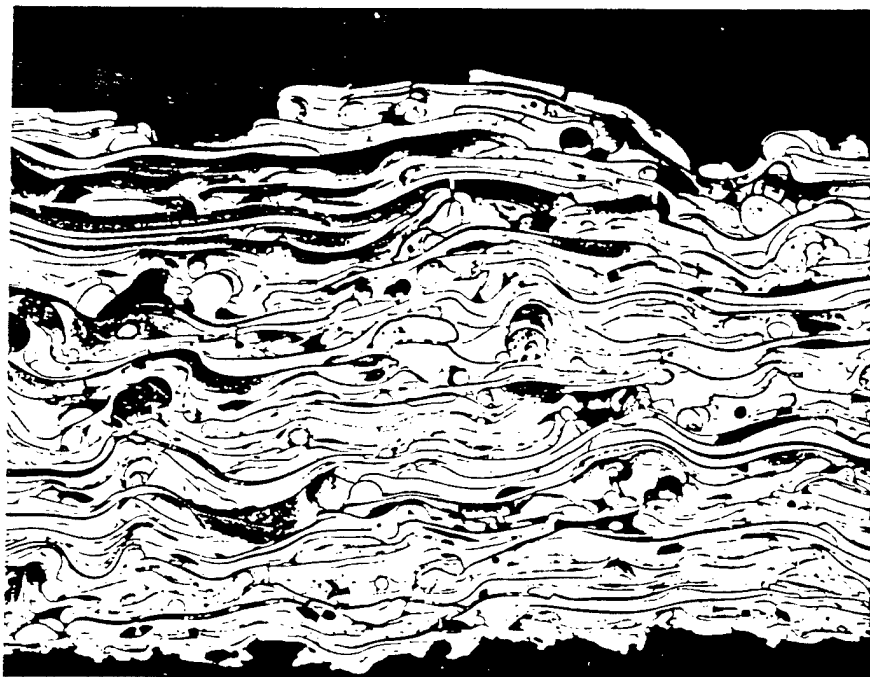coating after 650°F, 6 hour bake.

172

43

Figure 4.2-27.   (Specimen A6, 500X)   Cross section of Versalloy 50
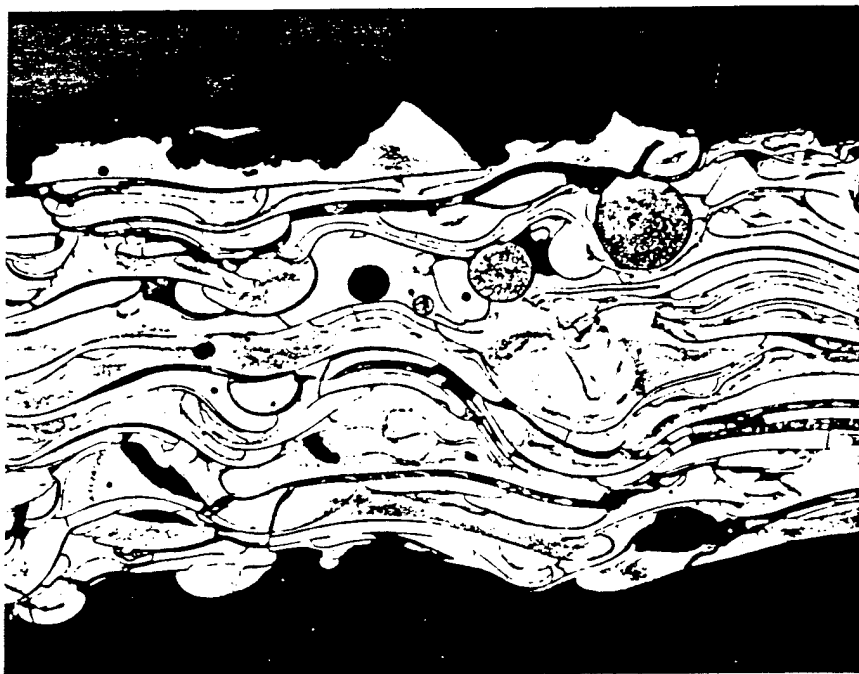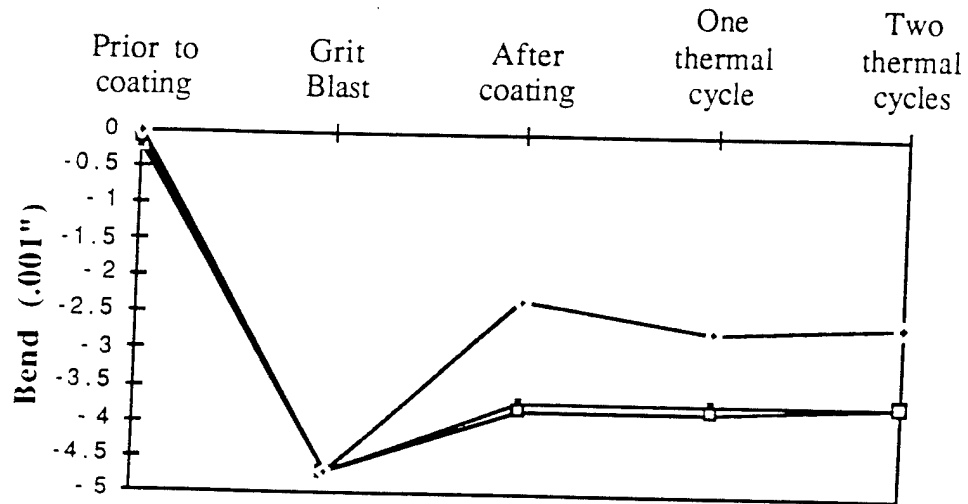coating after 900°F, 6 hour bake.

Figure 4.2-28.   (Specimen A6, 500X)   Cross section of Versalloy 50
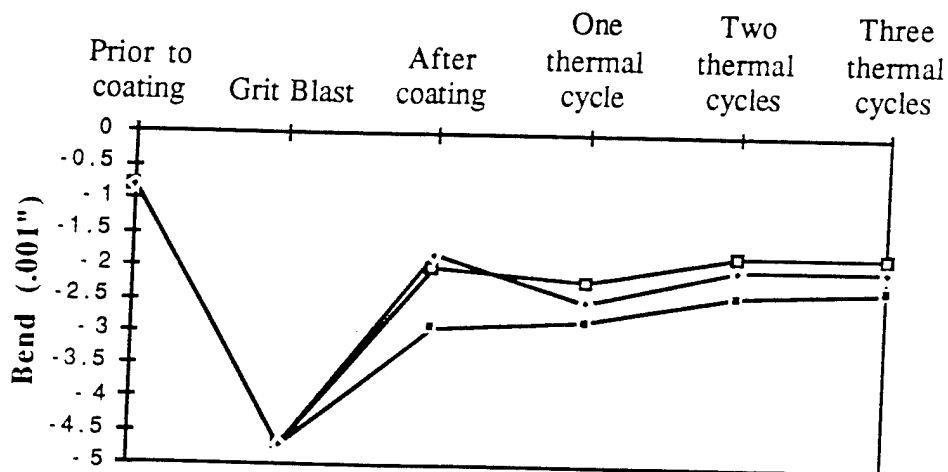coating after 900°F, 6 hour bake.

Internal Stress

Thermal Cycle: 375°F, 3 Hours

Figure 4.3-1.   Effect of thermal cycling at 375° F on internal stress.

Internal Stress

Thermal Cycle: 650°F, 3 Hours

Figure 4.3-2.   Effect of thermal cycling at 650° F on internal stress.

Internal Stress

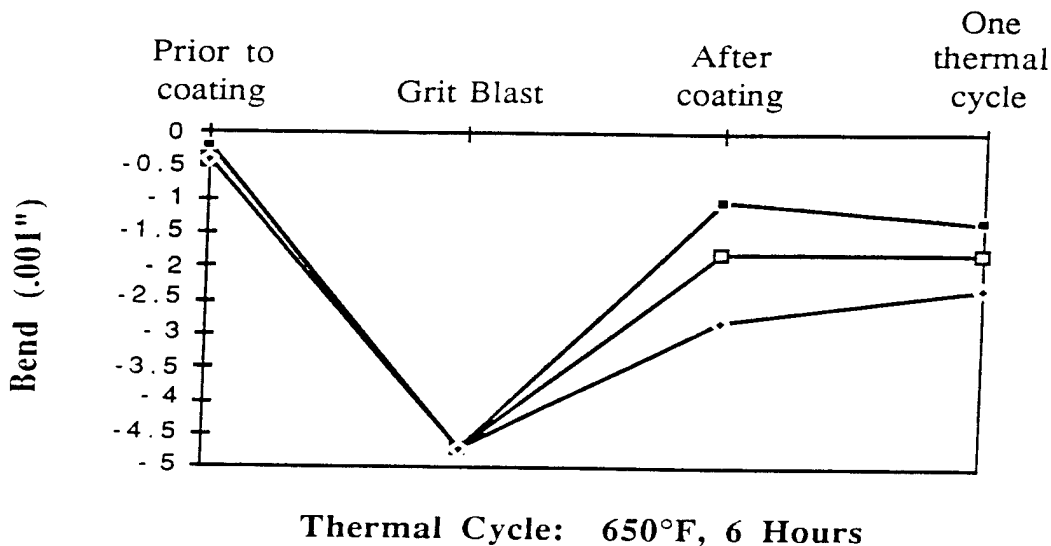Thermal Cycle: 650°F, 6 Hours

Figure 4.3-3.   Effect of one thermal at 650° F on internal stress.

Due to the overshadowing effect of the grit blasting, it is difficult to determine the internal stress of the coating. The partial relief of the compressive stress induced by grit blasting may be due to tensile stresses in the coating or may be due to the spraying process, either thermal or mechanical impact effects. The net result of the spraying process, including surface preparation, is a slight compressive stress at the surface of the part.

4.4   Hardness Tests

The results of microhardness measurements are shown in Figure 4.4-1. The microhardness of the as sprayed coating is significantly higher (755 HV_{500}) than that of the unsprayed alloy (514 HV_{500}). This can be related to the difference between the amorphous structure of the coating, and the crystalline structure of the unsprayed alloy.

There is no significant effect on hardness following a low temp bake (375° F, 6 hours). However, after baking a specimen at 650°F for 6 hours the hardness increased to 830 HV_{500} and after baking a specimen

at 900° F for 6 hours the hardness increased to 912 HV_{500}. This compares to chrome which had a value of 829 HV_{500}. A larger sample size is required to confirm these results.
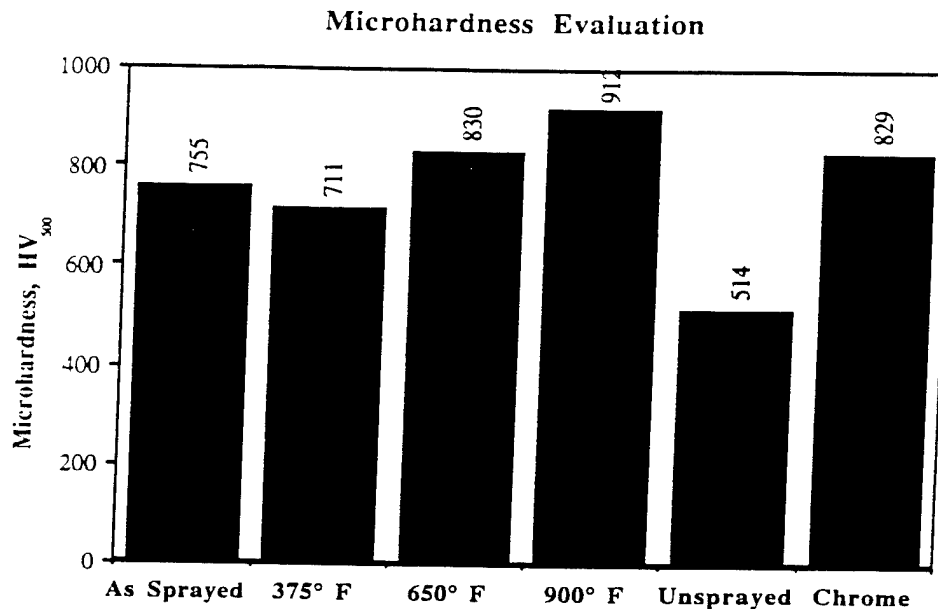
Microhardness Evaluation

Figure 4.4-1.   Microhardness of sprayed coating and chrome plate.

4.5   Corrosion Tests

Red corrosion products were evident on all sprayed panels after 24 hours of testing in an acetic acid salt spray environment and the test was discontinued after 72 hours. Photographs of the panels appear in Figures 4.5-1 through 4.5-3. The bent panels were more severely corroded than the flat panels due to cracking of the coating in the bend area. However, there was only slight if any difference in the degree of corrosion between the baked and unbaked panels.

Because acetic acid salt spray testing is significantly more aggressive than neutral salt spray testing, the test was repeated using the worn Taber abrasion test panels in a neutral salt spray cabinet maintained and operated in accordance with ASTM B117. The worn chrome Taber abrasion test panels were also included for comparison. Red corrosion products were again evident after 24 hours of testing on both the

sprayed and chrome plated panels and the test was discontinued after 48 hours.

Photographs of the Taber abrasion panels appear in Figures 4.5-4 and 4.5-5. Of the three sprayed panels, panel 2 was the most severely corroded and panel 1 the least. This corresponds to the coating thicknesses shown Table 4.5-1. Corrosion resistance improves with increasing coating thickness, especially if the coating contains cracks or porosity.

Table 4.5-1.   Taber abrasion test panel coating thickness.

Panel	Approximate Coating Thickness (inch)
1	0.010
2	0.005
3	0.0075

Comparing the sprayed panels to the chrome plated panels, corrosion was more severe on the sprayed panels in both the unworn areas and in the Taber abrasion wear scar. The extreme corrosion in the wear scar of the sprayed panels was expected due to thinning of the coating during wear test. But the lack of corrosion in the wear tracks of the chrome plated panels was unexpected and is thought to be due to lower surface roughness. A higher surface roughness will result in differences in oxygen availability between high and low points on the surface and contribute to the formation of corrosion cells. Surface roughness measurements were taken on representative panels and average values are shown in Table 4.5-2.

Table 4.5-2.   Typical surface roughness measurements.

Surface	Surface Roughness (R_a)
Metal spray, as sprayed	250
Metal spray, abrasion wear track	130
Metal spray, ground	48
Chrome plate, as plated	55
Chrome plate, abrasion wear track	10

As seen in the table, the surface roughness for chrome plate is lower in the abrasion wear track area than in the as plated area of the panel.

Because the substantially higher surface roughness of the metal spray coating (250 R_a) may be a significant factor when comparing corrosion test results to the chrome plated specimens and testing was then performed with sprayed specimens ground to a surface roughness closer to that of chrome plate. Specimen coating thicknesses and surface roughnesses are shown in Table 4.5-3.
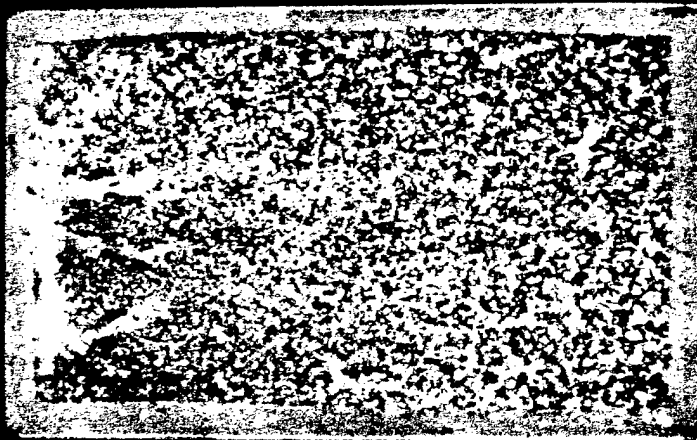
Table 4.5-3.   Corrosion panel coating thickness and surface roughness measurements.

Coating Type	Panel	As Coated Thickness (mils)	Ground Thickness (mils)	As Coated Surface Roughness (R_a)	Ground Surface Roughness (R_a)
Metal Spray	11	10.0	5.0	412	102
	12	10.0	7.5	406	212
	13	10.0	4.4	289	79
	14	10.0	3.9	311	79
	15	6.0	-	238	-
	16	6.0	-	248	-
	18	8.0	3.4	280	108
	19	4.0	-	260	-
	20	4.0	-	272	-
Chrome Plate	C1	1.7	-	46	-
	C2	4.1	-	61	-
	C3	2.6	-	53	-
	C4	5.0	-	57	-

Red corrosion products were apparent on all specimens after 24 hours of testing and the test was discontinued after 48 hours. There was no obvious difference between the sprayed panels which were ground (Figures 4.5-6 and 4.5-7) and the panels which were tested in the as sprayed condition (Figure 4.5-8) indicating that the effect of surface roughness is minimal compared to other factors such as coating porosity. Comparing the sprayed panels to chrome plate, corrosion was again more severe on the sprayed panels.
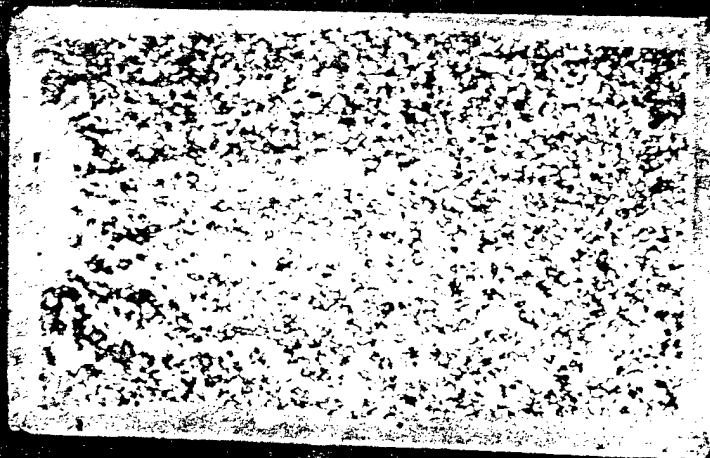
Panel 5
Versalloy 50
Thickness: 4.0 mils
Baked @ 650°F, 3 hours
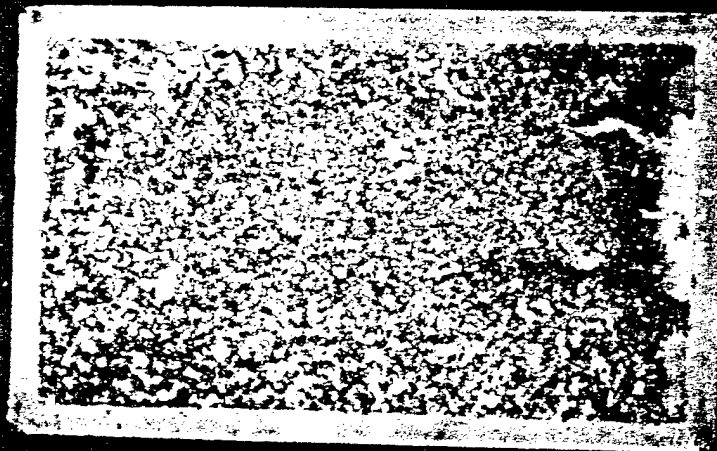
Panel 1
Versalloy 50
Thickness: 6.5 mils
Baked @ 375°F, 3 hours

Panel 7
Versalloy 50
Thickness: 6.0 mils
No bake

Figure 4.5-1. Corrosion test panels after 72 hours in acetic acid salt spray.

Panel 4
Versalloy 50
Thickness: 5.5 mils
Baked @ 650°F, 3 hours

Panel 2
Versalloy 50
Thickness: 7.5 mils
Baked @ 375°F, 3 hours

Panel 8
Versalloy 50
Thickness: 6.0 mils
No bake

Figure 4.5-2. Corrosion test panels after 72 hours in acetic acid salt spray.

Panel 6
Versalloy 50
Thickness: 4.5 mils
Baked @ 650°F, 3 hours

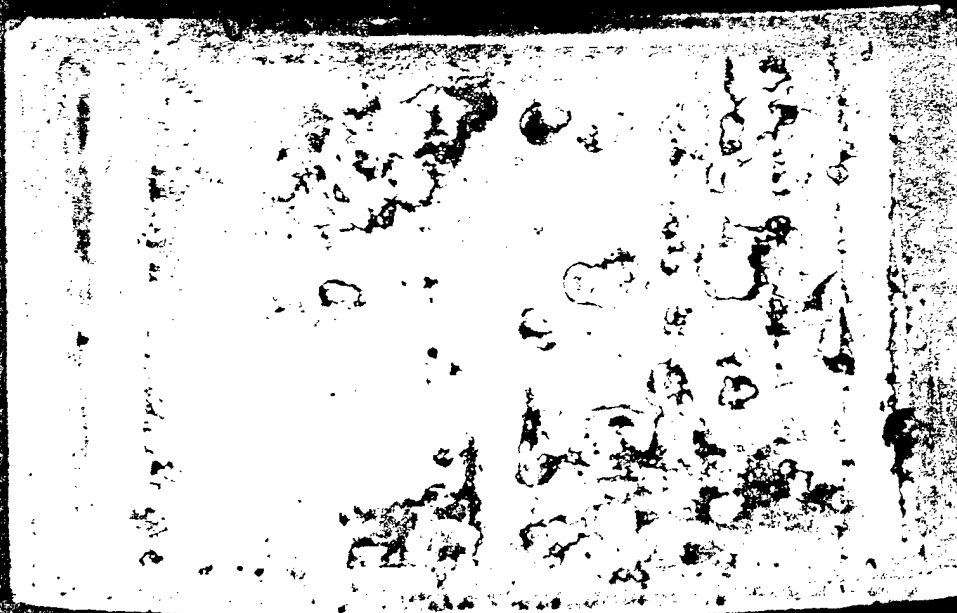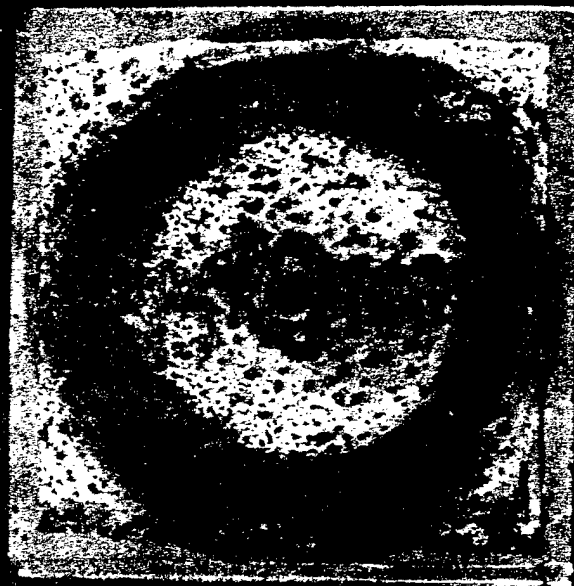Panel 3
Versalloy 50
Thickness: 5.5 mils
Baked @ 375°F, 3 hours

Panel 10
Versalloy 50
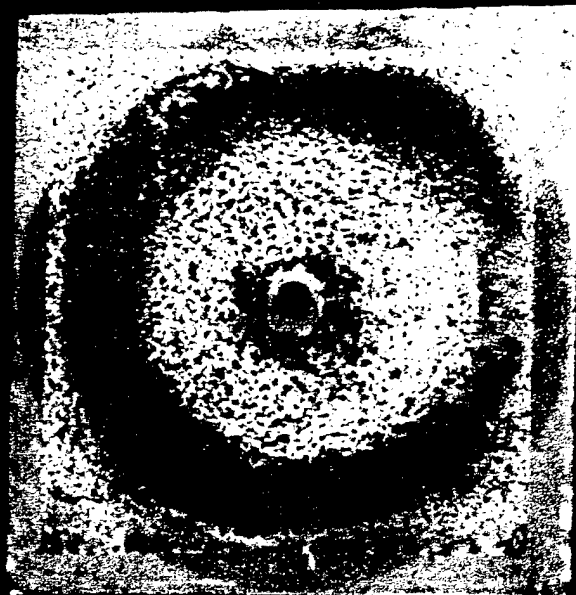Thickness: 5.0 mils
No bake

Figure 4.5-3.   Bent corrosion test panels after 72 hours in acetic acid salt spray.

181

Panel 3
Versalloy 50
Thickness: 7.5 mils

Panel 2
Versalloy 50
Thickness: 5 mils

Panel 1
Versalloy 50
Thickness: 10 mils

Figure 4.5-4.   Versalloy 50 taber abrasion panels after 48 hours in neutral salt spray.

Panel C3
Chrome
Thickness: 4.5 mils

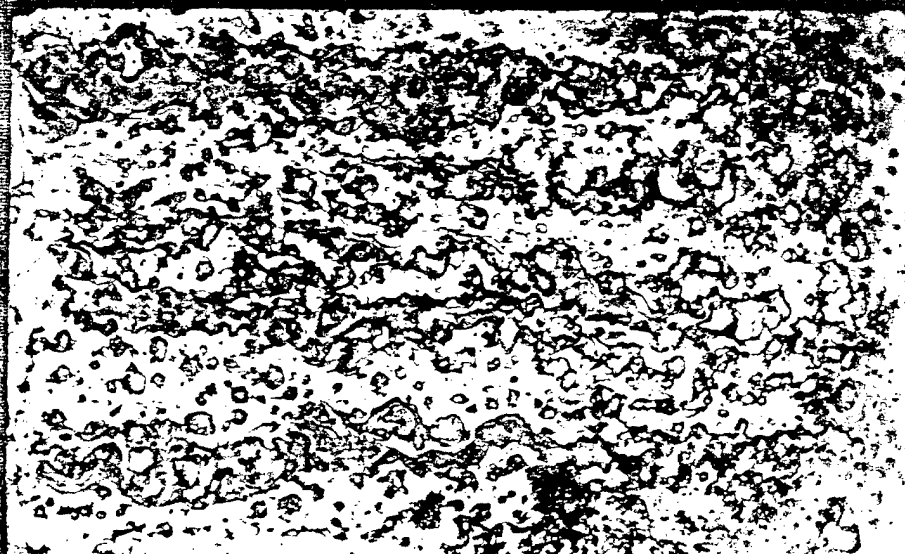Panel C2
Chrome
Thickness: 6.5 mils

Panel C1
Chrome
Thickness: 5.5 mils

Figure 4.5-5. Chrome plate taber abrasion panels after 48 hours in neutral salt spray.

Panel 11
Versalloy 50
Ground thickness: 5.0 mils

Panel 12
Versalloy 50
Ground thickness: 7.5 mils

Panel 13
Versalloy 50
Ground thickness: 4.4 mils

Figure 4.5.6.   Ground corrosion test panels after 48 hours in neutral salt spray.

Panel 14
Versalloy 50
Ground thickness: 3.9 mils

Panel 18
Versalloy 50
Ground thickness: 3.4 mils

Figure 4.5-7. Ground corrosion test panels after 48 hours in neutral salt spray.

Panel 16
Versalloy 50
As sprayed thickness: 6.0 mils

Panel 20
Versalloy 50
As sprayed thickness: 4.0 mils

Panel 15
Versalloy 50
As sprayed thickness: 6.0 mils

Panel 19
Versalloy 50
As sprayed thickness: 1.0 mils

Figure 4.5-8.   As sprayed corrosion test panels after 48 hours in neutral salt spray.

186

Panel C2
Chrome plate
Thickness: 4.1 mils

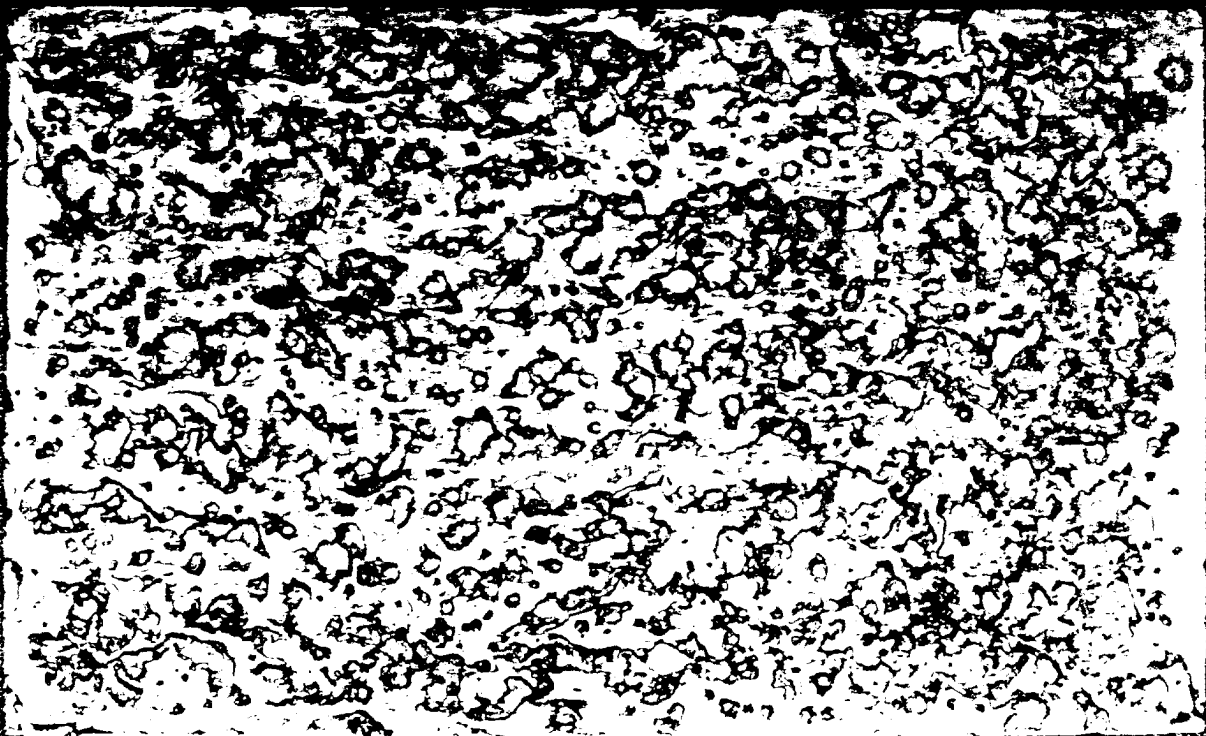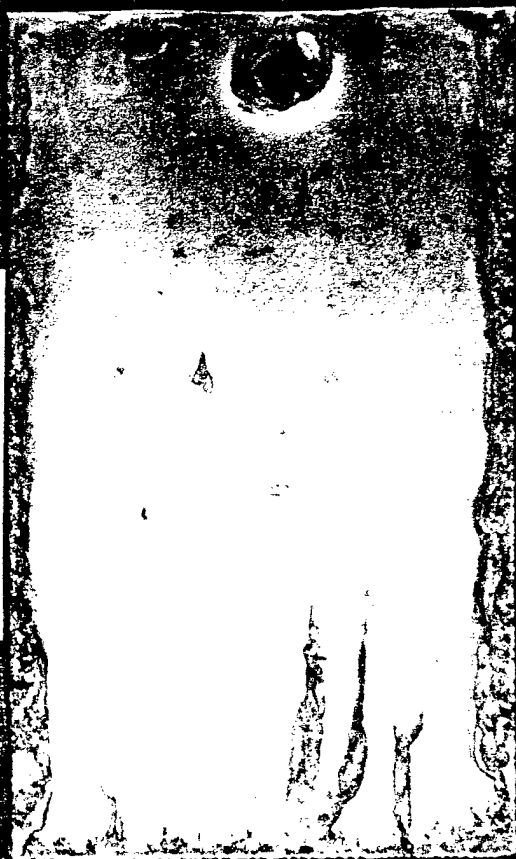Panel C4
Chrome plate
Thickness: 5.0 mils

Panel C1
Chrome plate
Thickness: 1.7 mils

Panel C3
Chrome plate
Thickness: 2.6 mils

Figure 4.5-9. Chrome corrosion test panels after 48 hours in neutral salt spray.

4.6 Abrasion Test

Taber wear indices (TWI) were calculated using the following equation:

$$\text{Taber Wear Index} = \frac{(A - B) \cdot 1000}{C}$$

A = Weight of test specimen before abrasion, milligrams
B = Weight of test specimen after abrasion, milligrams
C = Number of cycles of abrasion recorded

The lower the TWI, the better the abrasive wear resistance of the coating. Taber abrasion wear test results are shown in Figure 4.6-1.

There was a significant difference in wear indices between the metal spray coating and chrome plate. Because the spray coated panels had a higher surface roughness than the chrome plated panels, this difference may have influenced the test results. To determine the extent of any influence, one of the worn spray coated panels was retested for 1000 cycles under the same conditions. The Taber wear index was found to be 17.0 which is close to the original values obtained, thus indicating minimal influence by surface roughness.
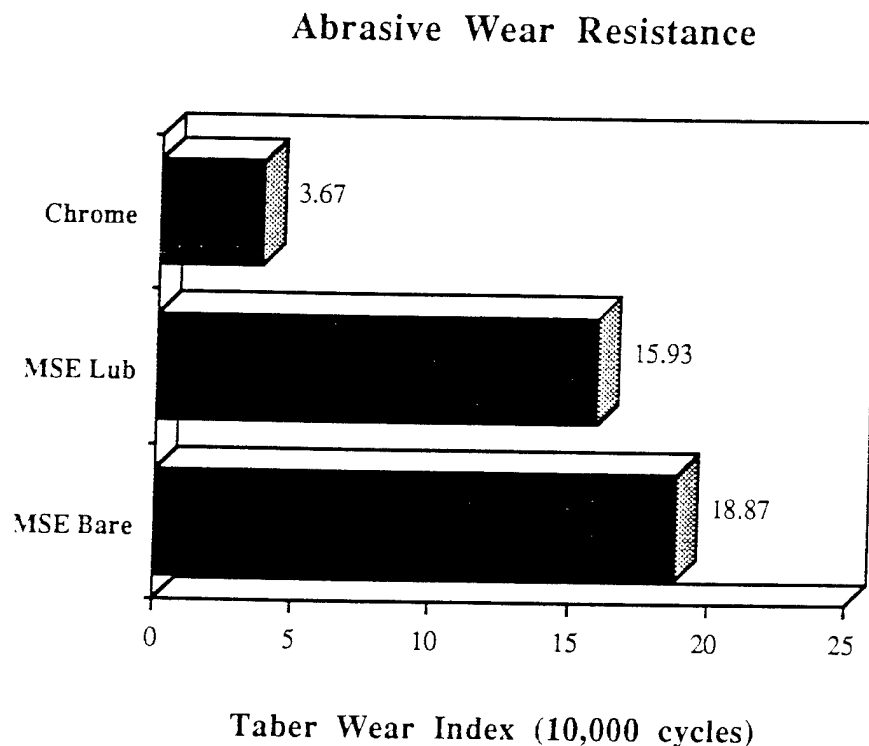
Abrasive Wear Resistance

Taber Wear Index (10,000 cycles)

Figure 4.6-1.   Taber abrasion wear results.

4.7   Adhesion Tests

The sprayed coating was found to have excellent adhesion to the 15-5 PH stainless steel and the 6Al4V titanium round bars. The coating was cut through to substrate with a saw, and a knife was used to probe the edges of the cut. Upon examination of the cut, no evidence of lifting or peeling of the coating was found (Figure 4.7-1, (a) and (b)). For AISI 4130 steel, the adhesion was lower than for the previous two substrates. The same test was performed using the knife, but in some areas, it was possible to pry the coating from the substrate (Figure 4.7-1, (c)). A loss of adhesion also occurred on the AISI 1018 steel bend specimen. The specimen was bent on a 1.0 inch diameter and examined in the bend area for loss of adhesion. As can be seen in Figure 4.7-1, (d), the coating lifted from the substrate at the bend and could be pryed from the substrate with a knife.

4.8   Materials Compatibility and Workability Tests

(a) Photographs of the specimens after shot peen appear in Figures 4.8-1 through 4.8-3. The adhesion of the coating to 15-5 PH steel was excellent. None of the specimens showed any loss of adhesion. The 6Al4V titanium specimens also showed excellent adhesion with only a slight loss appearing on two of the specimens. Adhesion of the coating to heat treated 4340M was not as high. Some degree of adhesion loss was noted on all of the specimens, and was particularly high on specimen 2. These results are consistent with the findings of the adhesion testing, section 4.7 of this report.

Testing was repeated with chrome plate applied to the same substrate materials for comparison (Figures 4.8-1.1 through 4.8-3.1). As with the sprayed coating, the adhesion to 15-5 PH steel was excellent. The adhesion of chrome plate to 4340M was superior to the sprayed coating with no loss of adhesion apparent .

The 6Al4V titanium specimens appear in Figure 4.8-2.1. The center specimen was not shot peened due to the poor condition of the coating after plating. Initially all of the specimens resembled the center specimen but were reworked by the shop in an attempt to enhance adhesion. Despite rework, the adhesion of Versalloy 50 was superior to chrome plate on this substrate.
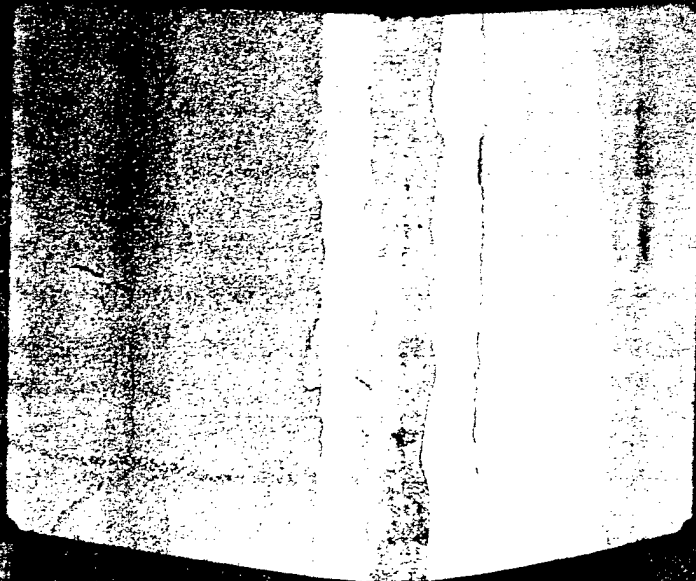
(a)   6A14V titanium substrate.   No loss of adhesion.

(b)   15-5 PH stainless steel substrate.   No loss of adhesion.

(c)   AISI 4130M steel substrate.   Moderate loss of adhesion.

(d)   AISI 1018 steel.   Moderate loss of adhesion.

Figure 4.7-1.   Adhesion test specimens.

(b) In comparing the grinding characteristics of the metal spray coating to chrome, the machine operator found the spray coating much easier to grind, requiring wheel dressing approximately one third as often.

(c) The general appearance of the material compatibility specimens after 500 hours of neutral salt spray exposure is shown in Figure 4.8-4. The specimens were cross sectioned and photographs were taken at the coating/substrate interface.

The coating appears to be galvanically compatible with 15-5 PH stainless steel. As shown in Figure 4.8-5, neither the coating nor the 15-5 PH substrate is preferentially corroded. The coating appears to be galvanically incompatible with 4340M steel and 6Al4V titanium. Preferential corrosion of the 4340M substrate is apparent in Figures 4.8-6 through 4.8-8, indicating that the substrate is more galvanically active than the coating. Preferential corrosion of the coating occurred when applied on a substrate of 6Al4V titanium indicating that the coating in more galvanically active than the substrate (Figures 4.8-9 and 4.8-10).
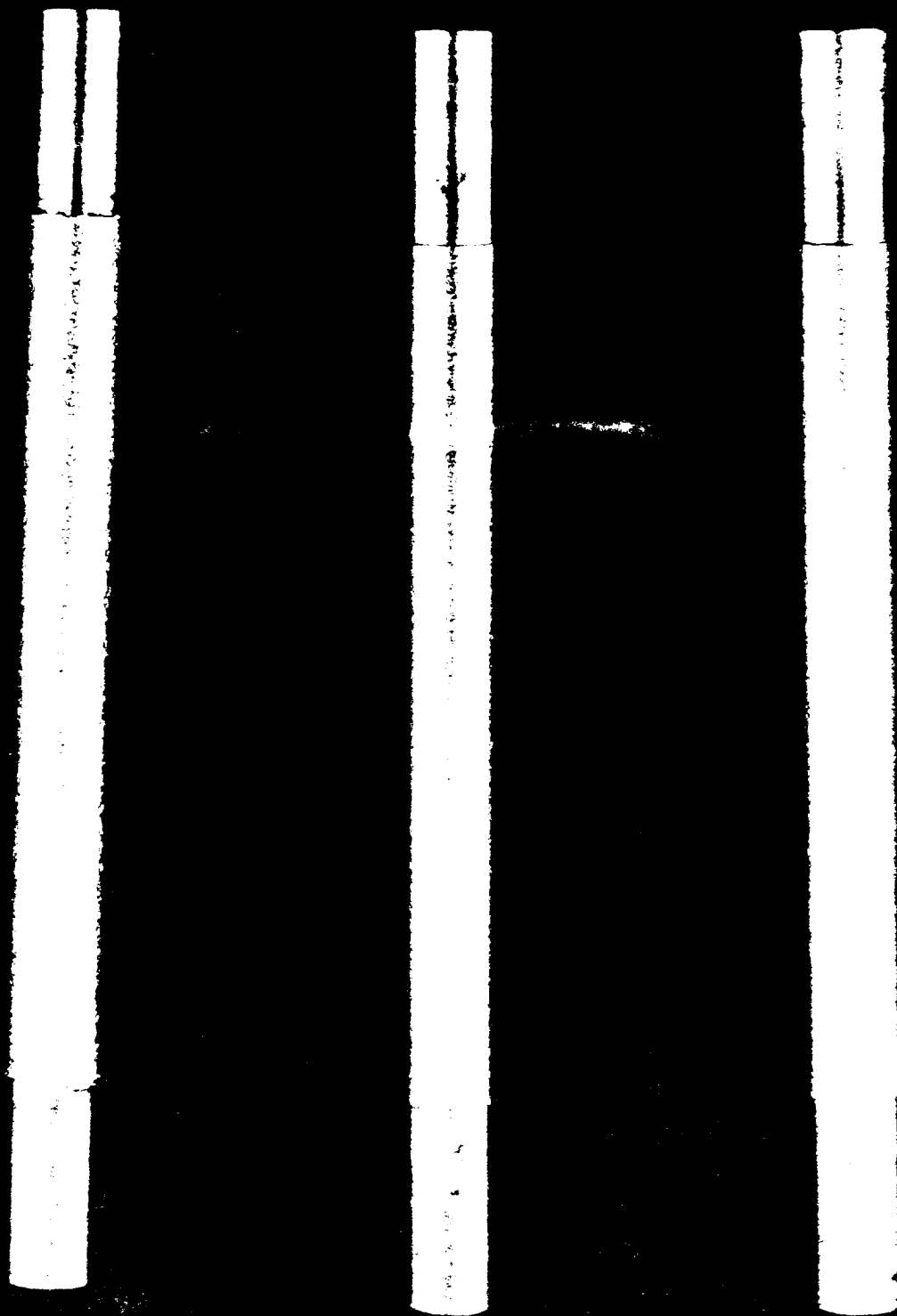
Figure 4.8-1.　Shot peened Versa by 50 coating on 15-5 PH
stainless steel substrate　No loss of adhesion.

190

Figure 4.8-1.1. Shot peened chrome plate on 15-5 PH stainless steel substrate. No loss of adhesion.
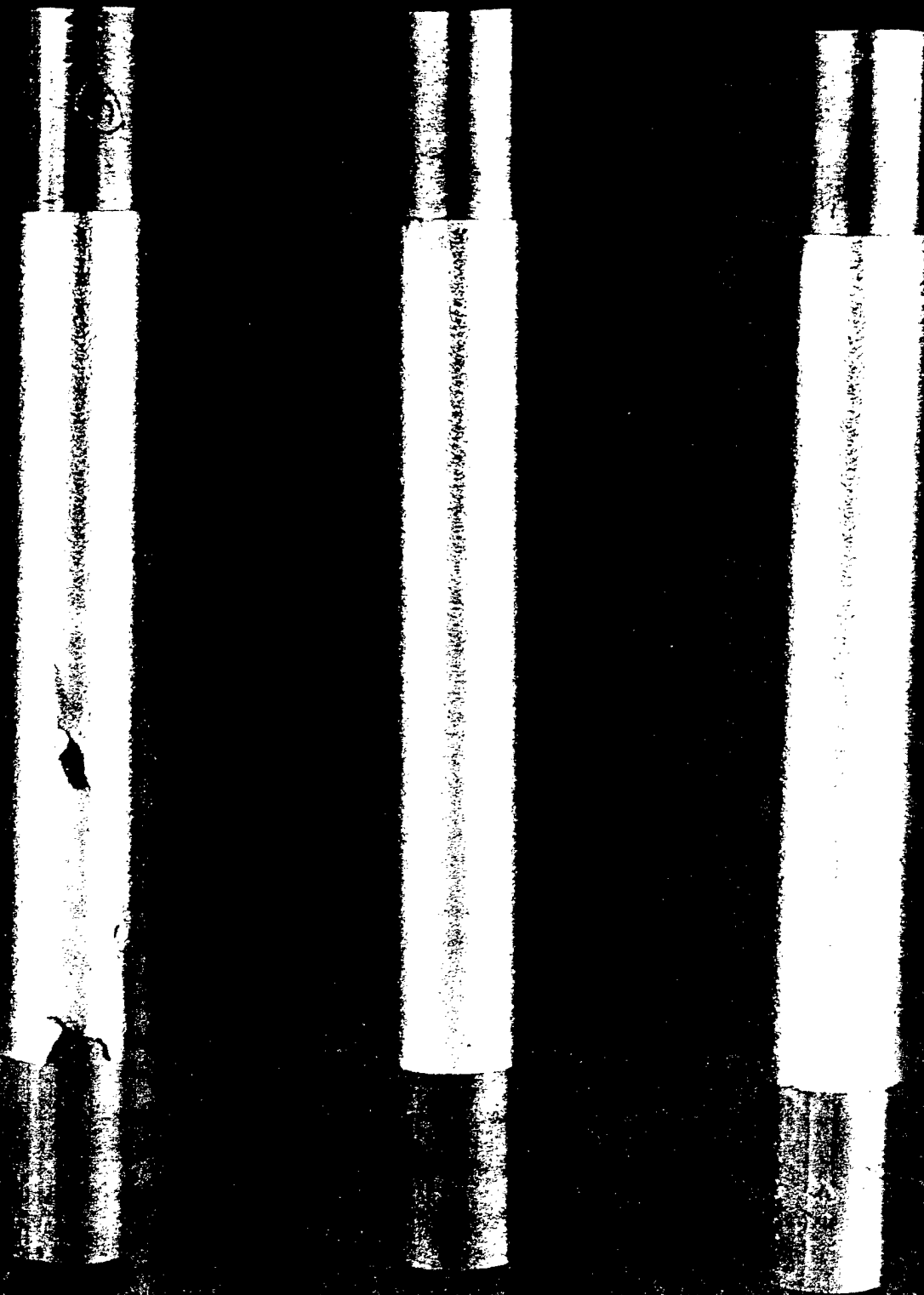
Figure 4.8-2. Shot peened Versalloy 50 coating, on 6A∣4V titanium substrate. Slight loss of adhesion.

194
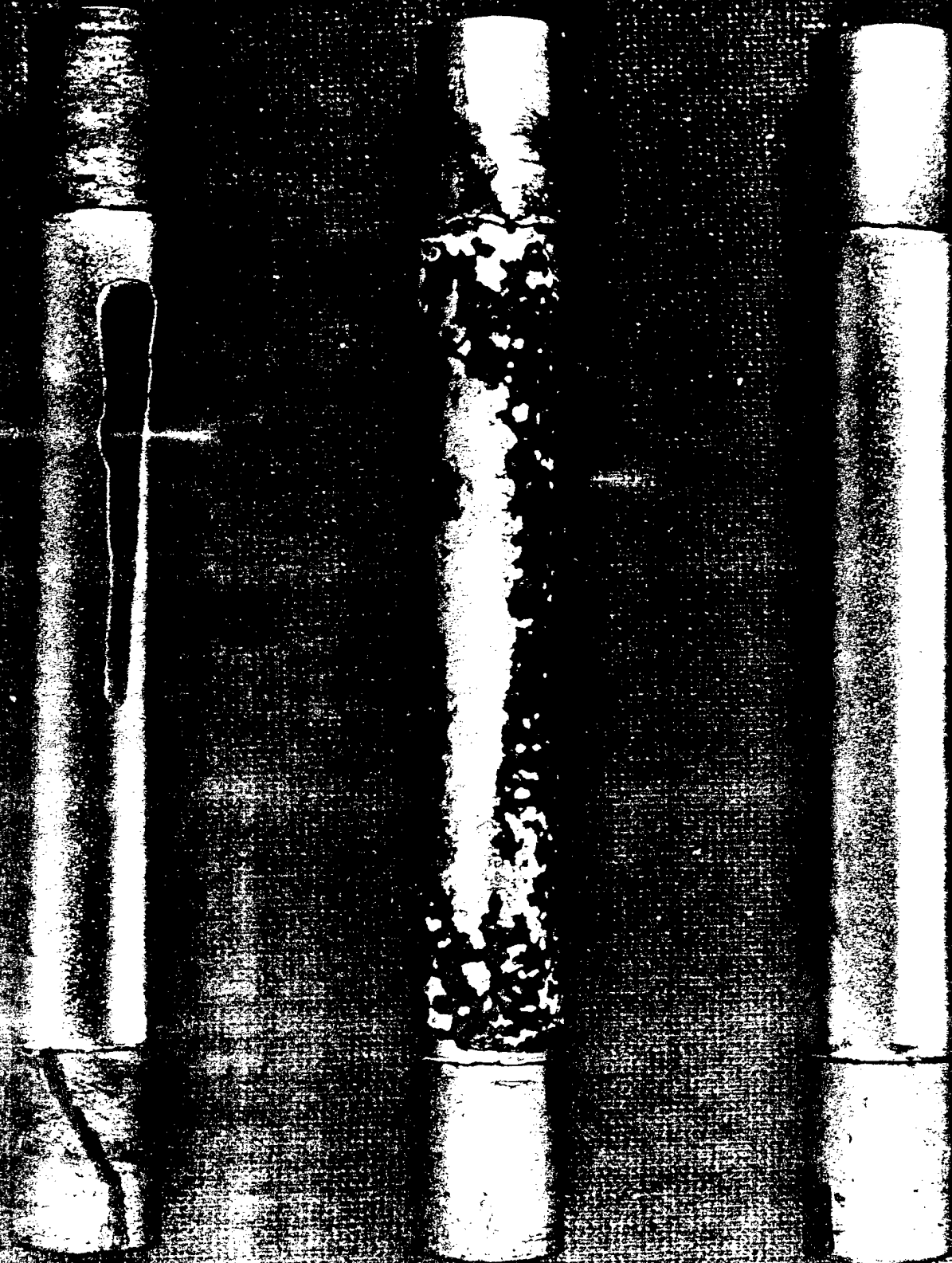
Figure 4.8-2.1. Shot peened chrome plate on 6Al4V titanium substrate. Severe loss of adhesion on one specimen, slight loss on second and no loss on third.
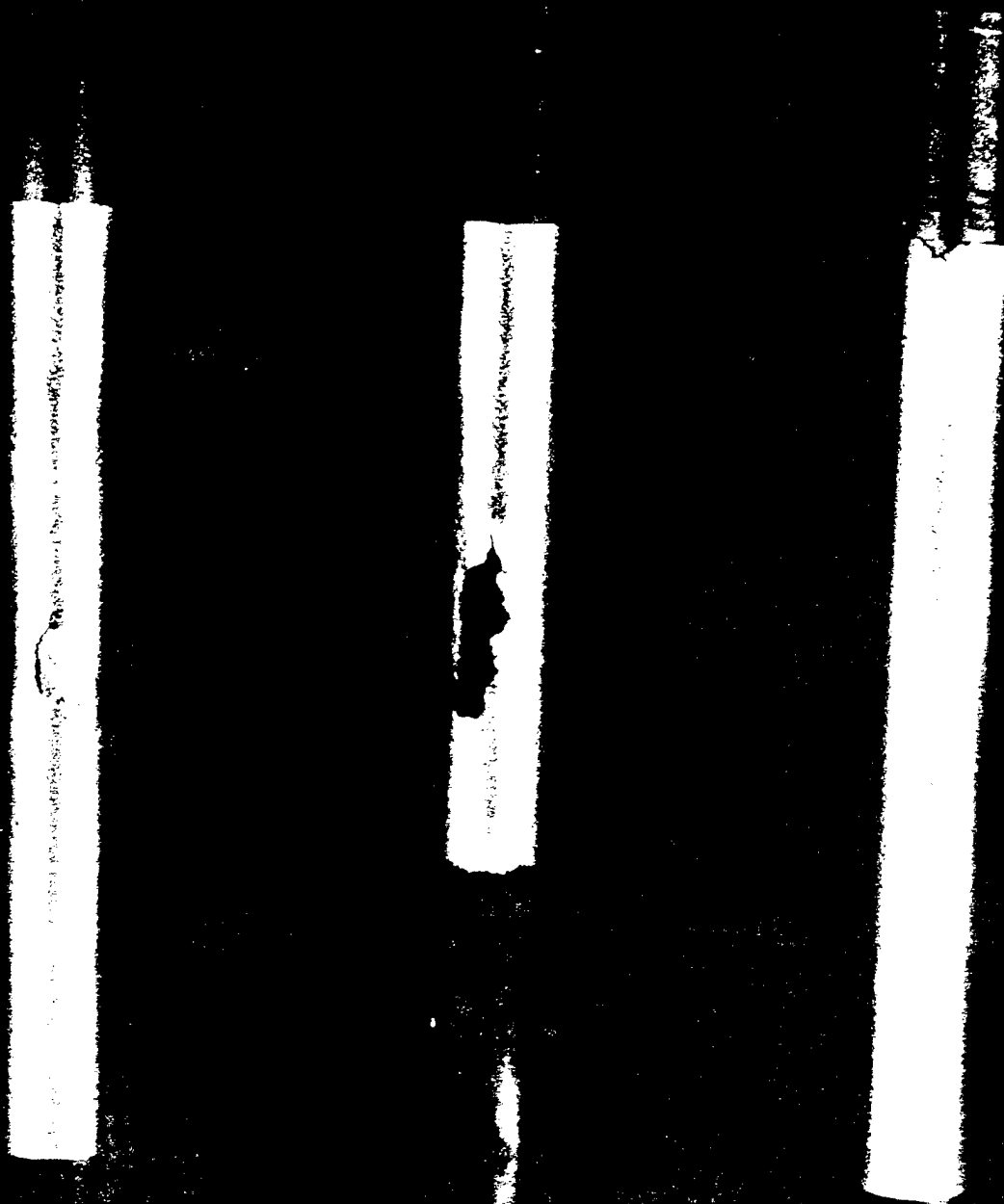
Figure 4.8-3. Shot peened Versalloy 50 coating, on AISI 4340M steel substrate. Slight loss of adhesion on two specimens, more severe loss of adhesion on the third.

196
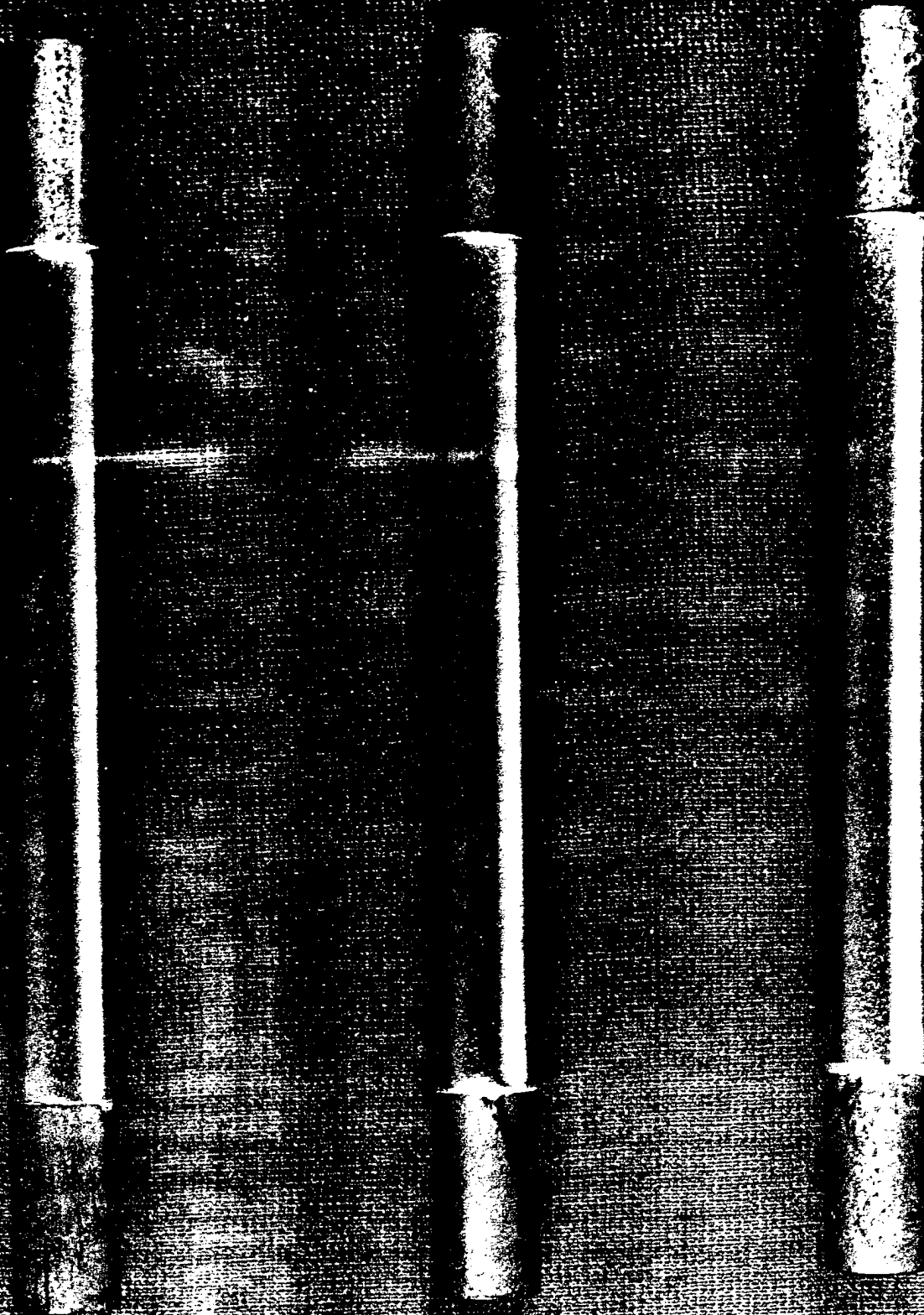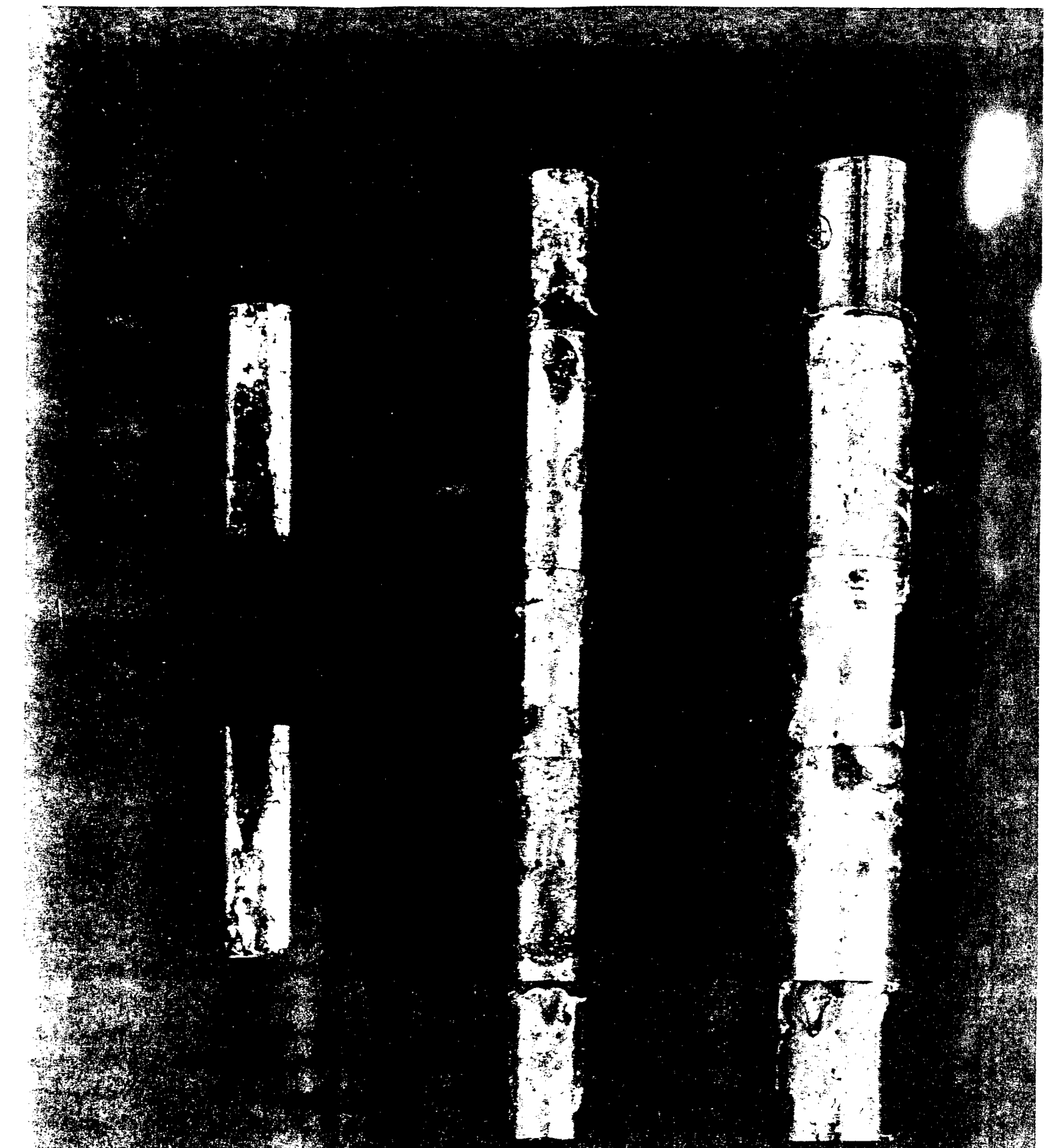
Figure 4.8-3.1. Shot peened chrome plate on AISI 4340M steel
substrate. No loss of adhesion.

Substrate: AISI 4340M steel.

Substrate: 15-5 PH stainless steel.

Substrate: 6Al4V titanium.

Figure 4.8-4.   Galvanic compatibility specimens after 500 hours in neutral salt spray.

Figure 4.8-5.   Cross section of Versalloy 50 coating on 15-5 PH stainless steel after 500 hours in neutral salt spray.

Figure 4.8-6. Cross section of Versalloy 50 coating on AISI 4340M steel after 500 hours in neutral salt spray.

200

Figure 4.8-7. Cross section of Versalloy 50 coating on AISI 4340M steel after 500 hours in neutral salt spray.

Figure 4.8-8. Cross section of Versalloy 50 coating on AISI 4340M steel after five hours in neutral salt spray.

Figure 4.8-9. Cross section of Versalloy 50 coating on 6A14V titanium after 500 hours in neutral salt spray.

Figure 4.8-10. Cross section of Versalloy 50 coating on 6Al4V titanium after 500 hours in neutral sa... ...ty.

75

4.9 Fatigue Test

S/N curves (maximum stress vs. fatigue life cycles) for bare, metal sprayed and chrome plated specimens are shown in Figure 4.9-1.
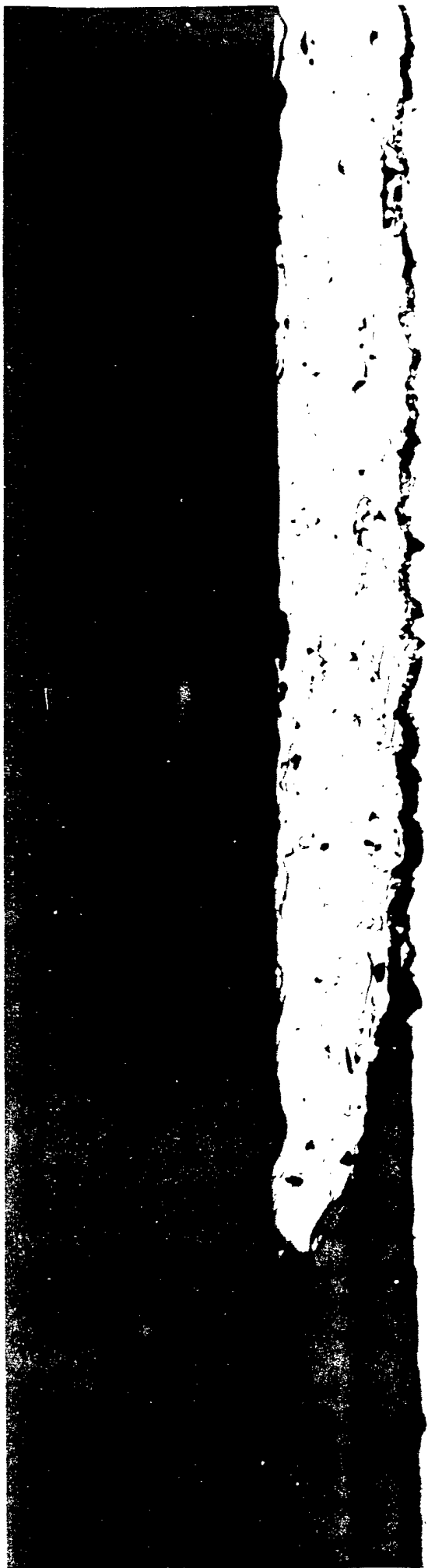
Fatigue Evaluation

Fatigue Life, Cycles
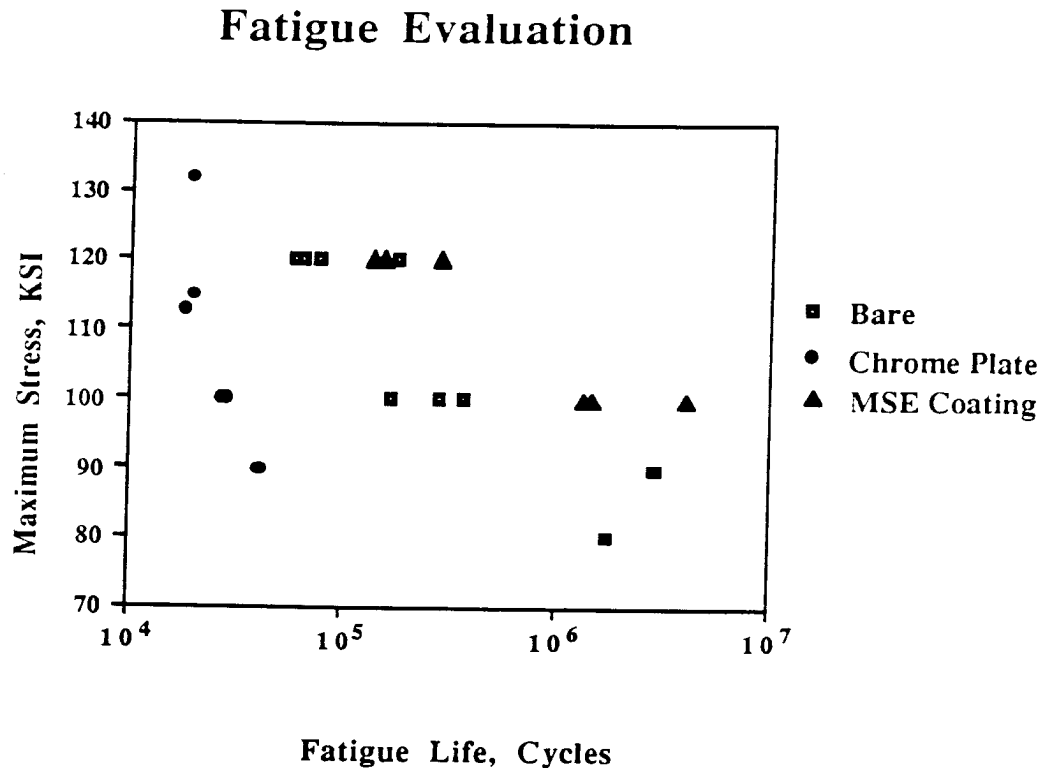
Figure 4.9-1.   S/N curves for unnotched 4130 alloy steel sheet, $F_{tu} = 180$ ksi, bare, spray coated and chrome plated.

The curve for the bare specimen establishes a base line against which to compare the effects of chrome plate and the spray coating on the fatigue life of the substrate material. As can be seen in the figure, chrome plate has a significant effect on the fatigue life of the steel, reducing it by as much as an order of magnitude. The metal spray coating however, enhanced the fatigue life to such an extent that runout occurred at 100 ksi and at 120 ksi, the fracture occurred outside the coated test region on three of the four specimens tested. Enhancement of fatigue life has been reported for other thermally applied coatings and may correspond to the residual compressive stresses that were reported in the Internal Stress section of this report. Typical failed fatigue specimens appear in Figure 4.9-2.
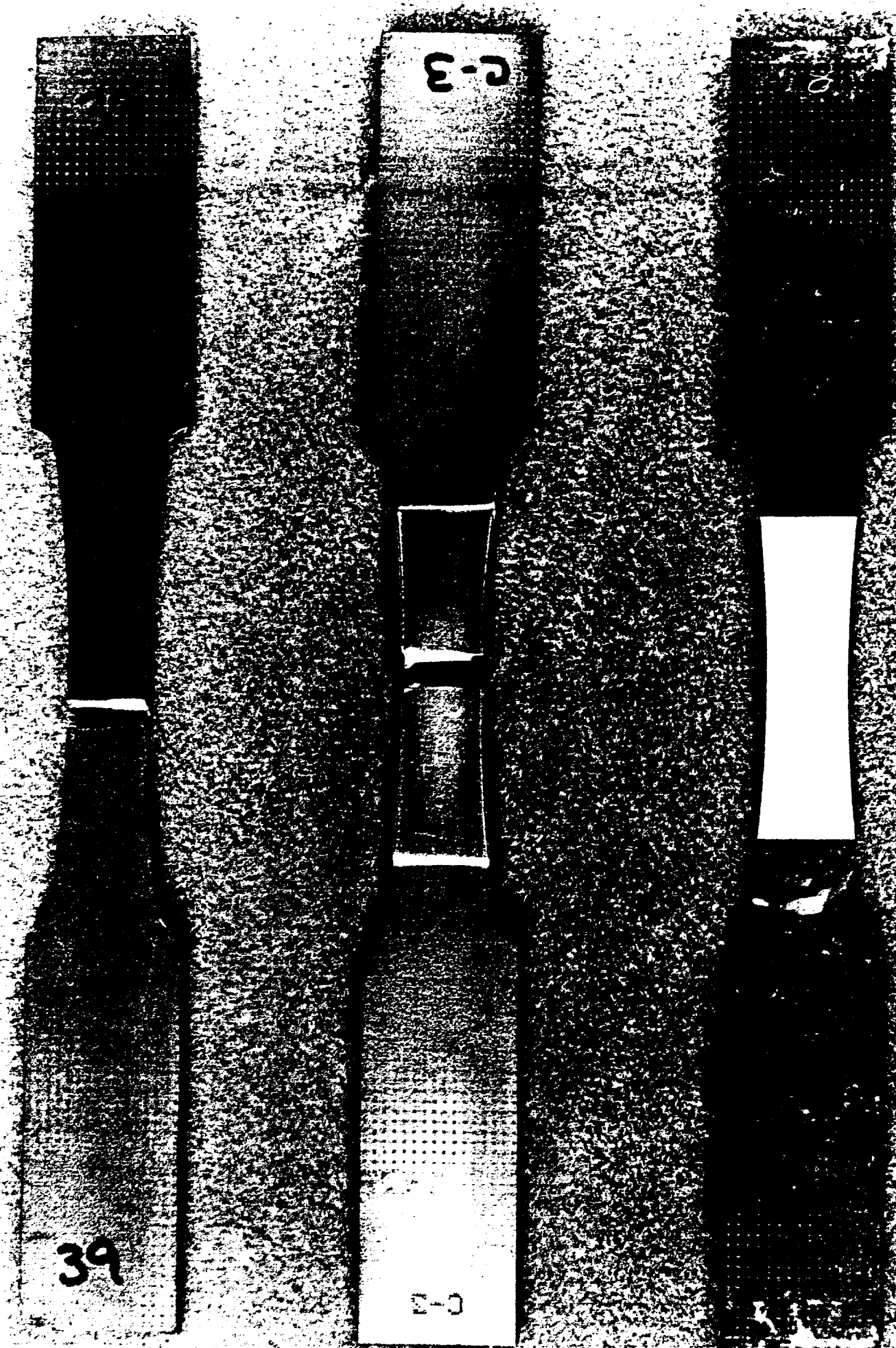
Figure 4.9-2. Typical failed fatigue specimens

CONCLUSIONS

The chemistry of the alloy appears to be preserved during the spraying process; however, the physical structure is not. The unsprayed alloy is crystalline in structure compared to the amorphous structure of the sprayed coating.

The performance of the sprayed coating compared to chrome plate varied among the tests performed. Most notably, the coating enhanced the fatigue strength of 4130 steel compared to a reduction caused by chrome plate. The coating exhibited excellent adhesion to 15-5 PH stainless steel and 6Al4V titanium, a substrate extremely difficult to electroplate.

The coating has a relatively high hardness, however did not perform well in abrasion testing compared to chrome. This is perhaps due to the layered structure of the coating. Although the coating did not perform as well as chrome in corrosion testing, refining the spraying process to reduce coating porosity should significantly enhance corrosion test performance.

APPENDIX B

ASM Handbook, Volume 18, pages 835-836

roethylene (PTFE) particles, have also been codeposited. As much as 30 vol% of the particles can be attained in both electroless and electroplated coatings (Ref 2).

In some applications, only limited areas of a component are subjected to wear. If the deposition of precious metals is involved, then it may be economically desirable to coat these areas selectively. Such limited coverage can be achieved by jet plating, laser-enhanced and laser-jet plating, and by physically masking off areas not to be plated, as in photolithography (Ref 3).

In jet plating, a fine jet of the plating solution is directed onto the areas to be coated. Because the current is constrained within the jet, only the areas where it is applied become coated. The jet also provides rapid ion transport to the depositing surface and therefore permits high deposition rates. In laser-enhanced plating, the heating effect of the laser enhances mass transport locally. It can also influence the deposition kinetics such that metal is not plated outside of the heated area. Laser-jet plating, which is a combination of jet and laser-enhanced plating, can provide improved deposit characteristics. The jet then acts as a waveguide for the laser.

The principal electrochemically deposited materials used in tribological applications are chromium, nickel, and both precious and soft metals. The characteristics of each type of deposit are described in this article. References 4 to 11 provide additional information relevant to electrochemically deposited metals and alloys used in tribological applications.

Chromium

Hard chromium coatings are widely used because of their low coefficient of friction and good wear properties. They are deposited at higher temperatures and current densities than decorative chromium. The plating solution for hard chromium has a lower ratio of chromic oxide to sulfuric acid (the main constituents of the solution) than that used for decorative coatings. The thickness of hard chromium deposits varies from about 0.1 to 100 μm (0.004 to 4 mils), whereas decorative thicknesses usually range from about 0.1 to 0.2 μm (4 to 8 μin.). Very strict antipollution regulations govern the discharge of solutions containing hexavalent chromium ions, which are used for hard-chrome plating. Therefore, plating solutions that contain mostly trivalent chromium ions are of interest. These solutions generally contain formic acid or one of its salts. Carbon will codeposit in these solutions. The deposits can therefore be heat treated to precipitate a chromium carbide.

The hardness of hard chromium varies from about 900 to 1100 on the Knoop and Vickers hardness scales. These values are considerably higher than the hardness of bulk chromium. Deposits from trivalent solutions are softer than those that are plated from hexavalent chromium solutions. However, after heat treating at about 700 °C (1290 °F), a hardness comparable to that of hard chromium can be achieved (Ref 12).

Table 1 Coefficients of friction

Couple	Static coefficient	Sliding coefficient
Chromium-plated steel versus itself	0 14	0 12
Chromium-plated steel versus steel	0 15	0 13
Steel versus steel	0 30	0 20

Source. Ref 13

Chromium deposits are characterized by high internal tensile stresses that can reach 1000 MPa (145 ksi). These stresses can reduce the fatigue properties of coated components. Hydrogen is also codeposited with chromium and can diffuse into components, causing hydrogen embrittlement. Heat treatments are typically required to relieve the stresses and hydrogen effects, but can reduce the hardness.

The coefficients of friction of hard chromium against hard materials are generally the lowest of any electrochemically deposited coatings. The actual values vary considerably, depending on the test method, the mating surfaces of the materials, and the degree of lubrication. Some values of static and sliding coefficients of friction are listed in Table 1. The static coefficient is calculated from the force to initiate movement of one component of a couple against the other. The force to maintain movement enters into the calculation of the sliding coefficient. It is important to note that only coefficients of friction obtained under the same conditions can be compared. The values should not be considered as absolute.

The wear rates of hard chromium can vary greatly, depending, again, on the type of test. The rates also vary with the mating material and whether adhesive or abrasive wear predominates. Some dry abrasive wear data from a Taber abrasion test for three different chromium deposits labeled CrA, CrB, and CrC are shown in Fig 1. The Taber test measures, for a certain number of cycles, the weight loss that results from abrasion with resilient, abrasive wheels at a load of 9.8 N (1 kgf). Figure 1 shows that deposit CrC had less wear than deposit CrA.

Figure 2 presents data obtained in a Falex wear test for the same three chromium deposits. In this test, a pin is rotated between two V-shaped blocks. Deposit CrA showed less wear than deposit CrC, illustrating the effect of a lubrication test method on the results. Figure 1 also shows that the chromium coating improved the abrasion resistance of the steel substrate. The hardest chromium deposits do not necessarily exhibit the least wear. The low friction coefficients and good wear properties of chromium have been attributed to a self-healing Cr_2O_3 film that forms on the surface. In general, hard chromium has a lower wear rate than either electroplated or electroless nickel, which are the two competing materials. This effect is also illustrated in Fig 1 and 2.

Under corrosive wear conditions, chromium coatings do not protect substrates if they crack in response to high internal stresses. Pulse plating can reduce the internal stresses and the resulting cracking of the deposit. The effects of pulse plating and deposition temperature on the wear rate of chromium deposits are shown in Fig 3. The improved wear resistance at higher pulse frequencies and temperatures corresponds to increases in hardness. The wear resistance in some applications can also be improved by the inclusion in the deposit of hard particles or those of a solid lubricant (Ref 15).

Chromium is widely used for wear resistance in automotive and aircraft components, such as
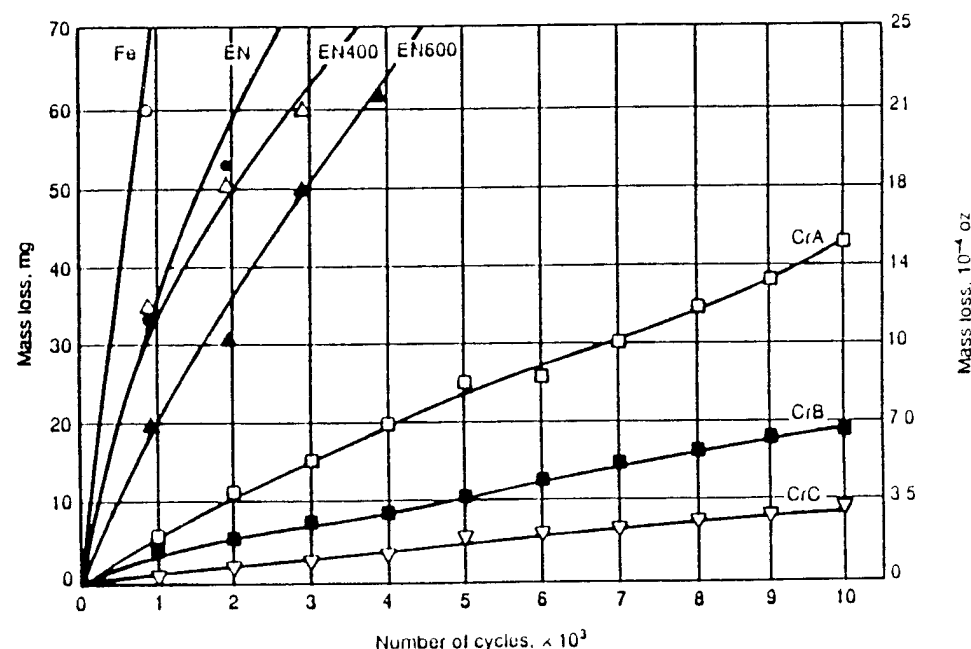

Fig 1 Effect of number of cycles on mass loss in the Taber abrasion test for uncoated steel substrate (Fe), three chromium deposits (CrA, CrB, CrC), and three electroless nickel deposits: as-plated nickel (EN), heat treated at 400 °C (750 °F) (EN400), and heat treated at 600 °C (1110 °F) (EN600). Source: Ref 1
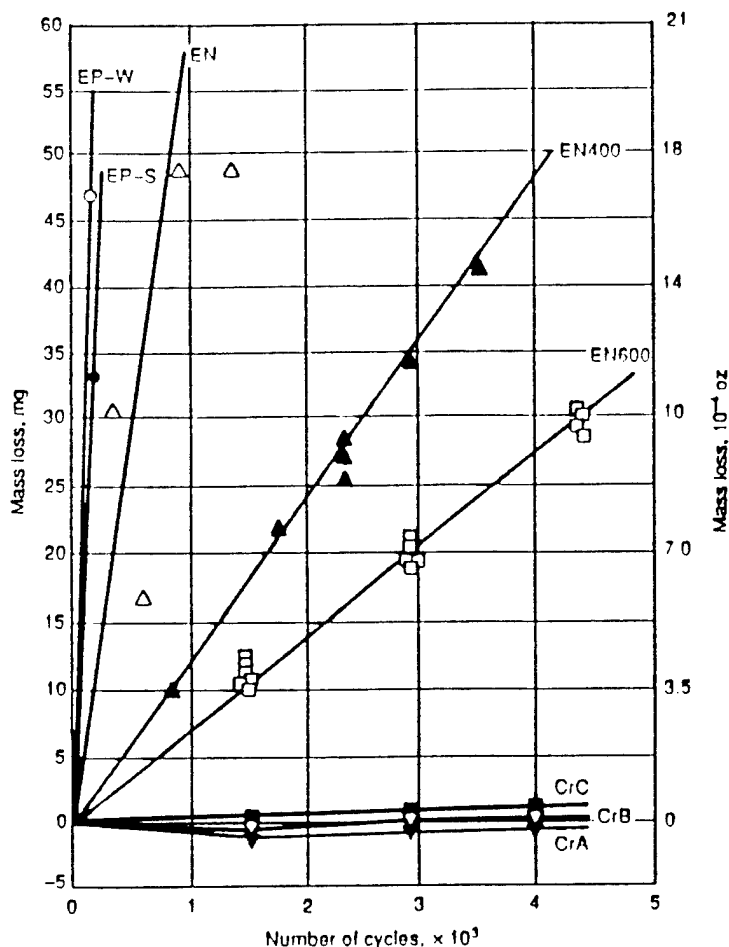
Fig 2 Effect of number of cycles on mass loss of plated pin versus steel blocks in a Falex test for same three chromium deposits (CrA, CrB, CrC) and same three electroless nickel deposits (EN, EN400, EN600) shown in Fig 1. Effects on two electroplated nickels from a sulfamate solution (EP-S) and a Watts solution (EP-W) are shown. Source: Ref 1
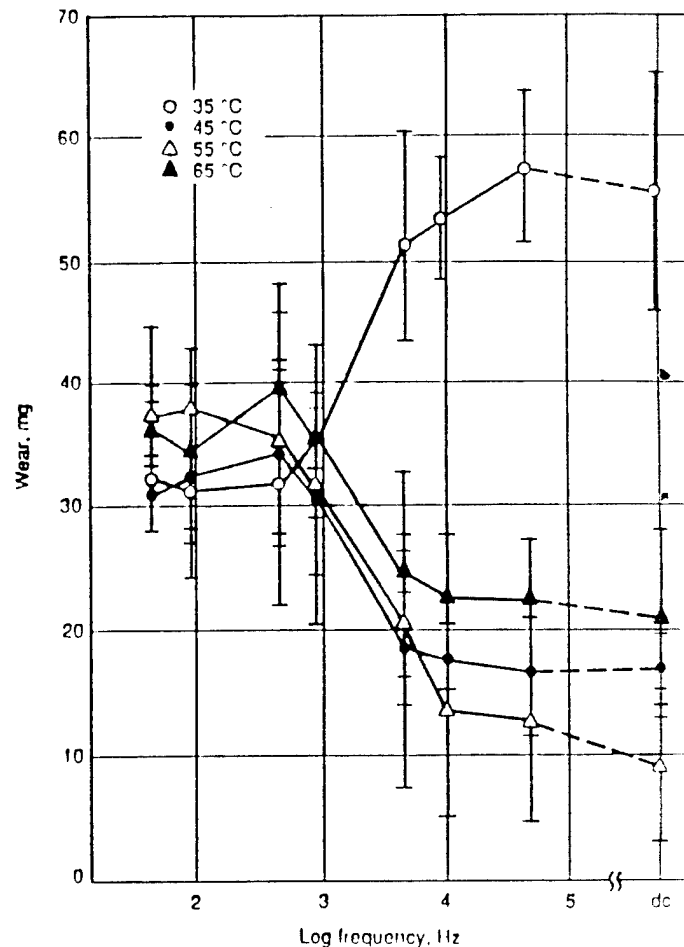
Fig 3 Effect of pulse frequency and solution temperature on mass loss of chromium deposits in a Taber abrasion test. dc, direct current. Source: Ref

pistons and shock absorbers (Ref 13). Other applications include coatings on drills, taps, dies, extrusion screws, and rolls. The wear resistance of gun barrels can also be improved by chrome plating. Salvaging of worn parts by chromium electrodeposition is an important industrial application.

Most of these applications require relatively thick chromium deposits. Thick deposits have a nodular surface structure, which is shown in Fig 4. Cracks that are due to high internal stresses are also visible. The nodular structure is too rough for some applications and therefore requires a mechanical finishing operation. Machining tools are usually plated with a thin chromium deposit, which is smooth and does not need to be finished (Ref 16).

Electroplated Nickel

The most widely used solution for plating nickel for wear applications is the Watts solution. Its main components are nickel sulfate, nickel chloride, and boric acid. Organic addition agents in the plating solution can increase the hardness and wear resistance mainly by decreas-

ing the grain size. Nickel usually is deposited with a tensile internal stress. Some sulfur compounds can cause the stress to become compressive, but also make the deposit more brittle, especially under elevated-temperature conditions. The nickel sulfamate plating solution produces low-stress deposits. It is possible to codeposit such metals as tungsten and molybdenum with nickel, even though they cannot be plated alone in aqueous solutions. Inclusion of hard particles or those of solid lubricants can also improve the wear or friction properties of electroplated nickel.

Improved wear resistance resulting from the incorporation of SiC particles is shown in Fig 5. In the test on which the data of Fig 5 are based, a plated block was pressed against a lubricated steel ring. Further improvement that was due to phosphide precipitates in heat-treated Ni-P-SiC coatings is also seen in this figure.

The hardness of nickel deposits can vary from about 150 to 500 on the Vickers scale. The hardness depends on the plating conditions, that is, current density, solution pH and temperature, and composition. Pulse plating can increase the hardness. The coefficient of friction and wear

rates of electroplated nickel are generally gr than those of chromium. The lower wear ra electroless, compared with electroplated, r can be seen in Fig 1 and 2. The widest u electroplated nickel for wear applications an undercoat for chromium. If thick deposi

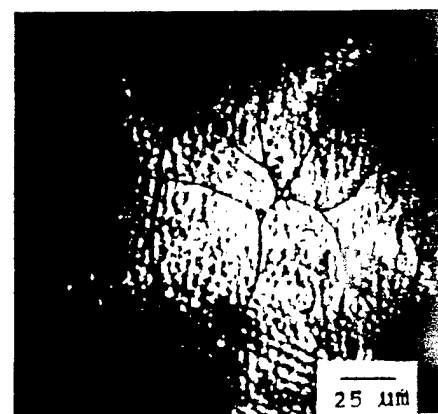**Fig 4** Optical micrograph of electrodeposited mium showing nodular structure and cr